Point-of-Care Sensors for Therapeutic Antibiotic Monitoring

Natascha Kappeler

Division of Medicine and London Centre for Nanotechnology
University College London

Supervisors:
Prof. Rachel A. McKendry
Dr. Daren J. Caruana

Industrial Supervisors from Sphere Medical Ltd., Cambridge:
Dr. Steve Fowler
Dr. Russell Keay

Thesis submitted for the degree of
Doctor of Philosophy at University College London

April 2014

I, Natascha Kappeler, confirm that the work presented in this thesis is my own. Where information has been derived from other sources, I confirm that this has been indicated in the thesis.

To my parents

Doris and Franz

“The product that the PhD researcher creates is not [only] the thesis - [...]

The product of their study is the development of themselves."

Sir Gareth Gwyn Roberts

(1940 – 2007)

Abstract

Antibiotics are some of the most effective drugs saving uncountable lives since their introduction more than 70 years ago. However, drug-resistant bacteria are rapidly spreading and posing one of the gravest threats to human health. Furthermore, the evolution of resistance is outpacing the discovery and development of new antibiotics. Therefore, stewardship of our existing and precious antibiotics is urgently needed.

The objective of this thesis is to develop point-of-care sensors for therapeutic antibiotic monitoring, particularly for vancomycin, which not only allow prudent antibiotic use, but very importantly lead to better health outcomes associated with lower healthcare costs.

The sensor development is approached with two different detection techniques: I) colourimetric detection via visible spectroscopy, and II) nanomechanical detection via cantilever array sensors.

I) The thesis' main focus was to develop a colourimetric vancomycin assay that builds on the point-of-care bench top device 'Pelorus' of our industrial partner – Sphere Medical Ltd. in Cambridge, UK. The assay could be successfully developed and benchmarked to UCLH's gold standard. It includes extraction from whole serum prior to a labelling reaction that permits subsequent quantification via visible spectroscopy. Free and bound drug concentrations can be quantified within minutes, which is crucial for the determination of antibacterial activity and an advantage over current routine assays. Furthermore, the labelling reaction produced a novel molecule, which was structurally characterised. The developed assay could be patented with recent PCT entry.

II) Nanomechanical detection of active free antibiotic concentration in human serum via cantilever arrays could be demonstrated. Combined with equilibrium theory, it led to better understanding of the biophysical mode of action improving treatment, dosage and drug discovery. It could be published in an article in *Nature Nanotechnology.*

This project has been early stage proof-of-concept work. The next step towards commercialisation should involve clinical evaluation from whole blood and may further extend to multi-analyte and hand-held sensors for therapeutic monitoring.

Outcomes of My Doctoral Study

PATENT

Title of Invention: **Analyte Extraction Apparatus and Method.** Inventors: Natascha Kappeler, Rachel A. McKendry, Daren J. Caruana, Russell Keay, David M. Pettigrew. Applicants: Sphere Medical Ltd, Cambridge, UK & UCL Business PLC, London, UK. Application Number: 1302774.3, Reference Number: RZ/P43636GB, Pages: 1-31, Filing Date: 18th February 2013, PCT Date: 18th February 2014.

PUBLICATIONS

Rachel A. McKendry & Natascha Kappeler: **Sensors: Good vibrations for bad bacteria.** *Nature Nanotechnology*, *8*(7), 483–484, 2013. doi:10.1038/nnano.2013.127.

Natascha Kappeler: **Thoughts on an education.** *Nature Nanotechnology, 8*(11)*,* 794–796, 2013. doi:10.1038/nnano.2013.239.

Joseph W. Ndieyira, Natascha Kappeler, Stephen Logan, Matthew A. Cooper, Chris Abell, Rachel A. McKendry & Gabriel Aeppli: **Surface-stress sensors for rapid and ultrasensitive detection of active free drugs in human serum.** *Nature Nanotechnology*, *9*(3), 225-232, 2014. doi: 10.1038/nnano.2014.33.

Natascha Kappeler: **Review: Cantilevers for Biological Monitoring.** *Contemporary Physics*. In preparation - deadline: 1st May 2014.

GRANT

Principle Investigator: Rachel A. McKendry, Co Investigator: Natascha Kappeler. Title: **Early-Stage Development of Novel Glycopeptide Antibiotics against Multidrug-Resistant Superbug Infections.** *UCL Therapeutic Innovation Fund.* Underpinning Funding: NHS, National Institute for Health Research, NIHR University College London Hospitals Biomedical Research Centre, NIHR Biomedical Research Centre at Great Ormond Street Hospital for Children NHS Foundation Trust and University College London, and Wellcome Trust. Funding: £ 50,000.

IMAGE DESIGN

François Huber, Hans Peter Lang & Christoph Gerber: **Nanomechanical Sensors: Measuring a response in blood.** *Nature Nanotechnology*, *9*(3), 165-167, 2014. doi:10.1038/nnano.2014.42.

Acknowledgments

A tremendously large and very special thank you goes to Prof. Rachel McKendry for being simply the perfect supervisor to me, as well as for her inspiration, her guidance, her support on all kinds of issues and, of course, for giving me the opportunity to do my PhD in her group. Furthermore I am very thankful that she has enabled me to develop and improve my professional and personal skills in various different ways. For example by strengthening my network of important contacts, supporting my attendance at different management courses, strongly encouraging my interest in public engagement, providing the environment to mature and grow into an independent scientist and constantly supporting the progression of my scientific career with publications and being co-investigator on a grant application. Many thanks go to Dr. Daren Caruana, my subsidiary supervisor, for all his support, for his great enthusiasm and for providing the essential additive point of view on my PhD project. I would like to express my gratitude to my industrial supervisors - Dr. Steve Fowler and Dr. Russell Keay and to my two former industrial supervisors - Dr. David Pettigrew and Dr. Peter Laitenberger from Sphere Medical Ltd. in Cambridge for giving me a very interesting industrial insight and for their assistance and ideas. It is great to be part of such an excellent team, to get inputs from different environments and to work at this interdisciplinary interface.

Furthermore I would like to thank Dr. Joseph Ndieyira from the LCN, who also played an important role in my PhD. A special thank goes to Dr. Antonio Jesús Ruiz Sánchez for his support and his assistance especially in the field of organic and analytical chemistry. Another very special thank goes to Alexander Wright, who has been my first student and a great pleasure to work with, for doing a perfect job in proof reading my whole thesis. Many thanks go to Dr. Abil Aliev and Dr. Stephen Hilton for their assistance with the nuclear magnetic resonance (NMR) measurements and purification, all the very interesting discussions and their enthusiasm, to Dr. Carolyn Hyde for her help with the mass spectrometry experiments, and to Dr. Anne Dawnay for performing the comparison with the gold standard assay at the University College London Hospital (UCLH).

ACKNOWLEDGMENTS

A great thanks goes to all other present and former members of Rachel McKendry's group, especially to Dr. Eleanor Gray for all her support, the great explanations especially in the field of genetics and virology, and all the very productive discussions. To Valérian Turbé for the great atmosphere in the office and in the lab, and for being my rock. To Kristina Schlegel for her friendship and for being part of the famous team Venice along with Val. To Dr. Tania Saxla and Kailey Nolan for their friendship, all their help and the great atmosphere in the office. To Benjamin Miller for the great atmosphere in the lab and for very last proof readings. To Dr. Rodolfo Hermans for being extremely helpful in various issues, for the legendary ladies nights and for being a great friend. To Joe Bailey for his friendship, introduction to the British way of life and for being a brilliant honour lady. To Dr. Manuel Vögtli and Dr. Daniel Engstrom, who I sadly miss at the LCN, for still being very supportive and becoming good friends. And to Dr. Richard Thorogate for managing the laboratories and the consumables.

Many thanks go to Prof. Gabriel Aeppli, the co-Director of the LCN, for his support and the enjoyable short conversations in Swiss German; to Dr. Frederique Guesdon for dealing with the health and safety issues; and to Nipa Patel, Rosie Baverstock-West, Gosia Janczak, Joanna Rooke and Denise Ottley for their help with any kind of administrative issues.

Furthermore I would like to extend my acknowledgments to all the co-workers in Sphere Medical Ltd. and the LCN for the wonderful working atmosphere and all the very pleasant conversations during and after work. Many thanks go to the other members of our INASCON 2013 organising committee, who are, asides from Val and Kristina, Thuong-Thuong Nguyen, Michael Gerspach, Tim Wootton and Samir Aoudjane, for sharing such a great experience and becoming friends through thick and thin. I would also like to thank Dr. Dessislava Nikolova, Angie Ma, Jenny Oberg and Dr. Maurice Mourad, who I sadly miss at the LCN, for all the fruitful discussions, their support, friendship and the continuing visits in London.

ACKNOWLEDGMENTS

A very special thank goes to Prof. Christoph Gerber for being my personal mentor, for all his inspiration and patronage; and together with Dr. Hans Peter Lang, Dr. Natalija Backmann, and Dr. François Huber all from the University of Basel, for supporting my work with cantilever arrays and for always welcoming me back in Switzerland.

Many thanks go to the University College London (UCL), Sphere Medical Ltd., The Engineering and Physical Sciences Research Council (EPSRC), and Health Tech and Medicines Knowledge Transfer Network (KTN) for providing the essential financial support. An additional thank goes to UCL's Graduate School for supporting my attendance inclusive talk at the Antimicrobials 2013 conference in Sydney, Australia; and moreover for reviving my public engagement activities by awarding me with a bursary to attend the Science Festival 2012 in Cheltenham, UK. In the same context, I would like to thank Dr. Steve Cross, the head of UCL public engagement, for offering me the opportunity to perform my very first stand-up comedy routine as therapeutic window leading to my stage name "Swiss Nano". Many thanks go to Daniel Friesner from the Science Museum for his unbreakable enthusiasm and support for the still ongoing organisation of an antibiotic awareness day.

Then a very personal thank you to my friends from the continent, particularly Angie, Simone, Thomas, Audrey, Anita, Beth, Corina, Saadet, and Adi, for their friendship, support and understanding; and of course my "NANOs", namely Meli, Nele, Susanne, Sonja, Lucas, This, Dario, Andy, Luki, Tinu, and Petz, for all their visits, brilliant and supportive discussions, and the great annual short trips colloquially know as "Nanoreisli".

Then I owe a huge thank you to my London family, Chloe, Hannah, Hilary, and Tony, for introducing me into the life of the British and the English language, for receiving me in their family, their support and the many enjoyable years. Last but not least, I would like to thank my parents, to whom I dedicate my thesis, for their love and immensely strong support.

Contents

CONTENTS

CONTENTS

CONTENTS

List of Figures

LIST OF FIGURES

LIST OF FIGURES

List of Tables

Abbreviations

ac	alkaline conditions
AFM	atomic force microscope
AM	amplitude modulation
AU	absorbance unit
AUC	area under the curve
BASF	Badische Anilin- und Soda-Fabrik (Baden Aniline and Soda Factory)
BSA	bovine serum albumin
C. difficile	*Clostridium difficile*
CE	"Conformité Européenne"
cfu	colony-forming units
COSY	correlated spectroscopy
CPE	carbapenemase-producing *Enterobacteriaceae*
CSV	comma-separated values
D*Ala*	L-*Lysine*-(ε-Ac)-D-*Alanyl*-D-*Alanine*
DCPIP	2,6-dichlorophenolindophenol
ddH_2O	distilled and deionised water
DI	distilled
Diprivan	diisopropyl intravenous anaesthetic
D*Lac*	L-*Lysine*-(ε-Ac)-D-*Alanyl*-D-*Lactate*
DNA	deoxyribonucleic acid
e-beam	electron beam
EMIT	enzyme multipled immunoassay techniques
E. coli	*Escherichia coli*
EPSRC	Engineering and Physical Sciences Research Council
ESI	electrospray ionisation
FBS	foetal bovine serum
FDA	Food and Drug Administration
FM	frequency modulation
FPIA	fluorescence polarisation immunoassay

ABBREVIATIONS

G6PDH	glucose-6-phosphate dehydrogenase
GISA	glycopeptide-intermediate *Staphylococcus aureus*
GlcNAc	N-acetylglucosamine
HCAI	healthcare associated infections
HOMO	highest occupied molecular orbital
HPLC	high-performance liquid chromatography
HSA	human serum albumin
I	interesting spin
ICI	Imperial Chemical Industries
ICU	intensive care unit
IR	infra-red
ISFET	ion-sensitive field effect transistor
IUPAC	International Union of Pure and Applied Chemistry
IV	intravenous
KTN	Knowledge Transfer Network
LCN	London Centre for Nanotechnology
Ltd.	Limited
LUMO	lowest unoccupied molecular orbital
MEMS	micro-electro-mechanical system
MHRA	Medicines and Healthcare Products Regulatory Agency
MIC	minimal inhibitory concentration
MPC	mutant prevent concentration
MRSA	methicillin-resistant *Staphylococcus aureus*
MSW	mutant selection window
MurNAc	N-acetylmuramic acid
NAD	nicotinamide adenine dinucleotide
NDM-1	New Delhi metallo-beta-lactamase-1
NEMS	nano-electro-mechanical system
NHS	National Health Service
NMR	nuclear magnetic resonance
NOE	nuclear Overhauser effect

NOESY	nuclear Overhauser effect spectroscopy
OR	operation room
PEEK	polyetheretherketone
PEG	polyethylene glycol (in our case: tri-ethylene glycol)
PG	peptidoglycan
PoC	point-of-care
ppm	parts-per-million
PSD	position sensitive detector
RNA	ribonucleic acid
ROESY	rotating frame nuclear Overhauser effect spectroscopy
S	source spin
S. aureus	*Staphylococcus aureus*
SAM	self-assembled monolayer
S_EAr	electrophilic aromatic substitution
SFM	scanning force microscope
SI	International System of Units (abbreviated from French: Système international d'unités)
SNI	Swiss Nanoscience Institute
SOI	silicon-on-insulator
SPR	surface plasmon resonance
STM	scanning tunnelling microscope
TDM	therapeutic drug monitoring
TLC	thin layer chromatography
TOCSY	total correlation spectroscopy
TVM	therapeutic vancomycin monitoring
UCL	University College London/London's Global University
UCLH	University College London Hospital
UV	ultraviolet
VCSELs	vertical cavity surface emitting lasers
VIS	visible
VISA	vancomycin-intermediate *Staphylococcus aureus*

VRE	vancomycin-resistant *Enterococcus* or vancomycin-resistant *Enterococci*
VRSA	vancomycin-resistant *Staphylococcus aureus*
VSE	vancomycin-sensitive (susceptible) *Enterococcus* or vancomycin-sensitive (susceptible) *Enterococci*
VSSA	vancomycin-susceptible *Staphylococcus aureus*
WEF	World Economic Forum
WHO	World Health Organization
WHS	whole human serum

CHAPTER 1: Introduction

Antibiotics are some of the most effective drugs, saving uncountable lives since their introduction more than 70 years ago. Former deadly diseases such as syphilis, gonorrhoea and bacterial pneumonia have become curable. One could argue that their widespread use has contributed to the dramatic rise of average life expectancy. However, resistant bacteria are naturally evolving and by administering antibiotics we increase the evolutionary pressure fuelling their Darwinian selection. Consequently, as the use of antibiotics has increased, numerous drug resistant bacterial infections have emerged and continue to spread. In the last couple of years, it has become obvious that the evolution of resistant bacteria is outpacing the discovery and development of replacement drugs. Furthermore, with high global mobility, resistant strains of bacteria can spread very rapidly. This is one of the gravest threats to human health and has recently been classified alongside dangers such as terrorism and global warming (Davies 2011).

The objective of this thesis is to develop point-of-care sensors for therapeutic antibiotic monitoring, which not only allow the prudent use of our existing antibiotics whilst ensuring that their concentrations stay above the mutant prevention concentration, but also lead to better health outcomes associated with lower healthcare costs (Imamovic and Sommer 2013). Such a sensor will be a key tool for antibiotic stewardship and for personalised medicine. It will reduce the therapeutic decision time and enable the drug dose to be titrated to the desired active target concentration according to the patient's individual drug adsorption, distribution, metabolism and excretion characteristics. Furthermore, it will detect accumulation or changes in the drug clearance rate and provide early detection of faults in the drug delivery system.

The development of these sensors focuses particularly on the antibiotic vancomycin and is approached with two different detection techniques: I) colourimetric detection via visible spectroscopy, and II) nanomechanical detection via cantilever array sensors. This thesis is an 'industrial CASE studentship' between University College London, UK as an academic partner and Sphere Medical Ltd. in Cambridge, UK as an industrial partner.

1.1 Objectives of the Thesis

The funding scheme 'industrial CASE studentship' by the Engineering and Physical Sciences Research Council (EPSRC) provides a first-rate, challenging research training experience, within the context of a mutually beneficial research collaboration between academic and industrial partners. In the present case, the unique research collaboration is based on the active integration of Sphere Medical's expertise in highly innovative medical monitoring devices especially for the critical care environment and London Centre of Nanotechnology's breakthrough in specific surface chemistry for antibiotic capturing. Hence this project, which has been originally entitled "Nanomechanical Point-of-Care Devices for Antibiotic Monitoring" (Laitenberger, McKendry, and Ndieyira 2010), gives the unique opportunity to merge the interests of industry with the aims of the university. Moreover it provides a multidisciplinary training at the interface of biology, chemistry, physics, engineering and medicine whilst involving interactions with researchers from universities, companies and clinics.

The main objective of this PhD thesis is the development of the next generation of point-of-care (PoC) sensors for therapeutic antibiotic monitoring, particularly for the glycopeptide antibiotic vancomycin. In order to achieve this challenging goal, two detection technologies are investigated:

I) **Colourimetric detection** of vancomycin measured with visible spectroscopy builds on Sphere Medical's Pelorus bench top device. The goal is to specifically elute vancomycin out of the biological matrix and then to label it with Gibbs reagent to induce a detectable colour change. This approach of labelling phenol moieties with Gibbs reagent and measuring it spectroscopically builds on Sphere Medical's work with the anaesthetic propofol in the Pelorus bench top device (Pettigrew, Laitenberger, and Liu 2012; Liu et al. 2012). The main focus of this thesis has been laid on to the development of this first detection technique. Therefore its experimental study spans over three consecutive chapters. The benchmarking experiments according to Sphere Medical's Pelorus device are presented in

chapter 5 on page 71 et seqq. The development of the colourimetric detection of vancomycin, including the labelling reaction, extraction protocol and subsequent patent filing, are discussed in chapter 6 starting on page 120. Further characterisation of the 'vanGibbs' molecule especially important for patent validation can be found in chapter 7 from page 198 onwards.

II) **Nanomechanical detection** of vancomycin binding to a mimetic bacterial cell wall layer on cantilever array sensors. This approach, builds on previous work by Prof. Rachel McKendry and colleagues, has shown that cantilever array sensors offer a unique tool to study surface-active drugs and the nanomechanical consequences of drug-target binding interactions. Therefore cantilever array sensors paired with specific surface chemistry for antibiotic capturing establish an ideal basis for a nanomechanical sensor for therapeutic vancomycin monitoring (Watari, Ndieyira, and McKendry 2010; Ndieyira et al. 2008; McKendry et al. 2002; Sushko et al. 2008; J. Zhang et al. 2006; Shu et al. 2005; McKendry 2012; Watari et al. 2007). This approach is described in chapter 8 starting on page 229.

Along with developing each technique for therapeutic antibiotic monitoring at the point-of-care, the overarching aim is to evaluate the feasibility of miniaturising the different detection techniques for patient attached real-time monitoring devices. Therefore, the two techniques were deliberately chosen as an overall miniaturisation development process. As schematically illustrated in figure 1.01, this development includes the progression from the current gold standard with a laboratory-based device, over a bench top device with intermittent near-patient monitoring capabilities, to a future patient attached sensor chip with the ability to monitor in real-time.

Therefore, the first technique (I) is a simple, robust and low cost bench top device. Due to its similarities with the Pelorus system, this technique also benefits from a close proximity to the market. The second technique (II) is the development towards a future sensor chip, which aims to be incorporated into the patient's intravenous lines for real-time continuous monitoring. However with the current read-out system, cantilever array sensors, as the second technique (II), are still closer to be applicable in a bench top device than in an intravenous sensor chip. Therefore it represents the transition from a bench top device to a future patient attached sensor.

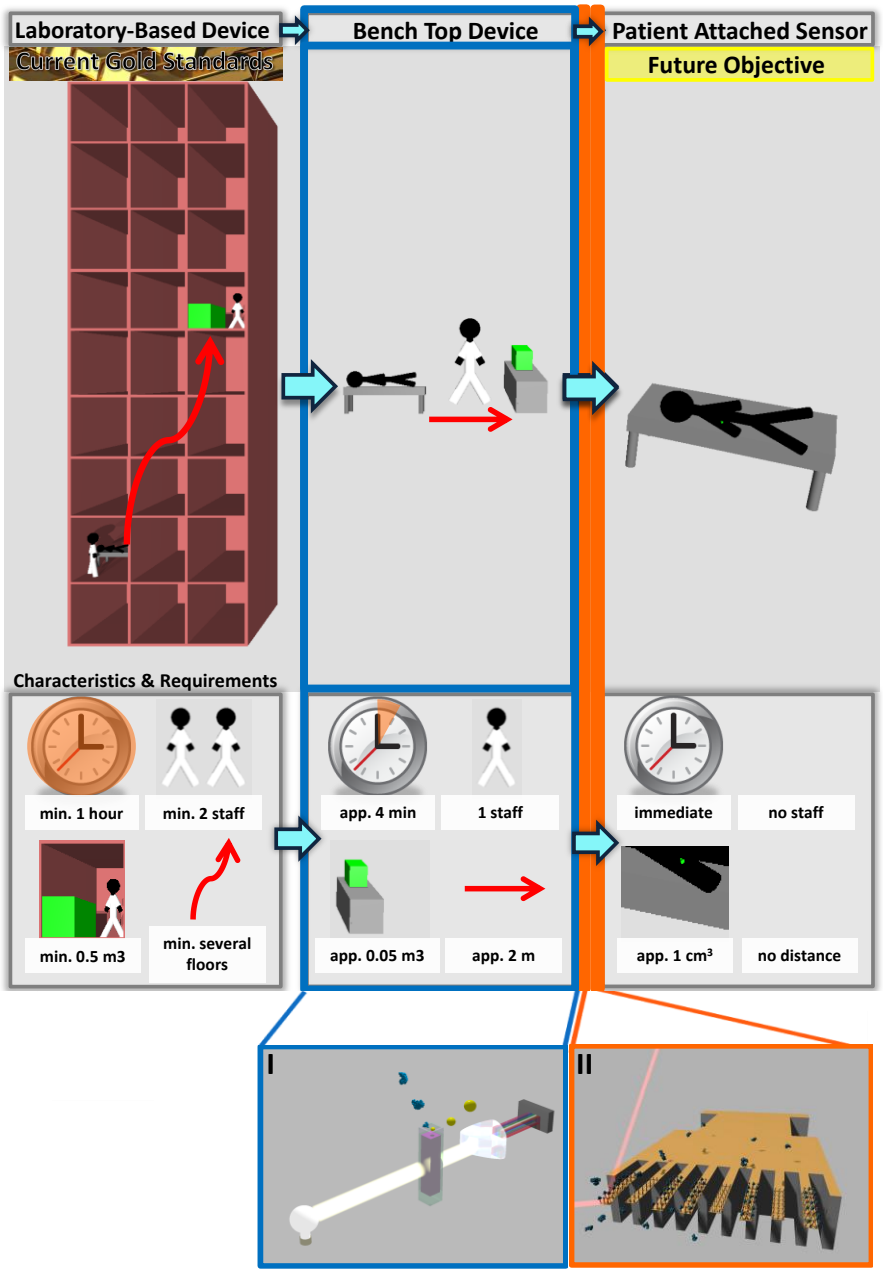

Figure 1.01: Overarching miniaturisation development process investigated in this thesis. This development includes the progression from the current gold standards with a laboratory-based device, over a bench top device with intermittent near-patient monitoring capabilities, to a future patient attached sensor chip with the ability to monitor in real-time. From the left to the right not only are the dimensions of the devices scaling down, but also the requirements in time, staff, transportation distance and administration are diminishing resulting in minimal associated costs. The two schematics at the bottom depict the different detection techniques used to approach the different stages in the miniaturisation development process: I) colourimetric detection via visible spectroscopy, and II) nanomechanical detection via cantilever array sensors.

1.2 Requirements for PoC Therapeutic Drug Monitoring Sensors

In order to study and examine these two techniques, sensors, biosensors and their characteristics have to be first defined in general terms. Furthermore, if sensors are used at the PoC, requirements of PoC tests have to be described.

Sensors are devices that measure an input signal and convert it, often several times, into an electrical signal which can then be read out by an instrument or an observer. Ideally sensor technologies should be an optimal compromise between specificity, sensitivity, simplicity, speed and costs. (Scheller et al. 2001; Thévenot et al. 2001; D'Orazio 2003)

The Medicines and Healthcare Products Regulatory Agency (MHRA), which is a UK government agency responsible for ensuring medicines and medical devices, defines a PoC test as follows: 'Any analytical test performed for a patient by a healthcare professional outside of the conventional laboratory' (MHRA 2010). This definition includes rapid tests for monitoring and/or diagnostic purposes at or near the site of patient care. PoC tests are often transportable, portable and handheld instruments, which enable patient, physician and the care team to receive a quicker result that allows immediate clinical management (Luppa et al. 2011).

Consequently, a PoC therapeutic drug monitoring sensor, which monitors an analyte, the drug, and generates a concentration dependent signal, needs to fulfil the following requirements:

- Sensitive to clinically relevant drug concentrations.
- High specific for the required drug with very low interference or cross-reactivity with other drugs or blood components (e.g. serum proteins, antibodies, antigens, hormones).
- Rapid.
- Simple, not require specialist equipment and staff.
- Cost effective.

- Robust and stable in the application and storage environment.
- Safe in case of any malfunction.
- Sterile, nontoxic and preferably the part in direct contact with sample should be disposable.
- Quantify free and bound drug fraction: An additional benefit for a therapeutic antibiotic monitoring sensor, particularly for vancomycin, would be the option to monitor free and active drug concentration. Since it is commonly accepted that a drug bound to blood serum proteins, will have a reduced biological activity, this in turn affects the distribution in the body, elimination rates, tissue penetration and presence at the site of infection. Hence it is mainly the unbound fraction of the antibiotic which is active against the infecting organisms (Shin et al. 1991; Butterfield et al. 2011; Sun, Maderazo, and Krusell 1993; Zeitlinger et al. 2011; Stein and Wells 2010). Serum binding and its effect are further discussed in chapter 3.3.3.

Moreover according to PoC sensors for therapeutic antibiotic monitoring, the recent published “UK Five Year Antimicrobial Resistance Strategy 2013 to 2018” by the Department of Health and the Department for Environment Food & Rural Affairs listed PoC sensors as urgent requirement for new or improved rapid diagnostic ‘as well as to reassess the appropriateness of the diagnosis and treatment’ (Department of Health 2013). Furthermore, they list the use of PoC sensor for improvement in knowledge of antibiotics and antibiotic resistance, and as a key tool for antibiotic stewardship (Department of Health 2013).

1.3 Thesis Outline

The objective of this thesis is to develop point-of-care sensors for therapeutic antibiotic monitoring. Due to the multidisciplinary approach of this development with two different detection assays, it has been decided that the investigation of each technique is separated into different chapters. Each chapter consists of a first subsection covering the technique specific introduction, followed by a subsection listing the corresponding materials and methods, a third subsection presenting and discussing the results, and a fourth and last section drawing the conclusions. Moreover, since the main focus of the thesis is the development of the colourimetric technique, its experimental study spans over three consecutive chapters. Consequently, the thesis is organised as follows:

- Chapter 1 gave a concise introduction and describes the thesis' objectives as well as the requirements seeking to be fulfilled by the different techniques.

- Chapter 2 provides a general overview of antibiotics and antimicrobial resistance, which is a major threat to human health and a global challenge that urgently needs to be tackled. Furthermore, it discusses antibiotic stewardship and drug discovery.

- Chapter 3 describes the antibiotic vancomycin including pharmacological characteristics with special focus on serum binding and its effect on antibacterial activity. It also lists the so far unmet clinical needs seeking to be addressed in this thesis.

- Chapter 4 reviews the need for the therapeutic drug monitoring technologies whilst emphasising its health economic importance with special focus on antibiotic monitoring. Additionally, it presents the current gold standards for therapeutic vancomycin monitoring and a profile of our industrial partner, Sphere Medical Ltd., Cambridge, UK.

- Chapter 5 is the first of three consecutive chapters describing the investigation of colourimetric detection via visible spectroscopy. This part contains proof-of-principle and benchmarking experiments with reference to Sphere Medical's Pelorus device, which colourimetrically quantifies the anaesthetic propofol.

- Chapter 6 is the largest chapter in the thesis. It presents the development of the colourimetric detection of vancomycin, including the labelling reaction, extraction protocol from serum, free and bound drug quantification, comparison to a gold standard technique and subsequent patent filing.

- Chapter 7 is the last chapter related to the colourimetric detection of vancomycin. It discusses the characterisation of the vanGibbs molecule and the labelling reaction mechanism by NMR and mass spectrometry studies.

- Chapter 8 describes the nanomechanical detection of vancomycin by cantilever array sensors, which is the second detection technique investigated in this thesis.

- Chapter 9 is the final chapter and summarises the key findings and conclusions. Furthermore, it outlines ideas for future work.

- The appendix includes the statistical analysis from chapter 6.

CHAPTER 2:

Antibiotics, Resistance, Stewardship and Drug Discovery

One of medicine's greatest success stories in the 20th century was the discovery and development of antibiotics and antibacterial agents for the treatment of bacterial infections. Countless lives were saved and previous lethal illnesses such as syphilis, gonorrhoea and bacterial pneumonia, that were predominately incurable, could suddenly be cured. In more recent times, some antibiotics have even shown to be effective as antiviral or anticancer drugs (Demain and Sanchez 2009; Davies and Davies 2010).

However, the implementation and reliance of antibiotic therapy has led to a significant problem. Bacteria are acquiring mutations which can make them resistant to antibiotics, due to a variety of factors. The resistant bacterium may then be selected by further use of antibacterial drugs according to Darwin's theory of 'survival of the fittest' and 'natural selection' (Darwin 1859). The resistance acquiring factors include the naturally stochastic appearance of genetic variations paired with short generation times, the ability to pass genetic information such as genes encoding resistance and multi-resistance between individuals from the same or different genera, and the increased mutagenesis of 'hypermutable' strains found in natural bacterial populations (Walsh and Wright 2005; Williams and Bardsley 1999; Livermore 2007; Blázquez 2003).

Recent discoveries of mutation mechanisms, induced by growth-limiting stress, add an additional perspective to the evolution of resistance. Stressors include hypoxia, starvation, oxidative stress and antibiotics (Shee, Hastings, and Rosenberg 2013; MacLean, Torres-Barceló, and Moxon 2013). In the last ten years, work has shown that some antibiotics, including β-lactams, quinolones and aminoglycosides, can induce mutagenesis (Davies and Davies 2010; Kohanski et al. 2007; Miller et al. 2004). The resulting mutations may give resistance to the same antibiotic (Cirz et al. 2005), to

different or even a wide range of antibiotics (Kohanski, DePristo, and Collins 2010; Pérez-Capilla et al. 2005).

Hence, the widespread use of antibiotics amongst humans and animals has created a global problem in spreading resistance acquisition. Unfinished treatments, overuse in agriculture and farming, misuse against viral infections and usage for prophylaxis has accelerated the pace at which bacteria are able to overcome the bacteriostatic and bactericidal mechanism implemented by many types of antibiotic agents. The typical antibiotic-resistance mechanisms include efflux pumps, target gene-product modifications, and inactivation of the antibiotic compound by enzymes. (Dantas et al. 2008; Spellberg, Bartlett, and Gilbert 2013)

Consequently, a combination of multi-resistant bacterial strains and a lack of new potent antibacterial drugs is a global healthcare problem (Butler and Cooper 2011; Cooper and Shlaes 2011; Ledford 2012; Howell 2013; Davies 2011; Chan 2013; McKendry and Kappeler 2013).

Additionally, very recent studies have confirmed that bacteria are not only acquiring resistance against antibiotics, but also against broad-spectrum antimicrobial agents such as triclosan (Drury et al. 2013). Due to its antibacterial and antifungal activity, triclosan is a commonly used additive in various consumer products such as antibacterial soaps, shampoos and toothpastes (Thompson et al. 2005). Moreover, it has become a recommended treatment in surgical units for the decolonisation of patients, whose skin is carrying methicillin-resistant *Staphylococcus aureus* (MRSA) (Coia et al. 2006a; Coia et al. 2006b).

These alarming developments show beyond dispute that the responsibility of protecting antibiotic efficacy lies in our hands. There can be no doubt that we urgently need to tackle the global challenge of antimicrobial resistance.

In simple terms, there are three areas of focus underpin the fight against developing antibacterial resistance. The first is traditional practices in infection prevention and control, the second is improved antibiotic stewardship, while the third is the development of new antibacterial drugs (Spellberg, Bartlett, and Gilbert 2013).

This chapter provides a general overview of antibiotics and antibiotic resistance including terminology (2.1), history (2.2), the lack of antibiotics and the rise in resistance as our global challenges (2.3).

2.1 Definition of Antibiotics, Antimicrobials and Antibacterials

The word “antibiotic” is derived from “antibiosis”, which originated from the Ancient Greek and means ‘against life’. It is believed that this term was introduced by the French mycologist Jean Paul Vuillemin (1861 – 1932) in 1889 when he described the characteristic of a group of drugs, which showed activity against microorganisms (Calderón and Sabundayo 2007).

In 1947, Selman A. Waksman (1888 – 1973), a Ukrainian-born American inventor, biochemist and microbiologist, published one of the first definitions for the term “antibiotic”. He concluded that “An antibiotic is a chemical substance, produced by microorganisms, which has the capacity to inhibit the growth of and even to destroy bacteria and other microorganisms. The action of an antibiotic against microorganisms is selective in nature, some organisms being affected and others not at all or only to a limited degree; each antibiotic is thus characterised by a specific antimicrobial spectrum. The selective action of an antibiotic is also manifested against microbial versus host cells. Antibiotics vary greatly in their physical and chemical properties and in their toxicity to animals. Because of these characteristics, some antibiotics have remarkable chemotherapeutic potentialities and can be used for the control of various microbial infections in man and in animals.” (Waksman 1947).

Historically, Waksman's definition did not include semi- and fully synthetic antibiotic agents, however, this was later extended to include synthetic agents (von Nussbaum et al. 2006).

In conclusion, 'antibiotic(s)' is an umbrella term for a whole range of compounds with antimicrobial activity. However, it is important to distinguish between antimicrobial medicines/medication/drugs/agents[1], which include antifungal, antiparasitic and antibacterial agents, and a wide range of less specific or non-specific chemicals, metals, plants or natural compounds with antimicrobial activity (von Nussbaum et al. 2006). They span from disinfectants such as iodine (Coia et al. 2006a; Coia et al. 2006b), alcohols (Coia et al. 2006a; Coia et al. 2006b; Marshall et al. 2004), and detergents with additives like triclosan (Drury et al. 2013; Thompson et al. 2005). Further, they include, for instance, the metals copper (Casey et al. 2010; O'Gorman and Humphreys 2012) and silver (Percival, Bowler, and Russell 2005), which are broadly applied in healthcare facilities (Ojeil et al. 2013). Moreover, organic acids including citric and lactic acids (Eswaranandam, Hettiarachchy, and Johnson 2006), and plant extracts including essential oils such as garlic, tea tree oil and thymol[2] (Smith-Palmer, Stewart, and Fyfe 1998; Selim 2011; Kollanoor Johny et al. 2010; Ogata et al. 2005; Nostro et al. 2007), are known to have antibacterial activity (Windler, Height, and Nowack 2013). However,

[1] For simplicity, these four terms are treated as synonyms within this thesis.

[2] Thymol is the colloquial name of 2-isopropyl-5-methylphenol and it serves as structural basis for bromothymol blue (BTB). BTB is a pH indicator changing its colour from yellow to blue above a pH of 7.6. It is typically one compound of the universal pH indicator paper (Scudi 1941; Mertens et al. 2004; Foster and Gruntfest 1937). Coloured compounds serving as pH indicators are further discussed in chapter 5.1.1.3. Due to its phenolic moiety, thymol was described by Harry D. Gibbs to react with 2,6-dibromoquinonechoroimide in a similar manner to phenol resulting in a blue coloured indophenolic compound (Gibbs 1926b; Gibbs 1926a; Adam et al. 1981). The Gibbs reagent and its mechanism plays an important role in the first detection technique investigated in this thesis and will be discussed in chapter 5.1.2. Furthermore, it resembles the anaesthetic propofol structurally, which will be further discussed in this thesis (see chapter 5.1.3 and 5.3.2). Therefore, it is often used as internal standard in different propofol monitoring experiments (Cussonneau et al. 2007; Dawidowicz and Fornal 2000; Liu et al. 2012; Dawidowicz et al. 2006; Dawidowicz and Kalitynski 2005; Hornuss et al. 2007; Miekisch et al. 2008; Adam et al. 1981; Dawidowicz, Kobielski, and Pieniadz 2008a). And to close the circle, phenolic compounds including propofol and especially dipropofol, which on the first glance resembles the structure of triclosan, were reported to have antimicrobial activity (Ogata et al. 2005).

most of them are applied locally to disinfect surfaces or on wounds and are not administered in patients.

To determine whether a compound is a therapeutic agent, or more specifically an antimicrobial agent, the following two definitions provided by the German physician and scientist Paul Ehrlich (1854 – 1915), need to be considered. For the international medical congress in 1913, Paul Ehrlich wrote an "Address in Pathology on Chemiotherapy" (Ehrlich 1913) and he defined "The only substances, therefore, that can be used as therapeutic agents are those in which the ratio between organotropic effect and parasitotropic effect is a favourable one, and that can be easily ascertained by experimental comparison of the *dosis toxica* with the *dosis tolerata.* The only substance that can be considered therapeutic agents are those of which is a fraction of the *dosis tolerata* is sufficient to bring about therapeutic effects." (Ehrlich 1913, p. 355) Ehrlich's second definition is "Corpora non agunt nisi fixata. When applied to the special case in point this means that parasites are only killed by those materials to which they have a certain relationship, by means of which they are fixed by them. I call such substances 'parasitotropic'." (Ehrlich 1913, p. 353) In other words, this suggest that "A drug will not work unless it is bound" (Rang et al. 2007, p. 8).

Nowadays, the term 'antibiotic(s)' is widespread and used synonymously with antibacterials. Therefore, in the context of this thesis, it was decided that the word 'antibiotic(s)' will be synonymous with antibacterials, unless otherwise declared, even though it is not entirely correct.

2.2 The History of Antibiotics, Resistance and Drug Discovery

The history of antibiotics and antibiotic resistance are closely linked. The starting point for such a topic is also particularly tricky to specify.

2.2.1 Antibiotic and Antibiotic Resistance Timeline

For example, one could argue that the history of antibiotics and antibiotic resistance began almost four billion years ago when the first bacteria and other microorganisms began to populate the world (Wright 2010; Fernandes 2006). It is likely that the competition between bacteria, for limited resources began at the same time and has not stopped since (DeLong and Pace 2001; Fernandes 2006). Bacteria compete by producing chemical that kill or inhibit the growth of competitor organisms. The development of resistance was the process by which microorganisms evolved in order to overcome the effects of these chemicals.

Resistance mainly develops via a process of random genetic mutations that are changes of the microorganism's genetic material. Certain mutations in the genome will confer a specific phenotype to the organism, which in some cases is favourable in protection against harmful toxins and chemicals. Should a mutation arise that limits the effect of an antibiotic agent, the surviving microorganism is described as "antibiotic resistant". In Darwinian terms referring to 'natural selection' and 'survival of the fittest' (Darwin 1859), the mutated and selected microorganism is the fittest in this specific environment and subsequently survives and proliferates. The same applies to a bacterium or microorganism that randomly evolved a more potent chemical and is able to obtain more resources and will thrive (Sommer, Dantas, and Church 2009; Dantas et al. 2008; Walsh and Wright 2005).

Consequently, in the face of this exposure to chemicals over a long time, it is not too surprising that microbes have evolved complex machinery for sensing, responding to and metabolising chemicals harmful to them (Wright 2010). In conclusion, one could argue that antibiotics on planet earth have been "invented" by microorganisms

including bacteria and the simultaneous development of antibiotic resistance has evolved as a natural by-product of the process (Spellberg, Bartlett, and Gilbert 2013).

In more practical terms, the history of antibiotics begins when humans first developed substances to treat bacterial diseases. However, it is hard to specifically date when humans first used substances against bacterial growth. There is evidence that several natural substances with known antibacterial effect, such as various roots, honey and moulds, were used in ancient Egypt and China (Wainwright 1989).

On the other hand, it seems fairly straightforward to put a start date to antibiotic resistance history as it basically is the same as the first application of an antibacterial substance. Since in simple terms, one can say that with every single use of an antibacterial chemical the evolutionary pressure on bacteria rises. Antibiotics increase the selective pressure on bacterial populations, allowing the resistant bacteria to thrive whilst the susceptible bacteria die off. In some cases, antibiotics even induce mutagenesis, for example, by stimulating the production of reactive oxygen species (Dwyer, Kohanski, and Collins 2009; Kohanski, DePristo, and Collins 2010) or induction of DNA damage that activates error-prone polymerases (Miller et al. 2004; Cirz et al. 2005; Pérez-Capilla et al. 2005). Moreover, bacteria have the ability to pass their resistance to other bacteria via conjugation. This can occur between bacteria from different genera (Theuretzbacher 2013; Davies and Davies 2010; von Nussbaum et al. 2006; Fernandes 2006; Alekshun and Levy 2007; Gould 2011).

The beginning of the antibiotic era could alternatively be defined by Waksman's definition (see chapter 2.1). This would require us to look for the first use of a "chemical substance, produced by microorganisms, which had the capacity to inhibit the growth of, or even to destroy bacteria and other microorganisms" (Waksman 1947). However, providing a conclusive answer for the very first use of an antibiotic in modern ages would be particularly difficult (Foster and Raoult 1974).

2.2.2 Golden Era of Antibiotic Drug Discovery

Undoubtedly amongst the most famous people associated with antibiotic's history is Sir Alexander Fleming (1881 – 1955), a Scottish biologist and pharmacologist. By 1928, Fleming was already a well-known researcher for his work on *Staphylococcus* and the antibacterial property of lysozyme (Fleming 1922). His laboratory was often untidy with bacterial cultures left out on the benches. Upon his departure for a holiday, his laboratory was left in a similar state, with culture plates stacked one on top of the other. On his return, six weeks later, he found his culture contaminated with mould. Furthermore, the colonies of *Staphylococci*, which had surrounded the mould, had undergone lysis. He interpreted this observation as the activity of an anti-bacterial substance produced by the fungus. He identified this fungus as *Penicillium rubrum*. Thus Fleming named this substance penicillin (Fleming 1929). In further experiments he found that this substance prevented growth of *Staphylococci* and other bacteria even when it was diluted several hundred times. This natural antibacterial drug gave humanity the first effective treatment against several diseases such as diphtheria, gonorrhoea, pneumonia, scarlet fever and syphilis. During the Second World War, penicillin saved countless lives by helping treat bacterial infections contracted by war-wounded soldiers. In 1945 Fleming, Howard Flory (1898 – 1968), an Australian pathologist, and Ernst Chain (1906 – 1979), a German biochemist, were awarded the Nobel Prize for Medicine for their discovery of the first natural antibiotic, penicillin (Fleming 1929; Fernandes 2006; Ligon 2004).

However, already before Alexander Fleming's discovery, several scientists associated a connection between the appearance of mould and the disappearance of bacteria. For the sake of brevity, only two of them are subsequently presented. In 1871, Sir John Scott Burdon-Sanderson (1828 – 1905), a British physiologist, reported that culture liquid, which was covered with the mould *Penicillium rubrum*, lacks bacteria (Burdon-Sanderson 1871). Four years later, John Tyndall (1820 – 1893), an Irish physicist demonstrated in several studies the previous observed antibacterial activity of *Penicillium*. However, he concluded that the bacteria in the liquid, covered by the

mould, died due to the lack of oxygen and consequently did not deem these findings relevant (Tyndall 1881; Landsberg 1949; Foster and Raoult 1974).

A couple of years after Burdon-Sanderson and Tyndall, a fairly different approach was undertaken by Paul Ehrlich, who has previously been introduced in subsection (2.1). Ehrlich had worked extensively on immunology, antiserum to combat diphtheria, standardising therapeutic serums and on a new technology for in vivo staining. In the course of the latter, he came across methylene blue, which was later taken on by his friend Robert Koch (1843 – 1910), a German physician and pioneering microbiologist, for his research on pathogens causing tuberculosis (Gensini, Conti, and Lippi 2007). In 1908 Paul Ehrlich was awarded the Nobel Prize for Physiology or Medicine for providing a theoretical basis for immunology as well as for his work on serum (Raju 1998). Based on these previous studies, Ehrlich theorised that a drug with antimicrobial activity could be discovered which does not kill the human host. He called it a "bewitched bullet" (Ehrlich 1913). To find such a "magic bullet", Ehrlich's team conducted a survey of hundreds of systematically modified chemical compounds (Schwartz 2004; Foster and Raoult 1974). In 1909 they discovered 'Salvarsan' (3-amino-4-hydroxyphenylarsenic, arsphenamine, or compound 606), which only one year later got introduced as the first effective organic compound against syphilis (Lloyd et al. 2005; von Nussbaum et al. 2006; Schwartz 2004). His methodical search for a specific cure for an identified disease can be seen as the introduction of targeted chemotherapy. He is therefore considered as the creator of the field of chemotherapy (Schwartz 2004). Ehrlich also described the process of the development of drug resistance and the therapeutic index of a drug as the ratio between the average minimum effective dose and the average maximum tolerated dose in a group of subjects, which is still in use today (Ehrlich 1913; Rang et al. 2007).

Following Ehrlich's Salvarsan, the next synthetic antibiotic Prontosil, a sulfonamid, was discovered many years later in 1932 (Schwartz 2004; Otten 1986). After five years of testing thousands of various azo dyes compounds, Gerhard Domagk (1895 – 1964), a German pathologist and bacteriologist, discovered that one compound is remarkably effective against *streptococcal* sepsis in mice. In 1939, Gerhard Domagk was awarded

the Nobel Prize in Physiology or Medicine “for his discovery of the antibacterial effects of Prontosil” (Raju 1999).

The successful development of penicillin in 1928 showed that many antibiotics could be awaiting discovery. Therefore, the golden era of antibiotic drug discovery began in the 1940s by screening of natural products and systematic search of antibacterial producing microorganisms (von Nussbaum et al. 2006; Lewis 2012; Fernandes 2006; Walsh and Wright 2005; Singh and Barrett 2006). One of the pioneers of this time was Selman A. Waksman, who was previously introduced in subsection 2.1. He exploited bacteria’s ability to produce their own antibiotics and systematically tested them. His main interest was for *Streptomyces*, which are the largest genus of Gram-positive actinobacteria. In 1943, this testing led to the discovery of streptomycin, the first antibiotic used to treat tuberculosis. In 1952 Waksman received the Nobel Prize in Physiology or Medicine for his “ingenious, systematic and successful studies of the soil microbes that have led to the discovery of streptomycin.” (Ginbserg 2005; Lewis 2012)

As already highlighted at the beginning, it is impossible to tell the history of antibiotics without resistance. This applies to penicillin as well. By the late 1950s, up to 85% of clinical isolates of *Staphylococci* were found to be resistant against penicillin (Williams and Bardsley 1999). Consequently from the 1960s to the 70s, the development of antibiotic resistant bacteria added urgency to the search for new antibiotic compounds. However, with screening of natural products nearly no new antibacterial substances were found anymore. Therefore, semi-synthetic modifications of existing antibiotics seemed to be very promising. This approach was less risky and deemed successful due to the known toxicity and selectivity of the parent antibiotic. (Fernandes 2006; Kappeler 2010)

However, by the early 1980s after two decades of deriving analogues, this method seemed to be exhausted whilst bacteria resistance continuously thrived, fuelled by the extensive and uncontrolled use of antibiotics, especially in hospitals and agriculture (Levy and Marshall 2004; Sommer, Dantas, and Church 2009).

In the late 80s and 90s researchers started to screen small drug libraries and re-tried the synthetic chemistry approach. However, the yield has been very poor, so that many companies returned to known natural compounds. Figure 2.01 presents a timeline for antibiotic research. (Fernandes 2006; Lewis 2012; Wright 2010; Gwynn et al. 2010)

2.3 Lack of Antibiotics and Rise in Resistance our Global Challenges

Today the most up-to-date methods, such as microbial gene cloning, genome sequencing, protein expressions, high-throughput screening and combinatorial libraries, have not led to an improved yield of new antibiotics. In the past 40 years, less than a handful of new antibiotic classes have been launched (Cooper and Shlaes 2011). Furthermore after decades of little success, pharmaceutical companies are 'pulling the plug' on antibiotic discovery. Most of them have either left the field, such as Merck (New Jersey, U.S.A.) and Eli Lilli (Indiana, U.S.A.), or have hugely downsized their effort (Lewis 2012). Hence as Dr Margaret Chan, Director-General of the World Health Organization (WHO), recently announced "In terms of new replacement antibiotics, the pipeline is virtually dry" (Chan 2013). Therefore, it is beyond dispute that the rise in antimicrobial resistance and the lack of new antibiotics in the antimicrobial drug discovery pipeline are two interlocking global challenges, which urgently have to be tackled (Butler and Cooper 2011; Cooper and Shlaes 2011; Ledford 2012).

Metaphorically, it can be seen as a constant 'arms race' of bacteria against humans and vice versa. This is as a very good example of the "Red Queen Hypothesis" proposed by Leigh Van Valen (1935 – 2010), an American evolutionary biologist, in 1973 (Van Valen 1973). The hypothesis describes how any evolutionary system must develop continuously to maintain its fitness relative to coevolving and competing systems (Woodford and Livermore 2009; Woodford 2003). The 'Red Queen' refers to the character in Lewis Carroll's novel "Alice Through the Looking Glass", who told Alice "Now, here you see, it takes all the running you can do, to keep in the same place" (Carroll 1871). Similarly, we have to do all the 'running' we can do in order to keep up with the evolution of antimicrobial resistance.

However, the emergence of new highly-resistant bacteria, such as carbapenemase-producing *Enterobacteriaceae*[3] (CPE) and New Delhi metallo-beta-lactamase-1 *(*NDM-1) producing bacteria (Kumarasamy et al. 2010), as well as the re-emergence of old enemies, such as the well-known hospital 'superbug' MRSA, are clear evidence that we are limping behind.

Dr. Margaret Chan emphasised at several occasions, including last year's conference on "Combating Antimicrobial Resistance: Time for Action" in Copenhagen, that antibiotic resistance could bring "the end of modern medicine as we know it. Things as common as 'strep throat' or a child's scratched knee could once again kill"(Chan 2013). Furthermore, there is a greater risk "that hospitalization kills instead of cures" (Chan 2013). Supporting this, the Chief Medical Officer for England, Professor Dame Sally Davies, recently announced the "antibiotic apocalypse" and said "that we might not see global warming" since "the apocalyptic scenario is that when I need a new hip in 20 years I'll die from a routine infection because we've run out of antibiotics" (Davies 2011). Moreover, she rated antibiotic resistance as one of the gravest threats to human health alongside dangers such as global warming and terrorism (Davies 2011). Supporting this, the recent annual report on global risks from the World Economic Forum (WEF) stated "the greatest risk [...] to human health comes in the form of antibiotic-resistant bacteria" (Howell 2013).

[3] *Enterobacteriaceae* is a family of Gram-negative bacteria including the genera *Salmonella*, *Klebsiella*, *Shigella*, *Yersinia* with the species *Yersinia pestis*, *and Escherichia* with the species *Escherichia coli* (*E. coli*).

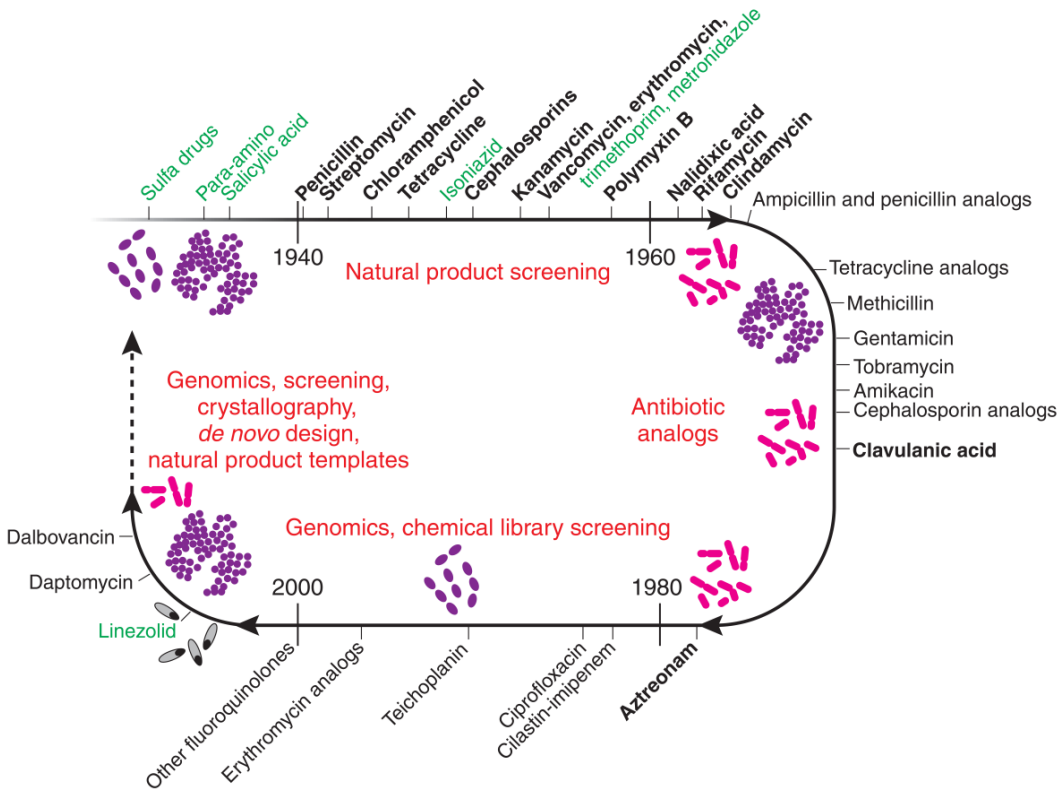

Figure 2.01: A timeline for antibiotic research. New antibiotic classes are highlighted in bold letters. Antibiotics originated from natural product are shown in black and those that are synthetic are written in green letters. Technologies used in antibacterial drug discovery are shown in red letters. Gram-positive bacteria are drawn in purple and Gram-negative bacteria are in pink. *Clostridium difficile* (*C. difficile*) is shown in black. The almost closed loop indicates the current risk of returning to the pre-antibiotic era. Schematic adopted from Fernandes 2006.

CHAPTER 3:

The Glycopeptide Antibiotic – Vancomycin

Antibiotics are subdivided into several different classes. One class is the glycopeptide antibiotics. Glycopeptide antibiotics are originally natural compounds active against Gram-positive bacteria and produced by several genera of actinomycetales, which are an order of the actinobacteria. Actinomycetales form branching filaments, which appear like the mycelia of a fungus and therefore were initially classified as actinomycetes. Actinobacteria are Gram-positive bacteria, which can be terrestrial or aquatic and they play a vital role in turnover of organic matter (Malabarba, Nicas, and Thompson 1997; Servin et al. 2008).

This chapter is divided into three subsections. The first subsection (3.1) presents a concise history of vancomycin. The second subsection (3.2) shows vancomycin's structure, explains its mode of action and discusses a mechanism of resistance. The third and last subsection (3.3) discusses vancomycin's pharmacology with focus on pharmacokinetics and pharmacodynamics.

3.1 History of Vancomycin – the Glycopeptide Antibiotic

Vancomycin is the archetype of the glycopeptide antibiotics and was first described in 1956 (McCormick et al. 1956; McCormick, McGuire, and McGuire 1962). Three years earlier, in a natural products screening program by the pharmaceutical company Eli Lilly (Indianapolis, USA), Dr. Edmund Carl Kornfeld (1919 – 2012), an American organic chemist, and his team collected a soil sample in Borneo. In this soil sample they found an unknown microbe and they were able to isolated a new antibacterial substance out of it (Moellering 2006; Griffith 1981). This substance was produced by *Amycolatopsis orientalis* (formerly designated as *Streptomyces orientalis*). It became the name "vancomycin" after the word "vanquish" (Levine 2006).

Already two years after its isolation, vancomycin got approved by the US Food and Drug Administration (FDA) for treatment of Gram-positive infections in hospitals. However, due to its toxicity it was used only for infections where other antibiotics, like β-lactam, failed. Therefore the introduction of semi-synthetic penicillins overshadowed vancomycin. However with rise of MRSA infection in hospitals, vancomycin has become one of the drugs of last resort worldwide. MRSA is one of many examples demonstrating that human induced evolutionary pressure causes bacteria resistance. *Staphylococcus aureus* mutated from a harmless methicillin-susceptible skin bacterium, with which typically everyone is colonised, to a multi-resistant highly infectious 'superbug' (Marshall et al. 2004; Chen 2013).

Due to the widespread and often indiscriminate use of vancomycin, the first resistant bacteria to glycopeptides antibiotics were observed in 1987 as vancomycin-resistant *Enterococci* (VRE) emerged (Johnson et al. 1990). Approximately ten years later, further vancomycin resistant bacteria developed, such as vancomycin-intermediate *Staphylococcus aureus* (VISA) (also termed GISA for glycopeptide-intermediate *Staphylococcus aureus*) and afterwards vancomycin-resistant *Staphylococcus aureus* (VRSA) (Hiramatsu 2001; Hopewood et al. 2007; Kahne et al. 2005; Gould 2010).

3.2 Vancomycin's Structure, Mode of Action and Resistance

The structure elucidation of vancomycin took many years to solve (Marshall 1965; Perkins 1969; Williams and Kalman 1977; Sheldrick et al. 1978) and its final structure was not found until 1981 (Harris and Harris 1982). Since then vancomycin's structure and its non-covalent binding interactions have been extensively studied by X-ray crystallography (Schäfer, Schneider, and Sheldrick 1996; Loll et al. 1998; Nitanai et al. 2009) and nuclear magnetic resonance (NMR) methods (Williams et al. 1983; Williams 1984; Pearcea and Williams 1995).

The core structural element of vancomycin and all glycopeptide antibiotics is a linear heptapeptide backbone consisting of seven amino acid residues. Five aromatic amino

acids are invariant and their residues are cross-linked together to build the characteristic rigid concave shape (figure 3.01 A). This backbone structure provides a further name for this antibiotic class – dalbaheptides (Hubbard and Walsh 2003).

The activity of the glycopeptide antibiotics results from their ability to inhibit bacterial cell wall biosynthesis. Their mode of action targets peptidoglycan, a conserved structural feature of bacteria, which is vital for their mechanical integrity. The peptidoglycan cell wall is an excellent antibiotic target because it occurs exclusively in bacteria and has no counterpart in mammalian cells, which is a very crucial for an effective antibiotic as described by Ehrlich (Ehrlich 1913). The peptidoglycan is a robust mesh-like carbohydrate polymer, which is made of alternating units of N-acetylglucosamine (GlcNAc) and N-actylmuramic acid (MurNAc). Each MurNAc is attached to a pentapeptide, which terminates in L-*Lysine*-((*Glycine*)$_5$)-D-*Alanyl*-D-*Alanine* (**D*Ala*-D*Ala***) (figure 3.02 A and B). Attached to the inner membrane in the cytoplasm, these two units become cross-linked to GlcNAc-MurNAc-pentapeptide. Afterwards all these cross-linked units get exported to the outer membrane where transglycosylase enzymes polymerise them to long chains. This transfer to the outer membrane takes place via lipid carriers, undecaprenyl phosphates ($C_{55}H_{91}O_4P$), which are embedded in the membrane. Lastly these units get cross-linked via transpeptidase enzymes to the existing cell wall (Schouten et al. 2006; Schneider and Sahl 2010).

Glycopeptide antibiotics recognise and bind strongly to the pentapeptide terminating in **D*Ala*-D*Ala*** and thus inhibit release of the building block unit from the lipid carrier (figure 3.01 A and 3.02 A). Consequently transglycoslation and transpeptidation (cross-linking) cannot be carried out, which prevents the essential cell wall formation and turnover. This causes a loss in mechanical integrity, leading to lysis of the bacterium due to the high osmotic pressure inside the bacterial cell. In contrast to glycopeptide antibiotics, β-lactam antibiotics, such as penicillin, inactivate several proteins involved in the transglycoslation and transpeptidation. This inactivation also causes lysis of the bacterial cell due to loss of mechanical integrity. The proteins to which the β-lactam antibiotics are binding to are summarised as penicillin-binding proteins (PBPs). Both

antibiotic target sides are indicated in figure 3.02 A. (Ndieyira et al. 2008; Kahne et al. 2005; Nagarajan 1994; Allen and Nicas 2003; Rang et al. 2007; Kappeler 2010; Hiramatsu 2001; McKendry 2012)

The binding interaction between vancomycin and the **D*Ala*-D*Ala*** dipeptide is characterised by five hydrogen bonds (figure 3.01 A). Due to these interactions the antibiotic is forming a groove with its binding pocket along the peptide (figure 3.01 B and C). (Williams 1996; Williams 1984; Kannan et al. 1988; Nagarajan 1994; Kahne et al. 2005)

There are different mechanisms causing resistance against vancomycin. Two examples are briefly presented below.

i) One example of a resistance mechanism is the subtle change from an amide to an ester in peptidoglycan's precursor occurring in VRE. This change from D-*Alanyl*-D-*Alanine* to D-*Alanyl*-D-*Lactate* (from **D*Ala*** to **D*Lac***) results in the deletion of a single hydrogen bond from the binding pocket and the subsequent creation of destabilising lone pair-lone pair interactions between the peptide and the antibiotic. These changes in interaction render the antibiotic therapeutically ineffective (figure 3.01 D). (Arthur et al. 1996; Arthur et al. 1992; Nagarajan 1994; Cooper and Williams 1999)

ii) Another example is the mechanism employed by the different clinical strains of VRSA. All of them feature a significant thickened cell wall in comparison to vancomycin-susceptible *Staphylococcus aureus* (VSSA). This thickened cell wall impairs the penetration of vancomycin molecules and consequently prevents them from reaching the peptidoglycan precursor. (French 2006; Hiramatsu 2001; Holmes, Johnson, and Howden 2012; Calfee 2012; Gould 2011; Chen 2013; Woodford and Livermore 2009)

The firstly presented resistant mechanism will be further exploited for the nanomechanical detection of vancomycin described in chapter 8.

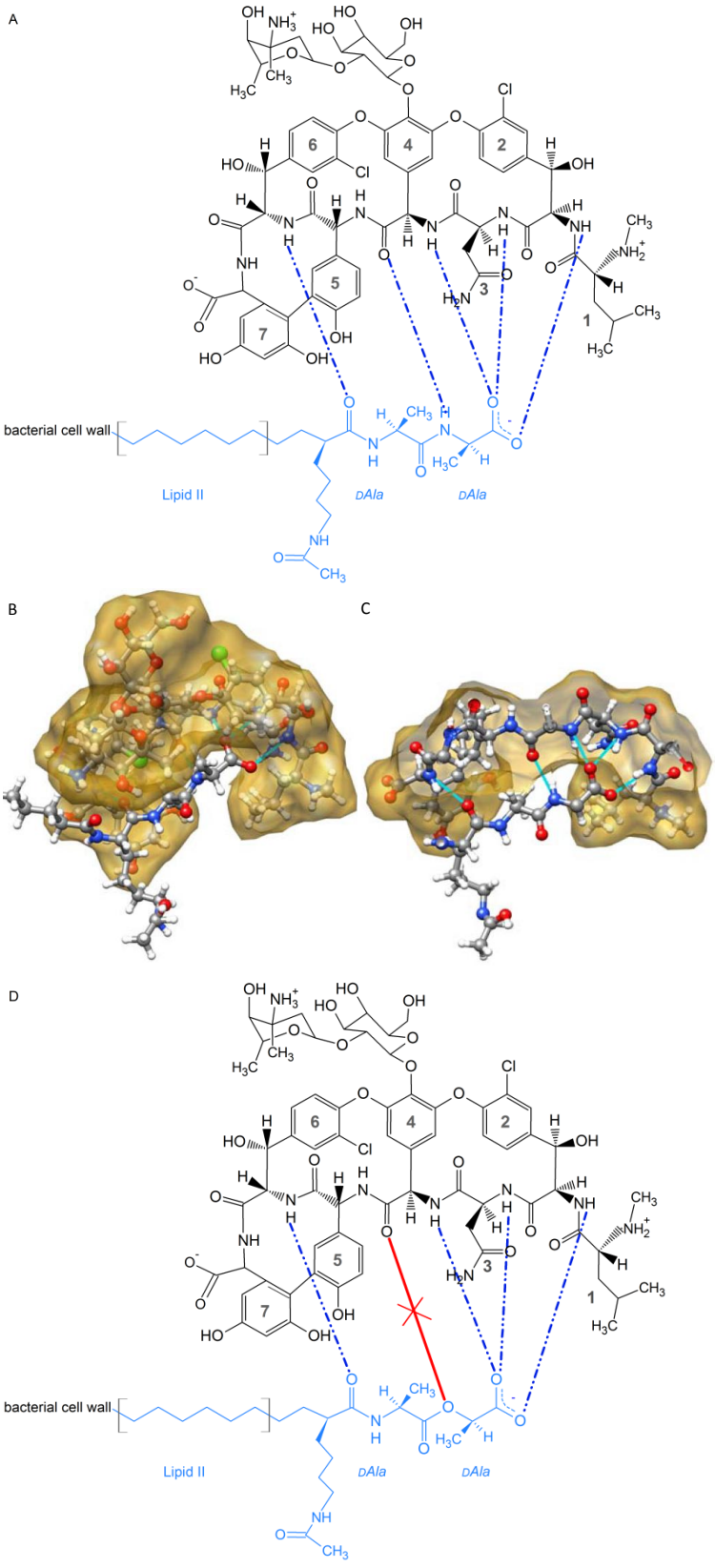

Figure 3.01: Vancomycin's structure, its mode of action and one example for a resistance mechanism.

A) Lewis' structure of vancomycin binding to D*Ala*-D*Ala*. The dotted blue lines indicate five hydrogen bonds.

B) Three-dimensional model of vancomycin binding to the dipeptide of the peptidoglycan precursor. For improved visibility of the groove, an artificial surface in yellow is drawn around the vancomycin molecule.

C) A cross section through (B) shows the interaction of the vancomycin binding pocket with the dipeptide. The five hydrogen bonds are shown with turquoise lines.

Schematics B and C courtesy of Dr. Manuel Vögtli.

D) Resistance mechanism occurring in vancomycin-resistant *Enterococci* (VRE). The exchange of the dipeptides's terminal from a D*Ala* to a D*Lac* replaces an amide with an ester. This subtle change results in a deletion of one hydrogen bond (indicated by the red line) and adds destabilising lone pair-lone pair interactions, which renders the antibiotic ineffective.

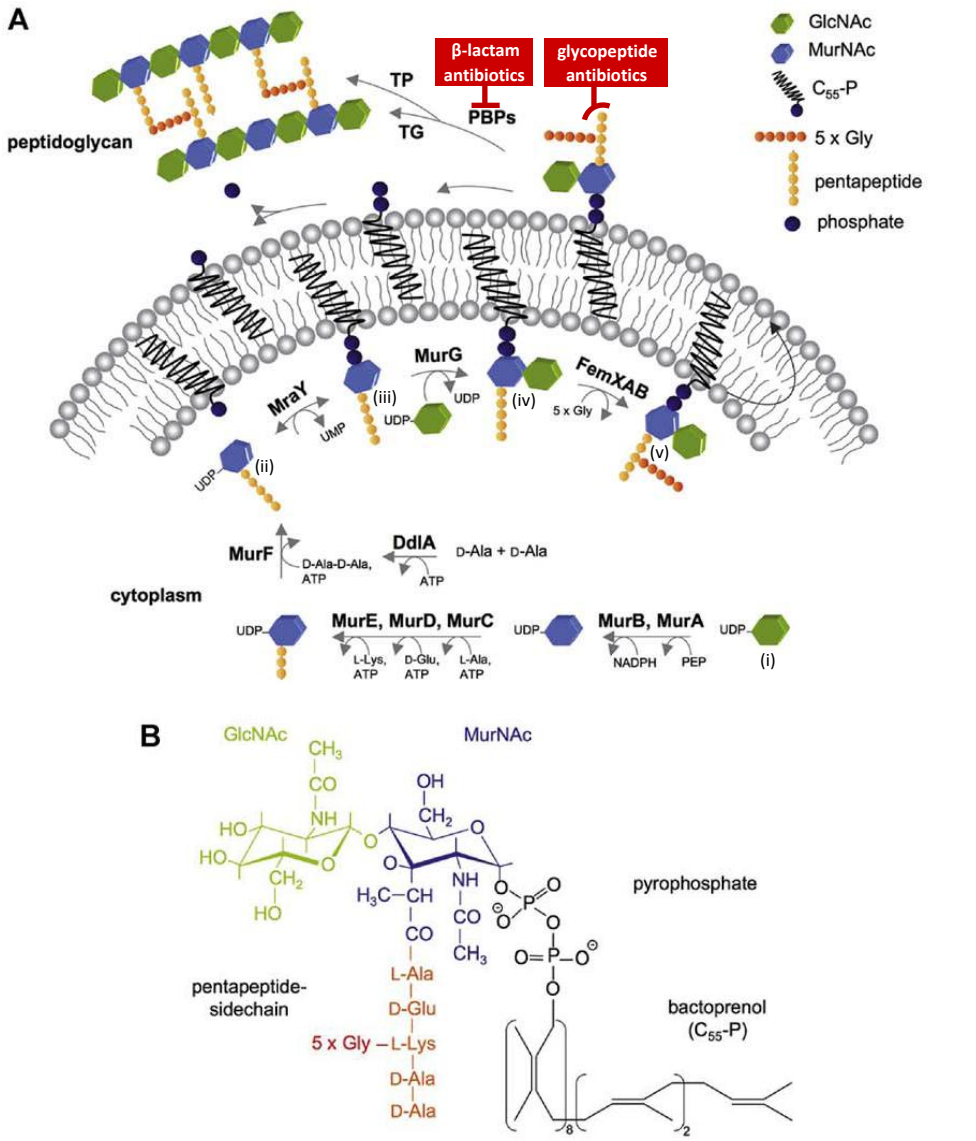

Figure 3.02: Peptidoglycan biosynthesis as an antibiotic target. A) Schematic representation of cell wall biosynthesis of *S. aureus*. The synthesis starts in the cytoplasm with the conversion of UDP-N-acetylglucosamine (UDP-GlcNAC) (i) to the soluble precursor UDP-MurNAc-penta-peptide (ii). The conversion is sequentially catalysed by the enzymes MurA to MurF. Then, (ii) gets linked via another phosphate to the membrane embedded lipid carrier, undecaprenyl phosphate (C_{55}-P), by MraY. The whole complex, C_{55}-P-MurNAc-pentapeptide (iii), is also called lipid I. The translocase, MurG, subsequently cross-links UDP-GlcNAc to the muramoyl moiety of lipid I, producing a precursor of lipid II (C_{55}-P-GlcNAc-pentapeptid) (iv). In *S. aureus*, 5 glycines are added to this precursor catalysed by FemXAB enzymes leading to the final structure of lipid II (v) which is further detailed in schematic B. Afterwards, lipid II is translocated across the membrane by a mechanism which is still the subject of scientific debate. On the membrane outside, the peptidoglycan unit is incorporated into the growing network through the activity of penicillin-binding proteins (PBPs) by transglycosylation (TG) and transpeptidation (TP) reactions. The red boxes indicate the antibiotic target sites of β-lactam and glycopeptide antibiotics. It has to be emphasised that other classes of antibiotics also target the peptidoglycan biosynthesis. **B) Chemical structure of lipid II produced by *S. aureus*.** The colour coding refers to schematic A. Both schematics adapted from Schneider & Sahl 2010.

3.3 Vancomycin's Pharmacology

This chapter gives a concise overview of vancomycin's pharmacology to provide the required background for the assessment of the clinical needs for a PoC sensor for therapeutic antibiotic monitoring, which is summarised in chapter 4.3. This chapter consists of four subsections. The first subsection (3.3.1) describes the current dosing strategy of vancomycin and its administration. The second subsection (3.3.2) defines pharmacokinetics and pharmacodynamics. The third (3.3.3) and the fourth subsection (3.3.4) discuss vancomycin's pharmacokinetics and pharmacodynamics respectively.

3.3.1 Current Vancomycin Dosing Strategy

Vancomycin has been used clinically for more than 50 years and is one of the antibiotics of last resort. It is effective against serious Gram-positive bacterial infection, such as MRSA and *Clostridium difficile* (*C. difficile*). Traditionally vancomycin has been considered bactericidal (kills bacteria) against most of the Gram-positive bacteria, such as *S. aureus* and *Pneumococci*, but bacteriostatic (stops bacteria from reproducing) against *Enterococci* (Roberts, Lipman, et al. 2008; Saribas and Bagdatli 2004; French 2006). Vancomycin is generally used to treat septicaemia, endocarditis, pseudomembranous colitis, catheter-related blood stream infections, skin and soft tissue infections and as prophylaxis for certain procedures and implants. It is also valuable in treatment of severe staphylococcal infection in patients allergic both to penicillins and cephalosporins.

The normal route of vancomycin administration is intravenous as opposed to oral, since the drug is not able to cross the gastrointestinal mucosa due to its size and its hydrophobicity. For treatment of *C. difficile* and associated pseudomembranous colitis, vancomycin must be given orally as intravenous administration will not achieve the minimum therapeutic concentration in the gut lumen (Rang et al. 2007).

The British National Formulary (BNF) recommends peak serum values for vancomycin to be in the range of 25 to 40 µg/ml which corresponds to 17.3 to 27.6 µM of vancomycin, and trough values should be in the range of 10 to 15 µg/ml and 15 to 20 µg/ml for complicated infections, which corresponds to 6.9 to 10.4 µM and 10.4 to 13.8 µM vancomycin respectively. For paediatrics, the peak serum values can reach 60 µg/ml which corresponds to 41.4 µM of vancomycin, and trough values are typically measured in the range of 5 to 10 µg/ml which corresponds to 3.5 to 6.9 µM vancomycin (Eiland, English, and Eiland 2011; Miles et al. 1997; Gordon et al. 2012; Nandí-Lozano, Ramírez-López, and Avila-Figueroa 2003).

Vancomycin is typically administered in two daily dose of 1 g or sometimes in smaller doses more frequently, such as four times 500 mg (Tobin 2002; Thomson et al. 2009; Kitzis and Goldstein 2006). However, some studies suggest that continuous infusion may be more favourable than the formerly used single dosage or intermitted regimes, especially for infections with *S. aureus*, which show an elevated vancomycin minimal inhibitory concentration (MIC) (Roberts, Kirkpatrick, and Lipman 2011; Roberts, Lipman, et al. 2008; Rello et al. 2005). A lower pharmacokinetic (see subsection 3.3.2 and 3.3.3) variability and better cost-efficiency was observed (Jelassi et al. 2011). Nevertheless this is still a controversial topic and other studies did not see a significant improvement in the pharmacodynamics of vancomycin with continuous infusion (Rybak et al. 2009a; Wysocki et al. 2001). Consequently, further studies can be expected (Roberts and Lipman 2009).

3.3.2 General Definition of Pharmacokinetics and Pharmacodynamics

A very simplified definition is “what the body does to the drug” is termed pharmacokinetics and “what the drug does to the body” is termed pharmacodynamics (Rang et al. 2007).

The following two bullet points provide a more extended description:

- The word pharmacokinetics has its origin in Ancient Greek and is derived from the two terms *pharmakon* "drug" and *kinetikos* "to do with motion". It describes the relationship of drug concentrations over the course of time attained in different body regions during and after dosing. This includes absorption, distribution and metabolism and excretion, which is often abbreviated as ADME or LADME if liberation is taken into account. Hence it describes how the body affects a drug from administration until elimination. (Rang et al. 2007; Craig 2003)

- Pharmacodynamics, on the other hand, is derived from Greek word *dynamikos* "powerful" and describes the effect of the drug on the human body itself, on microorganism or on parasites within or on the human body. This includes the mode of action of the drug as well as the relationship between the concentration and effect. It can be concluded that pharmacokinetic parameters are related via pharmacodynamics to the pharmacologic effect. (Rang et al. 2007; Craig 2003)

3.3.3 Pharmacokinetics of Vancomycin

Despite more than half a century of clinical experience and many studies, there are large differences in the published vancomycin model parameters leading to great variance and intense debate with regards to the pharmacokinetics values. This is especially the case for several patient populations, such as children, immuno-compromised, intensive care and dialysis patients, for whom the pharmacokinetic parameters can be significantly different (Helgason, Thomson, and Ferguson 2008; Lomaestro 2011; Rybak et al. 2009b; Eiland, English, and Eiland 2011; Miles et al. 1997; Gordon et al. 2012).

Similar accounts for protein binding, which is observed and reported for antibiotics over many years and still remains a very contradictory topic. There are still no standardised pharmacodynamic models that take protein binding into account, even though there are many studies proving its importance to the efficacy of the antibiotic and consequently to the health outcome and for the prevention of antimicrobial resistance. In this context, Zeitlinger and colleague's paper bears the provoking title "Protein Binding: do we ever learn?" (Zeitlinger et al. 2011). It reports that literature suggest that the proportion of

vancomycin bound to proteins can vary between 10 – 82% with 55 % often quoted as the mean fraction bound. It is believed that vancomycin is predominately binding to serum albumin which is the most abundant plasma protein in mammals. However, it is also known to bind to other proteins including alpha-1-acid glycoprotein. (Bohnert and Gan 2013; Butterfield et al. 2011; Cantú et al. 1990; Ackerman et al. 1988; Zokufa et al. 1989; Rodvold et al. 1988; Kitzis and Goldstein 2006; Shin et al. 1992; Shin et al. 1991; Zeitlinger et al. 2011; Dawidowicz, Kobielski, and Pieniadz 2008a; Fournier, Medjoubi-N, and Porquet 2000).

The volume difference in serum between various patient groups such as children, the elderly, obese or dialysis patients is expected to be significant. Additionally, critical ill patients may suffer from physiological changes that alter the pharmacokinetics of drugs including antibiotics, which may lead to sub-therapeutic concentrations or changes in drug clearance especially in dialysis patients (Roberts et al. 2011; Roberts and Lipman 2009; Udy et al. 2010; Roberts, Kirkpatrick, and Lipman 2011). Furthermore especially in paediatric care, there is little data guiding the dosing and monitoring of vancomycin leading to a wide variety of doses and dosing frequencies resulting in reduced success in achieving the recommended plasma concentrations (Miles et al. 1997; Eiland, English, and Eiland 2011; Gordon et al. 2012; Kitzis and Goldstein 2006). Nandí-Lozano and colleagues reported that from 70 paediatric patient treated with vancomycin less than 20% were in the therapeutic range (Nandí-Lozano, Ramírez-López, and Avila-Figueroa 2003).

Additionally, most, if not all, gold standard drug monitoring methods only measure the total antibiotic concentration and do not distinguish between bound and free fractions, even though studies have suggested that the correlation between free and total fraction is poor (Zeitlinger et al. 2011; Estes and Derendorf 2010; Butterfield et al. 2011).

3.3.4 Pharmacodynamics of Vancomycin

Pharmacodynamics of antibacterials deals with the relationship between drug exposure and antimicrobial effect (Craig 2003). Pharmacodynamically, the antibiotic activity is dependent on the interaction between drug concentrations at the site of infection, bacterial load, phase of bacterial growth and the MIC of the pathogen. A change in any of these factors will affect the pharmacodynamics of the antibiotic against the particular pathogen and therefore may not only affect the therapy outcome but also predispose development of antibiotic resistance. (Roberts, Kruger, et al. 2008; Levison 2004)

Various different studies show that vancomycin's pharmacodynamic characteristics, despite the similarity in mechanism, are not fully comparable to the pharmacodynamics profile of the β-lactam antibiotics, such as penicillin. Hence vancomycin is neither a solely time-dependent killer nor a solely concentration-dependent killer. Instead its clinical effectiveness is related to both the time above the MIC and the total amount of antibiotic, which is best described with the pharmacodynamics parameter: AUC over MIC, which is typically abbreviated as AUC/MIC (figure 3.03 A). AUC stands for the area under the curve and is a measure for the total exposure of an antibiotic to an organism (Rybak et al. 2009b; Muppidi et al. 2012; Stein and Wells 2010; Avent et al. 2013; Dhand and Sakoulas 2012; Udy et al. 2010; Roberts and Lipman 2009; Rybak 2006; Holmes, Johnson, and Howden 2012; Estes and Derendorf 2010; Gould 2011; Butterfield et al. 2011; Thomson et al. 2009). In theory, to accurately determine the AUC, multiple serum concentration measures are needed. However, in practice with the current gold standards of therapeutic antibiotic monitoring, this is nearly impossible. The current gold standards of therapeutic antibiotic monitoring are further discussed in chapter 4.1.

Two other aspects play an important role in the pharmacodynamics of vancomycin. These are (i) the so called 'MIC creep' and (ii) the mutant selection window (MSW) in combination with the mutant prevention concentration (MPC).

i) MIC creep: The increasing use of vancomycin since the mid 1980s is associated with a decreasing bacterial susceptibility (Dhand and Sakoulas 2012). The MICs of vancomycin VSSA, which previously have been characterised with a vancomycin MIC of below 1.5 mg/l, are now quite often observed creeping into the range of 1.5 to 2 mg/l. These elevated MICs of VSSA are referred to as the 'vancomycin MIC creep'. Such less susceptible VSSA are currently much more frequent in various healthcare settings around the globe than vancomycin non-susceptible strains such as VISA, which has a vancomycin MIC ranging from 4 to 8 mg/l, and VRSA with a vancomycin MIC of > 16 mg/l (Dhand and Sakoulas 2012; Estes and Derendorf 2010; Wang et al. 2013). These less susceptible bacteria are the cause for prolonged bacteremia, treatment failures, increased mortality and higher relapse possibilities, which poses strong evidence for the urgent need for therapeutic vancomycin monitoring (Kitzis and Goldstein 2006; Rybak et al. 2009a; Holmes, Johnson, and Howden 2012; Pumerantz et al. 2011; Estes and Derendorf 2010; Chen 2013; Calfee 2012; van Hal, Lodise, and Paterson 2012; Muppidi et al. 2012; Dhand and Sakoulas 2012).

ii) Mutant selection window (MSW) and mutant prevention concentration (MPC): Various studies suggested that inappropriately low antibiotic dosing is contributing to the increasing rate of antibiotic resistance. Consequently for many antibiotics a MSW could be identified, within which it is proposed that resistant mutants are selected (Firsov et al. 2006; Roberts, Kruger, et al. 2008; Imamovic and Sommer 2013). Since this MSW is typically in the concentration range from between MIC and MPC, attention should be paid to the antibiotic dosing strategy. The MPC is defined as the concentration required to prevent emergence of bacteria with single step mutations in a population of at least 10^{10} cells (figure 3.03 B). Not only should the blood concentration of the antibiotic kept above the MIC of the bacteria in question, it should also be able to deal with the most resistant subpopulation in this colony. Therefore the concentration should be above the MPC, which may be achieved by maximising antibiotic exposure by administering the highest recommended dose to the patient. In taking this approach into account, the selection of resistant mutants

will be prevented and further development or resistance will be limited. (Roberts, Kruger, et al. 2008; French 2006)

Following on this, the next chapter (4) describes therapeutic drug and vancomycin monitoring and its health economic importance. Furthermore, it also summarises the assessment of the clinical needs for a PoC sensor for therapeutic antibiotic monitoring.

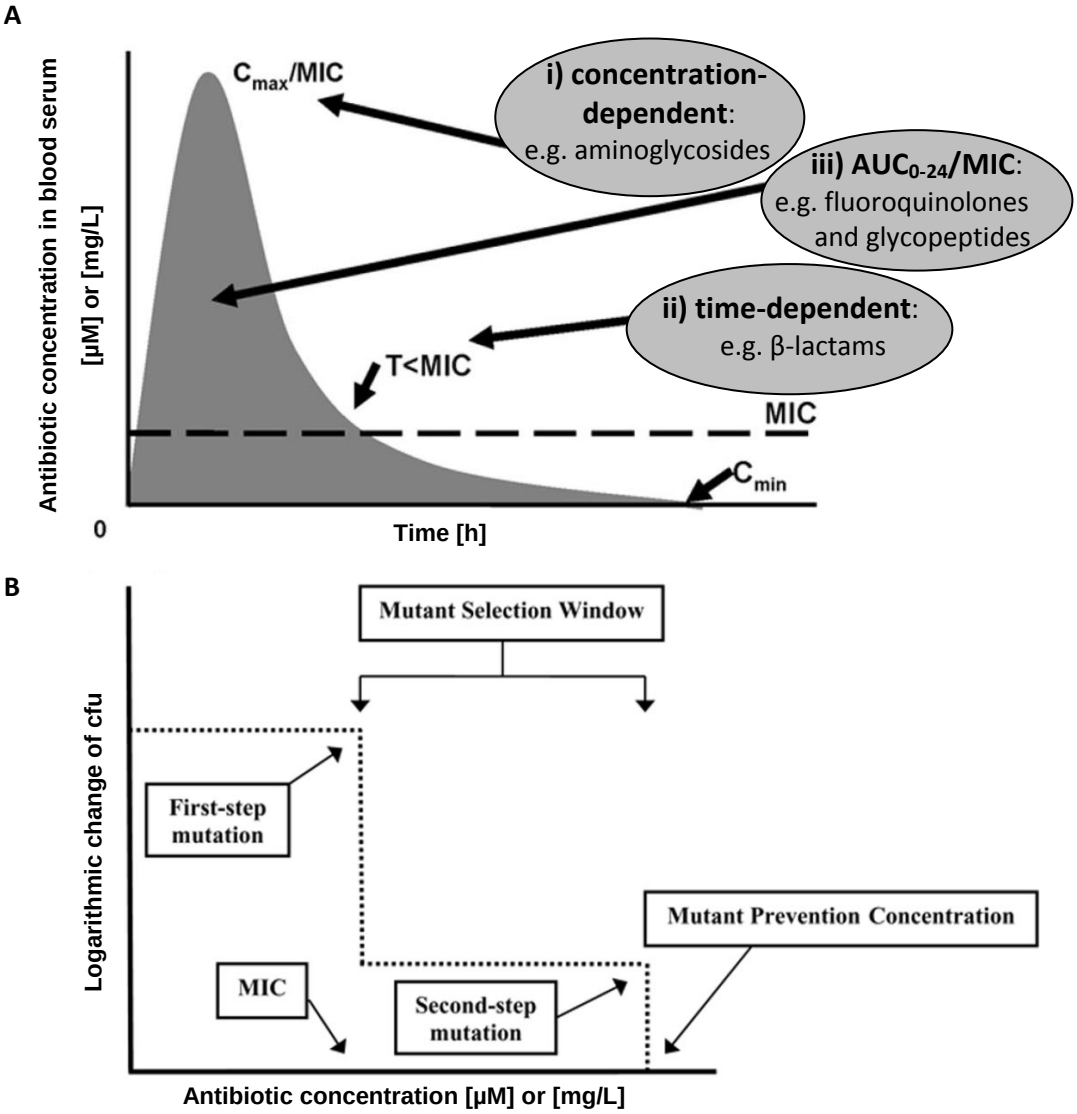

Figure 3.03: Pharmacodynamics of antibiotics. A) Schematic of fundamental pharmacodynamic parameters on a concentration vs. time diagram. Typically three models are differentiated which describe the clinical efficacy of the various antibiotic classes best: i) concentration-dependent killing is defined via the ratio of maximum serum antibiotic concentration (C_{max}) to MIC: C_{max}/MIC; which is for example exhibited by aminoglycosides, ii) time-dependent killing is expressed by the time (T) for which the antibiotic concentration exceeds the MIC: T>MIC; which is associated with β-lactam antibiotics, and iii) area of the concentration time curve during 24 hours illustrated by AUC_{0-24} divided by the MIC: AUC_{0-24}/MIC; which for example is largely displayed by fluoroquinolones and glycopeptides, as both antibiotics show concentration- and time-dependent killing. C_{min} depicts the minimum serum antibiotic concentration. **B) Mutant selection window (MSW) and mutant prevention concentration (MPC) depicted against the logarithmic change of the colony-forming units (cfu) and the antibiotic concentration.** This graph represents the reduction of bacterial colonies with increased antibiotic exposure. For bacteria to survive the first 'drop' (MIC), a first mutation is required. Then to survive the second 'drop' (MPC), they have to acquire a second mutation, which is less likely. If the antibiotic concentration is between the two 'drops' in the MSW, selection of the resistant bacteria may occur. Both schematics adapted from Roberts, Kruger, et al. 2008.

CHAPTER 4:

Therapeutic Drug and Vancomycin Monitoring

Therapeutic drug monitoring (TDM) is a model example of the multidisciplinary approach to patient care defining modern healthcare practices and personalised medicine. Nursing staff, clinicians, pharmacist and scientist are all involved in the adjustment and optimisation to tailor the treatment to individual patient's needs. TDM enables the drug dose to be titrated to the desired target concentration within the therapeutic range according to patient's individual drug adsorption, distribution, metabolism and excretion. Repeated measurements allow the detection of accumulation or changes in the drug clearance rate and additionally may provide early detection of faults in the drug delivery system. As a result, TDM is often implemented for drugs with a narrow therapeutic range, pharmacokinetic variability and target concentrations that are difficult to monitor. Moreover, it is also of great benefit where special care is requires, such as paediatrics or intensive care settings. (Gross 2002; Kang and Lee 2009)

This chapter is divided in four subsections. The first subsection (4.1) describes the current gold standards in therapeutic vancomycin monitoring (TVM). The second subsection (4.2) discusses the health economic importance of TVM. The third subsection (4.3) summarises the assessment of the clinical needs for a PoC sensor for therapeutic antibiotic monitoring. The fourth and the last subsection (4.4) presents a profile of our industrial partner, Sphere Medical Ltd., Cambridge, UK.

4.1 Current Gold Standards in Therapeutic Vancomycin Monitoring

The administration of many therapeutic drugs, including vancomycin, is routinely guided by therapeutic drug monitoring (TDM). The current gold standards for therapeutic vancomycin monitoring are immunoassays, such as the enzyme multiple immunoassay technique (EMIT) and the fluorescence polarisation immunoassay (FPIA). According to

the literature, the latter seems to be one of the most popular assays in clinics (Tobin 2002; Wilson, Davis, and Tobin 2003; Yu, Zhong, and Wei 2010; White 2000).

The mode of operation of these two immunoassays, EMIT and FPIA, is described below:

- The working principle of an EMIT is based on competition between vancomycin in the samples, which can be either serum or plasma, and the vancomycin labelled with the enzyme glucose-6-phosphate dehydrogenase (G6PDH) provided within the assay for the antibody binding sites (figure 4.01 A). The enzyme is from the bacteria *Leuconostoc mesenteroides* and therefore requires a bacterial coenzyme, which is employed in the assay. This bacterial origin assures that endogenous serum G6PDH is not interfering. The antibodies are monoclonal mouse anti-vancomycin antibodies and the enzyme activity of the labelled vancomycin decreases upon binding to them. Active enzyme converts oxidised nicotinamide adenine dinucleotide (NAD) to NADH resulting in an absorbance change at 340 nm, which can be measured spectrophotometrically. Consequently, the vancomycin in the sample and the unbound enzyme labelled vancomycin included in the assay are directly proportional. ("Package Insert: VANC2 COBAS® from Roche Diagnostics" 2012; Wild 2013)

- The change of tumbling rates for free and bound molecules is exploited for FPIA. The absorbance of light is depending on the orientation of the molecule relative to the direction and polarization of the exciting light. The subsequent emission as fluorescence by electronically excited molecule is typically polarised. However, if tumbling molecules rotate during the excitation period the orientation of the fluorescence polarisation may be randomised. Consequently, the faster the tumbling, the less polarisation is measured. FPIA makes use of competitive-binding assay principle. In a vancomycin focused device, fluorescein-labelled vancomycin, which is generically called 'tracer', competes with added sample vancomycin for the antibody-binding sites (figure 4.01 B). Again the sample can be either serum or plasma and the used antibodies are

mouse anti-vancomycin antibodies. The complex of a tracer bound to an antibody rotates slower than the free tracer. Further, if their rotation rate is low relative to the rate of the emission of fluorescence than a polarised emission occurs. Contrarily, free tracer, that rotates rapidly, results in unpolarised emission. Consequently, the vancomycin in the sample is proportional to the free tracer and can be determined via measuring the degree of polarisation of the fluorescence emission. ("Package Insert: AXSYM® SYSTEM Vancomycin II from Abbott" 2005; Dandliker et al. 1973; Jolley et al. 1981; Schwenzer, Wang, and Anhalt 1983; Wild 2013)

Conclusively, all of these currently used techniques require a sample collection into specialised container and transport to a specialised laboratory with trained staff, which is either located within or outside the hospital. This process is expensive, laborious, time-consuming and requires a lot of administrative work (see subsection 4.2). Moreover, the inevitable delays between tests and results means that important therapeutic decisions are delayed and patient pathways can become slow and cumbersome (Cooper and Shlaes 2011; Tobin 2002; Wilson, Davis, and Tobin 2003; Begg, Barclay, and Kirkpatrick 1999; Yu, Zhong, and Wei 2010; Jesús Valle, López, and Navarro 2008). Additionally, as previously mentioned, routine drug monitoring only measures the total antibiotic concentration even though protein binding varies. This could be problematic as it is generally accepted that only the free drug fraction is pharmacologically active. Moreover, studies have suggested that the correlation between free and total fraction is poor. Therefore, one might conclude that the total vancomycin concentration is not predictive for the free amount of the antibiotic and as a result it is recommended to routinely monitor the free drug concentrations (Berthoin et al. 2009; Estes and Derendorf 2010; Butterfield et al. 2011).

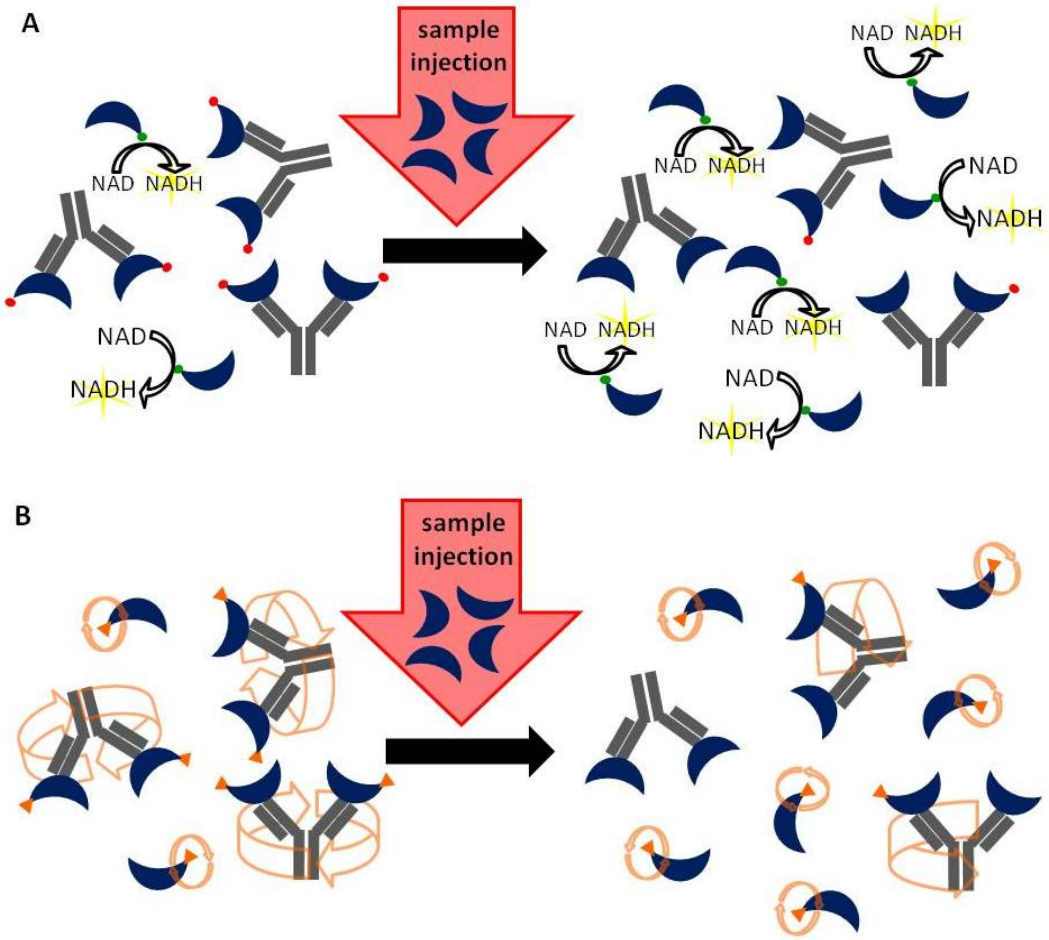

Figure 4.01: Schematic illustration of the working principles of TVM gold standard assays. A) EMIT. The assay provides monoclonal mouse anti-vancomycin antibodies shown in grey and vancomycin molecules labelled with the enzyme G6PDH shown as dark blue crescent shape with either a green or a red dot. If the labelled vancomycin is free, the enzyme is active, which is illustrated with the colour green as opposed to red, and oxidises NAD to NADH. NADH can be spectrophotometrically detected at 340 nm depicted as a yellow star in the background. Upon sample injection, the vancomycin molecules in the sample, shown as dark blue crescent shape, compete with the labelled vancomycin for the antibody binding sites. Consequently, the amount of vancomycin in the sample is directly proportional to the amount of unbound labelled vancomycin, which can be spectrophotometrically quantified. **B) FPIA.** Comparable to the EMIT, the assay provides monoclonal mouse anti-vancomycin antibodies shown in grey and vancomycin molecules labelled with fluorescein shown as dark blue crescent shape with an orange triangle. Upon light absorbance the fluorescein-labelled vancomycin molecules get excited and consequently emit fluorescence. If fluorescein-labelled vancomycin is bound to the antibody, the emitted fluorescence is polarised because the tumbling rate of this larger complex, illustrated as orange arrows, is low relative to the emission rate. Contrarily, the free vancomycin rotates rapidly and results in unpolarised emission. If vancomycin containing sample is added, those vancomycins compete together with the labelled molecules for the antibody binding sites. Therefore, vancomycin in the sample is directly proportional to free fluorescein-labelled vancomycin, which can be quantified by the degree of polarisation of the emitted fluorescence.

4.2 Health Economic Importance of Therapeutic Vancomycin Monitoring

The health economic case for therapeutic vancomycin monitoring has been analysed in different countries. In 2002, NHS Bristol launched a survey to study vancomycin TDM in different institutions (Tobin 2002). They questioned 310 participants from UK NHS hospitals, UK public health laboratories, UK private hospitals and other European and non-European hospitals. According to this survey, the cost of a vancomycin assay itself is only £4, but increases to £35 if the costs associated with taking blood, the transport to the microbiology laboratory within or outside the institution, time for paperwork, running the assay, result reporting and interpretation are included. Strikingly this total cost to monitor a patient's drug level on a single basis exceeds the drug cost for twice-daily 1 gram intravenous dosing. The survey reported that the number of assays requested differed greatly from laboratory to laboratory by up to 5 to 7500 assays per year. Around 65% of all assays only received their results in one day. At that time, almost exclusively, 97% of the respondents were using the fluorescence polarisation immunoassay (FPIA) "FLx/TDx" from Abbott Diagnostics (Maidenhead, UK).

Similar studies in Spain (Fernandez de Gatta et al. 1996; Portolés et al. 2006), in the U.S.A. (Paladino et al. 2007) and in France (Jelassi et al. 2011) led to comparable results as found by the NHS survey in 2002. They all support the case for the urgent development and complete reappraisal of therapeutic drug monitoring for vancomycin.

Furthermore a recent study published by Touw et al. in "the European journal of hospital pharmacy science" (Touw et al. 2007) presented the results of cost-effectiveness study of TDM. Their study published results on aminoglycoside and vancomycin treatments and showed statistically significant increased death rate (6.3%), length of stays in hospitals (12.3%), hearing loss (46.3%) and renal impairment (34.0%), and consequently higher total charges (6.3%) in hospitals that did not have pharmacist-managed therapies, which included TDM combined with results interpretation by using mathematical derived pharmacokinetic models which then advised the physicians

correspondingly. Conclusively, they recommend that vancomycin therapy is guided by TDM, especially in patient populations at risk, such as intensive care unit (ICU) patients, oncology patients and patient receiving concomitant nephrotoxic medication, since vancomycin's nephrotoxicity is usually associated to additional administration of nephrotoxic drugs (Paladino et al. 2007).

4.3 Summary of Needs for Therapeutic Vancomycin Monitoring

As laid out above, the following points highlight the unmet clinical need for therapeutic antibiotic monitoring. There are clear arguments for the implementation of TDM in general, as well as the application of TDM to antibiotic monitoring. Finally, there is a particular need for vancomycin monitoring, which cannot be met with the current gold standard techniques.

i) TDM in general is assuring that the drug concentration stays within the drug's therapeutic range. Hence, its main benefits are the improvement in efficacy, the attenuation of the toxic side effects, and the viability of personalised drug management according to the patient's individual needs. Therefore, it results in a better health outcome, which is besides the improvement in healthcare also associated with lower costs. Furthermore, in terms of the continuous and real-time monitoring at the PoC, it allows personalised drug management according to patient's individual drug adsorption, distribution, metabolism, and excretion. Moreover, it detects accumulation or changes in the drug clearance rate and additionally may provide early detection of faults in the drug delivery system. Consequently, it will be a crucial step towards personalised medicine.

ii) Aside from the previously mentioned general advantages of TDM, therapeutic antibiotic monitoring is a very valuable tool for antibiotic stewardship by ensuring that the antibiotic concentration stays above the MPC throughout the entire treatment period. This will promote prudent use of current antibiotics and reduce the development of resistance.

iii) In particular, the following list provides arguments for the need of a real-time, continuous and low cost PoC sensor for therapeutic vancomycin monitoring, which is currently an unmet clinical need:

a. Vancomycin has a very narrow therapeutic window paired with a narrow therapeutic index and severe adverse side effects (Begg, Barclay, and Kirkpatrick 1999; Roberts and Lipman 2009).

b. Vancomycin has to be kept effective as long as possible and therefore prudent use via antibiotic stewardship has to be promoted (Williams and Bardsley 1999).

c. Vancomycin's most reliable pharmacodynamics parameter requires several measurements for an accurate estimation, which is almost impossible with current gold standards. Consequently, it is normal for a single trough concentration measurement to be taken prior to the next dose (Tobin 2002). (Rybak et al. 2009b; Muppidi et al. 2012; Stein and Wells 2010; Avent et al. 2013; Dhand and Sakoulas 2012; Udy et al. 2010; Roberts and Lipman 2009; Rybak 2006; Holmes, Johnson, and Howden 2012; Estes and Derendorf 2010; Gould 2011; Butterfield et al. 2011; Thomson et al. 2009).

d. Vancomycin pharmacokinetics differs hugely in different patient populations and may even be subject to change in the course of treatment due to different factors such as the disease state and its progression. Furthermore, the pharmacokinetics of certain patient groups, such as children, critically ill, renal impaired, immuno-compromised, diabetic, dialysis patients and in those taking a combination of other drugs, where contraindications may arise, are usually neglected in general drug dosing models, which are derived from population averages (Roberts et al. 2011; Roberts and Lipman 2009; Udy

et al. 2010; Roberts, Kirkpatrick, and Lipman 2011). Therefore, continuous monitoring at the PoC, which puts immediate intervention into practice, is sought after.

e. Vancomycin has a variable protein bound proportion, namely from 10 – 82 % (Zeitlinger et al. 2011; Sun, Maderazo, and Krusell 1993; Kitzis and Goldstein 2006; Cantú, Yamanaka-Yuen, and Lietman 1994). Therefore the inter-patient variability and the disease state dependent protein levels are resulting in a challenging prediction for the ratio of bound/inactive and free/active antibiotic fractions (Estes and Derendorf 2010). Furthermore, the current gold standard drug monitoring methods only measure the total antibiotic concentration (Butterfield et al. 2011).

f. The MIC creep is leading to an inevitable increase in vancomycin dosing regimens, which renders the already narrow therapeutic window even narrower (Dhand and Sakoulas 2012). Consequently, the likelihood that the antibiotic concentration will fall below the lower limit or reach toxic concentrations by exceeding the upper limit is increasing. Hence, one could conclude that alongside the rise in vancomycin's MIC, the desire for therapeutic vancomycin monitoring increases as well.

g. Furthermore, the possible change from intermittent dosing to continuous vancomycin infusion regimens would support continuous monitoring very well (Roberts, Kirkpatrick, and Lipman 2011; Roberts, Lipman, et al. 2008; Rello et al. 2005; Jelassi et al. 2011). Since the therapeutic vancomycin monitoring sensor could be incorporated into the intravenous line (IV) of the vancomycin drip.

Hence, these arguments strongly demand a simple, rapid, reliable and regular measurement of the free vancomycin concentration. Therefore, the main objective of my PhD thesis is the development of sensors to monitor antibiotic levels in real-time at the PoC in collaboration with our industrial partner, Sphere Medical Ltd., Cambridge, UK. A profile of Sphere Medical Ltd. can be found in the following subsection (4.4). The focus of this thesis is the glycopeptide antibiotic vancomycin. It serves as a starting point for the mid-term aim to extend these sensors to other antibiotics. However, this lies beyond the scope of my thesis. Ultimately, the ideal and very ambitious long-term goal would be to expand the capability of these sensors towards other drugs, disease and health markers to make them indispensable multi-analyte sensors for future personalised healthcare.

4.4 Industrial Partner – Sphere Medical Ltd., Cambridge, UK

Sphere Medical Ltd. is a medical device company developing a range of monitoring and diagnostic products, which are designed to provide significant improvements in patient management in different hospital environments, such as critical care, operating theatre and emergency room. Their products are aiming to allow near real time measurement of blood gases, various electrolytes and drug levels with laboratory accuracy at the patient's bedside ("Sphere Medical Ltd.'s Homepage: About Sphere Medical" 2014). Currently they have three products, the Pelorus propofol measurement system (figure 4.02 A), the Proxima system (figure 4.02 B) and the cardiopulmonary bypass monitor.

The Pelorus system is directly relevant for this thesis and the Proxima system serves as future vision (see figure 1.01). Therefore, both systems are further presented below.

- The Pelorus propofol measurement system is the world's first commercial device that has the unique capability to rapidly quantify the concentration of the intravenous anaesthetic propofol in whole blood samples. Therefore it enables personalised sedation and intravenous anaesthesia management at the patient level in operating

room and ICU. It is a bench top device with a small footprint and its measuring time amounts to 5 minutes. ("Sphere Medical Ltd.'s Homepage: Pelorus Propofol Measurement System" 2014)

- The Proxima system is a disposable multi-parameter micronanalyser, which measures the blood gases, haematocrit and electrolytes. It is a patient attached sensor for arterial blood, which is engineered to return all blood back into the patient after measurement. The first generation of Proxima achieved FDA 510(k) clearance in March 2011. Furthermore its second generation successfully completed a clinical trial in November 2011 and achieved European CE ("Conformité Européenne") marking in December 2011 as a patient dedicated in-vitro arterial blood diagnostic analyser ("Sphere Medical Ltd.'s Homepage: About Sphere Medical" 2014). CE marking is a declaration by the manufacturer that their product meets the requirements of the applicable European Directives. ("Sphere Medical Ltd.'s Homepage: Proxima System" 2014)

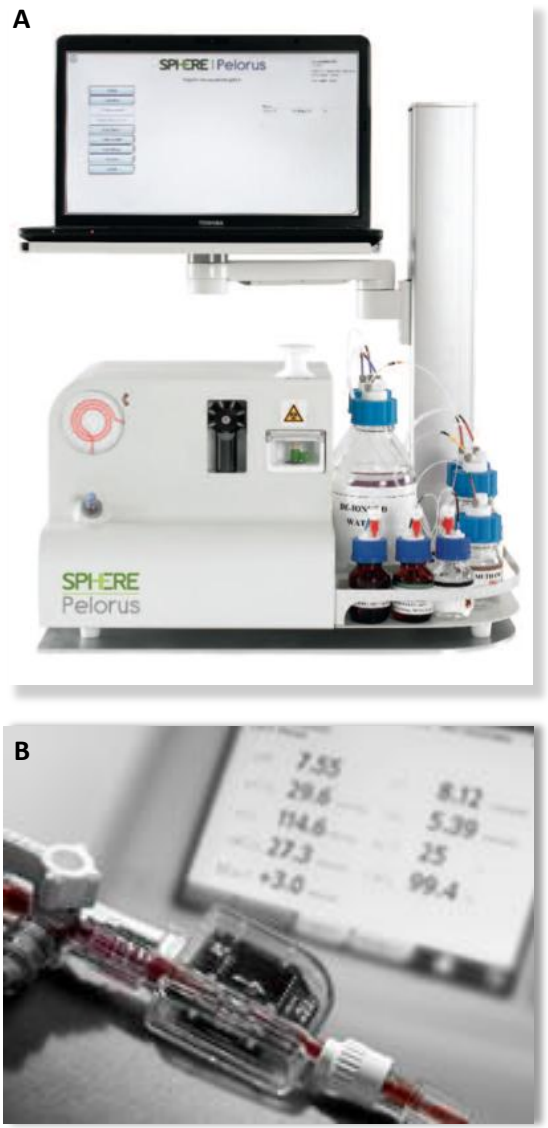

Figure 4.02: Point-of-care sensors developed by our Industrial Partner – Sphere Medical Ltd., Cambridge. A) Pelorus propofol measurement system. It measures rapidly the concentration of the intravenous anaesthetic propofol in whole blood samples and therefore enables an optimal therapy at the individual patient level. Image adopted from "Sphere Medical Ltd.'s Homepage: Pelorus Propofol Measurement System" 2014. **B) Proxima system.** It is a disposable multi-parameter micronanalyser of arterial blood, which is patient attached and measures the blood gases, haematocrit and electrolytes on demand in real-time. Image adopted from "Sphere Medical Ltd.'s Homepage: Proxima System" 2014.

CHAPTER 5:

Proof-of-Principle and Benchmarking of Colourimetric Detection

The main objective of this PhD thesis is the development of a PoC sensor for therapeutic antibiotic monitoring, particularly for the glycopeptide antibiotic vancomycin, which improves current practise in TDM. As described in the first chapter (1.1), through the development of each detection technique for a PoC application in healthcare settings, the overall aim is to miniaturise a PoC device to allow simple, cost effective and real-time monitoring of a specific analyte. In order for a sensor to be developed, it must meet the general requirements that were also established in chapter (1.1).

The starting point for this miniaturisation process is the colourimetric detection of vancomycin by visible spectroscopy (see figure 1.01), which builds on Sphere Medical's Pelorus bench top device that measures the anaesthetic propofol. The incorporation of colourimetric detection technique into a bench top device was the first objective and the main focus of this thesis. Hence, it is presented and discussed in three chapters (5, 6 and 7).

The objective of this chapter is to detail the development of the colourimetric assay with the initial proof-of-principle experiments followed by a set of benchmarking experiments against the existing Pelorus bench top device from Sphere Medical Ltd.

This chapter is built up on four subsections: The first subsection (5.1) introduces spectroscopy, the Gibbs reagent, a concise history about general anaesthesia and a description of the anaesthetic propofol. The second part (5.2) lists materials and methods including the experimental set-up. The third subsection (5.3) presents the results including preliminary discussions and continues into the final subsection (5.4) with the overall discussion and conclusion.

5.1 Introduction

This subsection introduces the theoretical background surrounding the development of a colourimetric or optical sensor for therapeutic antibiotic monitoring focusing on vancomycin. As described above this approach builds on Sphere's Pelorus bench top instrument, in which the anaesthetic propofol is extracted from whole blood and subsequently labelled with Gibbs reagent to determine its concentration in blood samples. This coupling reaction with Gibbs reagent induces a detectable colour change, which can be measured via visible spectroscopy.

Therefore this section contains an introduction to spectroscopy (5.1.1), with special emphasis on ultra-violet and visible spectroscopy, colourimetry and the Beer-Lambert-Bouger law, the coupling reaction with the Gibbs reagent (5.1.2) and the anaesthetic propofol (5.1.3). A further and more detailed discussion on the coupling reaction involving Gibbs reagent can be found in chapter 7.

5.1.1 Spectroscopy

Spectroscopy is an analytical method based on the analysis of the interaction between specific radiative energy and matter. There are various different spectroscopic techniques that exist to analyse different aspects of atomic and molecular structure. Since the radiative energy is associated with certain transitions in atoms or molecules, spectroscopic techniques correspond to a particular part of the electromagnetic spectrum. The most frequently used methods in chemistry are nuclear magnetic resonance (NMR), infra-red (IR), ultra-violet (UV) and visible (vis) spectroscopy. This thesis will focus on the latter two techniques.

Spectroscopy generally distinguishes between absorption and emission spectra. Absorption of electromagnetic radiation of the correct energy excites electrons of atoms, molecules or ions to make a particular transition from a ground to an excited state. The corresponding absorption spectrum records the energy and intensity of this specific radiation, which caused the particular excitation, against the entire initial range

of energies. The specific absorbance of a compound of interest can be either recorded as absorbance or transmittance and is dependent on several factors such as the probability of particular transitions occurring, the populations of the various energy states and the sample concentration. Contrariwise, emission spectra measure the radiation emitted by a compound of interest when it makes a transition from an excited to the ground state.

Both absorption and emission always take place in discrete quanta. This quantisation of electromagnetic radiation was first proposed by the German theoretical physicist Max Karl Ernst Ludwig Planck (1858 – 1947; Nobel Prize in Physics 1918) in 1900 (Born 1948). The equation describing this is:

$$\Delta E = h\nu = \frac{h\,c}{\lambda} \qquad 5.1$$

where ΔE is the difference between the ground and the excited state, h is Planck's constant ($\approx 6.63 \cdot 10^{-34}\,J \cdot s$), ν is the frequency of the absorbed radiation, c is the speed of light ($\approx 3 \cdot 10^{8}\,m \cdot s^{-1}$) and λ is the wavelength. This means that the energy of absorbed or emitted electromagnetic radiation must be a multiple of $h\nu$. (Kellner et al. 2004; Vollhardt and Shore 2005)

An important aspect of spectroscopy is the timescale. This is a fairly complex topic and will therefore not be discussed in great detail in this thesis. However, several points are particularly important and will need to be elaborated on. In particular, the spectroscopy methods that will be used to analyse compounds of interest will be discussed further.

Molecules are not static systems and are constantly in rotational and translational motion defined as Brownian motion with roughly 10^{21} collision per second (Chandrasekhar 1943). The atoms within the molecules are also vibrating. These vibrations have typical frequencies of 10^{12} to 10^{14} Hz and can be of the following types: stretching, bending, rocking, wagging and twisting. Every molecular system has its characteristic energy profile consisting of discrete electronic, rotational and vibrational states.

Upon absorption of the appropriate type of electromagnetic radiation, transitions into excited states of the aforementioned molecule specific energy states can be induced. These excited states usually last for short (< 10 nanoseconds), variable periods, whereupon they decay to their original ground states. Therefore, it is important to consider that if the spectroscopic method is faster than these frequencies, then one analyses a "snapshot" of the event. On the other hand, if the method is slower, then the result is an average measurement of the molecule in motion.

On this note, UV and visible spectroscopy are fast and so have the ability to give a snapshot of the current vibrational and rotational state of the molecule. NMR spectroscopy, on the other hand, is much slower resulting in an averaged view of the molecular motions within the sample. NMR spectroscopy is further presented in chapter 7, which describes the structural characterisation of the novel product. (Housecroft and Constable 2010; Vollhardt and Shore 2005; Kellner et al. 2004; Kalsi 2004)

5.1.1.1 Ultra-Violet and Visible Spectroscopy

UV and vis spectroscopy use high energy radiation, normally between 160 and 1250 kJ/mol. UV spectroscopy operates in the wavelength range of about 200 nm (which is the near ultra-violet part of the electromagnetic spectrum) to 400 nm while vis spectroscopy spans 400 nm to 800 nm reaching the beginning of the near infra-red region (see figure 5.01). This UV-vis range is especially important for the analysis of electronic structures of unsaturated molecules and the study of their conjugation width. Therefore UV/vis spectroscopy is often called electronic spectroscopy.

In most molecules, the electrons, with the exception of lone electron pairs, are occupying bonding molecule orbitals, such as σ and π molecular orbitals; hence the molecule is electronically in its ground state. Lone pairs are occupying non-bonding orbitals referred to as n-orbitals. During the absorbance of UV and visible radiation, valence electrons from occupied bonding and non-bonding molecular orbitals get excited and change to unoccupied anti-bonding molecular orbitals, such as σ^* and π^*

molecular orbitals. As a result, the molecule is in its electronically excited state. This absorbed energy is released either in a chemical reaction, by emitting light (fluorescence or phosphorescence) or as thermal energy. The absorbed wavelength λ is dependent on the energy difference between the occupied and the unoccupied molecular orbitals. Since the wavelength λ is inversely proportional to the energy E and the frequency ν, the higher the energy gap between the highest occupied molecular orbital (HOMO) and the lowest unoccupied molecular orbital (LUMO), also referred to as lowest anti-bonding molecular orbital, the smaller the wavelength that is needed.

σ-bonds, i.e. carbon-carbon bonds and carbon-hydrogen-bonds, have a energy gap to the anti-bonding orbitals that is too high and hence cannot be excited and subsequently observed with UV/vis spectroscopy. On the other hand, lone pairs and π-bonds, which are, amongst other functions, bridging the σ-bond in multiple bonds, have a smaller energy gap to the LUMO. Therefore they can be studied in the spectral range from 200 nm to 800 nm. Hence, as mentioned above, the UV/vis range is important in order to study unsaturated molecules and the extension of their conjugation. Conjugated molecules have a system of connected and overlapping p-orbitals (π-bonds) with delocalised electrons that stabilise the system and therefore lower both its overall energy and the energy gap between HOMO and LUMO. Consequently an electronic transition from a bonding or non-bonding to an anti-bonding molecular orbital can occur with lower energetic radiation, possibly via absorbance of light with a long wavelength in UV or even visible range. For conjugation, a continuous chain of atoms with overlapping p-orbitals and possibly additional overlapping lone pairs are needed. This can be achieved by alternating single and double bonds and in some types of ionic systems. Alternatively, in a more specific example, conjugation can occur by a five-membered ring with two alternating double bonds and an oxygen with its lone pair at position 1 (known as furan).

Besides their conjugation, aromatic compounds exhibit an additional stability due to the fulfilment of Hückel's rule, which is named after the German physical chemist Erich Hückel (1896 – 1980). Hückel's rule says a compound is aromatic (i) if it is planar,

(ii) every atom in its circle participates in the electron delocalisation by having p-orbital or a pair of unshared electrons, and (iii) if the number of its delocalised π electrons fulfils

$$4n + 2 \qquad 5.2$$

while $n \geq 0$ and an integer (Hückel 1931). Furthermore, additional examples for the extension of delocalisation beyond π-bonds to include lone pairs are aniline (also called phenylamine), phenol and benzaldehyde. The penultimate molecule will play an important role later on in this thesis.

Conclusively, UV/vis spectroscopy is a measure of the degree of conjugation in a molecule and reveals important information about the excited states of molecules. In general, the more conjugated systems a molecule has, the higher the absorption wavelength λ for the lowest energy gap and the lower the energy required for its excitations is needed.

Besides this measure for the degree of conjugation, one also obtains an estimation of how many groups in a molecule absorb light in the studied range. Such groups are named chromophores. However, there are different definitions for chromophores in use. Some experts name a whole delocalised system one chromophore and others specify each individual part contributing to the system as chromophores. Within this thesis it has been decided that the whole delocalised system will be referred to as one chromophore based on the fact that the electrons are not distinguishable within the delocalised system and hence this whole system is causing the specific absorption.

In a typical absorption spectrum, the wavelength of the peak with the maximal absorbance is called λ_{max} and is characteristic for the absorbent species. The transition with the highest maximal wavelength usually corresponds to the one from the highest occupied molecular orbital to the lowest unoccupied of all the molecular orbitals.

Robert Burns Woodward (1917 - 1979) and Louis Fieser (1899 – 1977), both American organic chemists, empirically derived a set of rules that predict the λ_{max} for a compound of interest in the UV/vis range. These rules are called Woodward's rules or Woodward-Fieser rules and can be applied to conjugated dienes, polyenes and carbonyl compounds. They take into account the type of chromophores, the substituent and the solvent's effects (Woodward 1941; Woodward and Clifford 1941; Woodward 1942a; Woodward 1942b; Fieser, Fieser, and Rajagopalan 1948; Slater 2002). These rules work well for conjugated systems with less than four double bonds.

For conjugated polyenes with more than four double bonds, one can use the Fieser-Kuhn rules, which gives an additional estimate of the maximum absorptivity ε_{max} of the molecule of interest (Kalsi 2004). However, both rules are not applicable to aromatic compounds or fairly large systems and are therefore not further discussed in this thesis. (Kellner et al. 2004; Vollhardt and Shore 2005)

As previously mentioned, besides the characteristic λ_{max} , the absorbent species can be additionally characterised by its specific molar absorptivity or molar absorption coefficient ε, which is completely independent of concentration and the cuvette size. How the absorptivity is defined and how it can be calculated is described in the following subsection (5.1.1.2), which presents the Beer-Lambert-Bouger law.

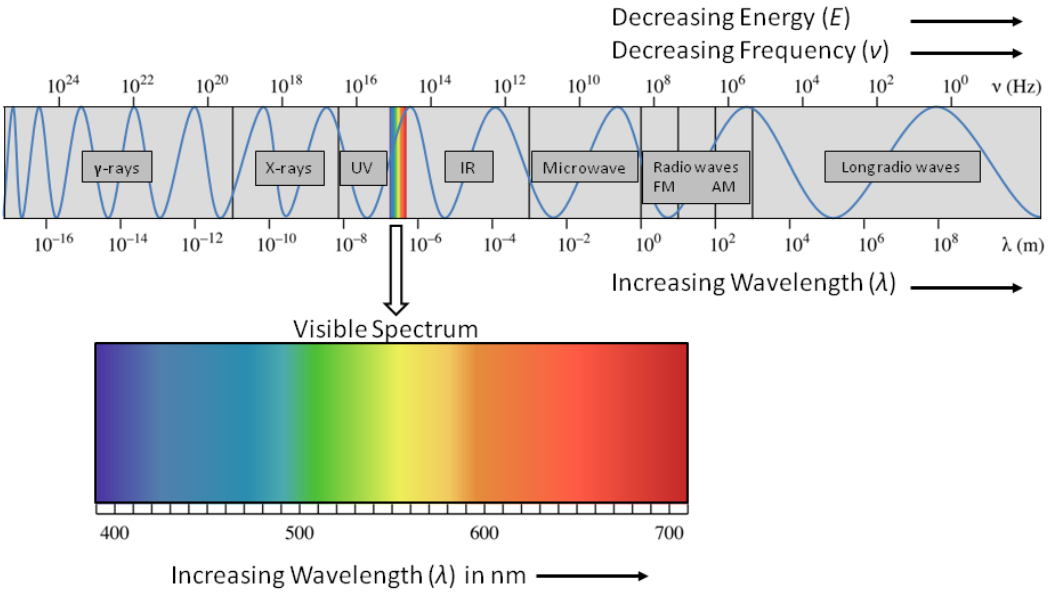

Figure 5.01: Electromagnetic spectrum including the visible spectrum. In this schematic the electromagnetic spectrum spans from γ-rays, X-rays, ultra-violet, through visible, infra red, microwave, to radio waves including frequency modulation (FM) and amplitude modulation (AM), and ends with long radio waves. It has to be highlighted that neither the borders between the different regions are exact and nor are the scales linear. Hence the schematic has to be seen as an approximation.

5.1.1.2 The Beer-Lambert-Bouguer Law

The law is widely known as the Beer-Lambert law only, even though it was discovered by Pierre Bouguer (1698 – 1758), a French physicist, astronomer and geodesist, and first presented in his book "Essai d'optique sur la gradation de la lumière" in 1729 (Bouguer 1729). He described the reduction of the radiation intensity according to the path length through an absorbent. In the year 1760 Johann Heinrich Lambert (1728 – 1777), a Swiss mathematician, logician, physicist, astronomer and philosopher, cited Bouguer's book and even quoted from it (Lambert 1760). In the same publication he described the cosine emission law also named Lambert's emission law, which will not be further discussed in this thesis. About a century later, in 1852, the German mathematician, chemist and physicist, August Beer (1825 – 1863) extended the Bouguer-Lambert law by adding the dependency of the transmitted light on the concentration of the absorbent (Beer 1852). (Perrin 1948)

Transmittance (T) is defined as the ratio of the final intensity of the emergent light (I_f) and the intensity of the incident light (I_i), hence it can be calculated as follows:

$$T = \frac{I_f}{I_i} \tag{5.3}$$

Values of transmittance T lie between 0 and 1, but experimentally it is often expressed as a percentage, therefore:

$$\mathrm{T}\,[\%] = \frac{100 \cdot \mathrm{I_f}}{\mathrm{I_i}} \tag{5.4}$$

If light passes through a sample it can undergo absorption, reflection, interference and scattering, hence the intensity of the emergent light (I_f) is reduced compared to the initial intensity (I_i). In order to measure the amount of absorbed light only, an appropriate reference has to be measured either prior to or after the compound of interest in a single beam spectrometer. In a double beam spectrometer the beam is split in two, which allows simultaneous measurement of sample and reference. A suitable reference might be the solvent without the compound of interest present.

The principle of spectrometers is described in subsection 5.2.2.1 of the materials and methods chapter. Typically, a spectrometer can be operated in either transmittance or absorbance mode. Absorbance (A) is calculated as the negative logarithm of the transmittance (T):

$$\mathrm{A} = -\log(\mathrm{T}) = \log\left(\frac{1}{\mathrm{T}}\right) = \log\left(\frac{\mathrm{I_i}}{\mathrm{I_f}}\right) \quad 5.5$$

As a result 100% transmittance corresponds to zero absorbance and vice versa. Since it is a logarithmic dependency, for a zero transmittance the absorbance continuously increases to infinite values. 1% transmittance corresponds to an absorbance of 2. Although absorbance is dimensionless, it is often reported in 'absorbance units' and abbreviated as AU. Usually UV/vis spectrometers operate up to 4 or 6 AU (Housecroft and Constable 2010).

Historically, the Beer-Lambert-Bouguer law was derived separately and independently. Lambert's law depended on Bouguer description and specified that the absorbance is proportional to the path length. Whilst Beer's law defined that the absorbance is proportional to the concentration of the absorbent. The modern derivation correlates the absorbance to the path length and the concentration of the absorbent. In this way both laws are combined.

This combined derivation derives the Beer-Lambert-Bouguer law as follows: The initial intensity reduces when light passes through a cuvette with a certain thickness containing a compound of interest in uniform concentration (c), which absorbs light. It has been assumed that the cuvette consists of infinitesimal slices with thicknesses of (dx). The reduction of initial intensity (dI) is proportional to the thickness of the slice (dx), the concentration and the initial intensity (I). Hence we can write that in term of the change in intensity (dI):

$$\mathrm{dI} = -\alpha\, \mathrm{c}\, \mathrm{I_i}\, \mathrm{dx} \quad 5.6$$

or

$$\mathrm{d\ln(I)} = -\alpha\, \mathrm{c}\, \mathrm{dx} \quad 5.7$$

where α is the proportionality coefficient. Since there are fewer photons compared to the incident light and it is proportional in magnitude to the number of absorbed

photons, dI is negative. To obtain the final intensity (I_f), which emerges from the sample, when it has been illuminated with the initial intensity (I_i), one has to sum all successive changes over the whole path length (l) respectively whole sample thickness, which results in the following integrals:

$$\int_{\mathrm{i}}^{\mathrm{f}} \mathrm{d}\ln(\mathrm{I}) = -\int_{0}^{\mathrm{l}} \alpha\, \mathrm{c}\, \mathrm{dx} \qquad 5.8$$

If the concentration (c) is uniform then it is independent from variable x and the equation can be expressed as follows, which is the Beer-Lambert-Bouguer law; however in an unconventional notation:

$$\mathrm{I_f} = \mathrm{I_i}\, \mathrm{e}^{-\alpha \mathrm{cl}} \qquad 5.9$$

The intensity decreases exponentially with the sample thickness and the concentration, and the law is often expressed as:

$$\mathrm{I_f} = \mathrm{I_i}\, 10^{-\varepsilon \mathrm{cl}} \qquad 5.10$$

or

$$log\frac{I_f}{I_i} = -\varepsilon\, c\, l \qquad 5.11$$

where ε is the molar absorption coefficient or molar absorptivity of the absorbent species at a certain frequency, formerly called the extinction coefficient, and related to the proportionality coefficient (α) by:

$$\varepsilon = \frac{\alpha}{\ln(10)} = \frac{\alpha}{2.303} \qquad 5.12$$

The molar absorption coefficient is dependent on the frequency of light absorbed by the molecular cross-section. As a result the coefficient is usually expressed as [M^{-1} cm^{-1}]. The greater the cross-section of the molecule for the absorbance, the stronger it absorbs and the greater the attenuation of the incident beam of light. Typical molar absorptivities for the UV and vis region are in the range of 10^3 to 10^5 M^{-1} cm^{-1}. Accordingly the absorbance (A) (formerly known as optical density (OD)) of a chemical species is the defined as the following dimensionless product:

$$\mathrm{A} = -\log\left(\frac{\mathrm{I_f}}{\mathrm{I_i}}\right) \qquad 5.13$$

which leads to the well known **Beer-Lambert-Bouguer law**:

$$\mathrm{A} = \varepsilon\, \mathrm{c}\, \mathrm{l} \qquad 5.14$$

Since the absorbance is calculated as the negative logarithm of the transmittance, the transmittance or the transmission (T) of a molecule can consequently be described as:

$$\mathrm{T} = \frac{\mathrm{I_f}}{\mathrm{I_i}} = 10^{-\varepsilon \mathrm{cl}} \qquad 5.15$$

The Beer-Lambert-Bouguer law derivation assumes a linear relationship between A and the absorbent concentration c.

However, it has to be emphasised that this is relationship is only true, if every absorbing particle can be contemplated independently and thus is not affected by other particles. That means that particles are not allowed to shadow each other, hence more than one particle along the same optical path will lead to deviations from the linear calibration curve. Consequently the Beer-Lambert-Bouguer law should only be used for dilute solutions where the absorbent concentration is equal or below 0.1 mol/l ($c \leq 0.1 \frac{mol}{l}$). For concentrations above this limit the actual concentration may be underestimated, which will lead to errors if the Beer-Lambert-Bouguer law is used. As a rule of thumb, absorbances in the range of 0.1 to 1 are less affected by this shadowing and therefore the law should be applicable. (Vollhardt and Shore 2005; Kellner et al. 2004; Housecroft and Constable 2010)

Furthermore, it has to be highlighted that analyses of two or more component mixtures by UV/vis can be challenging. In optimal cases, the different species in the same sample are not interfering with each other. Consequently the light absorption by these species is additive. Even simpler would be if the present components have their respective maximal absorbances in different regions of the spectra and do not show absorbances in the maximal absorbance regions of the other components. However, this is not always the case and strong interferences can preclude simple simultaneous determinations of concentration. Especially if the different compounds present are absorbing in similar wavelength regions. (Sawyer, Heineman, and Beebe 1984)

5.1.1.3 Colourimetry

Colourimetry is an analytical technique to determine the concentration of a coloured compound in solution. In a typical colourimeter, the light source emits only one specific wavelength according to the λ_{max} of the compound of interest. Usually the objectives for colourimetric detection are to follow a reaction, to determine the stoichiometry of a reaction or to measure the concentration of a known compound as a one-off measurement. The latter relates to Sphere's Pelorus device and will be the focus for our point-of-care sensor for therapeutic antibiotic monitoring.

The difference between colourimetry and spectroscopy is that colourimetric detection is limited to the colour intensity of a known compound, which depends on its concentration in the solution. On the other hand, visible spectroscopy intends to analyse the colour of the compound based on the absorption wavelength λ.

If a molecule has its λ_{max} above 400 nm, within in the visible range, then it appears colourful to the human eye. Generally, to predict the absorbed wavelength in relation to the observed colour by the human eye, one has to consult the visible spectrum of the electromagnetic radiation and find the wavelength of the complementary colour (see figure 5.02). To explain this principle, three examples will be discussed. The latter one will also serve the additional purpose of setting the stage for the following subsection (5.1.2) on Gibbs reagent labelling:

i) The first example is β-carotene orange (figure 5.03 A i), which is a well known pigment from various plants and fruits such as carrots, pumpkins and sweet potatoes. It absorbs radiation throughout the UV region of the electromagnet spectrum and also very strongly between 400 and 500 nm as a result of its eleven conjugated carbon-carbon double bonds. The wavelength with the maximal absorbance (λ_{max}) is at about 451 nm with two shoulders at approximately 478 and 430 nm, which is presented in figure 5.03 Aii (Khachik and Beecher 1987; Hornero-Méndez and Mínguez-Mosquera 2001; Khoo, Morsingh, and Liew 1979). This corresponds to the blue/cyan region of the visible light spectrum. However to

our eyes, it appears orange as this is the complementary colour of the transition between blue and cyan. The absorptivity of β-carotene at the $\lambda_{451\,nm}$ amounts to 139500 M^{-1} cm^{-1} (= $\varepsilon_{451\,nm}$) (Zechmeister and Polgár 1943).

ii) Phenolphthalein (figure 5.03 B i) has been chosen as the second example in anticipation of the vancomycin Gibbs coupling reaction product, which will be discussed in more detail in chapter 6. Phenolphthalein is a halochromic chemical, which means that its absorbance, and therefore its colour, is pH dependent. In a pH range of 0 to 8.2, the three aromatic rings of phenolphthalein are bonded over a tetrahedrally coordinated and hence sp^3-hybridised carbon atom, which is not contributing and also not extending the conjugation over the three aromatic rings within the molecule. Accordingly the molecule only absorbs in the UV region, which makes its appearance to humans colourless. However, as soon as the pH increases beyond 8.2 towards basic conditions, the central carbon atom loses a proton and becomes sp^2-hybridised. This leaves a p-orbital that connects the delocalised electron systems of the three aromatic rings together to a large extended chromophore absorbing at 553 nm in the green range of the spectrum (see figure 5.03 Bii) (El-Nahhal, Zourab, and El-Ashgar 2001). This makes molecule appear magenta to the human eye. Phenolphthalein's molar absorptivity at the maximal absorbance ($\varepsilon_{553\,nm}$) is usually given as 21000 M^{-1} cm^{-1} (Barnes and LaMer 1942). Due to its halochromic characteristics, phenolphthalein is a component alongside methyl red, bromothymol blue and thymol blue in universal indicators for pH tests (Foster and Gruntfest 1937).

iii) The last example is 2,6-dichlorophenolindophenol (see figure 5.03 Ci), which will be further abbreviated as DCPIP. It is a particularly relevant example for this thesis. DCPIP is the chlorine form product of the original Gibbs reagent reaction with phenol, which is further discussed in subsection 5.1.2. It has been used in proof-of-principle experiments for the colourimetric studies in order to initiate the development of the colourimetric antibiotic assay. DCPIP is a redox indicator or redox dye and so can quickly and reversibly change its colour depending on

whether it is predominantly in the oxidised or reduced form. The colour of its oxidised form is either blue in a basic environment or red in an acidic media. The latter can alternatively be more towards pink in more diluted solutions (Tillmans, Hirsch, and Reinshagen 1928; Kar, Mandal, and Palit 1969). The oxidised form has an extended conjugated system with a maximal absorption at 605 nm in basic media (see figure 5.03 Cii). The molar absorptivity is 21000 M^{-1} cm^{-1} at 605 nm (ε_{605nm}). This value was found experimentally (subsection 5.3.1) and fits exactly the manufacturer's information provided by Sigma-Aldrich. The reduced form splits the extended chromophore at the secondary amine resulting in smaller conjugated systems with larger energy gaps, which require higher energies and shorter wavelengths in order to get excited. Consequently it appears colourless to the human eye. In general such redox indicators are divided into two groups, the pH independent and the pH dependent ones. As already mentioned, DCPIP belongs to the pH dependent group. Its specific electrode potential (E^0), where it changes its redox form and consequently its colour, is pH dependent, namely +0.64 V at pH 0 and +0.22 V at pH 7 (Tillmans, Hirsch, and Reinshagen 1928). Therefore, besides being a redox dye, DCPIP can additionally be considered a halochromic chemical, comparable to phenolphthalein described in example two (ii).

DCPIP's acidic form is not stable and easily reducible. Therefore it is as an indicator for the presence and quantification of various chemicals such as thiols (Basford and Huennekens 1955) and ascorbic acid, commonly known as vitamin C (Owen and Iggo 1956; VanderJagt, Garry, and Hunt 1986). Vitamin C is a good reducing agent and turns the oxidised acidic form into the reduced colourless form. Therefore, if DCPIP is used for vitamin C quantification via titration, the endpoint is given by the appearance and persistence of the colour pink due to the accumulation of unreacted DCPIP in the acidic media. Since the reaction stoichiometry is one-to-one, the moles of DCPIP used to reach titration's endpoint equals the moles of ascorbic acid (VanderJagt, Garry, and Hunt 1986; Owen and Iggo 1956).

With these three examples it can be concluded that the connection between the absorbance wavelength and the colour appearance to the human eye can be generally described as follows. By increasing the wavelength from 400 nm to 800 nm and with the condition that the concentration of the absorbent species in the solution is high enough, at the lower range of the visible spectra the appearance is yellow, then orange, red, violet and blue-green at the end (see table 5.01). However, it has to be emphasised that this is a general principle and in some cases where the molecule absorbs over a large range of wavelengths this principle may not be applicable. (Vollhardt and Shore 2005; Atkins and De Paula 2002; Kellner et al. 2004; Kalsi 2004)

Figure 5.02: Prediction of the absorbed wavelength according to observed colours by the use of the colour wheel. The colour wheel is an abstract illustration of the circular organisation of the colour hues. It is used for the ascertainment of the complementary colours, which lay in opposition to each other in the wheel. According to the oxford dictionary a complementary colour is "a colour that combined with a given colour makes white or black". Complementary colours are the link between the observed colour and the prediction of absorbed wavelength for a coloured compound of interest.

colour apparent to human eye	prediction of absorbed (complementary) colour in vis spectrum	corresponding wavelength (λ) of absorption [nm]
yellow	violet	380 – 435
	blue	435 – 500
orange	cyan	500 – 520
red	green	520 – 565
violet	yellow	565 – 590
blue	orange	590 – 625
blue-green	red	625 - 740

Table 5.01: Visible spectrum's colour regions with approximate wavelengths. This table lists the main colour regions of the visible spectrum and the corresponding approximate wavelengths. It has to be highlighted that there are no clear cut-off points between the colours and that the wavelength values have to be seen as approximations. To see where the visible spectrum fits into the electromagnetic spectrum as a whole see figure 5.01. The following is an example for the absorbed wavelength prediction approach: If a compound in solution looks blue to the human eye, such as 2,6-dichlorophenolindophenol (DCPIP), one has to find the complementary colour to blue in the colour wheel (see figure 5.02), which is orange. According to the corresponding wavelength range in the table, one can predict that DCPIP's maximal absorbance wavelength within the visible spectrum should lie between 590 to 625 nm. However, it should be emphasised that this is a general principle and may in some cases not be applicable.

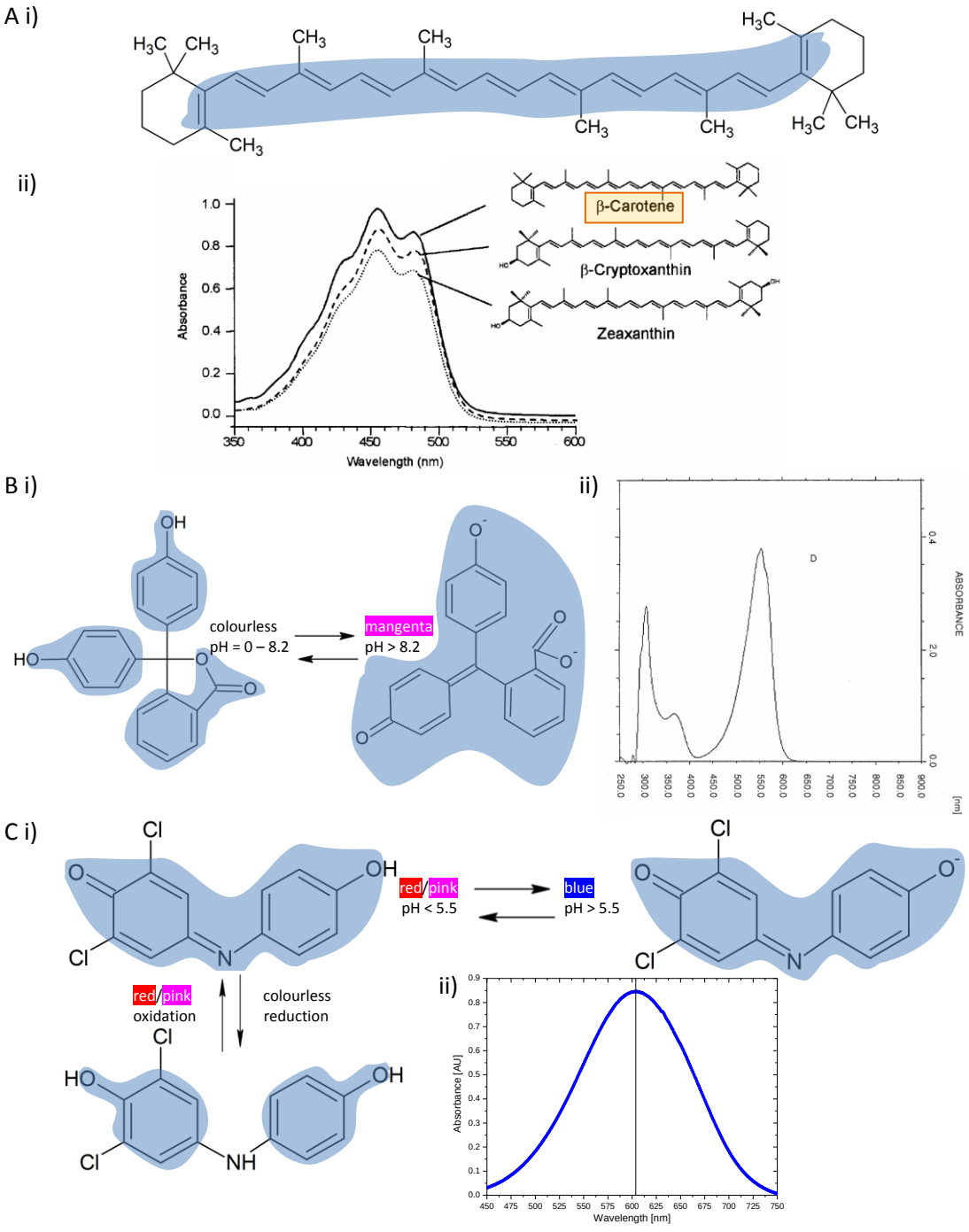

Figure 5.03: Three compounds as examples for colourimetric studies. A) β-carotene. i) Lewis' structure of β-carotene with the blue highlighted chromophore. ii) Typical UV/vis absorption spectra of various carotenoid pigments. Spectra adopted from Hornero-Méndez & Mínguez-Mosquera, 2001. **B) Phenolphthalein.** i) Lewis' structures of the colourless and mangenta form of phenolphthalein with highlighted chromophores. ii) UV/vis spectrum of phenolphthalein's basic form in a water methanol mixture. Spectrum adopted from El-Nahhal et al., 2001. **C) 2,6-dichlorophenolindophenol**. i) Lewis' structures with chromophores of the halochromic redox dye DCPIP. ii) Spectrum of the oxidised form of DCPIP in basic conditions.

5.1.2 The Gibbs Reagent and its Reaction

The first detection technique investigated in this thesis builds on the colourimetric detection of drugs. Vancomycin is of particular interest along with propofol in relation to the benchmarking experiments presented later in this chapter. Therefore, a detectable change in colour has to be introduced, which can subsequently be analysed and used for quantification of the compound of interest. In this thesis the colour change has been induced via the coupling of Gibbs reagent resulting in a brightly coloured product.

However, it has to be emphasised that this coupling reaction is not specific to the aforementioned compounds of interest. The Gibbs reagent has the ability to bind to various different phenolic moieties (Gibbs 1927a; Gibbs 1927b; Dacre 1971; Josephy and Van Damme 1984; Pallagi and Dvortsák 1986; Pallagi, Toró, and Müller 1994; Pallagi, Toró, and Farkas 1994; Pallagi, Toró, and Horváth 1999), some esters (Kramer, Gamson, and Miller 1959; Gamson, Kramer, and Miller 1959), certain thiols and sulfhydryl groups (Kramer and Gamson 1959; Harfoush, Zagloul, and Abdel Halim 1982; Harfoush 1983), nitroxyl groups (Pallagi, Toró, and Horváth 1999) and some amines (De Boer et al. 2007; Kovar and Teutsch 1986; Kallmayer and Thierfelder 2003; Annapurna et al. 2010).

Consequently for a specific labelling reaction, the use of vancomycin specific antibodies could be considered (Adamczyk et al. 2004; Adamczyk et al. 1999; Antoci et al. 2008; Cheng and Kim 2004; Fish et al. 2012; Hofmann, Anderson, and Marchant 2012; Rottman, Goldberg, and Hacking 2012; Varma, de Pedro, and Young 2007). Anti-vancomycin antibodies are commonly used in the current gold standards of therapeutic vancomycin monitoring, which are described in subsection 4.1 and figure 4.01 (Pfaller et al. 1984; Trujillo et al. 1999; Wan and Le 1999; Fong et al. 1981). Nevertheless, the approach using Gibbs reagent has been investigated in this thesis due to various reasons including cost effectiveness, simplicity (especially in readout) and the existing expertise of Sphere Medical with this technique. Their Pelorus device, which uses Gibbs reagent for labelling the anaesthetic propofol, is already on the market (see chapter 4.4). As such, the development of a compatible assay will potentially reduce the time taken for a vancomycin-focussed device to reach the market.

The following two subchapters provide a concise introduction into the history of the Gibbs reagent (5.1.2.1) and describe its reaction mechanisms including examples of application (5.1.2.2).

5.1.2.1 History of the Gibbs Reagent

The Gibbs reagent is named after an American chemist named Harry Drake Gibbs (1872 - 1934). Prior to the work with the compound carrying his name, H. D. Gibbs had been interested in arsenic occurrence in Californian wine (Gibbs and James 1905), and in phthalic anhydrides and quinones, specifically in anthraquinones (Gibbs 1923). In 1926 and 1927, he published a series of four papers concerning “phenol tests”. Whereas the first paper extensively reviewed all available tests and classified them (Gibbs 1926a), the second paper focused on the “nitrous acid test” (Gibbs 1926b). The third and fourth paper described the “indophenol test” and the study of the formation of the 2,6-dibromobenzenoneindophenol (figure 5.04 B) (Gibbs 1927a; Gibbs 1927b). Gibbs got this special indophenol by coupling 2,6-dibromoquinonechoroimide (figure 5.04 A) to the unsubstituted para-position of the hydroxyl group in a phenol. He suggested that the colour change upon completion of the reaction could be analysed via spectroscopic methods to determine the quantity of the phenolic compounds. Therefore, his work marked the beginning of the quantitative colourimetric assay for phenolic and hydoxypyridine derivates.

Later due to the toxicity of 2,6-dibromoquinonechoroimide, the chlorine version, 2,6-dichloroquinonechoroimide (figure 5.04 C), was adopted instead and has been further designated as the “Gibbs reagent”. The coupling reaction of Gibbs reagent to phenol yields the product 2,6-dichlorophenolindophenol (DCPIP), which was presented earlier as the third example for the prediction of the absorbed wavelength in relation to its apparent colour to the human eye in subchapter 5.1.1.3 and figure 5.03 C.

5.1.2.2 The Gibbs Reagent Reactions and their Applications

Gibbs proposed that the para-position to the hydroxyl group in the phenol should be unsubstituted and that the pH of the reaction influences the rate of indophenol formation. For example at pH 10, a colour change was detected within two minutes. Comparable findings have been made by D. Svobodová and colleagues in 1977 and 1978 (Svobodová et al. 1978; Svobodová et al. 1977). Furthermore, besides studying the influence of pH, different alcohols, mixing ratios of alcohol and buffer, and the ratio of the Gibb reagent to the phenol, they performed extensive investigations on stability and the yield of the reaction. For example, they found that maximum colour intensity for a reagent to phenol ratio is between 30 - 50 to 1, and the ideal pH lies between 7.5 and 10. However, the decomposition of the Gibbs reagent to 2,6-dichloroquinoneimine, which is the reactive species and crucial for the initiation of the reaction, is fastest at a pH of 8.5.

Despite their extensive studies on the optimal reaction conditions, they could not elucidate the detailed reaction mechanism (Svobodová et al. 1978; Svobodová et al. 1977). Various groups showed that the Gibbs reaction also works on some para-substituted phenols (Dacre 1971; Josephy and Van Damme 1984), and P. D. Josephy and A. Van Damme proposed the following reaction mechanism, which is presented in figure 5.04 D:

> First, the mechanism involves the solvolysis of the Gibbs reagent (1) to form 2,6-dichloro-p-benzoquinone monoimine (2). This reactive species attacks the para-position of the phenol (3). The resulting adduct (4) deprotonates to form the intermediate (5) which then loses a proton, H^+, and the para-substituent, R^-, to form 2,6-dichloroindophenol (DCPIP) (6).

However, this is only one example of a possible reaction mechanism and several other plausible alternatives have been proposed (Pallagi and Dvortsák 1986; Pallagi, Toró, and Müller 1994; Pallagi, Toró, and Farkas 1994; Pallagi, Toró, and Horváth 1999; Scudi 1941;

Rossi, Pierini, and Peñéñory 2003). Other alternative reaction mechanisms will not be discussed in this thesis for the sake of brevity.

Moreover, it has to be highlighted that an indophenolic moiety is produced in the aforementioned reaction, which would strongly suggest a blue colour. However, the product colour apparent to the human eye can vary from magenta, purple over blue to greenish blue depending on the solvents, the pH, the form in which the reagent is added, the presence or absence of metallic catalysts, and the time allowed for reaction (Scudi 1941; Dacre 1971; Svobodová et al. 1977). Similar observations are described for the Gibbs reaction with amines, for which the coupling product is expected to be yellow absorbing between 380 to 480 nm (see figure 5.04 E). This absorbance range is comparable to the activated Gibbs form, the 2,6-dichloro-p-benzoquinone monoamine, which was previously described and is shown in figure 5.04 D (2). However, J. V. Scudi observed that Gibbs reaction with creatine, creatinine, and phenylhydrazine give the expected yellow colour, but with uric acid and carbon disulfide yield in a yellow to pink (Scudi 1941). These observations were support by extensive studies of for example W. R. Fearon and D. N. Kramer and colleagues (Fearon 1944; Gamson, Kramer, and Miller 1959).

Due to this inducible colour changes, the Gibbs reagent assay has been or is still used to study, detect and quantify different molecules, such as cresols (Gibbs 1927c; MacManus-Spencer and McNeill 2005), vitamins B6 (Scudi 1941) and K (Scudi and Buhs 1941), uric acid (Fearon 1944), theophylline (also known as 1,3-dimethylxanthine) (Raybin 1945), methylthiouracil (McAllister 1950; Marsh and Hilty 1955), mercaptoimidazoles (McAllister 1951), porphyrilic acid of lichens (Wachtmeister 1954), anti-oxidants (Dacre 1971), catechols (Johnston and Renganathan 1987), opiates (Coop et al. 1995), whose presences also can get verified with a “Gibbs spray” on thin layer chromatography (TLC) plates (Baggi, Ram Rao, and Murty 1976), and drugs, such as the anaesthetic propofol (Adam et al. 1981; Pettigrew, Laitenberger, and Liu 2012; Liu et al. 2012) and as well as some antibiotics (Daabees et al. 1998; Krishna 2010), which will be

further discussed in chapter 6 and 7. The use of Gibbs reagent for therapeutic propofol monitoring will be further discussed in the next subsection (5.1.3).

Besides applications to study, detect and quantify molecules, the Gibbs reagent has also been utilised to measure enzymatic activity (Boyd and Eling 1984). Very recently C. S. Padidem and colleagues published a book chapter entitled “Sensor Enhancement Using Nanomaterials to Detect Pharmaceutical Residue: Nanointegration Using Phenol as Environmental Pollutant” in which they modified Gibbs reagent with gold nanoparticles for the detection of phenols (Padidem, Bashir, and Jingbo 2011).

All aforementioned publications followed the Gibbs reaction and the resulting colour change mainly optically by eye or via colourimetric readout systems. However, R. Compton and colleagues presented the electroactive characteristics of indophenol, which they exploited for indirect electrochemical detection of cannabinoids (Compton and Banks 2006; Lowe, Banks, and Compton 2005). Another study suggests the construction of a phenol-based sensor derived from colloidal chemistry in which the Gibbs reagent acts as the “detecting element” for colorimetric and electrochemical detection (Bashir and Liu 2009).

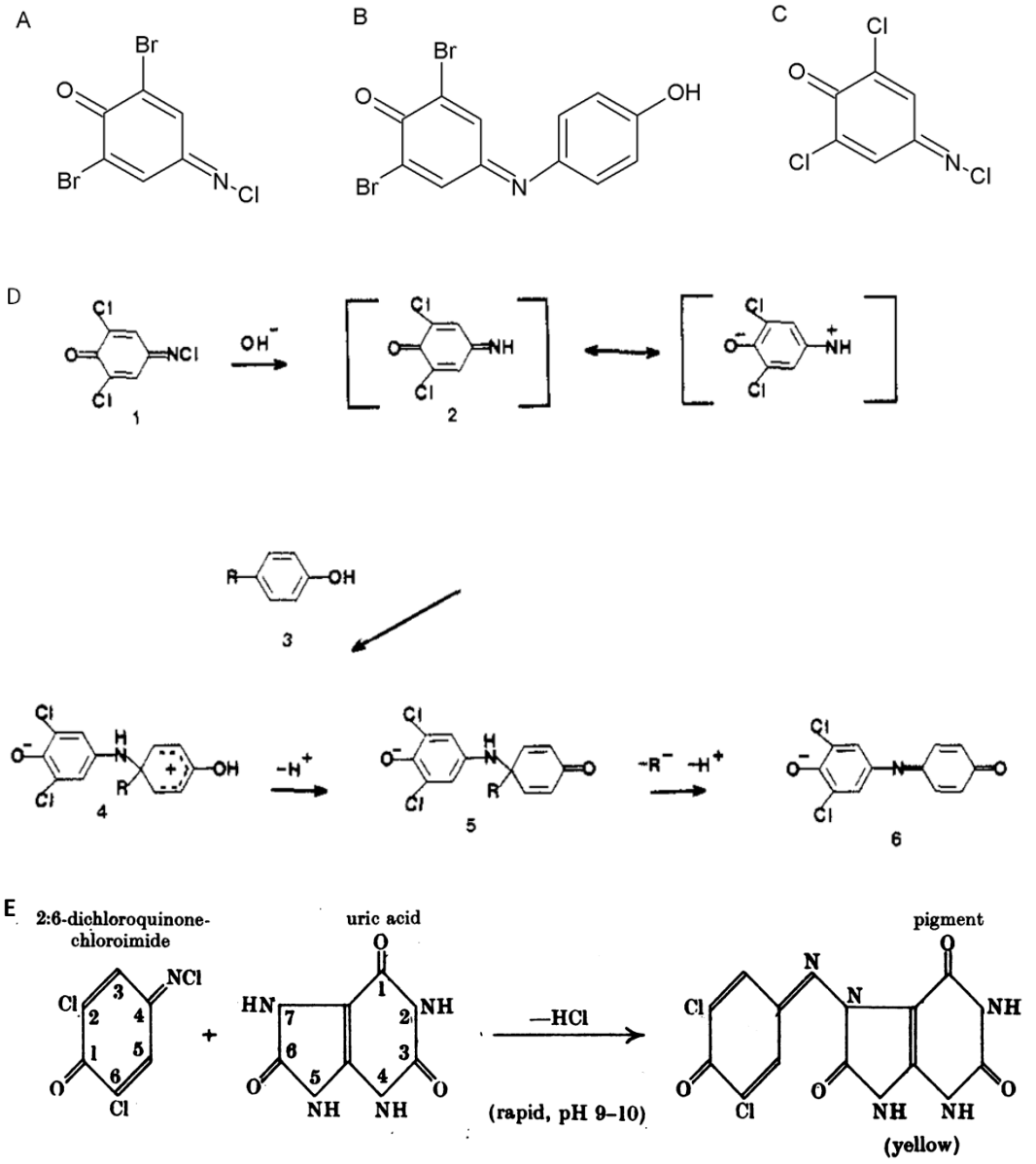

Figure 5.04: The Gibbs reagent and its reactions. A) Lewis' structure of 2,6-dibromoquinonechoroimide, which was the reagent H. D. Gibbs used to label compounds with phenolic moieties. B) Lewis' structure of 2,6-dibromobenzenoneindophenol, which is the product of 2,6-dibromoquinonechloroimide coupled to the para-position of a phenol. C) Lewis' structure of 2,6-dichloroquinonechoroimide, which is used instead of 2,6-dibromoquinonechloroimide and designated as the "Gibbs reagent". D) One possible reaction mechanism of Gibbs reagent coupling to a compound containing a phenolic moiety. First, the mechanism involves the solvolysis of the Gibbs reagent (1) to form 2,6-dichloro-p-benzoquinone monoimine (2). This reactive species attacks the para-position of the phenol (3). The resulting adduct (4) deprotonates to form the intermediate (5) which then loses a proton, H+, and the para-substituent, R^-, to form 2,6-dichloroindophenol (DCPIP) (6). Schematic adopted from Josephy & Van Damme, 1984. **E) A reaction scheme of Gibbs reagent coupling to a compound containing amines.** Schematic adopted from Fearon 1944.

5.1.3 The Anaesthetic Propofol

This subsection provides the literature review and background for anaesthetic propofol. Since propofol served as the precursor for the development of the colourimetric vancomycin assay in the benchmarking experiments, the information included in this section has been kept concise. The first part provides an insight into the history of general anaesthesia and anaesthetics followed by the second part, which is focused on the anaesthetic propofol.

The anaesthetic state consists of three main neurophysiological changes, namely loss of consciousness, loss of response to painful stimuli also called analgesia and muscle relaxation. For major surgical operations, the induction of anaesthesia is rapidly achieved with an intravenous agent, such as propofol. During surgery, the anaesthesia is maintained with either intravenous or inhalation anaesthetics given in combination with muscle relaxants and analgesics. (Rang et al. 2007)

5.1.3.1 Concise History of General Anaesthesia and Anaesthetics

The term anaesthesia takes its origin from Greek language and means “without sensation”. General anaesthesia is by no means a modern medical technique as its use has been recorded throughout history. Records indicate that the Egyptians, Greeks, Romans, Indians, Chinese and Babylonians were using some form of anaesthesia. The first attempts at general anaesthesia were most likely with herbs such as opium poppies. (Miller and Pardo 2011)

The origin of the anaesthesia known today can be dated back to 1772, when Joseph Priestly (1733 – 1804), an English scientist, discovered the nitrous oxide gas. About 30 years later, Sir Humphry Davy (1778 – 1829), a British chemist and inventor, experimented with it on himself (Davy 1839). Based on the euphoria experienced upon inhalation of the gas, he dubbed nitrous oxide ‘laughing gas’. He also observed that it “appears capable of destroying physical pain, it may probably be used with advantage during surgical operations” (Davy 1800). However, the analgesic effect of nitrous oxide

was ignored until Horace Wells (1815 – 1848), an American dentist, demonstrated its utility in dentistry in 1844. Since nitrous oxide anaesthesia showed inconsistency, the use of diethyl ether spread rapidly after William T. G. Morton (1819 – 1868), an American dentist and a former colleague of Horace Wells, demonstrated it successfully at a surgery in Boston in 1846. There have been several claims to the discovery of anaesthesia and it has been credited to many individuals including Crawford Long (1815 – 1878), an American surgeon and pharmacist, who performed a surgery in 1842 under ether induced anaesthesia, but did not publish his findings until 1849. In 1847, James Y. Simpson (1811 – 1870), a Scottish Obstetrician, proposed chloroform as a viable alternative to Ether. (Miller and Pardo 2011)

Less than 30 years later, intubation, for the purposes of anaesthesia administration, had been successfully performed for the first time. In 1902, the first barbiturate, barbitone (also known as barbital), was discovered by Emil Fischer (1852 – 1919), a German chemist and Nobel Prize winner, and Joseph von Mering (1849 – 1908), a German physician. It was commercially marketed under the names “Veronal” and “Medinal” by Bayer Pharmaceuticals, Germany. Significant advances have been seen in the mid-20th century due to halogenations and the subsequent introduction of non-flammable and safe vapours, which then gradually replaced chloroform and cyclopropane. Such halogenated hydrocarbons initially included halothane and later desflurane and sevoflurane. Furthermore, the first intravenous anaesthetic, sodium thiopental, was synthesised by Ernest H. Volwiler (1893 – 1992) and Donalee L. Tabern (1900 – 1974) at Abott Laboratories, Illinois, US, in 1934 and has been tested for the first time in the same year. (Miller and Pardo 2011)

5.1.3.2 Propofol

In 1980 J. B. Glen and colleagues reported for the first time the anaesthetic activity of ICI 35 868 in mice performed at the Biology Department of ICI (Imperial Chemical Industries), London, UK (Glen 1980; Adam, Glen, and Hoyle 1980). The active agent in ICI 35 868 was 2,6-diisopropylphenol, later called propofol, which was completely unrelated to the commonly used barbiturate or steroid agents. Due to its hydrophobic

characteristics, propofol has initially been dissolved in Cremophor EL®, which acted as a formulation vehicle to stabilise the compound in aqueous environment. Cremophor EL® is a registered trademark of the BASF Corporation (Badische Anilin- und Soda-Fabrik), Ludwigshafen, Germany. However, this additive led to adverse side effects and further research towards a new formulation was needed (Lambert 2008). The new formulation published in 1984 included soya bean oil, egg phosphatidate and glycerol and is highly comparable to the current formula of propofol (Glen and Hunter 1984). Two years later propofol was first introduced in Europe, then in 1989 it was approved by the US Food and Drug Administration (FDA) for induction and maintenance of anaesthesia. "Diprivan" is the market name for propofol and stems from the abbreviated version of diisopropyl intravenous anaesthetic. It is a small hydrophobic molecule and its structure can be described as a phenol with two isopropyl groups in ortho-position to the hydroxyl group of the phenol (figure 5.05 A) (Rang et al. 2007; Glass et al. 2010).

Propofol has a very fast onset and is therefore widely used as a continuous infusion during surgeries. Furthermore, it is used in critical care for sedation of mechanically ventilated patients. The main unwanted side effects are cardiovascular and respiratory depression. However due to airway management techniques, such as intubation and close patient monitoring, these adverse events are very rare in current clinical practice (Rang et al. 2007). The human body is generally able to metabolise propofol very rapidly without cumulative effects, which assures a fast recovery from anaesthesia (Green 2007).

In-vivo, propofol is highly protein bound with reported fractions from 97 to 99% depending on its total concentration (Dawidowicz et al. 2006; Dawidowicz, Kobielski, and Pieniadz 2008b) and on certain diseases states such as diabetes, renal and hepatic insufficiency (Bohnert and Gan 2013; Dawidowicz and Kalitynski 2005; Glass et al. 2010). Approximately 80% of the administered propofol is bound to human serum albumin (HSA), which is the most abundant plasma protein in mammals (Bhattacharya, Curry, and Franks 2000; Zeitlinger et al. 2011). Studies by A. L. Dawidowicz and colleagues indicated that increases in temperature leads to increased propofol binding to HSA.

Variations in the hydration layer around the protein may play a major factor in changes in free drug fraction (Dawidowicz, Kobielski, and Pieniadz 2008a). Figure 5.05 B illustrates the crystallographic structure of the HSA protein containing two bound propofol molecules labelled with PR1 and PR2 (Bhattacharya, Curry, and Franks 2000). The binding site of PR1 is an especially well known binding site for various drugs and endogenous ligands (Curry 2011; Ghuman et al. 2005; Yamasaki et al. 2013). Due to the fact that propofol is not the main focus of this thesis, propofol's general pharmacology including possible side effects is not further discussed.

A

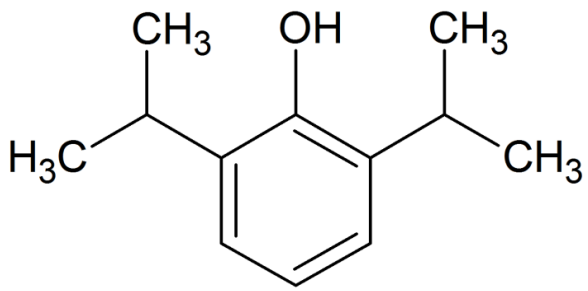

B

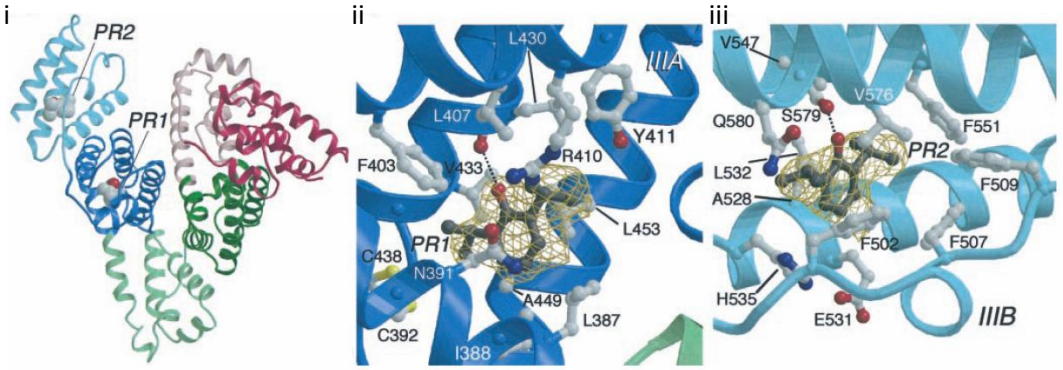

Figure 5.05: Propofol and the crystallographic structure of its binding sites on human serum albumin (HSA). A) Lewis' structure of 2,6-diisopropylphenol commonly known as propofol. B) The propofol binding sites on human serum albumin (HSA). i) Crystal structure of fatty acid free HSA containing two propofol molecules labelled with PR1 and PR2. ii) The propofol labelled with PR1 binds in sub-domain IIIA of HSA, which is an apolar pocket. The binding between the anaesthetic and the protein occurs mainly via two interactions. The first is a hydrogen bond (3.1 Å) between propofol's phenolic hydroxyl group and HSA's main-chain carbonyl oxygen of Leucine 430 (L430). The second is stacking of the propofol's aromatic ring with the sides chains of Leucine 453 (L453) and Aspargine 391 (N391). If fatty acids are present, propofol would compete with them for ligand binding. iii) The second propofol labelled with PR2 binds in a cavity located in sub-domain IIIB, which is mainly lined by aromatic residues of 4 phenylalanines (F502, F507, F509 and F551). The hydroxyl group of Serine 579 (S579) forms a hydrogen bond (2.9 Å) with propofol's hydroxyl group. In a similar way to the first binding pocket (ii), propofol binding could be prevented by ligands binding to fatty acid binding sites. Furthermore, it is believed that the binding site for propofol PR1 in the sub-domain IIIA has a higher binding affinity than the one for PR2 in IIIB (Bhattacharya, Curry, and Franks 2000). Moreover, later X-ray crystallography studies within the same group suggest that the binding site in sub-domain IIIA binds other endogenous ligands and drugs such as diazepam and ibuprofen (Curry 2011; Ghuman et al. 2005; Yamasaki et al. 2013). Schematic adopted from Bhattacharya et al., 2000.

5.1.3.3 Therapeutic Propofol Monitoring using Gibbs reagent

The clinically relevant concentrations for propofol range from about 1 to 10 µg/ml, which corresponds to 5.6 – 56.1 µM (Liu et al. 2012). Low concentrations in the range of 1.3 – 2.8 µg/ml are used to achieve sedation (Casati et al. 1999). Higher concentrations from 3 to 5 µg/ml in conjunction with adjuvants such as nitrous oxide and opiates are administered during surgery (Stuart et al. 2000). If propofol is used as a sole agent then the required concentration range is 6.0 – 8.0 µg/ml (Liu et al. 2012; Glass et al. 2010). The drug dosage is determined by population-based pharmacokinetic data and adjusted to individual patient biometrics (Langmaier et al. 2011). Currently in clinics, propofol is not directly monitored in real-time; however, patient's vital signs including ventilation, oxygen saturation, heart rate, blood pressure and level of consciousness are typically continuously monitored during administration of propofol to identify early signs of adverse events such as respiratory depression and hypotension (Rang et al. 2007; Sandiumenge Camps et al. 2000; Glass et al. 2010).

The validated methods for determining propofol concentration from blood and other biological samples are laboratory-based assays such as high performance liquid chromatography (HPLC), which require considerable time for sample preparation and analysis (Liu et al. 2012; Cussonneau et al. 2007; Dawidowicz and Fornal 2000; Langmaier et al. 2011). Furthermore, due to the fact that propofol is highly protein bound (see chapter 5.1.3.2), an additional sample preparation step, in which the red blood cells are lysed prior to the analysis, is highly recommended before HPLC analysis (Dawidowicz and Fornal 2000). However, this additional step increases the time required to carry out this already lengthy process. Therefore several different techniques have been suggested for a continuous real-time propofol measurement. These include the monitoring of exhaled air during surgery studied by various groups (Hornuss et al. 2007; Miekisch et al. 2008; Harrison et al. 2003). However, these methods have not demonstrated consistent and reliable results regarding the correlation of exhaled breath to blood propofol concentration (Liu et al. 2012).

Sphere Medical's Pelorus bench top device (see figure 5.06 A) has been designed for the rapid analysis of propofol directly from whole blood samples. A sample blood volume of 0.7 ml can be injected into the device and the propofol concentration is calculated in approximately 5 minutes (Pettigrew, Laitenberger, and Liu 2012; Liu et al. 2012). The measurement technology implemented in Sphere's device is based on a quantitative colourimetric principle via the coupling of Gibbs reagent where an intensely blue indophenolic compound is produced. As previously indicated in chapter 5.1.2, research by H. K. Adam and colleagues in 1981 established the viability of using Gibbs reagent for accurate estimation of the propofol concentration in blood. They described that propofol has a λ_{max} of 275 nm and its molar absorptivity is insufficient to allow quantification at levels occurring in biological fluids after therapeutic dosing (Adam et al. 1981). Just a year earlier, the same group were the first to report the anaesthetic activity of propofol (Glen 1980; Adam, Glen, and Hoyle 1980) (see chapter 5.1.3.2). As shown in figure 5.05 A, propofol is essentially a phenol with two isopropyl groups in the ortho-position to the hydroxyl group of the phenol. Therefore, it is likely to react with Gibbs reagent in a very comparable manner to phenol as described by Harry Drake Gibbs in 1927 (Gibbs 1927a; Gibbs 1927b) (see chapter 5.1.2.1 and figure 5.04). Adam et al. used HPLC separation followed by Gibbs coupling and subsequent quantification of propofol via UV/vis spectroscopy. They were able to detect and estimate the quantity of propofol at therapeutic levels and at concentrations as low as 25 ng/ml, which corresponds to 0.1 µM (Adam et al. 1981).

Sphere Medical's Pelorus device has implemented a solid phase extraction (SPE) method as opposed to HPLC, which was previously described by McGaughran and colleagues. They used SPE on a diluted whole blood sample followed by reaction with Gibbs reagent to produce the strongly coloured indophenolic product (McGaughran et al. 2006). The Pelorus device works after a similar principle in a fully automated manner without the requirement for sample preparation. After injection of a whole blood sample into the analyser, the sample gets diluted and the red blood cells are lysed. Propofol is then extracted via SPE and labelled with Gibbs reagent. Afterwards the instrument measures the concentration by absorption spectroscopy. The system is calibrated with two

calibration solutions containing low and high propofol concentrations respectively. Results from the Pelorus device were found to correlate linearly up to 12 µg/ml with a lower quantification limit of 0.75 µg/ml with an HPLC based method. Figure 5.06 B shows the correlation of the Pelorus 1000 to the reference HPLC method. It can be concluded that the Pelorus bench top device fulfils the requirements for monitoring propofol in whole blood samples with the required precision and accuracy in the clinically relevant range (Pettigrew, Laitenberger, and Liu 2012; Liu et al. 2012). Furthermore, in comparison to the currently validated methods for calculating the propofol concentration, the Pelours bench top device requires less space, staff, time, administration, shorter transportation distance and is consequently more cost effective (see figure 1.01).

A

B

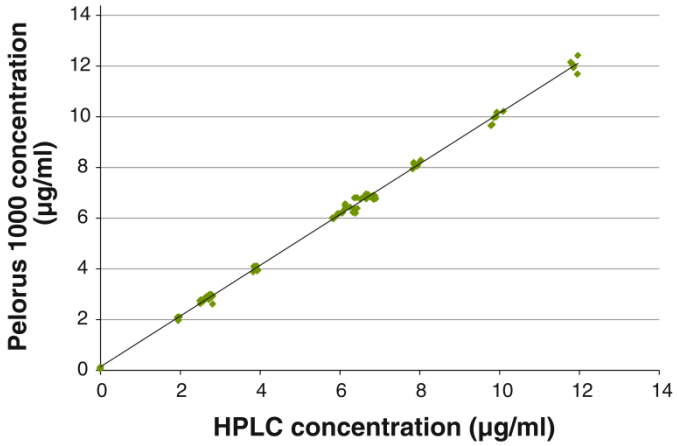

Figure 5.06: Sphere Medical's Pelorus bench top device and its correlation with a reference method. A) Photography of Sphere's Pelorus device. It is one of the first commercially available bench top devices for the rapid measurement of propofol. There are two series. The Pelorus 1500, which has CE (Conformité Européenne) mark as an in-vitro diagnostic (IVD) device for Europe and the Pelorus 1000, which is for research use only outside Europe. Image adopted from "Sphere Medical Ltd.'s Homepage: Pelorus Propofol Measurement System" 2014. **B) Scatter plot of the Pelorus 1000 versus the reference HPLC method.** The comparison shows a linear relationship over the range of 0 – 12 µg/ml. The data values were analysed with the 'Deming regression analysis'. It is a special 'total least squares' analysis which differs from the 'simple linear regression' in that it accounts for errors in both axes. The 'Deming regression analysis' results in a gradient of 1.001 with a 95% confidence interval of 0.992 – 1.010 and an offset of 0.14 µg/ml with a 95% confidence interval of 0.09 – 0.19 µg/ml. Schematic adopted from Liu et al., 2012.

5.1.4 Objectives for Proof-of-Principle & Colourimetric Benchmarking

The main objective of this thesis is the development of a PoC sensor for therapeutic antibiotic monitoring particularly for the glycopeptide antibiotic vancomycin. In order for a sensor to be developed, it must meet the general requirements that were established in the introduction in chapter 1.2.

As previously described, along with developing each detection technique for therapeutic antibiotic monitoring at the point-of-care, the overarching aim is to evaluate the feasibility of miniaturising the different techniques for patient attached real-time monitoring devices. The starting point for miniaturisation is the colourimetric detection of vancomycin by visible spectroscopy as schematically illustrated in figure 5.07, which builds on Sphere Medical's Pelorus bench top device that measures the anaesthetic propofol. This is the first out of two detection platforms studied in this body of work and it is also the technique on which my thesis was mainly focused on. Therefore, the colourimetric detection via visible spectroscopy is investigated and discussed in this chapter and in the following two chapters (6 and 7).

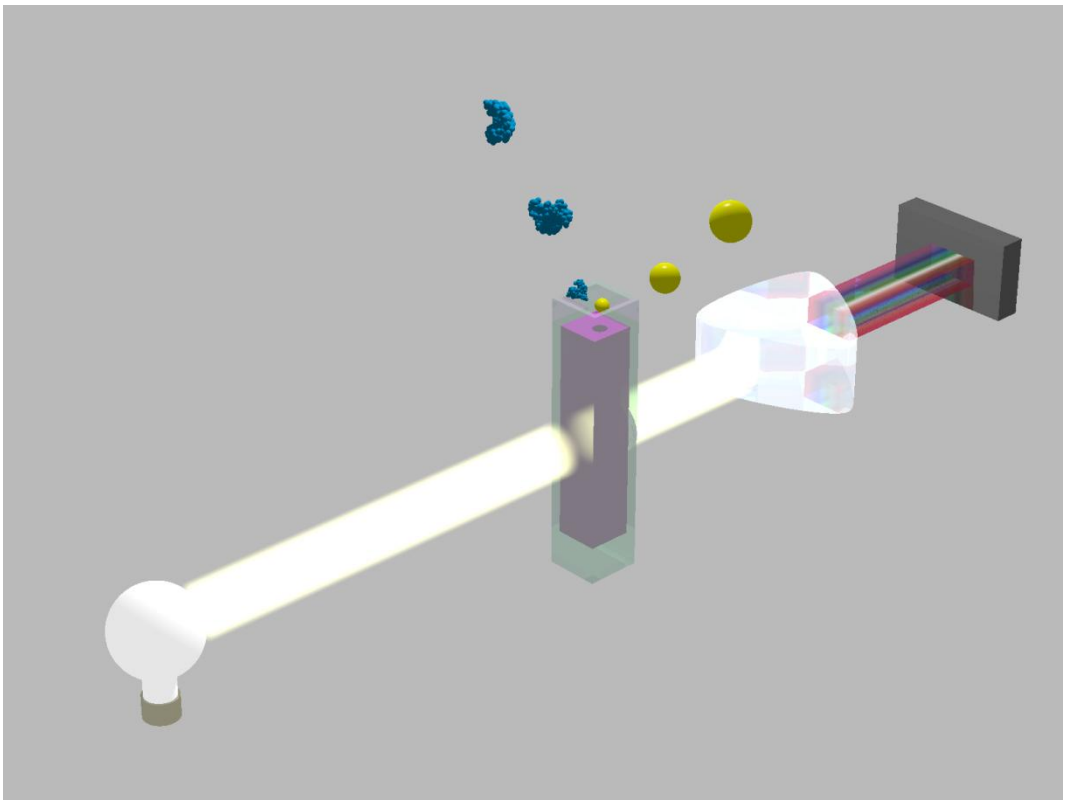

Figure 5.07: A schematic of the colourmetric detection of vancomycin via visible spectroscopy. The blue molecules depict vancomycin and the yellow spheres indicate Gibbs reagent. Upon coupling the colour changes and this can be detected via visible spectroscopy, thus quantifying the concentration of vancomycin. The colour change is indicated by the purple solution in the cuvette. The visible spectrometer is shown as a light bulb on the left and a prism and a detector on the right hand side. Even though this schematic is drawn with vancomycin molecules, it represents the general principle of colourimetric detection and could potentially work with many other drug molecules and different coupling reagents.

5.2 Materials and Methods

This chapter provides the information of the used materials and methods for the proof-of-principle (5.3.1) and benchmarking experiments for the colourimetric and optical detection assay (5.3.2). It is divided into three subchapters. The chemicals, including buffer solutions, solvents, phenolic compounds, and blood components, are described in the first subsection (5.2.1). The experimental set-up in the form of UV/vis spectrometer and the used cuvettes are presented in the second part (5.2.2). Lastly, the measurement procedure, data processing and analysis can be found in the third subsection (5.2.3).

5.2.1 Chemicals

All chemicals were purchased from Sigma-Aldrich (Dorset, UK), unless otherwise declared. They were handled, stored and disposed of in accordance with their safety guidelines stated in the corresponding 'material safety data sheets' (MSDS).

5.2.1.1 Buffer Solutions and Solvents

Borate buffer pH 10 solution was purchased from Fisher Scientific, which was initially used to either dissolve some phenolic compounds or was added to provide the required high pH for the Gibbs coupling. To dilute the hydrophobic propofol, a non-polar organic solvent is needed. According to Sphere's procedure acetonitrile (IUPAC: acetonitrile) was used. To dissolve the Gibbs reagent, methanol was used, which additionally provided the necessary primary alcohol for the solvolysis of Gibbs reagent to initiate the reaction.

5.2.1.2 Gibbs Reagent and Phenolic Compounds

2,6-dichloroquinone-4-chloroimide (IUPAC: 2,6-dichloro-4-chloroiminocyclohexa-2,5-dien-1-one) is referred to in this thesis as the Gibbs reagent (see figure 5.04). Although the original reagent H. D. Gibbs used for quantification of phenolic and hydoxypyridine derivates was 2,6-dibromoquinone-4-chloroimide, due to its toxicity it is not commercially available. Further information about the history of the Gibbs reagent can

be found in chapter 5.1.2. Two batches of Gibbs reagent were purchased with batch numbers 01705KJ and 02208KJ respectively. The first batch was used, unless otherwise declared. For the proof-of-principle experiments (5.3.1), the product of the original Gibbs reagent coupling reaction, sodium 2,6-dichloroindophenolate hydrate (IUPAC: 2,6-Dichloro-N-(4-hydroxyphenyl)-1,4-benzoquinoneiminesodium salt) was purchased. It is hereafter designated as DCPIP. For the experiments, it has been dissolved in different concentrations in either pure borate buffer or in borate buffer with 600 µM bovine serum albumin (BSA), to imitate the complex background of blood serum. BSA is listed in the next subsection '5.2.1.3 Blood Components'. The second set of the experiments (5.3.2), for benchmarking the colourimetric detection assay at UCL against Sphere Medical's system, used propofol. The anaesthetic propofol is marketed as 'Diprivan' (abbreviated version of diisopropyl intravenous anaesthetic), which is an opaque white emulsion with several ingredients such as oil and phospholipid and usually 1 % propofol (Rang et al. 2007). As a pure compound, propofol (IUPAC: 2,6-diisopropylphenol) is yellow in colour and liquid above 18 °C.

5.2.1.3 Blood Components

The experimental approach used to investigating the therapeutic monitoring of drugs needs to take into account the complex physiological background of whole human blood. It is possible that the constituent parts of human blood could interfere with the colourimetric detection of drugs using Gibbs reagent. For this reason, different blood components in increasing complexities have been studied. The starting point was fatty acid free bovine serum albumin (BSA). The albumin was dissolved in buffer in a concentration that mimics its concentration in normal blood serum. The amount of 600 µM BSA is well established and commonly used in the scientific community to mimic serum (Bohnert and Gan 2013; Bhattacharya, Curry, and Franks 2000). In the interest of brevity, buffer (and in subsequent subsections water with 600 µM dissolved BSA or fatty acid free human serum albumin (HSA)) are designated as pseudo-serum. Serum albumins are the most abundant plasma proteins in mammals. They are believed to be the proteins to which drug molecules predominately bind to (see 3.3.3) (Zeitlinger et al. 2011; Lin et al. 2013; Ndieyira et al. 2014). Wherever water or DI water is stated,

distilled and deionised water (usually abbreviated as ddH_2O, herein as water or DI water) was used. The water was purified with an ELGA Purelab Ultra water purification system (ELGA, Buckinghamshire, UK). A more detailed discussion about the serum binding particularly of vancomycin can be found in chapter 3.3.3.

5.2.2 Experimental Set-up

5.2.2.1 UV/vis Spectrometer

The used UV/vis spectrometer is an Agilent 8453 (Agilent Technologies, Santa Clara, California, US) in Dr. Daren Caruana's laboratory in the Department of Chemistry at UCL. It is a one light path spectrometer with two light sources, a deuterium lamp for the UV and a tungsten lamp for the visible range. Therefore it is capable of measuring a spectrum from 190 to 1100 nm. Its maximal absorbance value is 4 absorbance units ([AU]), which was experimentally established prior to the first experiments. The spectrometer's software is "UV-Visible ChemStation" software from Agilent Technologies.

5.2.2.2 Cuvettes

For the proof-of-principle experiments with DCPIP (chapter 5.3.1), disposable poly-methyl methacrylate (PMMA) cuvettes from Brand (BrandTech Scientific INC., Essex, Connecticut, US) have been used. However, due to the requirement of acetonitrile as solvent in the benchmarking experiments with propofol (chapter 5.3.2), the cuvettes had to be changed to the more stable disposable UV-cuvettes made of proprietary resin from Brand.

5.2.3 Measurement Procedure, Data Capturing and Analysis

The measurements were performed in a UV/vis spectrometer from Agilent Technologies with the "UV-Visible ChemStation" software. According to an empirical study performed prior to the first experiments, it was found that both light sources require a warm up

time. Therefore all experiments were performed after a 20 minute warm up period from when the bulbs were switched on. Since the Agilent 8453 spectrometer has only one light path, the reference or blank spectrum had to be captured first, which then was automatically subtracted from all further sample spectra. Different references had been studied, such as borate buffer, borate buffer with methanol, solely methanol, methanol and water mixtures and so on. The spectra data have been saved in comma-separated values (CSV) files by using the spectrometer's software. The CSV-files have been imported, plotted and analysed with Origin Pro 8.6 software (Origin Lab Corporation, Northampton, Massachusetts, USA).

Since these experiments served as the proof-of-principle and benchmarking experiments, the samples sizes were kept small and no statistical evaluation has been performed. The sample sizes for the proof-of-principle experiments (5.3.1) were two measurements of two independent samples (n = 2) and three measurements of one sample (n = 1). For the benchmarking experiments (5.3.2) three measurements of one sample were taken (n = 1). The included error bars indicate the corresponding standard deviation of the mean.

5.3 Results and Discussions

This chapter is separated into two parts. Firstly, chapter 5.3.1 demonstrates the proof-of-principle that colourimetric detection via visible spectroscopy has the potential to be an integral part of a PoC sensor for therapeutic drug monitoring. It focuses on the colourimetric detection of a known indophenolic compound using the Beer-Lambert-Bouguer law and showing a degree of sensitivity to clinically relevant drug concentrations. Secondly, chapter 5.3.2 presents the benchmarking experiments with propofol according to Sphere Medical's procedure used in their Pelorus device as described in subsection 5.1.3.3 (Pettigrew, Laitenberger, and Liu 2012; Liu et al. 2012). Since the development described herein is a consecutive process, preliminary discussions are added directly within these subsections, whilst the conclusion can be found in section 5.4.

5.3.1 Proof-of-Principle Experiments

The experiments with the commercially available end product of the Gibbs-phenol reaction, 2,6-dichlorophenolindophenol (DCPIP), served several purposes. Since the maximal absorbance wavelength (λ_{max}) and the molar absorption coefficient at this maximal absorbance wavelength (ε_{max}) are well known (see chapter 5.1.1.3 on page 84), the concentration estimation via the Beer-Lambert-Bouguer law could be directly executed without any dependency on a successful chemical reaction. Hence, independently of a reaction with two compounds and an unknown yield, it could be tested what absorbance values can be expected and whether the spectroscopic detection of clinically relevant concentrations is possible. Moreover, it may be a simple, reliable and 'coupling reagent free' calibration method for example for Sphere Medical's Pelorus device. Furthermore, it could be investigated whether detection in whole blood serum may be a possibility for the subsequent vancomycin colourimetric assay or whether the development of a specific extraction protocol cannot be circumvented, especially in relation to the non-specificity of the Gibbs coupling reaction. A direct detection assay without prior extraction would have several advantages, such as no loss of the compound of interest, increased rapidity, simpler instrumentation and consequently less associated costs, and no specificity concern according to the extraction process.

A successful monitoring assay has to meet several requirements including high sensitivity to clinically relevant drug concentrations, high specificity for the drug of interest and low interference or cross-reactivity with other drugs or blood components. To test the sensitivity of the colourimetric detection, DCPIP in different concentrations has been diluted in either borate buffer or borate buffer with 600 µM BSA. Subsequently, the absorbance spectra of different DCPIP concentrations have been captured via UV/vis spectrometer. For a therapeutic drug monitoring device, the unambiguous assignment of a single drug concentration to a single readout signal within and beyond the boundaries of the therapeutic range is crucial. Consequently, the concentrations of DCPIP have been chosen to include the clinically relevant range of propofol, which ranges from 1 to 10 µg/ml and that is equivalent to 5.6 – 56.1 µM of

propofol. Therefore, the DCPIP concentrations were chosen to range from 2 to 90 µM, which is equivalent to 0.6 - 26 µg/ml DCPIP.

Figures 5.08 A and B show overlays of the absorbance spectra of 2, 10, 30, 50 and 90 µM DCPIP in borate buffer and in pseudo-serum. Borate buffer and pseudo-serum without any DCPIP served as references. It should be highlighted that the small elevation at 632 nm is instrumental and typical for the spectrometer used. In figure 5.08 A, all spectra show clear distinctive symmetrical and typical indophenolic peaks with maxima at wavelength 605 nm (λ_{max}). The spectra of the highest concentration (26 µg/ml) shows a small drift on the left hand side of the peak, which to date is unexplained. A possible explanation could be that at these high concentrations the molecules are shadowing each other. Hence they cannot be regarded as independent chromophores. As previously described on page 83, absorbances over 1 AU are an indication that a shadowing effect may occur. This effect could cause deviations from the linear calibration curve, which will lead to inaccuracies of the Beer-Lambert-Bouguer law.

The spectra in pseudo-serum (figure 5.08 B) reveal that DCPIP's λ_{max} is bathochromic shifting approximately 30 nm towards red in the visible spectrum, from 605 to 632 nm. Furthermore, all maximal absorbances increased by values ranging from 0.04 to 0.06 AU. These values seem conserved over a fairly large concentration range of DCPIP spanning over more than a magnitude, which leads to the assumption that something constant within the sample must cause it. Consequently, it could not be increasing DCPIP and everything else such as proteins, which may denature and unfold in high pH, is subtracted by the reference. Therefore, this effect could not be explained and it was decided to not further investigate it. On the grounds of two reasons, (i) it is a conserved increase, which may result in higher sensitivity and (b) for which could be corrected for with a correction value.

As already highlighted above, the λ_{max} and ε_{max} of DCPIP are well known and therefore its concentration estimations via Beer-Lambert-Bouguer law (see chapter 5.1.1.2) can be directly applied. According to the manufacturer, DCPIP's absorption maximum can be

found at 605 nm (λ_{605nm}) and at this maximal wavelength it has a molar absorption coefficient of 21000 M^{-1} cm^{-1}. To calculate the DCPIP concentrations via Beer-Lambert-Bouguer law

$$A = \varepsilon \, c \, l \qquad 5.14$$

the absorbance values at 605 nm, have been divided by the known molar absorption coefficient at the maximal absorbance (ε_{605nm} = 21000 M^{-1} cm^{-1}) multiplied by the path length of the light (l = 1 cm), which results in concentrations (c). These calculated concentrations have been plotted against the diluted concentrations. Figure 5.08 C presents this concentration comparison of DCPIP in borate buffer. The y-error bars correspond to the range from two measurements taken at different time points after preparation (5 and 15 minutes) of two independent sets of samples (n = 2). X-errors are not indicated. However, it has to be highlighted that dilution errors of two kinds can occur and may contribute to a potential x-error. The first kind is an instrumental error arising from the Gilson micro pipettes and the second kind is an experimental error introduced by the experimenter. Both types were minimised or kept similar by generally good laboratory practices and specifically by strict and constant dilution procedures.

The same comparison of calculated to diluted concentrations is shown in figure 5.08 D for DCPIP in pseudo-serum. Additionally, a second set of concentrations according to the absorbance values at the shifted maximum wavelength, 632 nm, was calculated and plotted. Nonetheless, the molar absorption coefficient of 605 nm (ε_{605nm}) has been kept for these calculations. The y-error bars are standard deviations of the mean derived from three measurements taken at different time points after preparation (5, 10 and 20 minutes) on one sample (n = 1), which are consequently very small and not significant. In both figures (5.08 C and D) it can be observed that generally low concentration calculations are in fairly good agreement with the corresponding calibrated concentrations. However, high concentrations, even taking errors into account, do not correlate very well. This may again be caused by the shadowing effect within these high concentrations mentioned earlier, which could lead to deviations from

the linear calibration curve and resulting in inaccuracy of the Beer-Lambert-Bouguer law. It seems that the concentrations calculated with the bathochromic shifted absorbance maximum in serum ($\lambda_{max\ shifted}$ = 632 nm) (figure 5.08 D) fit slightly better the comparison with the concentration of the diluted solutions.

In conclusion, even though the samples sizes were kept small and at high concentrations a deviation has been observed, the proof-of-principle experiments were considered successful. The objective was to prove the principle of colourimetric detection by visible spectroscopy and to consequently show its potential as an integral part of a PoC sensor for therapeutic drug monitoring. It could be demonstrated that by using the Beer-Lambert-Bouguer law the concentrations can be estimated and the detection is sensitive in the clinically relevant concentration range. The observed deviation from the linear correlation for high concentrations are beyond the clinically relevant range and could, if required, be curbed by using an additional high calibration concentration. Furthermore, the experiments in serum showed promising results towards possible circumvention of a specific extraction protocol prior to the colourimetric detection. However, it has to be emphasised that this is just one aspect of direct detection in serum and interference, cross-contamination and Gibbs reagent's non-specificity still have to be further investigated. Besides the proof of principle, the DCPIP assay seems reliable, can be performed rapidly and is stable over at least 20 minutes. Hence it provides many characteristics for a potential calibration system for Sphere Medical's Pelorus device.

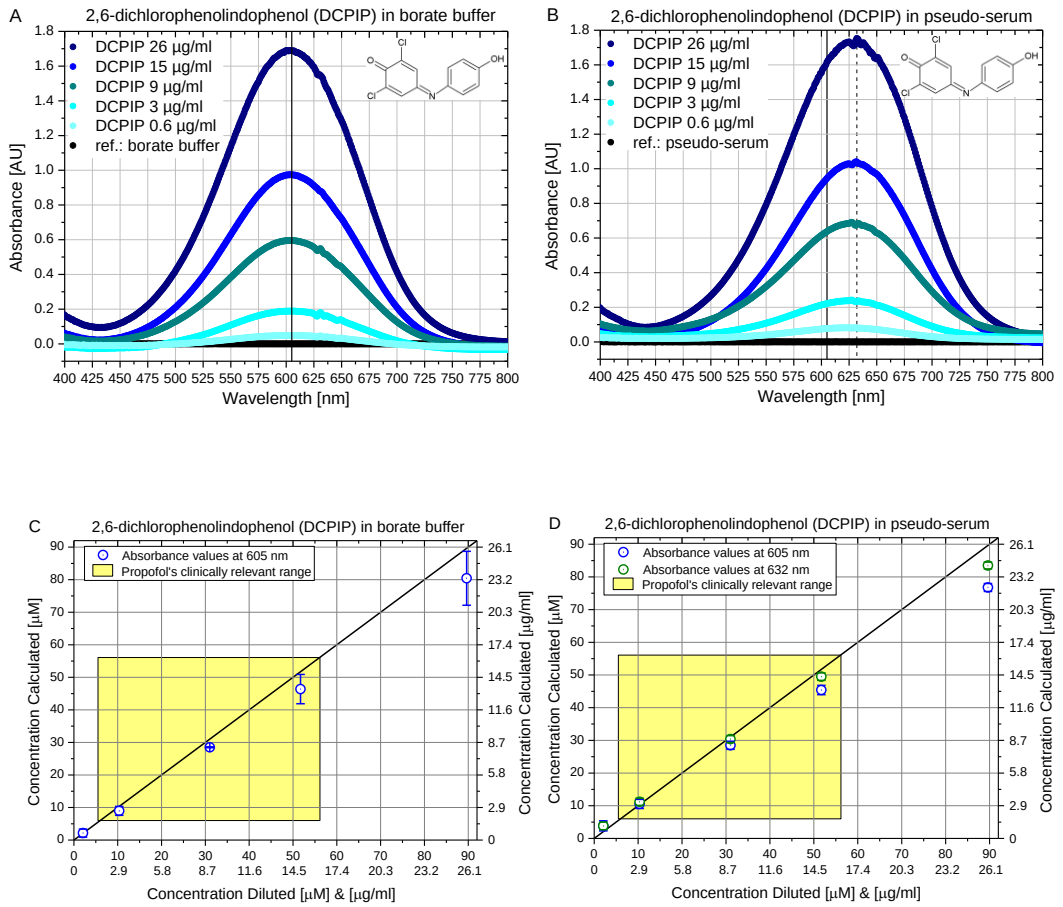

Figure 5.08: Proof-of-principle experiments with the commercially available product of the Gibbs-phenol reaction. A) Dilution series of 2,6-dicholorphenolindophenol (DCPIP) in borate buffer. Absorbance spectra of DCPIP in different concentrations in borate buffer. Reference is borate buffer. Vertical line at 605 nm corresponds to λ_{max} of DCPIP. **B) Dilution series of 2,6-dicholorphenolindophenol (DCPIP) in pseudo-serum.** Pseudo-serum corresponds to 600 µM BSA in borate buffer. Reference is pseudo-serum. Dashed line shows the bathochromic shifted λ_{max} (632 nm) in serum. **C) Beer-Lambert-Bouger law calculations of DCPIP's concentrations in borate buffer.** Error bars indicate the range obtained from 2 measurements of 2 independent samples (n = 2). **D) Beer-Lambert law calculations of DCPIP's concentrations in pseudo-serum.** Error bars are standard deviations derived from 3 measurements of 1 sample (n = 1) and are therefore very small and not significant.

5.3.2 Benchmarking Experiments with Gibbs Reagent and Propofol

The experiments to benchmark the colourimetric detection platform at UCL to Sphere Medical's Pelorus device were performed based on Sphere's experimental procedure, described in subsection 5.1.3.3 (Pettigrew, Laitenberger, and Liu 2012; Liu et al. 2012). A range of propofol concentrations were diluted in acetonitrile, which is the elution solvent for the solid phase extraction (SPE). Gibbs reagent was dissolved in methanol, which serves as the primary alcohol needed for the initial solvolysis required for the coupling reaction (see chapter 5.1.2.2). Gibbs reagent and borate buffer at pH 10, which provided the crucial alkaline pH, were added to the propofol/acetonitrile solution. Immediately after mixing, a colour change from a clear transparent to a striking blue colour was observed.

Figure 5.09 A shows the absorbance spectra of 0.8 mM Gibbs in methanol reacted with propofol in different concentrations (2, 4, 8, 12 and 20 µg/ml) according to the described procedure. The concentrations have been chosen to include the clinically relevant propofol concentrations ranging from 1 to 10 µg/ml corresponding to 5.6 – 56.1 µM. Sphere's Pelorus device measures the absorbance at a wavelength of 595 nm, which is marked with a dotted black line. The reference used in this experiment was the same reaction mixture but in the absence of propofol. All absorbance spectra showed the distinctive indophenolic peak at 595 nm. However, the two low concentrations (2 and 4 µg/ml) show large drift on the left hand side of the peak, which remains unexplained. However, since these experiments served as benchmarking experiments, repeats were not deemed necessary and no further investigations were performed.

To quantify the concentration of propofol in the sample, Sphere Medical uses two known calibrations solutions, 2.5 and 7.5 µg/ml of propofol, which are measured prior to the experiments and analysed via linear regression fit. According to these calibration samples the unknown sample concentrations are calculated via the Beer-Lambert-Bouguer law (see chapter 5.1.1.2),

$$A = \varepsilon\, c\, l \qquad 5.14$$

Following Sphere's procedure, the average of three spectra from three independent samples (n = 3) for 2 and 8 µg/ml of propofol were used to calculate the molar absorption coefficient of the coupling product at 595 nm (ε_{max}). Figure 5.09 shows these two absorbances including their y-errors, which are the standard deviations from the mean derived from the three independent samples (n = 3). The linear fit (depicted in red) through these values was forced to intercept zero and resulted in a slope of 0.017 ± 0.002 and an adjusted R^2 of 0.977. According to the Beer-Lambert-Bouguer law, the slope of a linear fit through data points arising from concentrations versus absorbances at a certain wavelength, presumably the maximal absorbance wavelength (λ_{max}) of the compound of interest, is a direct measure of the molar absorptivity at this wavelength ε. However, this only applies if the utilised cuvette has a path length (l) of 1 cm. Therefore, the molar absorptivity (ε_{max}) of the coupling product, Gibbs-propofol, was found to be 17000 ± 2000 M^{-1} cm^{-1}. This is comparable to the commercially available DCPIP, which has an $\varepsilon_{605\,nm}$ of 21000 M^{-1} cm^{-1} (see previous subsection 5.3.1 and third example on page 84).

After calculation of ε_{max}, all concentrations (2, 4, 8, 12 and 20 µg/ml) were treated as 'unknown' and the calculated $\varepsilon_{595\,nm}$ was used to estimate them via the Beer-Lambert-Bouguer law. Figure 5.09 C shows these calculated concentrations versus the diluted concentrations. The diagonal line indicates the region of the most optimal case, which would be if the calculated concentrations match exactly the diluted concentrations. 20 µg/ml is not shown due to the facts that it is double the upper end of the clinically relevant concentration range and showed a large deviation from the linear relationship. The latter observation however is in good agreement with the findings from the previous subsection (5.3.1) and the Pelorus device described in chapter 5.1.3.3, which report deviation from linearity above 12 µg/ml propofol (Pettigrew, Laitenberger, and Liu 2012; Liu et al. 2012). The calculated concentration, including accounted error bars, for the low concentration of 2 µg/ml correlates with the diluted concentration, but not the high concentration of 12 µg/ml propofol. The y-error bars correspond to the standard deviations of the mean derived from the three independent samples (n = 3). As discussed in the previous section (5.3.2), x-errors are not indicated.

However, despite these drifts and deviations, the experimental results were considered to be comparable to Sphere's results. Furthermore, the calculated $\varepsilon_{595\ nm}$ for the Gibbs-propofol molecule was in good agreement with DCPIP's $\varepsilon_{605\ nm}$.

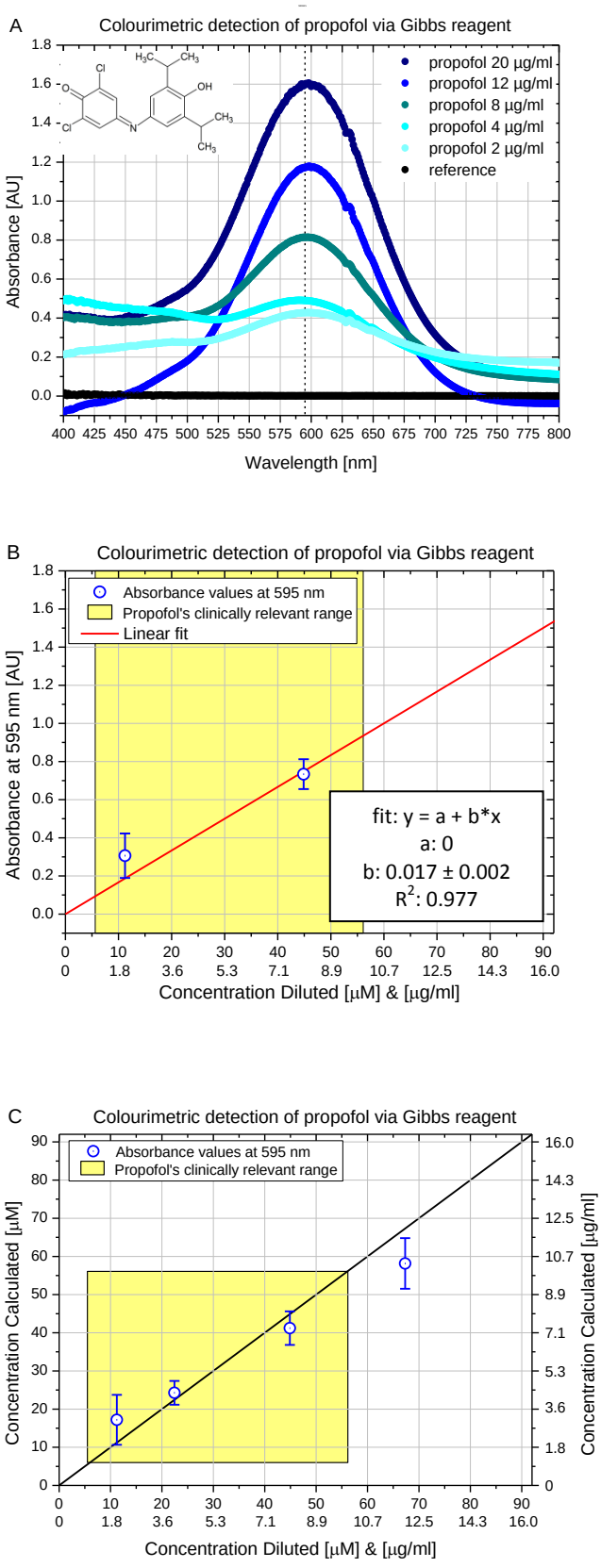

Figure 5.09: Benchmarking experiments for the colourimetric detection of propofol via coupling reactions with Gibbs reagent.
A) Dilution series of propofol labelled with Gibbs reagent. Absorbance spectra of 0.8 mM Gibbs in methanol reacting with different concentrations of propofol in acetonitrile. Borate buffer was added to the reaction mixture to provide the required high pH. The same mixture without propofol served as a reference. The dotted line at 595 nm marks the wavelength, which is used in Sphere Medical's Pelorus bench top device to calculate the drug's concentration. Elevation at 632 nm is instrumental and characteristic for the spectrometer used.
B) Estimation of the Gibbs-propofol's molar absorptivity. The differential absorbances of propofol reacted with Gibbs reagent are plotted against the corresponding concentrations. The indicated error bars are standard deviations of the mean derived from three independent samples (n = 3). According to the Beer-Lambert-Bouguer, the slope of the linear fit gives an estimate of the Gibbs-propofol's molar absorptivity ($\varepsilon_{595\ nm}$). It was found to be 17000 ± 2000 M^{-1} cm^{-1}. The yellow box highlights propofol's therapeutic window.
C) Beer-Lambert-Bouguer law calculations of propofol's concentrations. The calculated $\varepsilon_{595\ nm}$ was used to calculate the concentrations. These calculated concentrations were then plotted against the diluted concentrations. The error bars are standard deviations derived from three independent samples (n = 3). The yellow box highlights again propofol's therapeutic window.

5.4 Conclusion and Outlook

The proof-of-principle experiments with DCPIP in subsection 5.3.1 demonstrated that by using the Beer-Lambert-Bouguer law clinically relevant concentrations can be spectroscopically quantified. The experiments in serum showed promising results that a specific extraction may not be required. Furthermore, the DCPIP assay seems reliable, can be performed rapidly and is stable over at least 20 minutes. Hence, it fulfils many requirements for a potential calibration system. Consequently, it was proposed to Sphere Medical for their Pelorus device, in which it is in use nowadays.

The benchmarking experiments to the Pelorus device in subsection 5.3.2 were considered successful despite some drifts and deviations. Furthermore, the calculated $\varepsilon_{595\,nm}$ for the Gibbs-propofol molecule was comparable to DCPIP's $\varepsilon_{605\,nm}$.

In conclusion, it was deemed appropriate to move onto the development of the colourmetric detection of vancomycin, which will be further discussed in the next chapter (6).

CHAPTER 6:

Colourimetric Detection of Vancomycin

The main objective of this PhD thesis is the development of a PoC sensor for therapeutic antibiotic monitoring, particularly for the glycopeptide antibiotic vancomycin. The starting point of this development is the colourimetric detection of vancomycin by visible spectroscopy built on the principle of Sphere Medical's Pelorus bench top device.

The previous chapter presented the proof-of-principle with DCPIP and the anaesthetic propofol and benchmarking experiments to Sphere Medical's data. This chapter presents the first successful vancomycin-Gibbs colourimetric detection assay at clinically relevant concentration in whole blood within minutes. The work led to our patent submission "Analyte Extraction Apparatus and Method" (Kappeler et al. 2013).

In order for a sensor to be developed, it must meet the general requirements that were established in chapter 1.2. The last point is of particular importance for the therapeutic monitoring of vancomycin, as it states that an additional benefit for a sensor would be the option to monitor free and active drug concentration.

This chapter is divided into four subsections. The introduction in subsection 6.1 summarises the hypothesis, the unmet clinical needs and the findings from the previous chapter. Subsection 6.2 lists the additional materials and methods used hereafter. Subsection 6.3 presents the results including preliminary discussions and is structured in major milestones of the development process. It continues into the final subsection (6.4) with the overall discussion and conclusion.

In the following, chapter 7 will analysis the labelling reaction and the novel compound.

6.1 Introduction

To specifically develop an optical quantitative detection assay for the antibiotic vancomycin during my PhD several objectives have been considered. The first and most important one is the compatibility with Sphere Medical's existing Pelorus bench top device because of the associated market opportunities. Sphere Medical developed an assay to detect the anaesthetic propofol by labelling its phenolic moiety with Gibbs reagent (Adam et al. 1981; Pettigrew, Laitenberger, and Liu 2012; Liu et al. 2012). Gibbs reagent is named after Harry Drake Gibbs who used it 1927 to detect phenol and its derivates. Gibbs reagent induces a striking colour change by extending the conjugation in a molecule and the concentration of the newly produced light absorbing species can be accurately measured via visible spectroscopy (Gibbs 1926a; Gibbs 1926b; Gibbs 1927a; Gibbs 1927b). An extended explanation and discussion of the history of the Gibbs reagent, the reaction mechanisms and their applications can be found in the preceding chapter in subsection 5.1.2.

Vancomycin, as a heptapeptide, absorbs around 280 nm with values referenced between 280 – 282 nm (Nieto and Perkins 1971; Nagarajan 1994; "The Merck Index Online - Vancomycin" 2013) and has a molar absorptivity at 282 nm (ε_{282nm}) of 5943 M^{-1} cm^{-1} in water ("The Merck Index Online - Vancomycin" 2013). Herein, the maximal absorbance wavelength of vancomycin (λ_{max}) has been taken as 281 nm as it is the median of the aforementioned values. In conclusion, vancomycin can just about be detected in quartz glass cuvettes with a typical UV/vis spectrometer that ranges from about 200 to 1100 nm.

However, direct UV/vis detection of vancomycin in sample that additional contains proteins will be very complicated. Since due to their aromatic rings, which are paired with groups that are extending this delocalised system, the amino acid tyrosine (Tyr, Y) and especially tryptophan (Trp, W) absorb around 280 nm and consequently 282 nm as

well[4]. Tryptophan has a molar absorptivity at 282 nm (ε_{282nm}) of 5600 M^{-1} cm^{-1} and tyrosine an ε_{282nm} of 1200 M^{-1} cm^{-1} both measured in guanidinium hydrochloride dissolved in phosphate buffer at pH 6.2 (Gill and von Hippel 1989; Sułkowska 2002). Further if two cystines (Cys, C) residues are linked by a disulfide bond, they absorb around 280 and 282 nm as well. However, their effect is small as their molar absorptivity is only 100 M^{-1} cm^{-1} (Gill and von Hippel 1989).

Even though tyrosine and especially tryptophan are among the rarer amino acids in the average protein, they still influence the protein's absorbance characteristic due to their fairly large molar absorptivity. Human serum albumin (HSA), which is the most abundant plasma protein in humans, has one tryptophan and 19 tyrosines. Its counterpart in bovines, bovine serum albumin (BSA) has two tryptophans and 17 tyrosines (Sułkowska 2002; Zeitlinger et al. 2011). Since serum albumin's concentration in serum is about 600 µM, their absorbance will completely mask the absorbance of vancomycin in therapeutic concentrations of 4 to 28 µM (Bohnert and Gan 2013). Moreover, the Gibbs reagent may couple to tyrosines as it has a phenolic moiety. Even though the phenolic moiety is para-substiuted, as previously discussed, this may not prevent a successful Gibbs coupling (Dacre 1971; Josephy and Van Damme 1984) (see subsection 5.1.2).

Furthermore besides serum albumin, there are other proteins present in serum such as globulins, as well as electrolytes, antibodies, antigens, hormones and exogenous substances, which may absorb in this wavelength region as well. Therefore an absorbance enhancement possibly paired with an extraction procedure seems inevitable for an optical therapeutic vancomycin monitoring (TVM) device.

Moreover it has to be considered that solvents, including methanol, are absorbing in this wavelength region too and they may be required for the extraction of vancomycin from whole blood samples. The absorbances of solvents will be further discussed below in subsection 6.2.3 and figure 6.04.

[4] Phenylalanine has only one aromatic ring without a functional group or heteroatom that provides further extension of the aromatic ring's delocalised system and consequently has its maximal absorbance wavelength at around 260 nm (Ichikawa and Terada 1979).

Since vancomycin has several aromatic groups, including some phenolic moieties, one hypothesis is that Gibbs reagent couples to one or several of these. The resulting indophenolic structures would allow quantification via visible spectroscopy and therefore enhance the absorbance. The schematic in figure 6.01 illustrates a possible coupling reaction of the Gibbs reagent to position 6 in the 7th residue of vancomycin via an electrophilic aromatic substitution (S_EAr). Position 6 in the 7th residue of vancomycin is the para-unsubstituted position of the hydroxyl group at position 3. The 7th residue is a dihydroxy benzene (IUPAC: benzene-1,3-diol), which is colloquially know as resorcinol or resorcin.

It has to be highlighted that the addition may occur to another position of the vancomycin molecule such as the position 2 in the same residue (7th), other aromatic moieties that may become phenolic or to amine groups, as it was previously presented in subsection 5.1.2.2 (De Boer et al. 2007; Kovar and Teutsch 1986; Kallmayer and Thierfelder 2003; Annapurna et al. 2010). Moreover, these alternative additions could result in multiple coupling reactions accompanied with maybe even fragmentation of the vancomycin molecule. These alternative reactions as well as the structural characterisation of the novel product will be further discussed in chapter 7.

As indicated in the previous chapter in subsection 5.1.2.2, two references could be found describing Gibbs reagent reaction with antibiotics.

i) The first paper is by H. G. Daabees et. al. and presents the use of Gibbs reagent for the colorimetric detection of some antibiotics, namely amoxicillin (a β-lactam antibiotic), mixtures of amoxicillin with nystatin (an antifungal drug) and dicloxacillin (a β-lactam antibiotic), cefadroxil and cefoperazone (both cephalosporin antibiotics) (Daabees et al. 1998).

ii) The second reference is by P. S. N. H. R. Rao and colleagues and writes about the spectrophotometric detection of dobutamine (a symphathomimetic drug) and vancomycin with different chemicals including Gibbs reagent. However, the paper

could not be obtained online, via the British library or via email from the authors or their respective university. Only its abstract has been found in the search by the patent office. The abstract mentions “acidic conditions” and a maximal absorbance wavelength of 460 nm. Additionally, the thesis by K. B. M. Krishna presents briefly this paper in a literature review. He wrote: “Rao et al [P. S. N. H. Ramachandra Rao, T. Siva Rao, U. Viplava Prasad and C. S. P. Sastry. Spectrophotometric methods for the determination of dobutamine and vancomycin in formulations. Indian pharmacist. 2(9): 59-61(2003)] developed a spectrophotometric determination of dobutamine and vancomycin in pure samples and dosage forms based on the formation of yellow coloured (λ_{max} at 400 nm) and condensation product with ethylacetoacetate in sulfuric acid medium.“ (Krishna 2010). Consequently, it remains unknown whether they successfully managed to couple the Gibbs reagent to vancomycin and to which part of the molecule the addition occurred.

Moreover, Sphere Medical had previously tried to label vancomycin with Gibbs reagent. However, the obtained results were not conclusive. Conclusively, without a greater understanding of the reaction mechanism and a reduction in background interferences, this assay would not be viable as a commercial product.

Therefore, the main objective of this part of the thesis is to develop a method to label vancomycin and consequently gain the ability to quantify its unknown concentration in a complex sample matrix – ultimately whole blood. Besides the just described objective, further objectives have been previously discussed (subsection 4.3). They in particular include the urgent need for free drug quantification and the benefits for the health economic case of therapeutic vancomycin monitoring.

Hence the two main objectives for this section describing the colourimetric detection of vancomycin can be summarised as follows:

i) The first objective is to develop a method to label vancomycin for subsequent colourimetric quantification. This labelling reaction has to allow quantification in vancomycin's therapeutic range. The starting point will be the Gibbs reagent.

ii) The following objective is to demonstrate this method for a whole serum sample. If necessary, this may include the development of an extraction protocol prior to the labelling reaction. This extraction protocol will aim to reduce the complexity of the sample, remove interfering and cross-contaminating species and may additionally increase the concentration of the compound of interest, thus improve the accuracy and sensitivity of subsequent quantification for TVM.

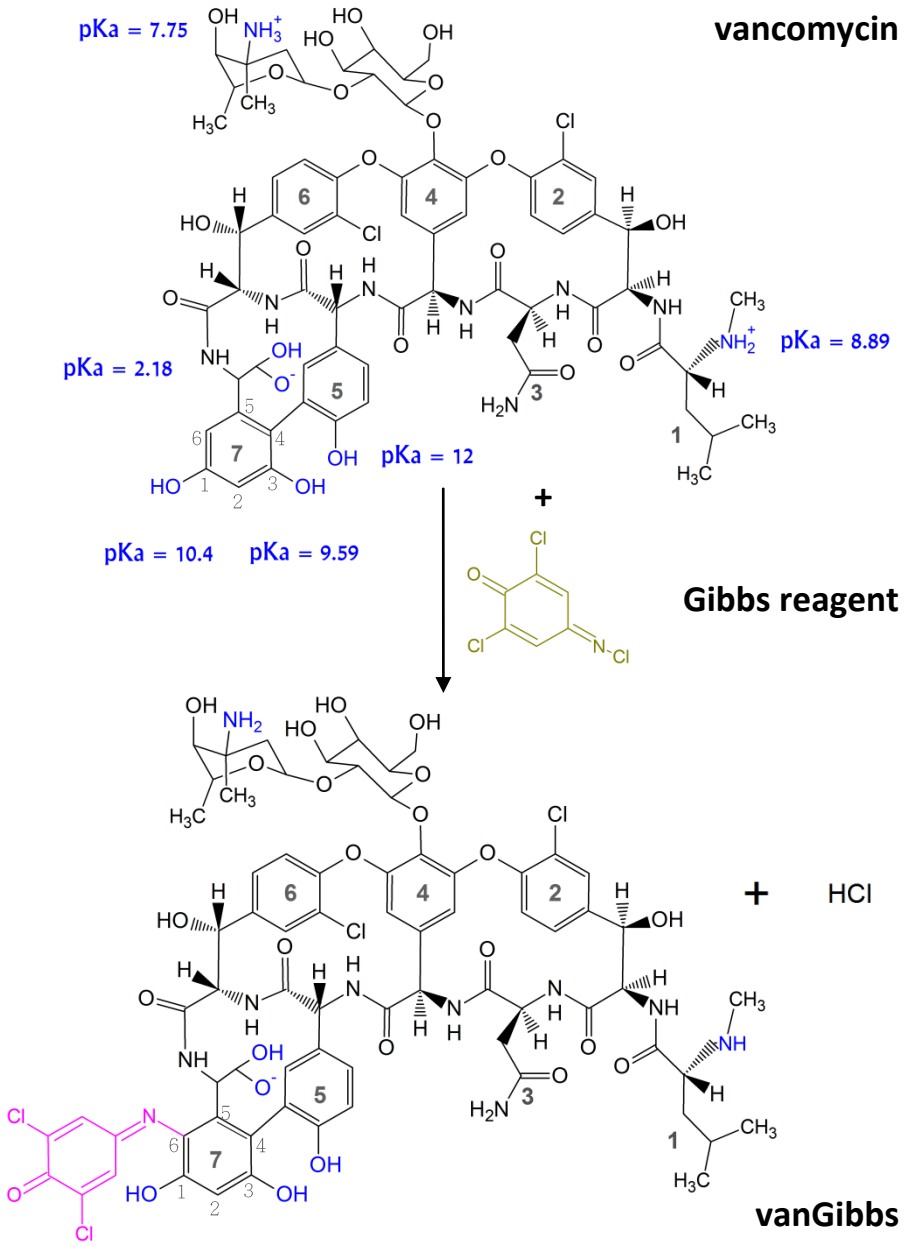

Figure 6.01: Hypothesis of Gibbs reagent coupling to vancomycin resulting in a novel vanGibbs molecule. Based on the theory of the Gibbs reaction, coupling to the para-unsubstituted position of the hydroxyl group at position 3 in 7th residues of vancomycin via an S_EAr seems a likely scenario. The coupled Gibbs molecule is indicated in purple in the vanGibbs molecule. One isomeric structure of vanGibbs was chosen as an example for many possible isomers. It has to be highlighted that the addition may occur to another position of the vancomycin molecule such as the position 2 in the same residue (7th), other aromatic moieties that may become phenolic or addition to amine groups. This could result in multiple additions accompanied with maybe even fragmentation, which will be further discussed in chapter 7. Furthermore, the coupling reaction requires high pH. Therefore the charged groups of the vancomycin scaffold were adjusted to an assumed pH of around 8.9 to 9.5 resulting in an overall charge change from $+1$ to -1. The pKa values were taken from Takács-Novák, Noszál, Tókés-Kövesdi, & Szász, 1993.

6.2 Materials and Methods

This subsection describes the materials and methods associated with the colourimetric detection of vancomycin. This materials and methods subsection is divided into three subchapters, namely chemicals (6.2.1), the experimental instrumentation (6.2.2) and measurement procedure, data processing and analysis including statistics (6.2.3).

6.2.1 Chemicals

All chemicals were purchased from Sigma-Aldrich (Dorset, UK), unless otherwise declared. They were handled, stored and disposed of in accordance with their safety guidelines stated in the corresponding 'material safety data sheets' (MSDS).

6.2.1.1 Buffer Solutions, Solvents and Antibiotic

Borate buffer pH 10 solution was purchased from Fisher Scientific, which was initially used to dissolve the antibiotic vancomycin and to provide the required high pH for the Gibbs addition. Later in the development process, vancomycin was dissolved in distilled and deionised water (usually abbreviated as ddH_2O, herein as water or DI water) and the necessary pH was achieved by adding 0.4 M sodium hydroxide (IUPAC: sodium hydroxide) in water. The water was purified with an ELGA Purelab Ultra water purification system (ELGA, Buckinghamshire, UK). Methanol was used in order to dissolve the Gibbs reagent. It also provided the required primary alcohol for the solvolysis of Gibbs reagent to initiate the reaction. The antibiotic vancomycin was purchased as vancomycin hydrochloride hydrate (IUPAC: (1S, 2R, 18R, 19R, 22S, 25R, 28R, 40S)- 48- {[(2S, 3R, 4S, 5S, 6R)- 3- {[(2S, 4S, 5S, 6S)- 4 - amino- 5 - hydroxy- 4, 6- dimethyloxan- 2- yl]oxy}- 4, 5- dihydroxy- 6- (hydroxymethyl)oxan- 2- yl]oxy}- 22- (carbamoylmethyl)- 5, 15- dichloro- 2, 18, 32, 35, 37- pentahydroxy- 19- [(2R)- 4- methyl- 2- (methylamino)pentanamido]- 20, 23, 26, 42, 44- pentaoxo- 7, 13- dioxa- 21, 24, 27, 41, 43- pentaazaoctacyclo [26.20.2.23, 6.814, 17.18, 12.129, 33.010, 25.034, 39] pentaconta- 3, 5, 8(48), 9, 11, 14, 16, 29(45), 30, 32, 34, 36, 38, 46, 49 - pentadecaene- 40 - carboxylic acid).

6.2.1.2 Blood Components

The experimental approach used to investigating the therapeutic monitoring of drugs, such as vancomycin, needs to take into account the complex physiological background of whole human blood. It is possible that the constituent parts of human blood could interfere with the colourimetric detection of vancomycin using Gibbs reagent. For this reason, different blood components in increasing complexities have been studied. As described in the previous chapter (5.2.1.3), fatty acid free BSA marked the starting point for mimicking normal blood serum. Later in the development process, fatty acid free HSA was used. Serum albumins are believed to be the proteins to which drugs predominately bind to (Zeitlinger et al. 2011; Lin et al. 2013; Ndieyira et al. 2014). A more detailed discussion about the serum binding particularly of vancomycin can be found in chapter 3.3.3.

After injection of a whole blood sample into Sphere's Pelorus device analyser, the sample gets diluted and the red blood cells are lysed. Propofol is then extracted via solid phase extraction (SPE) (Liu et al. 2012; Pettigrew, Laitenberger, and Liu 2012). Therefore, experiments were performed with foetal bovine serum (FBS) and whole human serum (WHS), marking the last complexity step before one would consider testing with human blood samples. FBS from both European and American bovine specimens were used in this investigation. In the course of this investigation no significant difference between those two types were found. WHS was extracted from a male donor of US origin with an AB blood type. The serum was endotoxin tested and sterile-filtered by the supplier.

6.2.1.3 Interferents

In order to investigate the specificity of the developed extraction protocol, four interferents were chosen based on their possible presence in patient blood samples and the presence of phenolic motifs in their structure. In light of the previously proven ability for Gibbs reagent to couple to the anaesthetic propofol; propofol, tyrosine, dopamine and paracetamol were selected (see figure 6.02). Tyrosine (IUPAC: (S)-

Tyrosine or L-2-Amino-3-(4-hydroxyphenyl)propanoic acid) was purchased as L-tyrosine, which is a crystalline white solid. Dopamine (IUPAC: 4-(2-aminoethyl)benzene-1,2-diol) was supplied as dopamine hydrochloride, which is a white powder. Paracetamol (IUPAC: N-(4-hydroxyphenyl)ethanamide or N-(4-hydroxyphenyl)acetamide) is alternatively named acetaminophen. It was bought as an over-the-counter preparation from the local pharmacist due to limited availability from Sigma-Aldrich (Dorset, UK). The active ingredient within one capsule was 500 mg paracetamol, which has been used as the basis for calculating the sample concentration. It has to be highlighted that this over-the-counter preparation also contains additives including maize starch, sodium laurilsulfate and magnesium stearate ("Leaflet: Boots Paracetamol 500 mg Capsules from Boots Pharmaceuticals" 2011). The objectives were to determine whether these four interferents are eluted out together with vancomycin and if so, whether they react with the Gibbs reagent to form an indophenolic motif that would absorb in the same region as vancomycin labelled with Gibbs. It has to be emphasised that these four interferents do not form an exhaustive investigation into potential interferents and further studies concerning this matter will need to be performed. For example a possible interferent may be salicylic acid which is the active metabolite of aspirin (Sneader 2000). Furthermore, depending on the results of these studies, these interferents could become the compound of interest for monitoring purposes in their own right. Expanding this research beyond the scope of propofol and vancomycin, a multi-analyte therapeutic drug monitoring device might be a feasible proposition in the future.

6.2.2 Experimental Instrumentation

6.2.2.1 UV/vis Spectrometer

As previously described in subsection 5.2.2.1, the used UV/vis spectrometer was a one light path spectrometer from Agilent (Agilent Technologies, Santa Clara, California, US) located in Dr. Daren Caruana's laboratory in the Chemistry Department of UCL.

6.2.2.2 Cuvettes

For the following vancomycin experiments, quartz glass cuvettes from Hellma (Hellma Analytics GmbH & Co. KG, Müllheim, Germany) were used instead of disposable cuvettes. This is due to the fact that absorbances below 300 nm wavelength were of interest as well. These could not be measured with the disposable cuvettes used since some plastics absorb below 300 nm. All cuvettes used had a path length (l) of 1 cm.

6.2.2.3 Solid Phase Extraction

The extraction protocol established hereafter is a solid phase extraction (SPE) technique that utilises Strata-X 33u Polymeric Reversed Phase (30 mg/1 ml sample) cartridges from Phenomenex® (Phenomenex, Macclesfield, Cheshire, UK) (see figure 6.03). According to the manufacturer, the named Strata-X reversed phase sorbent retains analytes by hydrophobic interactions, such as conventional C18 or C8 reverse phase columns, but also by hydrogen- and π-π bonding resulting in stronger retention of aromatic and polar analytes. This enhanced retention allows washing with organic solvents without breaking the interaction between the analyte and the stationary phase. Therefore, it is suitable for polar and non-polar analytes. Every cartridge was conditioned with 1 ml methanol and equilibrated with two times 1 ml of DI water prior to usage. SPE cartridges can be operated in a parallel manner with a vacuum manifold. Beside the significant reduction in time, it also has the advantage of completely drying out the polymer. Nonetheless, as discussed further in the following results chapter (subsection 6.3.3), the majority of the experiments were performed with gravity flow. Further information including the reasoning behind this choice can be found in the same subsection (6.3.3) and in the conclusion and outlook chapter (6.3.8).

6.2.2.4 Homogenous enzyme immunoassay

The last set of experiments presented in this chapter (6.3.8) is the direct comparison of the developed colourimetric TVM assay with a gold standard technique routinely employed in clinics. The different gold standard assays are discussed in chapter 4.1.

The hereafter used gold standard technique is the competitive, homogenous enzyme immunoassay "VANC2" from COBAS®, Roche (Roche, Basel, CH). It belongs to the group of the enzyme multiplied immunoassay technique, which are commonly abbreviated as EMIT (see chapter 4.1). This assay is the technique of choice in the diagnostic laboratories of the Whittington Hospital NHS Trust and the University College London Hospital (UCLH). The latter is where the prepared samples were sent to and kindly measured by Dr. Anne Dawnay.

The VANC2 assay has a lower detection limit of 1.7 µg/ml, which according to the technical support corresponds to 1.2 µM of vancomycin (conversion factor: µg/ml · 0.690 = µM) ("Package Insert: VANC2 COBAS® from Roche Diagnostics" 2012). This limit represents the lowest measurable analyte level that can be distinguished from zero and is calculated as the value lying two standard deviations above the measured value for zero (1 + 2 StDev, n = 21). The measuring range of the VANC2 is stated as 1.7 – 80.0 µg/ml of vancomycin, which corresponds to 1.2 – 55.2 µM. (Yeo, Traverse, and Horowitz 1989; "Package Insert: VANC2 COBAS® from Roche Diagnostics" 2012; Domke, Cremer, and Huchtemann 2000; Hermida, Zaera, and Tutor 2001; Domke 2002)

6.2.3 Measurement Procedure, Data Capturing and Analysis

6.2.3.1 Measurement Procedure and Data Capturing

The measurements were performed in a UV/vis spectrometer from Agilent Technologies with the "UV-Visible ChemStation" software. The basic measurement procedure was described in the previous chapter 5.2.3. However, in contrast to the disposable cuvettes, the quartz cuvettes had to be cleaned and reused. Therefore (and for other reasons stated later), it was decided to unconventionally use the absorbance spectrum of the empty quartz cuvette as a reference and blank respectively. This spectrum was captured prior to every new sample measurement or specifically every time the cuvette was changed. This unconventional procedure served several purposes. Besides the usual benefits, which include subtraction of cuvette surface imperfections and ambient light

changes that can affect spectrometers without cover, three main benefits supported this procedure.

1) By observation of the blank spectrum, the cleanliness could be guaranteed. Hence it can be seen as a quality measure for the cleaning procedure, which typically included water and acetone washes. This was especially important after protein rich samples, which denatured during the cleaning process and then had the tendency to stick to the inside of the cuvette.

2) The characteristic in the spectra, which resulted from constant constituent such as buffer and solvents like water and methanol (see figure 6.04), could be used for evaporation control, and if required, for the respective adjustment.

3) Furthermore, these characteristics served as indicators if there was an error introduced by the experimenter. Hence it served again as a quality control measure.

Besides these unconventional blank spectra from empty cuvettes, for each experimental series, spectra of appropriate references were also captured and subsequently subtracted as required during data analysis. These spectra included buffer solutions and solvents only, both inactivated and activated Gibbs reagent in various solutions, vancomycin in the corresponding solution mixture at neutral and high pH etc.
Water and methanol mixtures are prone to separation, which may result in false absorbance values and difficulties of evaporation factor estimation. Consequently it was decided that after the first experiments presented in chapter 6.3.1, the reaction mixtures should be shaken in an Eppendorf tube prior to addition into the cuvette for subsequent spectroscopic analysis. Furthermore, two spectra were recorded for each sample in order to ensure a level of consistency. The obtained data were saved in comma-separated values (CSV) using the export function of the spectrometer software.

6.2.3.2 Data Processing, Analysis and Statistics

The CSV-files were imported, plotted and analysed with Origin Pro 8.6 software (Origin Lab Corporation, Northampton, Massachusetts, USA). The solvent characteristics in the spectra could again be used as control indicating errors for instance in subtraction of the reference from the sample spectrum.

Whenever the sample sizes were large enough a statistical evaluation was performed. This included a one-way analysis of variance (ANOVA) and when the results indicate significance a post hoc Fisher's least significant difference (LSD) test followed. These tests were calculated using Microsoft Office Excel (Microsoft Corporation, Redmond, Washington, USA). Summaries of these calculations including formulae can be found in the appendix chapter A starting on page 347.

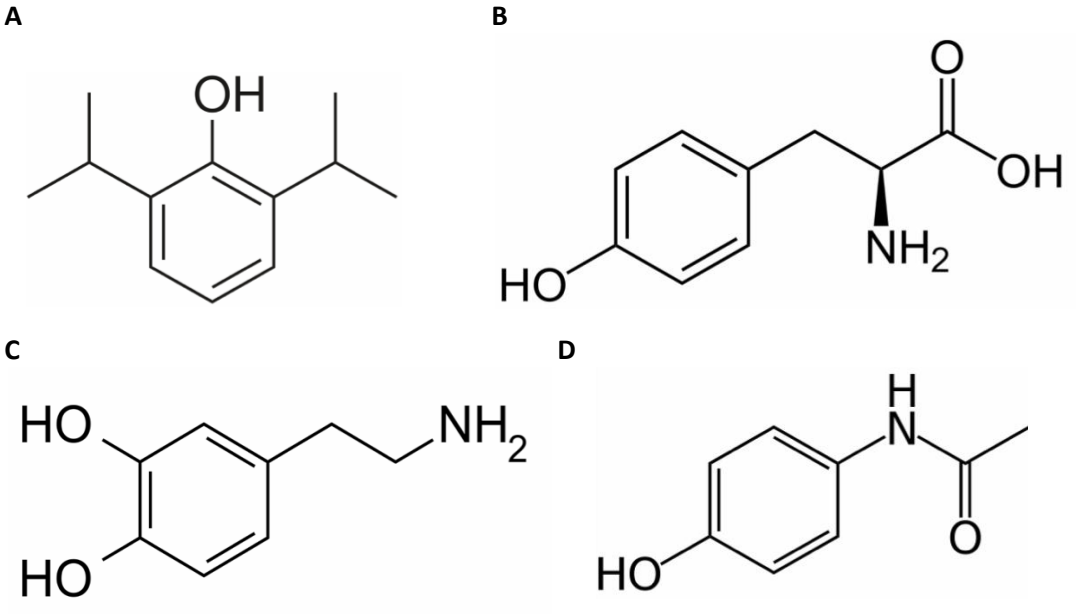

Figure 6.02: Chosen interferents with phenolic motifs, which may couple to Gibbs reagent and affect the vancomycin quantification. A) Propofol. The coupling of Gibbs reagent to the para-unsubstituted position of propofol is well established and results in an indophenolic structure with a at 595 nm (see chapter 5.3.2) (Pettigrew, Laitenberger, and Liu 2012; Liu et al. 2012; Adam et al. 1981). **B) Tyrosine.** Tyrosine (Tyr or Y) is a non-essential amino acid meaning it can be synthesised by the human body. Its phenolic moiety is para-substituted. **C) Dopamine.** Dopamine is a neurotransmitter and its structure consists of a dihydroxy phenol, where one para position to the hydroxyl group is occupied and one is free. **D) Paracetamol.** Paracetamol is also known as acetaminophen and is a widely used over-the-counter analgesic. In a similar way to tyrosine its structure consists of a para-substituted phenolic moiety.

Figure 6.03: Solid phase extraction (SPE). The SPE cartridge was a Strata-X 33u Polymeric Reversed Phase (30 mg/1 ml sample) cartridge from Phenomenex® (Macclesfield, Cheshire, UK). According to the manufacturer, the named Strata-X reversed phase sorbent retains analytes by hydrophobic interactions, such as conventional C18 or C8 reverse phase columns, but also by hydrogen- and π-π bonding resulting in stronger retention of aromatic and polar analytes. This enhanced retention allows washing with organic solvents without breaking the interaction between the analyte and the stationary phase. Therefore it is suitable for polar and non-polar analytes. Every cartridge was conditioned with 1 ml methanol and equilibrated with two times 1 ml of water prior to usage. SPE cartridges can be operated in a parallel manner with a vacuum manifold.

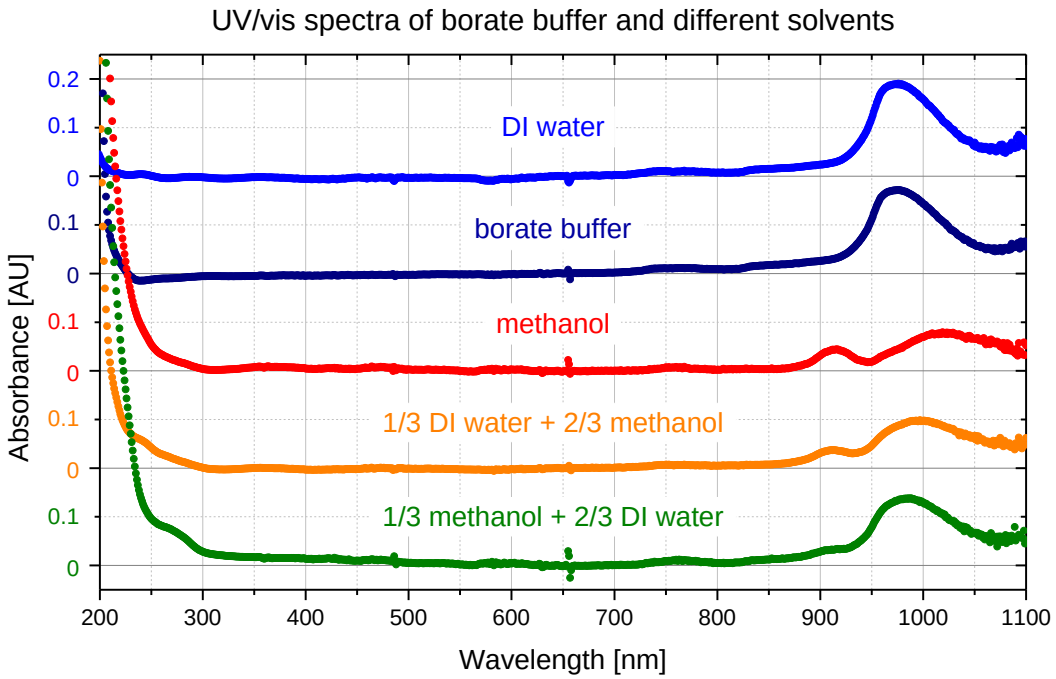

Figure 6.04: UV/vis spectra of borate buffer and various solvents. All spectra show distinctive characteristics in the wavelength region from 850 to 1100 nm. It is clearly visible that the solvent mixtures depict characteristics of both constituents according to their corresponding ratio. Furthermore, it is evident that methanol, especially in a mix with water, is absorbing around 281 nm and therefore is likely to mask absorbances of vancomycin. These specific characteristics of borate buffer and various solvents were used for quality measure during experiments and subsequent analysis including evaporation control and if necessary adjustment. The small elevations and drops at 486 and 656 nm are instrumental and specific for the used spectrometer.

6.3 Results and Discussion

The results herein report the colourimetric detection of vancomycin by successful labelling of vancomycin with Gibbs reagent, which is a key result of this thesis. This chapter presents selected consecutive major milestones of the development process for the colourimetric TVM assay. Due to the fact that it is a consecutive process some discussion and sometimes hypotheses had to be included to lead to the subsequent step.

This section is divided into eight parts. The first part (6.3.1) describes labelling of vancomycin at high concentrations. The second part (6.3.2) focuses on the detection in the therapeutic range and reports the first study in serum. The third part (6.3.3) presents the development of an extraction protocol for vancomycin from foetal bovine serum (FBS). The fourth part (6.3.4) contains the optimisation of the vancomycin to Gibbs reagent ratio. The fifth part (6.3.5) depicts the change from FBS to whole human serum (WHS). The sixth part (6.3.6) discusses the effect of serum protein binding on the vancomycin detection and studies the therapeutic monitoring of free and bound drug fraction. The seventh part (6.3.7) evaluates the selectivity of the assay with a subset of interferents. The eight and last part (6.3.8) presents the direct comparison of the developed vancomycin assay with a gold standard method that is routinely used in the microbiology laboratory of UCLH.[5]

6.3.1 Labelling of Vancomycin at High Concentrations

The starting point of the experimental procedure used herein is comparable to the one used for propofol described the precedent chapter in section 5.3.2. However, acetonitrile, as a polar aprotic solvent, could not be used for the dissolving of vancomycin. Therefore borate buffer, as a polar protic solvent, was chosen. The main reason for this choice was to not introduce another unknown solution to the

[5] Some experiments in the fourth, fifth, sixth and seventh subsection were carried out in conjunction with Alexander Wright. He is a medical student, who did a six month project in our group.

reaction mixture, since borate buffer was used previously in the benchmarking experiment to achieve the required alkaline pH. Retrospectively, this turned out to be one of the crucial changes, which made the coupling reaction work successfully.

Figure 6.05 A shows photographs of three quartz glass cuvettes. The first cuvette (i) contains 800 µM vancomycin in borate buffer, the second (ii) 800 µM Gibbs reagent dissolved in methanol mixed with borate buffer, and the third (iii) is a mixture of the first and the second showing the novel brightly purple coloured end product, which is hereafter called vanGibbs. The final concentrations in the mixture (iii) were 571 µM Gibbs reagent and 1710 µM vancomycin. The colour change occurs immediately after mixing the Gibbs and the vancomycin together.

The corresponding UV/vis absorbance spectra are drawn in figures 6.05 B and C. It has to be highlighted that all absorbance spectra were measured from 200 to 1100 nm. This will not be necessary in the final bench top device, since the vanGibbs molecule has its maximal absorbance in the visible region. However, full spectra were captured for quality and evaporation control, which was previously described in the materials and methods subsection 6.2.3.1. Furthermore, full spectra allowed additional study of the vancomycin peak at 281 nm.

The absorbance spectrum of vancomycin in borate buffer (i) appears transparent to the human eye. This observation agrees with the spectrum, which does not showing distinctive features above 350 nm that corresponds to the visible range. Additionally at the vancomycin maximal absorbance wavelength (λ_{max} = 281 nm) an elevation is apparent but not a clear distinctive peak. Furthermore, it seems as if at around 300 nm an additional peak may occur. These observations may be due to the high pH paired with a very high vancomycin concentration which is likely to result in a shadowing effect (see chapter 5.1.1.2). A theoretical calculation according to the Beer-Lambert-Bouguer law results in an expected absorbance of about 4.75 AU, which is a too large absorbance value to be measured with the spectrometer and supports the previous assumptions. The absorbance characteristic of vancomycin and its molar absorptivity will be further

discussed later in this chapter. Between 900 and 1100 nm the characteristics peak of borate buffer and water respectively is visible as previously presented in figure 6.04.

The spectrum of the Gibbs reagent (ii) shows high absorbances between 380 and 500 nm with two shoulders at about 415 and 460 nm. They are followed by decreasing absorbance values that are saturating after 800 nm at about 0.2 absorbance unit [AU] until the characteristic peaks of methanol mixed with water or borate buffer starts just before 900 nm. This UV/vis spectrum corresponds with Gibbs' yellow or brownish appearance. Its colour changes from initially faint yellow in neutral pH to yellow or brownish in alkaline pH. This colour change is associated with the formation of its reactive species, quinoneimine which is hereafter designated as 'activated Gibbs'.

Lastly, the spectrum of the brightly purple coloured product of Gibbs reagent coupled to vancomycin (iii) shows a distinctive bimodal peak from 500 to 620 nm with a maximum at around 589 nm, which is the yellow region of the visible spectra and therefore appears purple/violet to the human eye (see figure 5.03 and table 5.01). This observed wavelength of 589 nm is close to maximal absorbance wavelength (λ_{max}) of the product of the Gibbs reagent coupled to propofol, which absorbs the strongest at 595 nm. This wavelength is in the orange region and consequently appears blue to the human eye, which is very similar to DCPIP with a maximal absorbance wavelength (λ_{max}) of 605 nm (see chapter 5.3.1 and figure 5.09).

This experiment provided the first direct evidence of a successful coupling of Gibbs reagent to vancomycin and the yield of a novel product – vanGibbs – with a λ_{max} and corresponding colour that suggests an indophenolic motif as hypothetically proposed in figure 6.01. Additional experiments on the stability of this novel product showed a 0.6 ± 0.1 % difference in absorbance at λ_{max} after a period of 12 hours. The error corresponds to the standard deviation calculated from three independent experiments (n = 3).

To further study the coupling reaction and to understand the fairly complicated UV/vis spectra, concentration series were measured and the reaction stoichiometry was

studied. 800 µM of vancomycin dissolved borate buffer was gradually added to 571 µM of Gibbs reagent dissolved in methanol. Corresponding absorbance spectra were captured. Figure 6.06 A shows some of these absorbance spectra and figure B is a zoom in on the characteristic peak of the novel vanGibbs molecule. It has to be highlighted that the final vancomycin concentration ranged from 114 to 1713 µM which is several orders of magnitude higher than the therapeutic range (4 - 28 µM).

The spectrum with the highest absorbance at vanGibbs' λ_{max} appeared to be the reaction of 571 µM Gibbs with 457 µM of vancomycin shown in violet in figure 6.06 A and B. These concentrations correspond to a molar equivalent of 0.8 vancomycin to 1 equivalent of Gibbs reagent, which is good agreement with expectations based on the hypothesis of the Gibbs coupling to the position 6 of vancomycin's 7^{th} residue (see figure 6.01).

To further investigate the stoichiometry of the coupling reaction, four wavelengths according to their distinctive features in the absorbance spectrum were chosen as illustrated in figure 6.06 A. These wavelengths are 281 nm (dark gray line), 452 nm (dark yellow line), 589 nm (purple line) and 475 nm (blue line). Figure 6.06 C plots the absorbances of these wavelengths against the concentration ratios of vancomycin over Gibbs reagent. All absorbances are adjusted to the changing Gibbs concentration due to the gradual addition of vancomycin and subsequently subtracted from the Gibbs reagent only absorbances.

It is expected that the difference in absorbance values for the reaction product, vanGibbs (589 nm), is increasing simultaneously with the increase in starting material. This increase is expected until Gibbs reagent is depleted and then the absorbance values should saturate. Since a 1:1 reaction is expected this saturation should start at ratio 1. Additionally, a doubling of the value from 0.2 to 0.4 and from 0.4 to 0.8 is expected.

On the other hand, two scenarios could be possible for the vancomycin λ_{max} (281 nm). Firstly, it could show exactly the opposite behaviour to the vanGibbs wavelength. This would indicate that the Gibbs reagent is coupling to the chromophore responsible for

vancomycin's absorbance at 281 nm and extending this chromophore so that it is absorbing at 589 nm. Or secondly, the absorbance values for 281 nm could increase in a linear manner irrespective of the vanGibbs concentration, which would support that the Gibbs reagent is coupling to another position at the vancomycin molecule. As evident in figure 6.06 C, the latter scenario is fulfilled.

The absorbance around 452 nm was associated to the activated Gibbs reagents. Therefore, due to the adjustment these absorbances should stay around zero and not change upon different concentrations ratios. The same should be true for 975 nm, which is the characteristic peak of the solvent system, and therefore was influenced by the adjustment as well. The absorbance values in figure 6.06 C are in good agreement with all expectations.

In conclusion, this data set shows that the peak at 589 nm corresponds to the formation of the new coupling product and that the reaction stoichiometry seems to be around 1:1 vancomycin:Gibbs reagent. Furthermore, the results are suggesting that Gibbs reagent is not coupling to vancomycin's chromophore responsible for the absorbance at 281 nm.

Since the solvent system was changing constantly from sample to sample, no molar absorptivities were calculated so far. Due to the overlap of absorbances, the influence of Gibbs reagent absorbance upon the vanGibbs absorbance has to be studied firstly in order to be able to calculate the molar absorptivity of vanGibbs. It has to especially be evaluated whether these two absorbances at the vanGibbs are additive, overlaying or even interfering with each other (see chapter 5.1.1.2). However, as the molar absorptivity is strongly influenced by the molecule's environment including solvents and pH, the molar absorptivity will be calculated as soon as the optimal reaction conditions are established.

The next objectives presented in the following subsection (6.3.2) are coupling and consequently detection in vancomycin's clinical range (4 – 28 µM) and the test whether there may be a possibility to circumvent a specific extraction protocol.

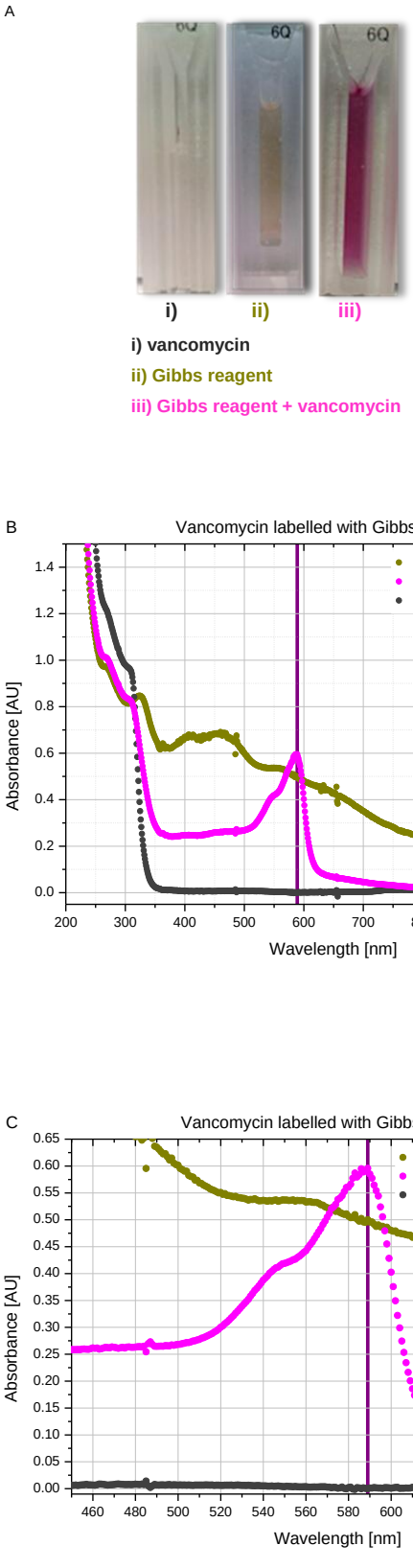

Figure 6.05: First vancomycin labelling with Gibbs reagent.
A) Photographs of the quartz glass cuvettes with the two starting materials and the end product of the vancomycin Gibbs reaction. i) 800 µM vancomycin in borate buffer, ii) 800 µM Gibbs reagent dissolved in methanol mixed with borate buffer, and iii) 1713 µM vancomycin reacted with 571 µM Gibbs reagent in borate buffer.
B) UV/vis absorbance spectra of the three cuvettes shown in image A. The absorbance spectrum of vancomycin in borate buffer (i) appears transparent to the human eye. This observation agrees with the spectrum, which does not showing distinctive features above 350 nm. Additionally at the vancomycin maximal absorbance wavelength (281 nm) an elevation is apparent but not a clear distinctive peak. This may be due to the basic pH and the large concentration of vancomycin in the sample. The spectrum of the Gibbs reagent (ii) shows high absorbances between 380 and 500 nm with two shoulders at about 415 and 460 nm. They are followed by decreasing absorbance values that are saturating after 800 nm at about 0.2 AU until the characteristic peaks of methanol mixed with water or borate buffer starts just before 900 nm. This UV/vis spectrum corresponds with Gibbs' yellow or brownish appearance. Lastly, the magenta spectrum is the product Gibbs reagent (ii) coupled to vancomycin (ii) and is hereafter called vanGibbs (iii).
C) Enlarged region from figure B. The vanGibbs spectrum shows a distinctive bimodal peak from 500 to 620 nm with a maximum at around 589 nm, which is indicated with a purple line. This maximal absorbance wavelength is in the yellow region of the visible spectra and therefore appears purple/violet to the human eye.

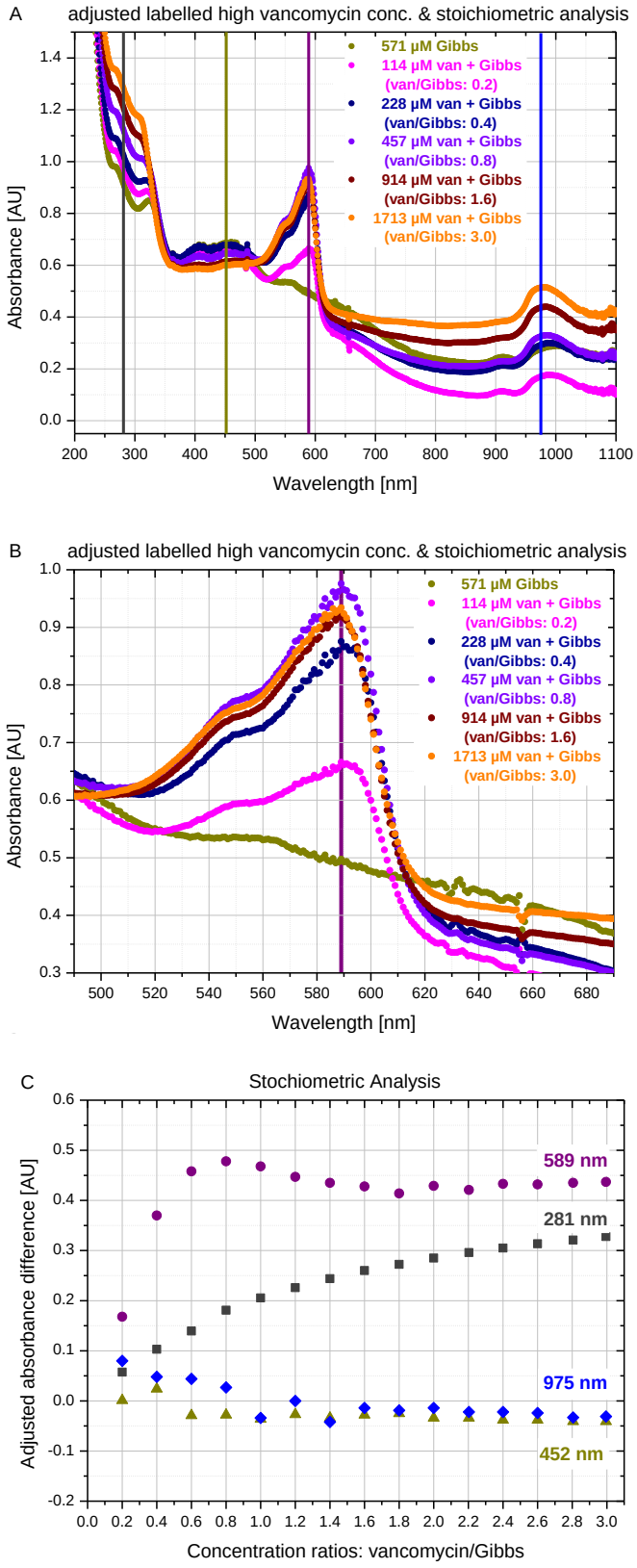

Figure 6.06: Vancomycin monitoring at high concentration and stoichiometric analysis.
A) Absorbance spectra overlay of several high vancomycin concentrations after the labelling reaction with Gibbs reagent including vertical lines that indicate the four wavelengths chosen for subsequent stoichiometric analysis. The vertical dark grey line marks the wavelength 281 nm, which is expected to be the λ_{max} of vancomycin. The dark yellow line indicates 452 nm, which seems to be associated with the Gibbs reagent. The purple lines is at 589 nm the λ_{max} of the new coupling product vanGibbs. Lastly the blue line highlights the wavelength 975 nm, which is within the region of the solvent system characteristic peaks.
B) Enlarged region from figure A. The spectrum with the highest absorbance at vanGibbs' appeared to be the reaction of 571 µM Gibbs with 457 µM of vancomycin shown in violet, which corresponds to a vancomycin over Gibbs concentration ratio of 0.8.
C) Stoichiometric analysis of the four chosen wavelengths against the concentration ratios of vancomycin to Gibbs reagent. All absorbances are adjusted to the changing Gibbs concentration due to the continuous addition of vancomycin and subsequently subtracted from the Gibbs reagent only absorbances, which were taken from the dark yellow spectrum in figure A and B. The x-axis corresponds to the vancomycin over Gibbs concentration ratios. This data set proves that the peak at 589 nm corresponds to the formation of the new coupling product and that the reaction stoichiometry seems to be around 1:1 vancomycin:Gibbs reagent.

6.3.2 Detection in Clinical Range and Preliminary Serum Studies

Building on the successful coupling of Gibbs reagent to vancomycin at high concentrations (114 – 1713 µM) in buffer, this chapter presents the first coupling and detection of vancomycin via Gibbs reagent in vancomycin's clinical range (4 - 28 µM) followed by time dependent and preliminary serum studies.

For this first set of experiments at vancomyin's clinical range, the same experimental procedure as for the experiments with high concentrations was chosen. Hence a specific volume of vancomycin in borate buffer (571 µM) was gradually added to Gibbs reagent in methanol (571 µM). This stepwise addition resulted in increasing vancomycin and decreasing Gibbs concentrations, which can nicely be observed in figure 6.07 A. It presents an overlay of selected absolute absorbance spectra of the described experimental procedure including the two starting materials, Gibbs reagent (571 µM) shown in dark yellow and the vancomycin (571 µM) in dark grey. All absorbances were normalised to a constant volume. The vertical line depicts the λ_{max} (589 nm) of the novel coupling product vanGibbs. The spectral region from 200 until 500 nm is comparable to figure 6.06 A and the vanGibbs peaks from about 525 until 625 nm are as expected much smaller. The decrease in Gibbs concentration resulting from the gradual addition of vancomycin can be observed. Concerning this matter, it is also evident that two spectra seem to behave slightly unexpected in comparison to the remaining spectra. The spectrum of '567 µM Gibbs + 6.8 µM van' shown in dark red colour seems a bit too high in absorbance, whilst the magenta coloured spectrum of '570 µM Gibbs + 2.3 µM van' on the other hand seems a bit too low. This may be due to the fact that this experimental procedure hinders a complete mixing of the buffer with the methanol. This hindrance was the reason that the experimental procedure was changed for the following experiments. Furthermore, since this set of experiments was performed to only check the feasibility of vancomycin detection at clinical concentrations via the Gibbs reagent coupling, the sample size was kept to a minimum (n = 1).

Figure 6.07 B illustrates an enlarged section of figure A. Additionally the absorbances were adjusted to a constant Gibbs concentration. As evident, the characteristic vanGibbs peak is hardly visible below a vancomycin concentration of 11.3 µM and the spectra are hardly distinguishable from the reference spectrum with solely Gibbs reagent. Nevertheless a steady absorbance increase at the λ_{max} of vanGibbs (589 nm) can be observed according to the increasing vancomycin concentrations. The graph figure 6.07 C plots the absolute absorbances at 589 nm in purple against the corresponding vancomycin concentrations. The blue box indicates the vancomycin's therapeutic window spanning from 4 to 28 µM. The dependency of concentrations and absorbances seems almost linear with an approaching saturation at the top end of the therapeutic window. The magenta data points reflect the differential absorbances at 589 nm derived by subtraction of the Gibbs only absorbance (shown on the left of the graph in dark yellow) from all vanGibbs absorbances. This subtraction is only legitimate if the absorbances of Gibbs and vanGibbs at 589 nm are additive, which at this point of the thesis was just an assumption and will further be evaluated and discussed.

The next objective was to study the time dependency of the coupling reaction because so far all presented spectra were captured almost directly after addition of vancomycin. Therefore, the concentration of vancomycin was chosen slightly above the upper limit of the clinical range at 30 µM and the Gibbs reagent's concentration was kept at 571 µM. Figure 6.08 A shows an overlay of several absorbance spectra from the two aforementioned compounds obtained at different time points after mixing. As usual, the vertical line marks the λ_{max} of vanGibbs. The previously established procedure for obtaining presumably only the absorbance for the vanGibbs molecule via subtraction was used again. Figure 6.08 B illustrates this procedure. The purple spectrum labelled with an a) is the reaction of 571 µM Gibbs reagent in methanol with 30 µM vancomycin in borate buffer. The dark yellow spectrum labelled with a b) is from 571 µM Gibbs reagent in methanol mixed with borate buffer. Hence the only difference between a) and b) was that a) had 30 µM vancomycin in the borate buffer and b) not. The magenta spectrum is the differential spectrum obtained as the subtraction of spectrum b) from a). The enlarged image in the top right corner depicts the vanGibbs wavelength area of

the differential spectrum. It can be observed that the shape of the vanGibbs peak seems different and not bimodal as in previous experiments. This observation will be further investigated in this chapter. Figure 6.08 C plots the differential absorbances at 589 nm against various time points after sample preparation. The data points in magenta are take from spectra in which vancomycin was dissolved in borate buffer. The depicted error bars correspond to standard deviations calculated from three independent experiments (n = 3). Immediately after mixing, a significant increase in absorbance to about 0.155 AU could be observed. After approximately four minutes the system seems to stabilise.

Comparable experiments have been performed in 10 % serum, which corresponds to 10 % BSA added to borate buffer. The difference in absorbance of the spectra with vancomycin and without vancomycin at a wavelength of 589 nm plotted versus time can is shown in violet in figure 6.08 C. These data points are obtained by only one experiment (n = 1) and consequently no error could be calculated. It can be observed that the differential absorbance signal is dropping from around 0.155 AU to 0.045 AU. Additionally, the stabilisation seems to take insignificantly longer. According to literature, the proportion of vancomycin bound to serum proteins can vary significantly between 10 – 82 % with 55 % often quoted as the mean fraction bound (Sun, Maderazo, and Krusell 1993; Butterfield et al. 2011; Cantú et al. 1990; Ackerman et al. 1988; Zokufa et al. 1989; Rodvold et al. 1988; Kitzis and Goldstein 2006; Shin et al. 1992; Shin et al. 1991; Zeitlinger et al. 2011). Although in this set of experiments only 10 % BSA was added to the borate buffer, the decrease in signal is about 70 %. Hence this absorbance decrease cannot be explained solely with binding of vancomycin to serum proteins and may arise due to further interference with the coupling reaction or with the optical read out method.

Conclusively, the first aim of this colourimetric detection to monitor vancomycin by specific labelling with Gibbs reagent could be successfully demonstrated. The newly formed compound seems to have its maximal absorbance wavelength (λ_{max}) at 589 nm and a molar absorptivity ($\varepsilon_{589\,nm}$) of around 7200 ± 300 M^{-1} cm^{-1} in a mixture of borate

buffer and methanol at a pH of approximately 10. Furthermore, this novel coupling reaction allows accurate detection at the upper limit of vancomycin's therapeutic window within four minutes. However, the finding that only 10% BSA in buffer reduces the absorbance signal by 70 % is clear evidence that an extraction protocol cannot be circumvented. Therefore the following chapter (6.3.3) presents the development of an extraction protocol from foetal bovine serum.

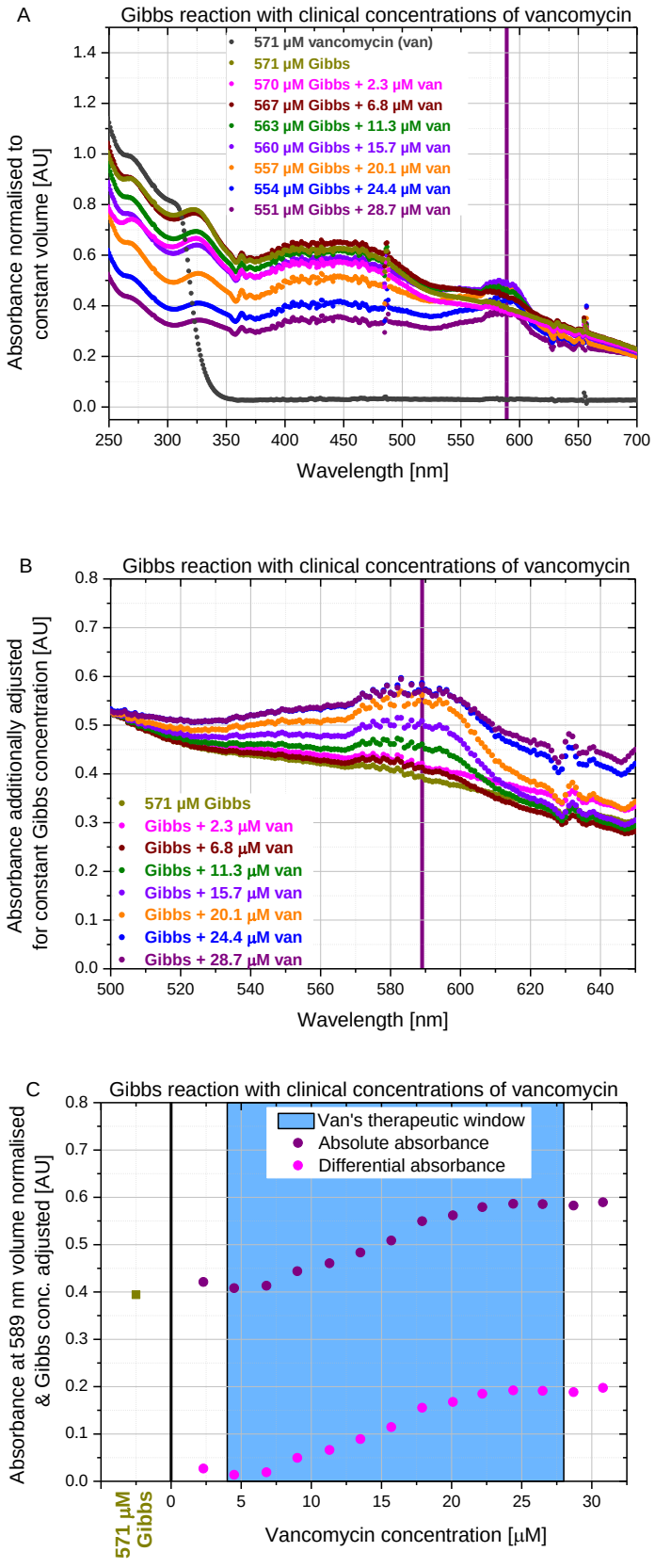

Figure 6.07: Therapeutic vancomycin monitoring at clinical concentrations.

A) Some absorbance spectra of vancomycin in clinical concentrations labelled with Gibbs reagent. Overlay of some spectra for which a certain volume of vancomycin in borate buffer (571 µM) was gradually added to Gibbs reagent in methanol (571 µM). These additions resulted in increasing vancomycin and decreasing Gibbs concentrations. All absorbances are normalised to have the same constant volume. The vertical line depicts the λ_{max} (589 nm) of the novel coupling product vanGibbs. The spectrum of '567 µM Gibbs + 6.8 µM van' shown in dark red seems a bit too high in absorbance, whilst the magenta coloured one of '570 µM Gibbs + 2.3 µM van' on the other hand seems slightly low.

B) Enlarged section of figure A. The absorbances are additionally adjusted to the gradual change in Gibbs reagent concentration. It can be observed that characteristic vanGibbs peak is hardly visible below a concentration of 11.3 µM vancomycin.

C) Relationship between concentration and absorbance. The absolute (shown in purple) and differential (in magenta) absorbances are plotted against the corresponding vancomycin concentrations. The blue box indicates vancomycin's therapeutic window (4 - 28 µM). The differences were obtained by subtracting the Gibbs value (in dark yellow) from the absolute absorbances. The dependency of concentrations and absorbances seems almost linear. The data points are obtained by one set of experiment (n = 1) and hence no error could be calculated.

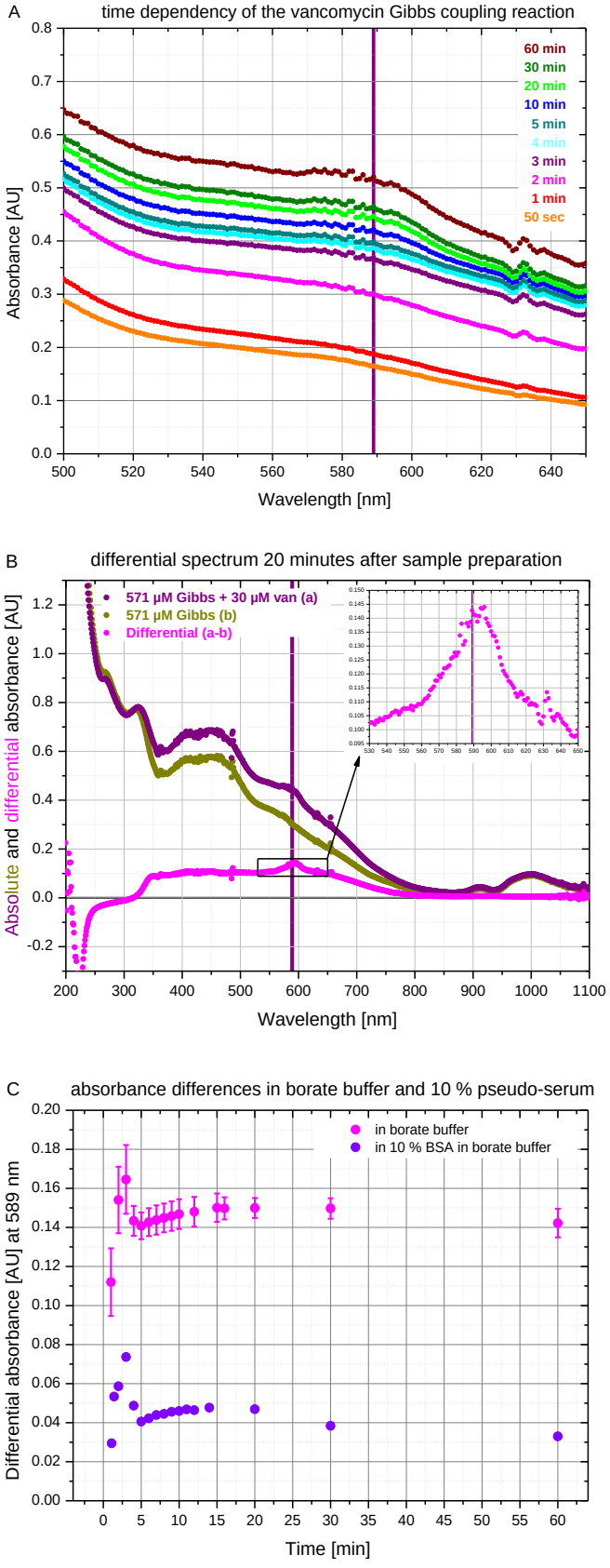

Figure 6.08: Time dependency studies of the Gibbs reagent coupling reaction and first serum trials.
A) Time dependency of this novel coupling reaction. Overlay of several absorbance spectra of Gibbs reagent (571 µM) reacted with vancomycin (30 µM) at different time points after preparation. Again the vertical purple line marks the λ_{max} of vanGibbs.
B) Absolute and differential spectra of Gibbs reagent with and without vancomycin 20 minutes after sample preparation. The purple spectrum (a) shows 571 µM of Gibbs reagent reacted with 30 µM of vancomycin. The dark yellow spectrum (b) is obtained from 571 µM Gibbs reagent in methanol mixed with borate buffer. Hence the Gibbs reagent is in exactly the same conditions as the reaction demands. Therefore the only difference between a) and b) is the presence and absence respectively of vancomycin. The enlarged image in the top right corner depicts the wavelength area of the new product vanGibbs. It can be observed that the shape of the vanGibbs peak seems not bimodal as in previous experiments.
C) Time dependency of absorbance differences in borate buffer and 10 % pseudo-serum. Differential absorbances at 589 nm of 30 µM of vancomycin labelled with Gibbs reagent are plotted against various time points after sample preparation. The magenta data points are taken from spectra in which vancomycin was dissolved in borate buffer. Whilst the violet data points are from spectra in which vancomycin was dissolved in borate buffer with 10 % BSA, herein called 10 % pseudo serum. The error bars for the measurements in borate buffer indicate the standard deviation derived from three independent experiments (n = 3). One set only (n = 1) was performed in 10 % pseudo-serum and consequently no error calculation could be performed.

6.3.3 Extraction Protocol Development from Foetal Bovine Serum

The finding that only 10% BSA in buffer could reduce the absorbance signal by 70 %, highlighted the need for specific extraction protocol for whole blood. Although this necessitates an extra step, the extraction process also aims to reduce the complexity of the sample, by removing some or ideally all of the interfering species. The extraction process can also be designed to pre-concentrate the substance of interest thereby increasing the diagnostic window which may be beneficial for very low drug concentrations. It can therefore improve the specificity and sensitivity of drug quantification.

For the purpose of the initial investigation, foetal bovine serum (FBS) was chosen as a biological matrix, and served as a useful development stepping stone to whole human serum (WHS). Historically, FBS has been widely used as a substitute for WHS in cell culture media (Tateishi et al. 2008; Freshney 2005; Gospodarowicz and Moran 1976). Additionally, Sphere Medical has used it during the development process of the Pelorus device. Therefore, it seemed a reasonable choice at the outset of this investigation.

The starting point in relation to the extraction set-up was chosen in accordance with Sphere Medical's existing bench top device for the anaesthetic propofol. By mimicking some aspects of Sphere's current methodology implemented in their commercially available Pelours device, there was greater scope for reducing the required time for a vancomycin-focussed device to reach the market. The Pelorus device uses solid phase extraction (SPE) (Pettigrew, Laitenberger, and Liu 2012). Although it might not be the most optimal type for the extraction of vancomycin, this SPE cartridge will be the starting point. As described in more detail in chapter 6.2.2.3 and figure 6.03, reversed phase SPE separates analytes based upon their polarity. Its stationary phase retains analytes by hydrophobic interactions, hydrogen- and π-π bonding which results in stronger retention of aromatic and polar analytes in contrast to conventional reversed phases such as C8 and C18.

However being optimised for propofol extraction, the extraction protocol has to be significantly modified. Propofol, as a small hydrophobic molecule, has a greater capacity for extraction in organic solvents such as acetonitrile. On the contrary, vancomycin, due to its polarity, is almost insoluble in pure organic solvents including methanol, ethanol, acetone and acetonitrile.

The procedure during the development process was as follows. The Gibbs labelling reaction mentioned previously (see chapter 6.3.1 and 6.3.2) has been used to detect the presence of vancomycin in the different washing and elution stages. Additionally, to account for possible unspecific coupling of the Gibbs reagent to numerous components present in serum, including proteins, hormones, antibodies, antigens, electrolytes and any exogenous substances, a reference preparation was treated the same way as serum spiked with vancomycin. Correspondingly, they were run in parallel through the SPE cartridge and labelled with Gibbs reagent. The UV/vis spectra of the reference preparations were subtracted from the sample spectra. It has to be emphasised that such a reference subtraction will not be possible in the actual bench top device. Therefore the procedure has to be optimised in such a manner that means subtraction is not required anymore.

This chapter describes the development process of the extraction protocol with major milestones listed below.

i) The first objective was to indentify a suitable solvent, an eluent, which disrupts the interaction between the compound of interest and the stationary phase of the SPE cartridge. Additionally this eluent must be different from the washing stages with which the unwanted components and interferents will be washed away prior to elution. Since it was previously found that borate buffer is not a requirement for the success of the coupling reaction and vancomycin can be dissolved in DI water while Gibbs is dissolved in methanol, various ratios of methanol to DI water were tested first. This approach was chosen on the grounds that no additional unknown

substance will be added to the system. As presented in figure 6.09, it was found that the most optimal mixing ratio is 1/3 water + 2/3 methanol.

However, before moving to the next objective, it had to be demonstrated that this solvent mixture allows detection in the clinical range in a comparable matter as previously described in chapter 6.3.2 and figure 6.07. Figure 6.10 presents the results from one set of experiments showing that this new mixture allows detection slightly below and in the therapeutic window of vancomycin. Since these experiments were performed prior to finalising the elution protocol, the sample size was kept to a minimum (n = 1). Consequently neither error calculations nor statistical analysis could be conducted. The Gibbs concentration used at this stage was 13.3 mM whilst the addition of 0.4 M sodium hydroxide in DI water was used to reach the necessary high pH. These conditions gave the highest absorbances in previous experiments and will be further optimised after the ideal elution protocol has been established.

Furthermore due to this concentration series, the molar absorptivity of vanGibbs could be roughly estimated again. This estimation would reveal changes according to the different Gibbs reagent ratio and the environmental alterations including slight adjustment in solvent mixture and pH as well as the omission of borate buffer. Figure 6.10 C depicts the differential absorbances obtained from the six different vancomycin concentrations. The linear fit through these data points forced to intercept zero resulted in a slope of 0.0073 ± 0.0003 and an adjusted R^2 of 0.991. Therefore, the molar absorptivity of vanGibbs ($\varepsilon_{589\,nm}$) in a mixture of 1/3 DI water + 2/3 methanol at a pH of approximately 13 seems to be around 7300 ± 300 M^{-1} cm^{-1}. This is in excellent agreement with the previously obtained $\varepsilon_{589\,nm}$ (6.3.2), which was 7200 ± 300 M^{-1} cm^{-1} in a mix of borate buffer and MeOH at a pH of approximately 10.

To assess whether a similar behaviour can also be observed if only vancomycin gets dissolved in this optimised eluent, comparable experiments were performed. If vancomycin would show an enhanced absorbance comparable to vanGibbs in these

conditions and if additionally the extraction protocol would be successful, then the use of a Gibbs coupling for absorbance 'enhancement' becomes futile. Figure 6.11 presents that vancomycin dissolved in 1/3 DI water + 2/3 methanol shows a bathochromic shift of its maximal absorbance wavelength to 304 nm (λ_{max}). The molar absorptivity at this shifted wavelength ($\varepsilon_{304\,nm}$) does not change significantly and is with 5600 ± 100 M^{-1} cm^{-1} very comparable to vancomycin in water ($\varepsilon_{282\,nm}$ = 5943 M^{-1} cm^{-1}) ("The Merck Index Online - Vancomycin" 2013).

Therefore, it can be concluded that molar absorptivity of vanGibbs ($\varepsilon_{589\,nm}$ = 7300 ± 300 M^{-1} cm^{-1}) remains also in the chosen eluent advantageous above vancomycin's molar absorptivity ($\varepsilon_{304\,nm}$ = 5600 ± 100 M^{-1} cm^{-1}). Furthermore, due to the Gibbs reagent coupling the optical detection requires only a visible light source and will work in disposable plastic cuvettes.

ii) The second objective was to develop a protocol that removes unwanted components and interferents from the serum. These could interfere with the quantification of vancomycin and lead to a masking or elevating effect on the detection signal. These components are endogenous, arising from the patient's blood or are exogenous substances such as drugs and microorganisms, which may be present as well. The serum used herein lacks only the proteins involved in blood clotting and contains all usual electrolytes, antigens, antibodies, and hormones.

Since the conditioning of the SPE stationary phase is performed with methanol followed by two DI water equilibration steps, DI water as a washing step was studied first. This starting point also considered the avoidance of a premature transition from DI water to methanol. This transition would inevitably lead to achieving the previously developed optimal elution solvent mixture within the stationary phase that consequently could result in partly or full loss of vancomycin. Another important aspect which had to be considered is that the same labelling reaction and the identical SPE cartridge are used for the anaesthetic propofol. Furthermore, both propofol and vancomycin are used in the critical care setting. Therefore, propofol contamination of a blood sample containing

vancomycin seems likely. Consequently at least one organic washing step had to be added to extraction protocol. However, as indicated above, this could have a significant effect on the protocol. Whilst changing from a watery washing step to an organic solvent, the previously developed elution condition for vancomycin will inevitably be achieved within the cartridge. This could lead to a potential loss of vancomycin. One way of circumventing this problem would be the application of a vacuum to the SPE cartridge, which will allow the stationary phase to dry out prior to the solvent change. Such a vacuum system will be integrated into a bench top device regardless, as a method for reducing the time the extraction protocol takes. However, such a system was not convenient in the laboratory environment. A lack of automation along with the need to have access to the SPE cartridges for application of solvent meant a continuous vacuum could not be maintained. Furthermore the sample loss from repeated venting and vacuum reapplication was too large. Therefore all experiments with gravity-assisted flow despite the increased time requirement. Several experiments with organic washing steps prior to the vancomycin elution were performed. For sample preparations with 29 µM vancomycin, absorbances of 0.18 ± 0.03 AU were obtained. The stated error corresponds to the standard deviation of three independent experiments (n = 3). These absorbances were in excellent agreement with the results presented in figure 6.09 B, where absorbances of 0.19 ± 0.01 AU were found without any washing steps. Additionally, they were also in very good agreement with the, according to the $\varepsilon_{589\,nm}$ (figure 6.10 C), calculated absorbance values of 0.21 ± 0.01 AU . Therefore, it was assumed that the level of loss due to gravity-assisted flow was negligible despite the unattainability of full dryness of the stationary phase.

iii) The last objective was to increase the sensitivity of quantification via pre-concentration of the analyte of interest in the eluate. This was achieved by reducing the volume of the eluent. It has been found that 0.5 ml of eluent with an initial sample volume of 1 ml is sufficient to wet the entire polymer within the cartridge and elute the vancomycin out without significant loss (figure 6.12).

In conclusion, the following extraction protocol was found to be ideal for eluting 29 µM vancomycin out of FBS (table 6.01):

Table 6.01:

Developed solid phase extraction protocol for the Strata-X 33 u Polymeric Reversed Phase SPE cartridges from Phenomenex®:

A) Conditioning of the SPE cartridge	
	1 ml methanol
B) Equilibration of the SPE cartridge	
	1 ml DI water
	1 ml DI water

C) Extraction	
#1	1 ml sample (spiked or reference/control)
#2	1 ml DI water (washing stage)
#3	1 ml DI water (washing stage)
#4	1 m methanol (washing stage)
#5	1 m methanol (washing stage)
#6	0.5 ml 1/3 DI water + 2/3 methanol (eluent)

Figure 6.13 presents this developed extraction protocol. The typical absorbance spectra of all Gibbs labelled stages from a reference preparation with only FBS (figure 6.13 A), a sample preparation additionally containing 29 µM vancomycin (figure 6.13 B) and the difference of the two aforementioned spectra (figure 6.13 C) are illustrated. The most distinctive feature of all differential spectra is the characteristic vanGibbs peak at 589 nm of the elute (#6) shown in magenta in figure C. It indicates the presence of the highest quantity of vanGibbs, which therefore leads to the conclusion that this must be the stage in which vancomycin is mainly eluted out of the column. Figure D plots the mean absorbance values at 589 nm of all extraction stages including their standard deviations derived from three independent experiments (n = 3). The lack of overlap in error bars suggests that there is significant difference between stage #6 and the other stages (#1 - #5). This statement is supported by statistical analyses, which are discussed and presented in the appendix A.3. A one-way analysis of variance (ANOVA) and post hoc Fisher's least significant difference (LSD) test were performed. The one-way ANOVA showed significance at the 5 % level. For the post hoc Fisher's LSD test a pairwise

comparison for each stage of the SPE was performed aiming to determine which data groups are significantly different from each other. It was found that the peak absorbance signal from the eluent (#6) is significantly different from all other stages of the SPE. However, the second organic washing step (#5) showed significant difference from the sample (#1) and from the first DI water wash (#2). This may indicate that some vancomycin extraction is occurring in this wash as well. Nevertheless, it is not significant from any of the other stages. Moreover, it is has to be emphasised that only a small number of repeats (n = 3) have been performed and further experiments would lead to a strengthening of the statistical analysis.

Furthermore, the recovery of vancomycin from the SPE cartridge could be roughly calculated using the established linear function and the corresponding molar absorptivity of vanGibbs ($\varepsilon_{589\,nm}$ = 7300 ± 300 M^{-1} cm^{-1}) in figure 6.10 C. This rough estimation results in vancomycin concentration of 12 ± 2 µM in the elute (#6). For the case of a total concentration of 29 µM vancomycin, this corresponds to a recovery from the SPE cartridge of 41 ± 10 %. The errors were derived from the standard deviation from three independent experiments (n = 3) and from the error of the linear fit. However, it has to be highlighted that this is only a rough estimation with only n = 1 sample size on the linear function side and n = 3 on the SPE cartridge side and consequently the error is fairly large. More accurate recoveries will be calculated later on in the development process.

The two photographs in figure 6.13 E show the reference (top) and the spiked (bottom) SPE stages after reaction with the Gibbs reagent. The characteristic magenta colour of the elute (#6) suggests the presence of vanGibbs. The yellow and orange colour of the wash stages (#2 - #4) indicates the presence of activated Gibbs reagent, more specifically the reactive quinoneimine intermediary. The darker orange for both samples (#1) lead to the assumption that Gibbs coupling (to unspecified components) is occurring within the collected sample of both the reference and the spiked preparation. This finding is strongly supported by the observed the peak around 600 nm in figures A and B. Since this peak is present in the reference and in the spiked FBS, it can be

assumed that it must be something within the serum and was not associated with vancomycin. However, since the subtraction of these peaks results in negative values resembling the shape of the peak (figure C), one may assume that the quantity of whatever it binds to is higher in the reference than in the sample preparation. Looking ahead, this is already a first indication of vancomycin's protein binding and may lead to first presumption that SPE is not disrupting the drug-serum binding. Further studies of the effect of serum binding with special focus on free and bound drug monitoring will be discussed in subsection 6.3.6. These peaks at around 600 nm in figures A and B decreases drastically in the first DI water wash (#2) and almost vanishes in the second one (#3). This corresponds of course with the differential signal in figure C, where an increase is observed. This finding and the consequent assumption that Gibbs reagent may couple to the serum proteins was supported by two observations.

i) The first observation was the decrease in viscosity observed during pipetting. During the initial transfer of the reference (pure serum) and sample (serum spiked with vancomycin) preparations into the SPE cartridges, it was observed that they were highly viscous. The subsequently collected sample (#1) and the first DI water wash (#2) were less and less viscous. And ultimately the viscosity of the second DI water wash resembled pure water.

ii) The second observation was made after UV/vis measurements. If the cuvettes were initially cleaned with acetone, instead of water, aggregates, which stuck to the inside of the cuvettes and made them less transparent, were noticed. This effect decreased from the collected sample (#1), to the first wash (#2) and ultimately was not observable in the second DI water wash (#3). Hence, it was assumed that the serum proteins become denatured in the presence of acetone.

It could not definitively be distinguished to what Gibbs binds to, but since proteins consist of phenolic-motif containing tyrosines, it was assumed that Gibbs may bind to them. This assumption was studied and it was found that Gibbs does indeed bind to serum proteins, specifically to serum albumins. Figure 6.14 presents one sets of experiments (n = 1) with various concentrations of two different types (BSA and HSA) of

serum albumins reacted with Gibbs reagent. Figure A and B depict BSA in concentrations of 75 µM, 150 µM, 300 µM and 600 µM dissolved in DI water reacting with 13.3 mM of Gibbs reagent. Figure C and D present exactly the same for HSA.

Figure 6.14 E presents the relationships between the differential absorbances at 589 nm for both serum types and the serum albumin concentrations. As previously mentioned in subsection 6.1, BSA has 17 tyrosines, while its counterpart in humans, HSA, has 19 tyrosines (Sułkowska 2002; Zeitlinger et al. 2011). It can be observed that for both serum protein types the spectra of 600 µM are almost indistinguishable from 300 µM, which supports the assumption that Gibbs reagent couples to the tyrosines. 17 and 19 tyrosines for each albumin molecule in a concentration of 600 µM BSA and HSA respectively would in the most ideal case demand at least 10.2 and 11.4 mM Gibbs reagent. However, previous experiments have suggested that an excess of Gibbs reagent seems to be required for a complete coupling reaction. Additionally it can be observed that the absorbances for HSA are slightly higher than for BSA. This would again support the theory of coupling to tyrosines as HSA has two tyrosines more than its bovine counterpart. However, since the sample size is kept minimal (n = 1), these are only assumptions and the enlarged absorbances may be within errors. Hence further experiments would lead to a strengthening of these findings and would allow statistical analysis. However, at this point in the development process, this study was not deemed relevant for the colourimetric detection assay since serum proteins can be removed with the just described extraction protocol. Therefore, the ability of Gibb reagent to couple to serum albumin was not further investigated. Nevertheless, it may be something to consider for a future multi analyte therapeutic monitoring device as serum albumin levels are useful prognostic marker and indicator for nutritional status, inflammation and protein deficit especially in ICU patients (Don and Kaysen 2004; Seve et al. 2006; Lai et al. 2011; Pan et al. 2013).

In conclusion, the proof that Gibbs is binding to serum albumin and absorbs at the same wavelength as vanGibbs adds another compelling argument for the necessity of an extraction protocol that removes serum proteins prior to the coupling reaction.

Additionally it shows that two DI water washes seem sufficient to elute the majority of the proteins out of the SPE cartridge. Consequently, this will increase the sensitivity and specificity of the subsequent colourimetric quantification of vancomycin, which is crucial since in a bench top device no reference spectra can be obtained. The inter-patient serum levels may vary drastically, which would have lead to falsely elevated absorbance signals limiting the ability to accurately detect the vancomycin concentration within the patient's blood.

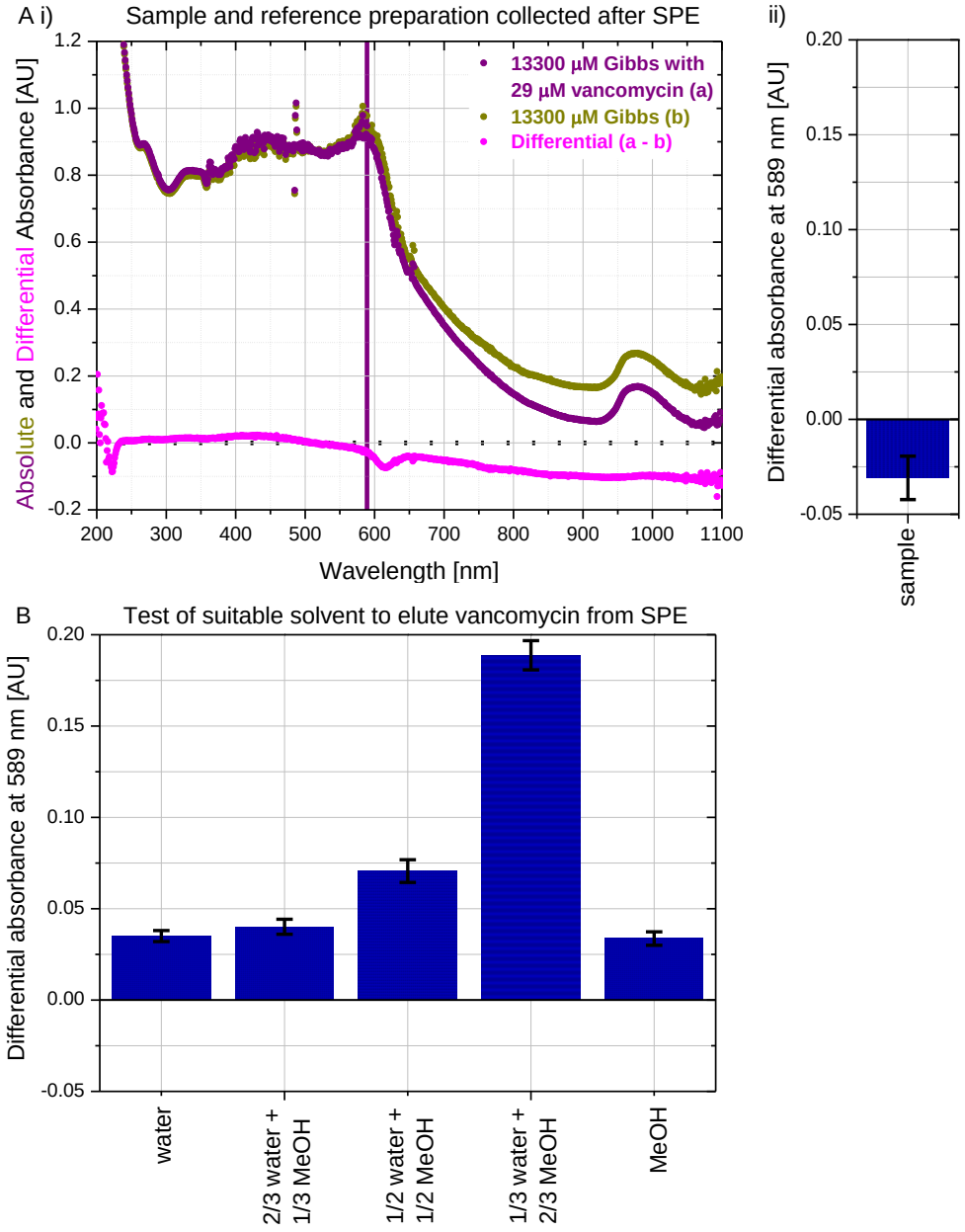

Figure 6.09: Test of a suitable solvent to elute vancomycin from the SPE cartridge. A) Sample and reference preparation collected after the passage through SPE cartridges. i) The dark yellow (a) and purple (b) curves represent 13300 µM Gibbs at high pH without and with 29 µM vancomycin respectively. The magenta spectrum (a – b) represents the difference of the two aforementioned spectra. The purple line highlights vanGibbs' λ_{max}. ii) The column chart represents the average of the differential absorbances at 589 nm. The error bar corresponds to the range obtained by two independent experiments (n = 2). The negativity suggests that not only vancomycin is retained in the SPE cartridge but presumably also a serum constituent. This observation will be further studied later on in this thesis. **B) After the sample and reference collection, several solvents were individually tested via the same procedure presented in the figures A.** As the coupling reaction already consists of water and methanol, various mixtures of these solvents were tested first. Again the error bar corresponds to the range obtained by two independent experiments (n = 2). It is evident that the most vanGibbs is eluted from the SPE cartridge with a ratio of 1/3 water + 2/3 methanol.

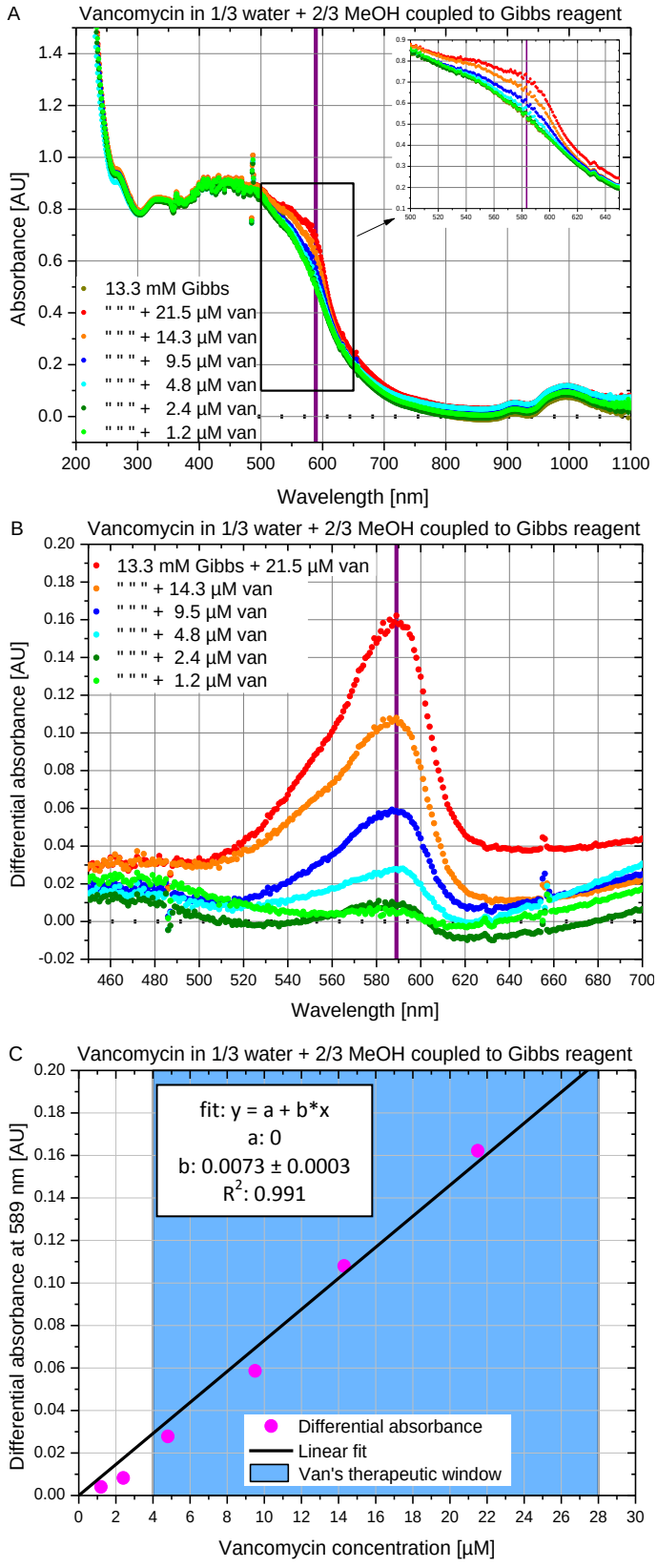

Figure 6.10: Test of potential eluent for the ability to optically detect therapeutic vancomycin concentrations via Gibbs reagent coupling.
A) Absorbance spectra of different vancomycin concentrations reacted with Gibbs in the solvent mixture chosen to be the eluent. Overlay of several absorbance spectra of Gibbs reagent (13.3 mM) reacted with therapeutic vancomycin concentration spanning from 1.2 to 21.5 µM. As usual the Gibbs reference spectrum is shown in dark yellow and the vertical line highlights the λ_{max} of vanGibbs. The enlarged image in the top right corner depicts the wavelength region where the vanGibbs peaks are occurring.
B) Enlarged overlay of the differential spectra obtained by subtraction of the Gibbs reference spectrum from the various spectra presented in figure A. The vanGibbs peak is evident down to a concentration of 2.4 µM vancomycin. However, as previously seen in figure 6.08 B, the peaks do not show an explicit bimodal shape as observed in the initial experiments (see 6.3.1).
C) Relationship between concentration and absorbance. The differential absorbances are plotted against their corresponding vancomycin concentrations. The blue box indicates vancomycin's therapeutic window (4 – 28 µM). The slope of the linear fit gives an estimate for vanGibbs' $\varepsilon_{589\,nm}$ in this potential eluent. It equals to 7300 ± 300 M^{-1} cm^{-1}. Since this experiment was performed prior to finalising the elution protocol, the sample size was kept to a minimum (n = 1).

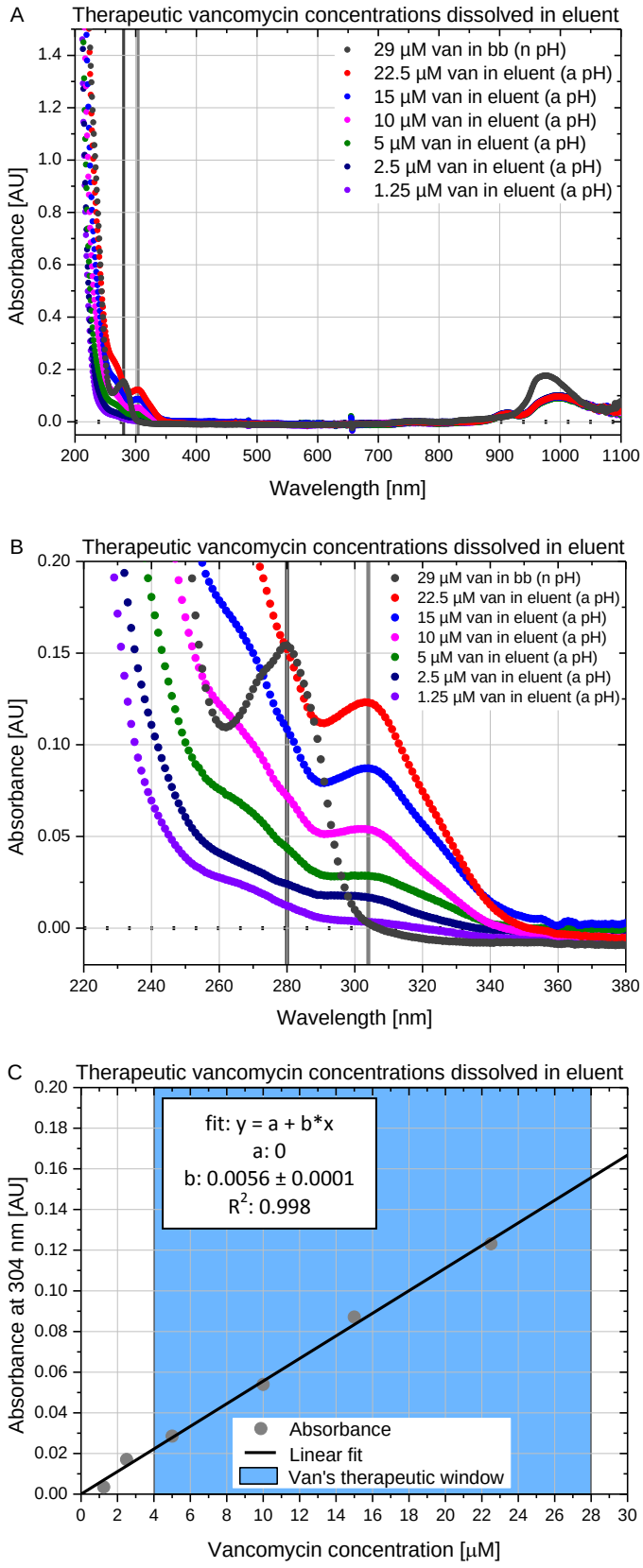

Figure 6.11: Assessment of pure vancomycin absorbances in the solvent mixture planned to be the eluent for the SPE.
A) Absorbance spectra of therapeutic vancomycin concentrations dissolved in the eluent. The absorbance spectrum of 29 µM vancomycin in borate buffer (bb) at neutral pH (n pH) has the λ_{max} around 281 nm highlighted with a dark grey line. The other six therapeutic concentrations were dissolved in the eluent with an alkaline pH (a pH). The λ_{max} in the eluent shifted to 304 nm marked with a grey line.
B) Enlarged section of figure A. Besides the two peaks discussed above it can also be observed that the region between 220 to 280 nm seems to be changing even though the ratios of methanol and water were kept constant. Hence it must be associated with vancomycin. This observation will not be further investigated in this thesis.
C) Relationship between concentration and absorbance. The absorbances at 304 nm are plotted against their corresponding vancomycin concentrations. The blue box indicates van's therapeutic window (4 – 28 µM). The slope of the linear fit gives an estimate for vancomycin's $\varepsilon_{304\,nm}$ in this potential eluent. It equals to 5600 ± 100 M^{-1} cm^{-1}, which is in very good agreement with vancomycin in water at neutral pH ($\varepsilon_{282\,nm}$ = 5943 M^{-1} cm^{-1}) ("The Merck Index Online - Vancomycin" 2013). Since the objective of this experiment was just a brief assessment, the sample size was kept to a minimum (n = 1).

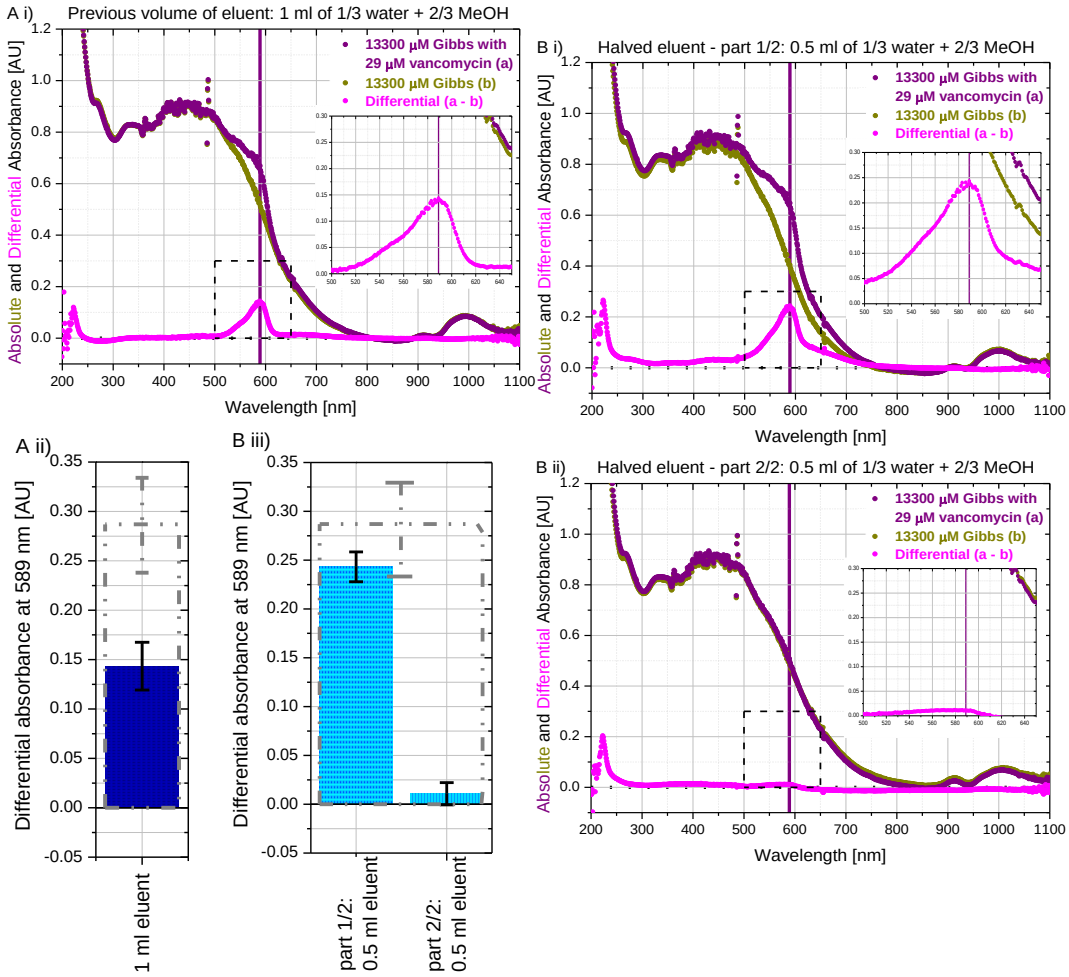

Figure 6.12: Feasibility test for the reduction of the eluent volume aiming to increase the sensitivity. A) Previously used eluent volume: 1 ml of 1/3 water + 2/3 MeOH. i) As usual the dark yellow (a) and purple (b) curves represent 13300 µM Gibbs without and with 29 µM vancomycin, whilst the magenta spectrum (a – b) represents their difference. The dashed box highlights the image part, which is enlarged on the right hand side. ii) The column chart represents the average of the differential absorbances at vanGibbs' λ_{max}. The error bar corresponds to the calculated standard deviation from three independent experiments (n = 3). It has to be highlighted that these absorbances are a bit lower than previous experiments. The grey dashed box including error bar indicates the expected differential absorbance if half of the eluent volume is used. **B) Halved eluent volume: 0.5 ml.** i) The figure presents the absorbance spectra obtained by elution with half of the previous eluent volume. The curves are displayed in a similar manner to figure A i. The expected increase in absorbance at 589 nm can be observed. ii) After the first elution with 0.5 ml, a second elution with the same volume was performed to check whether the first elution was sufficient to wet the entire polymer within the cartridge and to elute the vancomycin from it. It was found that the differential absorbance at 589 nm was almost zero. iii) The column chart designates the average differential absorbance at 589 nm for the first elution (part 1/2) shown in figure B i and the second one (part 2/2) shown in figure B ii. Again the error bars are the calculated standard deviations from three independent experiments (n = 3). It can be observed that the error bar of the expected absorbance, indicated in grey dashed lines, is overlapping the error bar of the absorbance of part 1/2. Furthermore, the error bar of the absorbance of part 2/2 intercepts zero. Therefore, it was concluded that 0.5 ml eluent is sufficient to elute vancomycin from the SPE cartridge without significant loss.

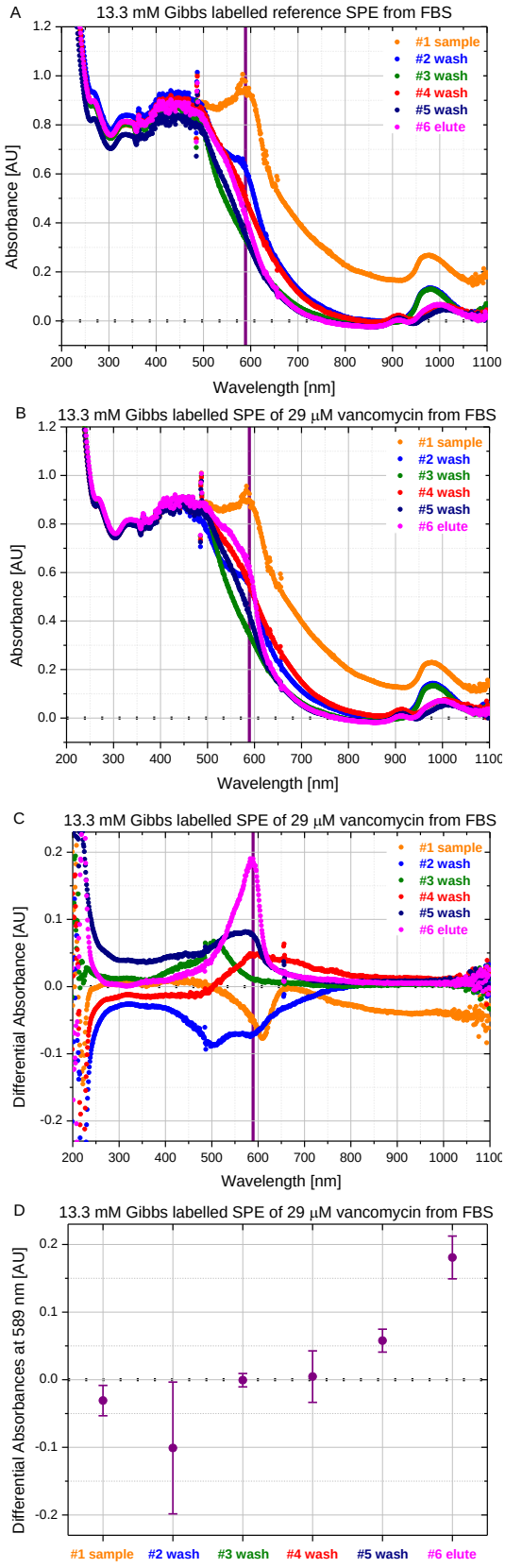

Figure 6.13: Developed extraction protocol of vancomycin from foetal bovine serum. A) Typical UV/vis absorbance spectra for solid phase extraction of the reference FBS without vancomycin. #1 sample refers to the first collected fraction from the SPE cartridge after adding the reference FBS into the cartridge. Four washes and the final elute were subsequently collected. 350 µl of each solution was transferred to an Eppendorf along with 50 µl of 13.3 mM Gibbs reagent in methanol followed by 40 µl of 0.4 M sodium hydroxide in water. 350 µl of the combined solution was then transferred to a cuvette for spectroscopic analysis. The purple line at 589 nm denotes the λ_{max} of vanGibbs. **B) Typical UV/vis spectra for SPE of spiked FBS with vancomycin.** The same procedure as described for graph A was applied to FBS spiked with 29 µM vancomycin. **C) Differential UV/vis spectra.** The corresponding absorbance values from spiked and reference FBS were subtracted from each other. **D) Average differential absorbances at 589 nm of all extraction stages and appropriate errors.** The elute (#6) has the highest absorbance indicating the highest vanGibbs quantity. The errors are standard deviation of the averages (n = 3). The lack of overlap in error bars suggests that the elute is significantly different from the other stages, which is supported by statistical analysis presented in the appendix on page 350. **E) Photography of the reference and the spiked SPE stages after reaction with the Gibbs reagent.** The characteristic magenta colour of the elute proves the presence of vanGibbs. The darker orange for both samples may suggest Gibbs coupling to serum proteins. Yellow and orange corresponds to the presence of activated Gibbs reagent.

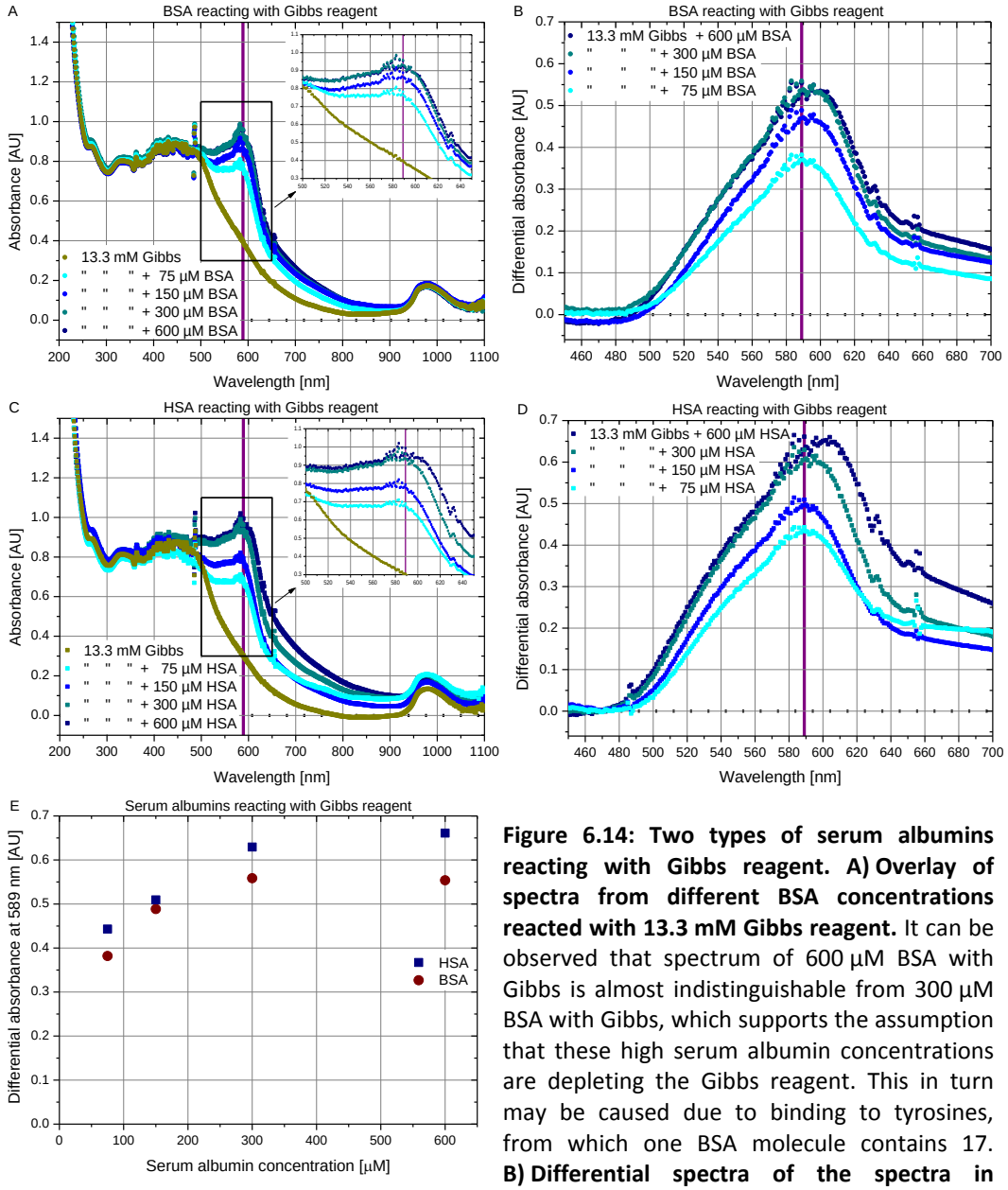

Figure 6.14: Two types of serum albumins reacting with Gibbs reagent. A) Overlay of spectra from different BSA concentrations reacted with 13.3 mM Gibbs reagent. It can be observed that spectrum of 600 µM BSA with Gibbs is almost indistinguishable from 300 µM BSA with Gibbs, which supports the assumption that these high serum albumin concentrations are depleting the Gibbs reagent. This in turn may be caused due to binding to tyrosines, from which one BSA molecule contains 17. **B) Differential spectra of the spectra in figure A.** The maximal absorbance wavelength of Gibbs-BSA is very similar to the vanGibbs, which is indicated with a purple line at 589 nm, whilst however the shape of the peak differs. **C) Overlay of spectra from different HSA concentrations reacted with 13.3 mM Gibbs reagent.** In general, the observations are very comparable to figure A. **D) Differential spectra of the preceding spectra in figure C.** Again the general observations are similar to figure A and B with the exception that the absorbances are slightly higher. These enlarged absorbances may be caused by the two additional tyrosines present in the HSA molecule. However, since the sample size is kept minimal (n = 1), these are only assumptions and the enlarged absorbances may be within errors. Hence further experiments would lead to a strengthening of these findings and would allow statistical analysis. **E) Relationships between concentration and absorbance.** All differential absorbances at 589 nm are plotted against the corresponding serum albumin concentrations. The previous made observation with saturation of the absorbance value can be observed. Furthermore, the slight enlarged absorbances of HSA can be seen as well.

6.3.4 Optimisation of the Gibbs Reagent Concentration

Some studies suggested that an excess of 25 – 30 times Gibbs reagent versus phenolic compound leads to a high maximal absorbance of the coupling product (Svobodová et al. 1978; Svobodová et al. 1977), which was also supported by previous experiments discussed in the previous subsection (6.3.3). Furthermore, since rapidity is a key requirement for a sensor quantifying drug concentrations, a fast reaction is sought after. Consequently based on the fundamental principle of Le Châtelier (Atkins and De Paula 2002), an excess of Gibbs reagent seems favourable.

However, since Gibbs reagent coupled to vancomycin has to best of our knowledge never been done before, there are no existing studies that suggest a similar ratio would have the same effect with vancomycin coupling. Moreover, there has to be a balance between a sufficient reaction velocity and a high sensitivity via enlarging the absorbance intensity whilst keeping the background absorbance of un-reacted Gibbs as low as possible, so that it is not masking and falsely elevated the absorbance of vanGibbs. As visible in figures 6.06 and 6.08, high concentrations of activated Gibbs is absorbing between 350 and 500 nm with two distinctive shoulders at around 410 and 460 nm. Afterwards the absorbance decreases until it reaches zero at approximately 800 nm. Since the maximal absorbance of vanGibbs (λ_{max} = 589 nm) lies within the decreasing slope, achieving the best balance of the arguments stated above is crucial. Furthermore, no subtraction of a reference spectrum for each individual sample is possible in a bench top device, which adds another compelling argument to a sensitive and accurate quantification of vancomycin.

Therefore this subsection presents the optimisation of the Gibbs reagent concentration for two different vancomycin concentrations. The concentrations were chosen at the two extremes, namely below (1 µM) and beyond (36.5 µM) the therapeutic window of vancomycin (4 – 28 µM). The objective was to estimate whether an optimum can be found suitable for the whole therapeutic window. The concentration beyond was chosen a bit larger in anticipation that the administrated vancomycin concentration will follow its trend of constant increase observed in the past (Kitzis and Goldstein 2006;

Rybak et al. 2009a; Holmes, Johnson, and Howden 2012; Pumerantz et al. 2011; Estes and Derendorf 2010; Chen 2013; Calfee 2012; van Hal, Lodise, and Paterson 2012; Muppidi et al. 2012; Dhand and Sakoulas 2012).

To not induce further potential for errors and for time efficiency reason, these experiments were performed in absence of a biological matrix in the elute mixture (1/3 DI water + 2/3 methanol). The optimisation was achieved via a several stages procedure, where in the Gibbs reagent concentrations systematically got narrowed to the most optimal concentration ratio range. The procedure was that the corresponding activated Gibbs reagent without vancomycin served as reference and was subtracted from the spectrum with vancomycin.

Figures 6.15 A presents some selected spectra of the described optimisation procedure for 36.5 µM of vancomycin. The spectra are averages from the three spectra, which were taken per individual Gibbs reagent concentration with and without vancomycin respectively. Spectra with solely Gibbs reagent are drawn with open spheres, whilst spectra with vancomycin are drawn with solid spheres. The 'av' in brackets indicates that all drawn spectra are average spectra from three independent experiments (n = 3).

It can be observed that especially the first shoulder of all Gibbs spectra around 400 nm decreases upon reaction with vancomycin. Hence this decrease could theoretically also be used to quantify the vancomycin concentration in the sample and seems to only depend on one compound namely the Gibbs reagent. However, since this decrease only ranged from -0.01 to -0.04 AU for a concentration slightly above vancomycin's therapeutic window, this approach was deemed irrelevant for this thesis and consequently was not further studied. To investigate the contribution of the Gibbs reagent absorbance to the vanGibbs absorbance at 589 nm, the molar absorptivity of Gibbs reagent was calculated and was found to be 28 ± 1 M^{-1} cm^{-1} ($\varepsilon_{589\,nm}$). Therefore it can be concluded that its contribution to the vanGibbs absorbance is almost negligible. Nevertheless for exact quantification of vancomycin in a sample, the absorbance value

obtained after subtracting the absorbance of the used Gibbs reagent should be adjusted for the decrease in Gibbs reagent upon reaction with vancomycin.

Figure 6.15 B plots the differential spectra of figure A. The absorbances at 589 nm from these differential spectra were plotted against the Gibbs reagent concentration. A bell shaped distribution of these data points was expected. On the left hand side of the bell shaped curve, where the Gibbs concentrations are low, the limiting factor of the reaction is the Gibbs concentration itself. Therefore, the concentration of the end product is correspondingly low resulting in a low absorbance at the vanGibbs maximal absorbance wavelength. Thus the predominant species is un-reacted vancomycin. Whilst increasing the Gibbs concentration, the reaction equilibrium shifts towards quantitatively more end product leading in increased absorbances at 589 nm. Heading over the maximum towards the right hand site of the bell shaped curve, where the Gibbs concentrations are high, the limiting factor are the quantities of vancomycin present in the sample. The resulting differential absorbances for the end product are low again, due to masking by the background absorbance of the activated Gibbs molecules. If no masking effect would occur, then a curve would be expected that saturates comparable in shape to figure 6.06 E. The saturation signal of this curve would correspond to approximately the initial vancomycin concentration.

Figure 6.15 C shows the absorbances at 589 nm for the two different vancomycin concentrations, 1 and 36.5 µM, drawn against a common logarithmic (base 10) scale of the various Gibbs reagent concentrations. The expected bell curve is visible for 36.5 µM but not for 1 µM of vancomycin. Consequently, 1 µM of vancomycin was deemed as tentative detection limit. The associated error bars are the standard deviations derived from three independent experiments (n=3). Within the region with the largest absorbances, the error bars are overlapping, which suggests that these concentrations are not distinct from each other.

The large variation also makes it hard to fit a model to the data points. To get an estimate where the maximum lies regarding to its x-value, the weighted arithmetic mean was calculated using the following formula (Hackbusch, Schwarz, and Zeidler 1996):

$$\bar{x} = \frac{\sum_{i=1}^{n} x_i \cdot y_i}{\sum_{i=1}^{n} y_i} \qquad 6.2$$

i represents the individual values of absorbances in the figure 6.15 C. In the numerator, all x and y-values are multiplied and subsequently summed, and in the denominator only y-values are summed. Consequently, the calculated means of the maxima were 6200 ± 900 µM Gibbs reagent for 36.5 µM vancomycin and 162 ± 1 µM Gibbs reagent for 1 µM vancomycin. The errors correspond to the standard deviations derived from three independent sets of experiments. The maxima are indicated in the figure 6.15 C with a dotted line and a box for the high concentration of vancomycin and with a dotted line for the low concentration respectively. However, it has to be emphasised that these calculated maxima are strongly dependent on the chosen concentrations and should therefore only be considered as an estimation.

Since the goal is to quantify unknown vancomycin concentrations in patient's blood samples, it is important to initially find a Gibbs concentration range, which preferably would be ideal for the whole therapeutic range. Therefore, the Gibbs concentrations were divided by the corresponding concentrations of vancomycin (1 and 36.5 µM) resulting in a multiple of the Gibbs reagent excess in relation to the antibiotic concentration. It was found that range between 100 to 150 times excess of Gibbs reagent seems to be ideal for both extreme concentrations. Additionally the differential absorbances of both concentrations seem to stay constant within excesses of up to 300 – 320 times and do not result in more than 13 % absorbances signal loss. This observation correlates with the calculated means of the maxima, which are 162 ± 1 µM for 1 µM and 170 ± 24 µM for 36.5 µM of vancomycin and consequently higher than 100 to 150 times excess.

To summarise, it was found that the range between 100 and 150 times excess results in highest absorbances. In comparison to previous study quoted at the beginning of this subsection (Svobodová et al. 1978), this optimised excess is roughly five to six fold larger than that observed in the original Gibbs reagent reaction. This may be another indication that several Gibbs reagent molecules are coupling to one vancomycin equivalent. This will further be discussed in the next chapter 7. Moreover, it was found that from an excess of 100 to presumably 300 – 320 times the decrease in absorbance signal is not more than 13 %.

Therefore, even though it cannot be unambiguously proven, it will be assumed for further experiments that in this optimised Gibbs region the Gibbs reagent and the vanGibbs absorbances are additive at vanGibbs's λ_{max} allowing subtraction of the Gibbs only absorbance from the total absorbance. However on the other hand, finding that such a large excess is the most optimal for the assay's sensitivity is less ideal for a TDM device, which must detect the whole therapeutic window of vancomycin. Since for quantification of an unknown vancomycin concentration within 4 to 28 µM, the optimal Gibbs reagent concentration lays somewhere between about 400 to 4350 µM. This challenge will further be discussed in the conclusion and outlook chapter (6.4).

To visualise the impact of this Gibbs reagent optimisation, figure 6.16 shows a comparison with the same vancomycin concentration. Graph A shows 29 µM of vancomycin reacted with the previously used Gibbs concentration, namely 13300 µM, which corresponds to an almost 460 times excess. Graph B shows the same antibiotic concentration reacted with a concentration within the optimal range according to the used vancomycin of 29 µM. The chosen concentration was 3625 µM of Gibbs reagent, which for 29 µM vancomycin correspond to an excess of 125 times. It can be observed, that the background absorbance of Gibbs reagent decreased significantly and consequently the characteristic bimodal shape of the vanGibbs peak in the raw as well as in the differential spectrum is more apparent and distinct. The absorbance at the vanGibbs wavelength (λ_{max} = 589 nm) increased from 0.18 ± 0.02 AU for a Gibbs concentration of 13300 µM to 0.26 ± 0.01 AU for 3625 µM. The errors correspond to

standard deviations derived from three independent experiments (n = 3). Hence it can be concluded that this optimised Gibbs concentration corresponds to a 45 % increase, which should directly translate into the same increase of assay sensitivity.

Therefore the next step was to test this expected sensitivity increase with a series in which therapeutic vancomycin concentrations (1.2 – 29 µM) in the eluent mixture were labelled with the novel optimised Gibbs reagent (3625 µM) in methanol. The experimental procedure was exactly the same as described in the previous chapter (6.3.3) for figure 6.10. The molar absorptivity ($\varepsilon_{589\,nm}$) there was found to be around 7300 ± 300 M^{-1} cm^{-1}. Figure 6.17 A and B show the characteristic bimodal vanGibbs peak for all spectra except for the spectra with only 1.2 µM vancomycin. This suggests that this concentration may lie beyond the current detection limit. Furthermore, it can be observed that the vanGibbs' λ_{max} has broadened with a slight hypsochromic shift. It seems to span from about 582 to 589 nm. This broadening will be kept under surveillance in the course of this thesis.

Figure 6.17 C plots the differential absorbances against their corresponding vancomycin concentrations. The slope of the linear fit gives an estimate for the novel vanGibbs' $\varepsilon_{589\,nm}$ with this optimised Gibbs reagent concentration, which was found to be 9100 ± 200 M^{-1} cm^{-1}. This is an increase of about 25 % in comparison to 7300 ± 300 M^{-1} cm^{-1}. It has to be highlighted that since this experiment was performed to only test the expected increase, the sample size was kept to a minimum (n = 1).

Therefore with this enlarged molar absorptivity and consequently increased sensitivity all further experiments presented hereafter will be performed with a Gibbs reagent concentration of 3625 µM. Furthermore, all differential absorbances will be multiplied by a factor 1.00267 to account for the decrease in Gibbs reagent upon coupling to vancomycin.

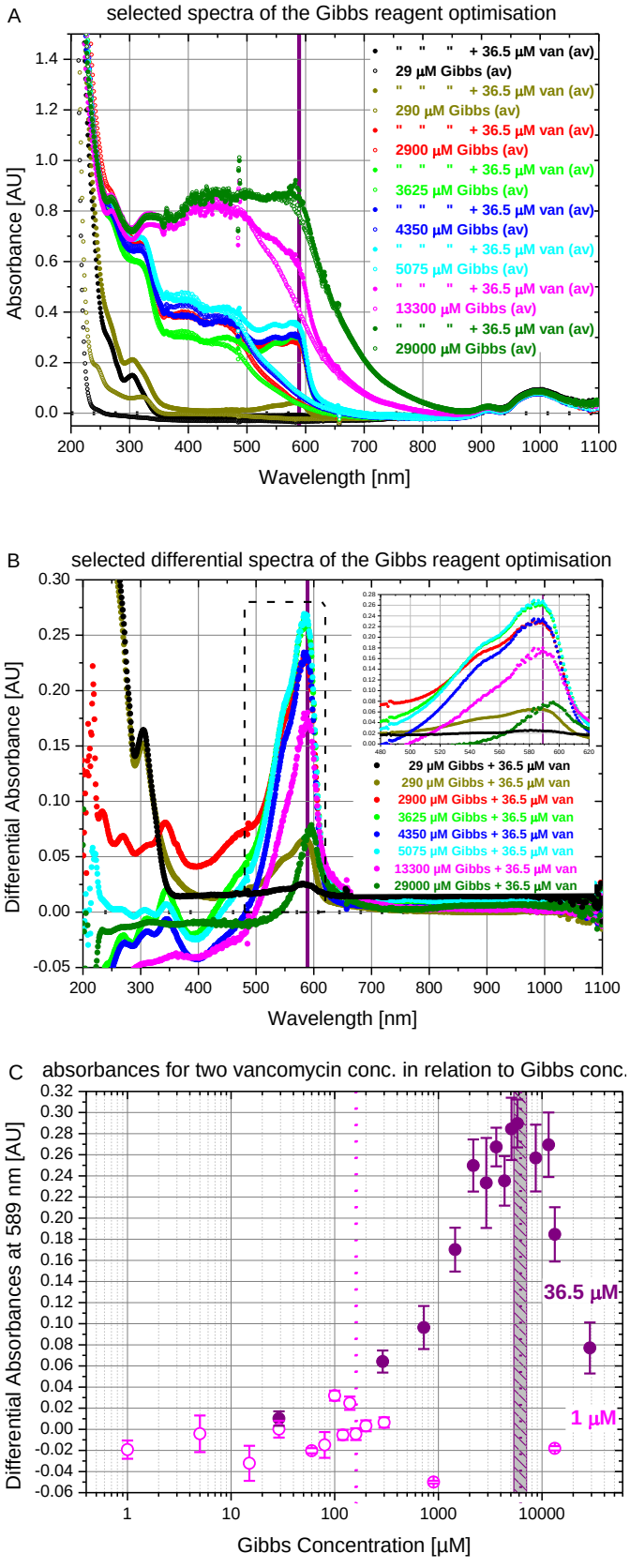

Figure 6.15: Optimisation of the Gibbs reagent concentration in relation to two constant vancomycin concentrations.
A) Selected spectra of different Gibbs concentrations only and the corresponding spectra where this Gibbs concentration had reacted with 36.5 µM vancomycin. The 'av' in brackets indicates that all spectra were average spectra obtained from three independent experiments (n = 3).
B) Differential spectra of the preceding spectra in figure A. The inset on the right shows a zoom of the region framed with a dashed box. It can be observed that 3625 µM (~ 100 x excess) and 5075 µM (~ 140 x excess) of Gibbs seem to result in highest absorbances.
C) Differential absorbances with errors at 589 nm of two vancomycin concentrations labelled with various different Gibbs concentrations versus this corresponding concentrations in logarithmic scale. The errors are standard deviations derived from three independent experiments. The expected bell curve is visible for 36.5 µM of vancomycin but not for 1 µM. This may be an indication that 1 µM is the detection limit, which will be further investigated hereafter. The dotted lines in the corresponding colours indicate the weighted arithmetic mean of the maxima of the concentrations, which are 6219 ± 873 µM for 36.5 µM and 162 ± 1 µM for 1 µM of vancomycin. The surrounding grey box of the maximum for 36.5 µM of vancomycin corresponds to its error, which was again the standard deviation derived from three sets.

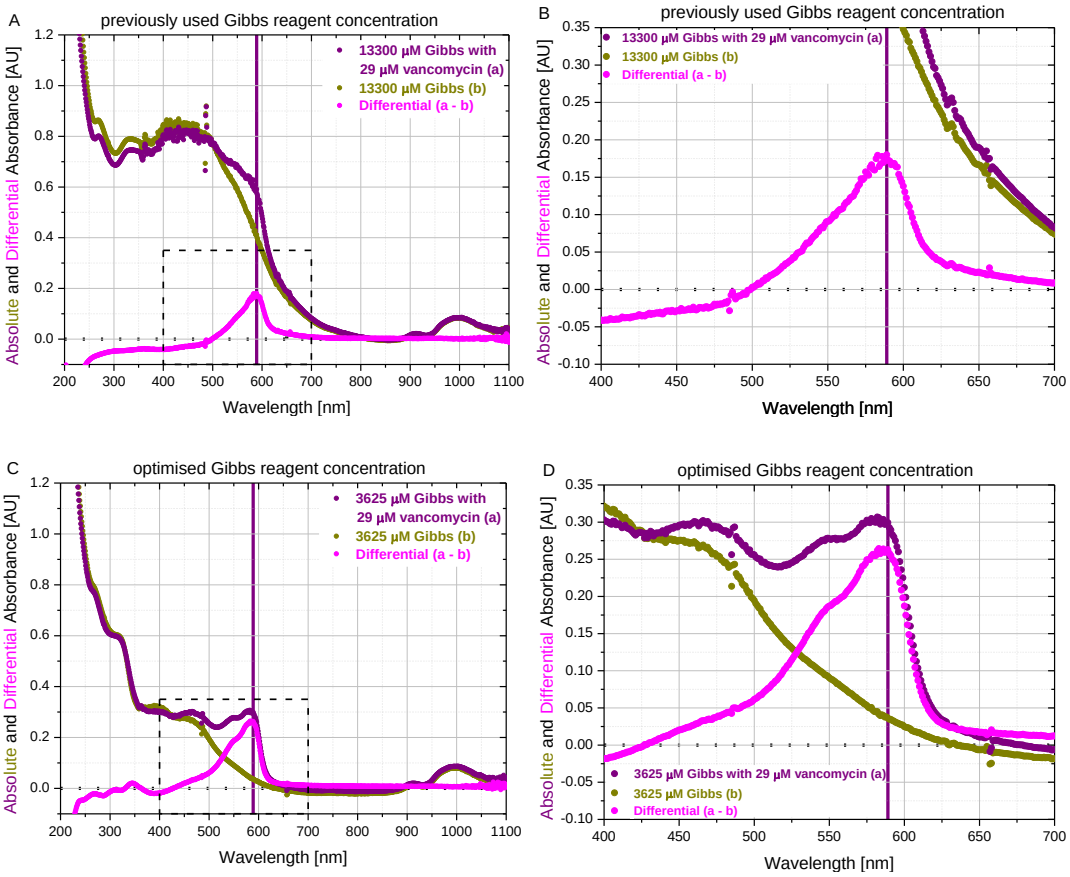

Figure 6.16: Comparison between the previously used Gibbs reagent concentration and the optimised concentration in reaction with 29 µM vancomycin. A) 29 µM vancomycin labelled with the previously used Gibbs reagent concentration of 13300 µM, which corresponds to almost 460 x excess. The dark yellow (labelled with an a) and purple (b) curves represent 13300 µM Gibbs at high pH without and with vancomycin respectively. The magenta spectrum (a – b) represents the difference of the two aforementioned spectra. The dotted box indicates the section of the graph, which is enlarged in figure B. **B) Enlarged section of figure A.** The differential absorbance value at 589 nm was found to be 0.18 ± 0.02 AU. All errors correspond to standard deviations derived from three independent experiments (n = 3). As previously observed, the shape of the vanGibbs peak is not bimodal as in the initial experiments (see 6.3.1). **B) 29 µM vancomycin labelled with a Gibbs reagent concentration within the optimal range for the corresponding vancomycin concentration, which was 3625 µM and that corresponds to an excess of 125 x.** The colour coding is the same as in figures A and B. **D) Enlarged section of figure C.** The differential absorbance value at 589 nm was found to be 0.26 ± 0.01 AU, which is a 45 % increase in comparison to the previously used Gibbs concentration. A similar increase is therefore expected for the colourimetric assay's sensitivity (see figure 6.17). Furthermore, it can be observed that the shape of the vanGibbs peak is bimodal again as in the initial experiments in the first chapter. This leads to the assumption that large excess of Gibbs reagent may lead to a slightly different molecule or molecules than a smaller excess. This will be considered for the following experiments as well as the vanGibbs characterisation presented in chapter 7.

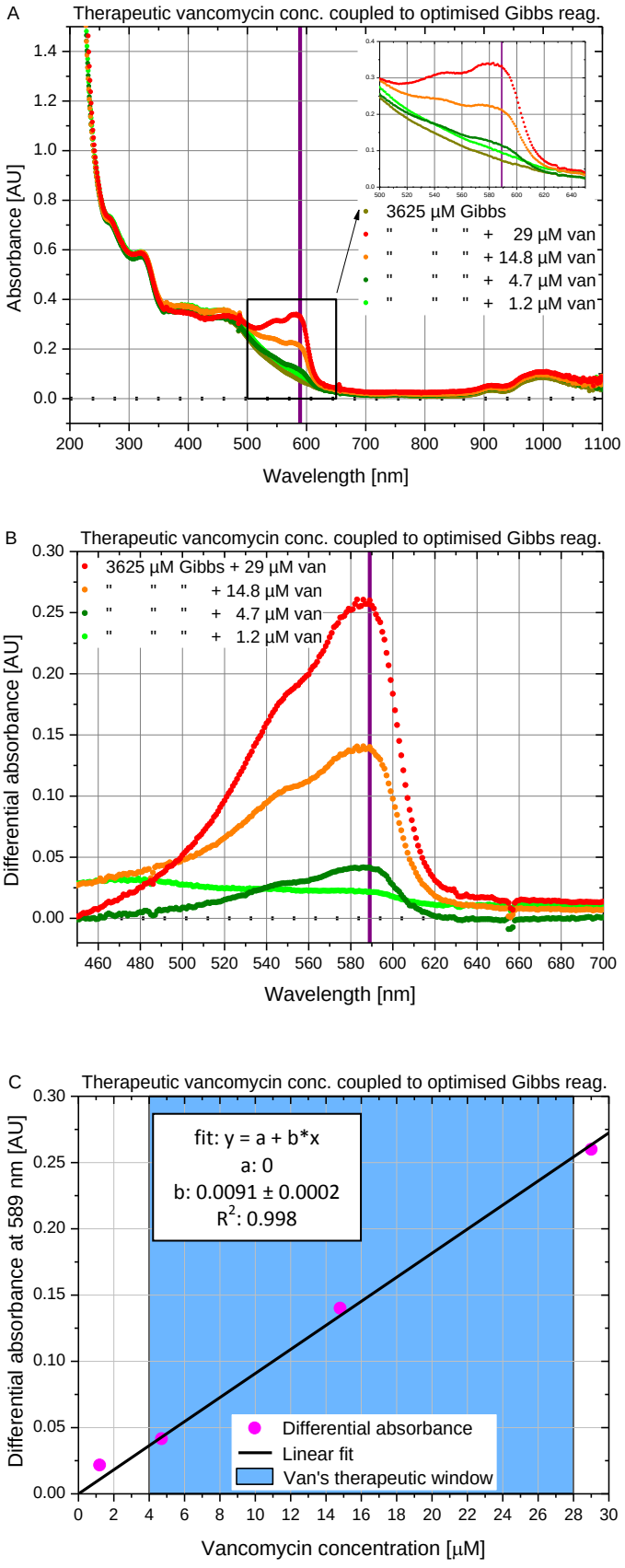

Figure 6.17: Test of expected sensitivity increase due to the optimised Gibbs reagent concentration.
A) Absorbance spectra of different therapeutic vancomycin concentrations reacted with the optimised Gibbs concentration. Overlay of several absorbance spectra of 3625 µM Gibbs reagent reacted with vancomycin concentrations spanning from 1.2 to 29 µM. The enlarged image in the top right corner depicts the region where the vanGibbs peak is occurring (λ_{max} = 589 nm).
B) Enlarged overlay of the differential spectra obtained by subtraction of the Gibbs reference spectrum from the various spectra presented in figure A. The characteristic bimodal vanGibbs peak is clearly visible in all spectra except in the spectrum of 1.2 µM. This suggests that this concentration lies beyond the current detection limit. Further, it seems that vanGibbs' λ_{max} has broadened with a slight blueshift (hypsochromic). It ranges from about 582 to 589 nm, which will be kept under further surveillance.
C) Relationship between concentration and absorbance. The differential absorbances are plotted against their corresponding vancomycin concentrations. The slope of the linear fit gives an estimate for vanGibbs' $\varepsilon_{589\,nm}$ with this optimised Gibbs reagent concentration. It equals to 9100 ± 200 M^{-1} cm^{-1}, which is an increase of about 25 % in comparison to 7300 ± 300 M^{-1} cm^{-1} (figure 6.10 C). Since this experiment was performed to test the expected increase with the optimised Gibbs concentration, the sample size was kept to a minimum (n = 1).

6.3.5 Change from Foetal Bovine to Whole Human Serum

After development of the extraction protocol (6.3.3) and optimisation of the Gibbs reagent ratio that lead in higher sensitivity (6.3.4dis), it was expected that changing from the foetal bovine serum (FBS) to whole human serum (WHS) is trivial and a matter of one set of experiments. But as evident in figure 6.18, this was not true and it seems that vancomycin partly change its elution condition according to serum type in which it is dissolved in.

Figure 6.18 A shows an overlay of the differential UV/vis spectra for all SPE stages from FBS and subsequently labelling with the previously established optimised Gibbs reagent concentration of 3625 µM.

Figure 6.18 B presents a comparable overlay but this time 29 µM vancomycin was dissolved in WHS as opposed to FBS. The differential spectra look fairly similar to figure A except of the first methanol wash (#4). The differential spectra of the first methanol wash (#4) shows also a vancomycin typical bimodal shaped peak slightly lower in absorbance than the peak from the elute (#6).

Figure 6.18 C compares all average absorbances with the associated errors at the vanGibbs λ_{max} (589 nm) for FBS and WHS. The stated errors correspond to standard deviations derived from three independent experiments (n = 3). The main difference between FBS and WHS is the extent of absorbance in the first methanol wash (#4), which is indicated with an arrow. This suggests vancomycin is additionally extracted from SPE carried out with WHS in the first methanol wash (#4).

This suggestion is strongly supported by statistical tests, which can be found in the appendix A.4. The ANOVA and the post-hoc Fisher's LSD tests of WHS showed that #4 and #6 are significantly different from the all other SPE stages and therefore suggesting that vancomycin is mainly extracted at these two stages of SPE. However, the analysis for FBS was not statistically significant at the 95 % confidence level. This may be due the fairly high absorbance of the collected sample (#1).

For WHS, the average absorbance values at the vanGibbs maximal absorbance wavelength (λ_{max} = 589 nm) are 0.178 ± 0.003 AU for #4 and 0.183 ± 0.015 AU for #6 and consequently fairly similar. However, it has to be highlighted that the concentration of the compound of interest in both elutes (#6) is artificially doubled due to pre-concentration achieved by halving the eluent volume (see subsection 6.3.3).

Calculations with the previously estimated $\varepsilon_{589\,nm}$ = 9100 ± 200 M^{-1} cm^{-1} (see subsection 6.3.4 and figure 6.17) gives a vancomycin content in the #6 for FBS of 10 ± 2 µM, which corresponds to a recovery from the SPE cartridge of 34 ± 7 %. Furthermore, it seems as if #1 and #5 may also have a bit of vancomycin eluted out. However, it has to be highlighted that the associated errors are large. The corresponding concentrations are 6 ± 5 µM for #1 and 3 ± 2 µM for #5, which in total would give a concentration of 19 ± 9 µM vancomycin and a total recovery of 66 ± 31 %.

On the other hand, concentration calculations for WHS yield in 20 ± 1 µM for #4 and 10 ± 2 µM for #6, which added results in 30 ± 3 µM of total vancomycin concentration. This in turn gives a recovery of 102 ± 4 %, which cannot be true. Especially not in light of #3 and #5, which also show a slight vancomycin content of 3 ± 1 µM and 7 ± 2 µM respectively. An addition of all these vancomycin contents would render an even higher recovery of 138 ± 31 %.

This finding suggests the hypothesis that one eluted species may be vancomycin bound to serum proteins and the other one free vancomycin. Therefore this falsely elevated recovery could be explained by the additional absorbance of the serum protein to which vancomycin is binding to. This is backed by previous findings (figure 6.14 in chapter 6.3.3) showing that Gibbs reagent is binding to serum albumins and resulting UV/vis spectra show maximal absorbance at the vanGibbs λ_{max}.

Moreover, this hypothesis is supported by the solvent difference between the two stages. The solvent for stage #4 is purely organic, whilst the solvent for #6 is an aqueous organic mixture, which demands a variation in the eluted species that changes this solvent preference.

Nonetheless it can definitively be assumed that both eluted species are associated with vancomycin, since this is the only difference between the control and spiked serum samples. The investigation of this hypothesis of bound and free vancomycin will be discussed in the next subsection 6.3.6.

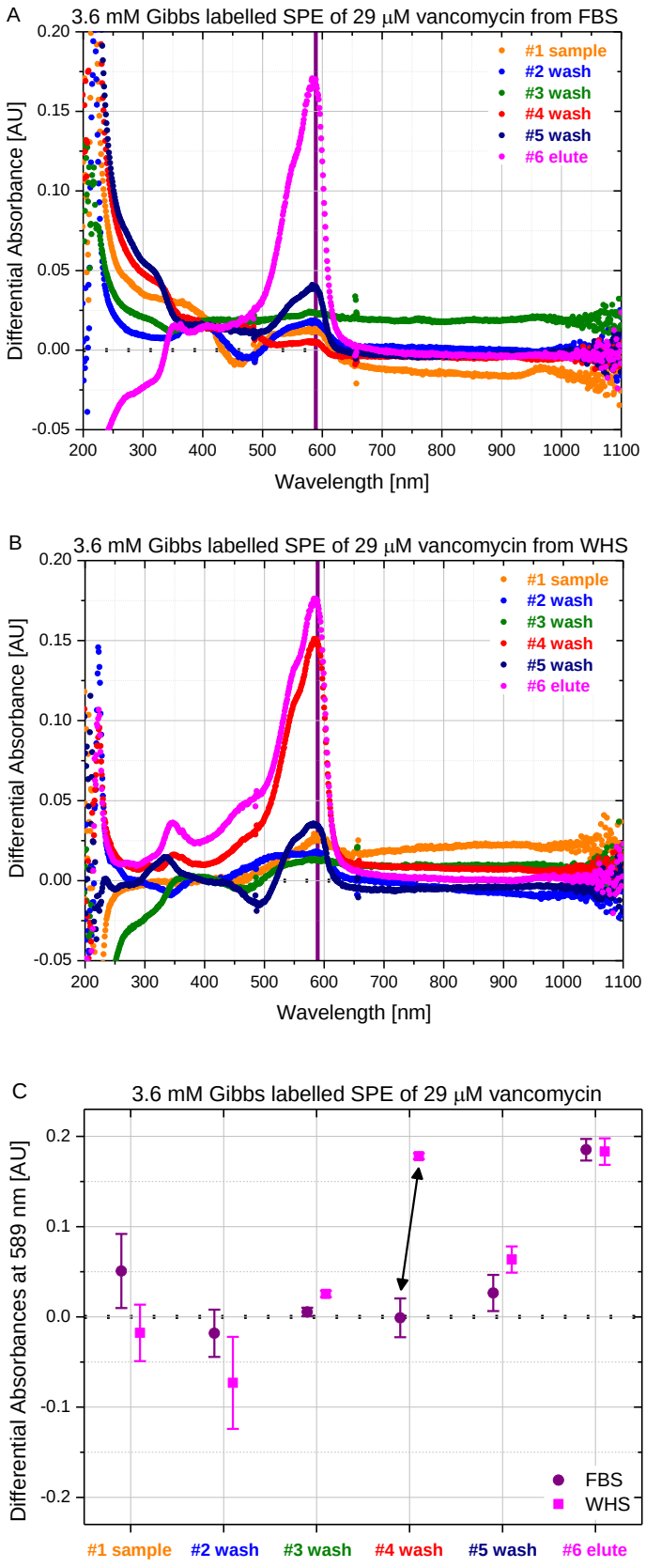

Figure 6.18: Comparison of elute compositions between FBS and WHS. Control and spiked with 29 µM vancomycin preparations of both serum types were used and subsequently subtracted. The vertical line denotes the λ_{max} (589 nm) of vanGibbs. **A) Differential UV/vis spectra of all elute stages from FBS SPE and subsequently labelled with 3625 µM Gibbs reagent.** The strong absorbance at 589 nm of the elute (#6) indicates that the majority of vancomycin is present. This figure is comparable to figure 6.13 C which shows the same overlay with the previously used Gibbs concentration. **B) Differential UV/vis spectra of all elute stages from WHS SPE and subsequent Gibbs coupling.** Similarly bimodal shaped peaks are observed for the first methanol wash (#4) and the elute (#6). **C) Average differential absorbances at 589 nm of all extraction stages and appropriate errors.** The main difference between FBS (purple) and WHS (magenta) is the extent of absorbance in the first methanol wash (#4) highlighted with an arrow. Statistical test showed that #4 and #6 were each significantly different from the other stages (appendix A.4). Concentration calculations yielded in 10 ± 2 µM vancomycin for #6 of FBS corresponding to a recovery of 34 ± 7 %. For WHS the concentrations were 20 ± 1 µM for #4 and 10 ± 2 µM for #6, which in addition results in a 102 ± 4 % recovery. This large recovery lead to the hypothesis that either #4 or #6 may be protein bound vancomycin.

6.3.6 Effect of Serum Protein Binding on Vancomycin Detection

As described in the prior subsection (6.3.5), whilst changing from FBS to WHS it became evident that vancomycin seems to change its elution conditions. In WHS it gets mainly eluted out in two stages, namely #4 and #6, as opposed to FBS in which its main fraction is detect in the eluent stage (#6). Furthermore, concentration and recovery calculations for WHS resulted in a more than 100 % recovery, which, amongst other indications, leads to the hypothesis that one eluted species may be vancomycin bound to serum proteins whilst the other one is free vancomycin. The bound vancomycin would therefore show an elevated absorbance value due to the additional absorbance of the protein, which may have been labelled with the Gibbs reagent as well.

To test this hypothesis and to figure out which stage contains which species, a constant vancomycin concentration (29 µM) was dissolved in a series of different concentrations of serum albumins in DI water. The concentrations span from 0, 75, 150, 300 to 600 µM BSA and HSA respectively. Each concentration was run through a SPE cartridge. Both the first methanol wash (#4) and the final elute (1/3 water +2/3 methanol) (#6) were collected and labelled with Gibbs reagent. As usual for each concentration a control preparation without vancomycin was treated similarly to allow subsequent subtraction.

Figure 6.19 summarises this one set experiment (n = 1) in four graphs. Graph A shows an overlay of the differential UV/vis spectra of the fourth SPE stage from five BSA concentrations plus FBS. Graph B presents the same as graph A but instead of BSA and FBS five HSA concentrations plus WHS are plotted. Graph C illustrates an overlay of the differential spectra of the final elute (#6) from five BSA concentrations and FBS, whilst the last graph (D) depicts the same as graph C but for five HSA concentrations and WHS. Generally, it can be noted that the graphs either show the characteristic bimodal vancomycin peak or basically no absorbance. Moreover, an either direct or a reverse dependency to the serum albumin concentrations can be observed.

In figures 6.19 A and B the highest absorbance at 589 nm have the spectra coloured in blue, which are obtained by 29 µM vancomycin dissolved in water only. This is the first

evidence that the pure organic solvent of stage #4 disrupts the binding of free vancomycin to the stationary phase of the SPE cartridge resulting in its elution. Then with increasing amount of serum albumins, the absorbances are decreasing. This matches the expectation since the quantity of free vancomycin is decreasing with increasing amount of proteins to which the drug can bind to. Furthermore in figure B, it can be observed that WHS is behaving comparable to 600 µM HSA, which again is expected as this is the concentration of albumin present in whole serum. However, its counterpart, FBS in figure A does not show any absorbance, which allows the assumption that in FBS almost no free vancomycin is present.

Then in the final elute (#6) graphs, C and D, the highest absorbance is measured for FBS and WHS respectively. Then the absorbances are decreasing from 600 µM, over 300 and 150 µM, to 75 µM. Both samples in which vancomycin was dissolved in water only (coloured in blue) show no absorbance in graph D and a negligible one in graph C. It has to be highlighted that for both graphs, C and D, the absorbance and therefore also the concentration is artificially doubled due to final elution with half of the volume of the initial sample. Summarised all these findings are proof that the fourth stage (#4) includes the free vancomycin fraction and the sixth stage (#6) incorporates the bound fraction.

Continuing from these findings, the next objective was to investigate whether and to which extent the serum proteins contribute to the absorbance at 589 nm of the bound fraction (#6). Firstly the vancomycin concentration in the free fraction could be directly calculated by execution of the Beer-Lambert-Bouguer law with the molar absorptivity $\varepsilon_{589\,nm}$ = 9100 ± 200 M^{-1} cm^{-1} estimated in the penultimate subsection (6.3.4) and figure 6.17.

Furthermore by calculating the vancomycin concentration from the two samples without protein (shown in blue in figures 6.19 A and B), the recovery of vancomycin from the SPE cartridge could be calculated. The recovery was found to be 95 ± 5 % (n = 2).

This was then taken into account for all further calculations with the assumption that the recovery is the same for the various samples as well as for the two extraction stages (#4 and #6). This assumption has not been tested.

On the basis of these calculated free concentrations, the expected bound fraction could be estimated (see table 6.02). It was found that all absorbances from the samples with BSA and HSA including the two water samples measured in the final elute (#6) match this expectations. This suggests that neither BSA nor HSA are contributing significantly to the absorbance at 589 nm, which would have led to a larger absorbance than expected.

For calculation of FBS and WHS, additionally data from the previous chapter (6.3.5 and figure 6.18) were taken with the aim to get a larger sample size (n = 4) and consequently more significant results. The measured absorbances for the bound fraction in FBS (graph C and figure 6.18 A shown in magenta labelled with '#6 elute') did not meet the expected values. Since FBS has basically no measurable absorbance in the free fraction (graph A and figure 6.18 A shown in red denoted as '#4 wash'), a large absorbance matching a bound vancomycin concentration of about 28.5 µM was expected. Instead a similar absorbances to WHS (see graph C and figure 6.18 B) were measured.

WHS, similar as observed in the previous chapter (6.3.5), shows a slightly higher absorbance than the expected value. The absorbances are about 9 ± 4 % too high, which corresponds to previous observations of more than 100 % recovery. It could be speculated that this enlarged absorbances may be due to binding to other proteins, such as for example alpha-1-acid glycoprotein which is also known to bind to vancomycin (Fournier, Medjoubi-N, and Porquet 2000; Zokufa et al. 1989; Dawidowicz, Kobielski, and Pieniadz 2008b; Sun, Maderazo, and Krusell 1993; Shin et al. 1991; Bohnert and Gan 2013) or interaction to other serum constituents including antibodies, antigens and hormones.

Figure 6.20 graphically summarises all calculations made in this section and compares the percentages of the two fractions, free and bound. It has to be highlighted that these calculations were based on an initial recovery value obtained by only two independent experiments (n = 2). Hence further experiments would lead to a strengthening of this finding and statistical analysis could be performed.

Nonetheless for further experiments and especially for the direct comparison with a gold standard TVM device presented in the last subsection (6.3.8) of these results and discussion section (6.3) the following findings will be used. The bound fraction in final elute obtained from a preparation with WHS should be corrected with factor of 0.778 ± 0.004 to account for the enhanced absorbance presumably caused by protein absorbance. The general recovery from the SPE cartridge seems to be about 95 ± 5 %.

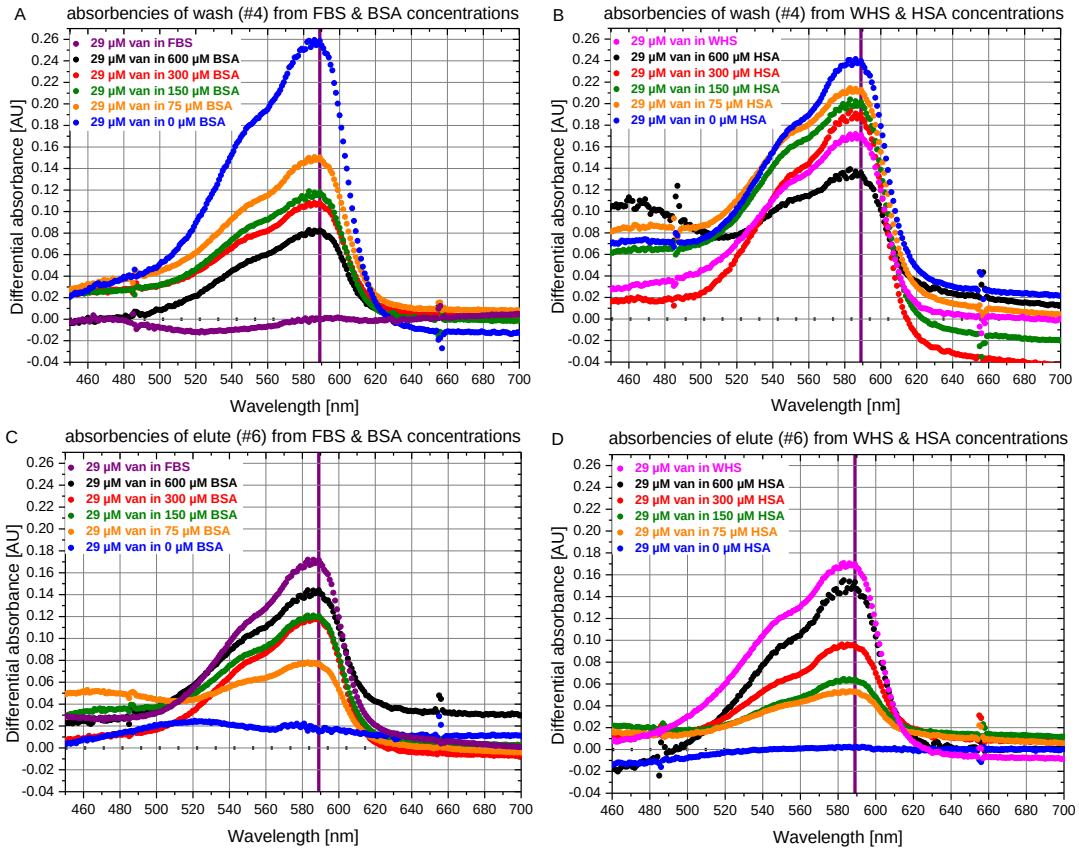

Figure 6.19: Effect of serum protein binding on vancomycin detection. 29 µM vancomycin was dissolved each individual serum albumin concentration plus FBS and HSA. **A) Overlay of differential UV/vis spectra of the fourth SPE stage (#4) from five concentrations of BSA plus FBS.** The different absorbances look reversely dependent on the protein concentration. The highest absorbance can be observed for the sample in which vancomycin was dissolved in water only. These two observations strongly suggest that the #4 stage includes the free vancomycin fraction. FBS seems to not incorporate much free vancomycin. **B) Differential UV/vis spectra of the first methanol wash (#4) from five concentrations of HSA plus WHS.** Generally, the observations are similar to figure A. Except that all absorbances are slightly higher suggesting more free vancomycin. Moreover, WHS absorbs between 600 and 300 µM. **C) Differential UV/vis spectra of the final elute (#6) from five concentrations of BSA plus FBS.** The differential absorbances show the opposite behaviour to figure A and B. They seem directly dependent on the serum protein concentrations. All these findings are clear evidence that the sixth stage includes the bound vancomycin fraction. The highest absorbance can be observed for FBS, whilst the lowest is for vancomycin in water. **D) Differential UV/vis spectra of the final elute (#6) from five concentrations of HSA plus WHS.** Again the observations are similar to figure C. Also the absorbance of WHS and FBS are highly comparable. It has to be highlighted that for both figures, C and D, the absorbance and therefore also the concentration is artificially doubled due to the final elution with half of the volume of the initial sample. Since these experiments had objective to test the hypothesis that one of these two stages contains the free and the other one the bound fraction, the samples size was kept to a minimum (n = 1). Continuing from these findings, table 6.02 and the following figure 6.20 are showing the percentages of the free and bound fractions. The objective is to investigate whether and to which extend serum proteins contribute to the absorbance at 589 nm of the final elute (#6).

Table 6.02:

29 µM vancomycin dissolved in...	#4 stage [µM]*	#4 stage [%]*	#6 stage [%] expected*	#6 stage [µM] expected*
FBS	1 ± 1	2 ± 1	98 ± 1	29 ± 1
600 µM BSA	10 ± 1	33 ± 2	67 ± 2	19 ± 1
300 µM BSA	13± 1	43 ± 2	57 ± 2	16 ± 1
150 µM BSA	14 ± 1	47 ± 2	53 ± 2	15 ± 1
75 µM BSA	17 ± 1	60 ± 3	40 ± 3	12 ± 1
0 µM BSA	29 (± 1)	100 (± 5)	0 (± 5)	0 (± 1)
WHS	21 ± 1	71 ± 3	29 ± 3	8 ± 1
600 µM HSA	16 ± 1	54 ± 3	46 ± 3	13 ± 1
300 µM HSA	22 ± 1	76 ± 4	24 ± 4	7 ± 1
150 µM HSA	23 ± 1	81 ± 4	19 ± 4	6 ± 1
75 µM HSA	25 ± 1	85 ± 4	15 ± 4	4 ± 1
0 µM HSA	29 (± 1)	100 (± 5)	0 (± 5)	0 (± 1)

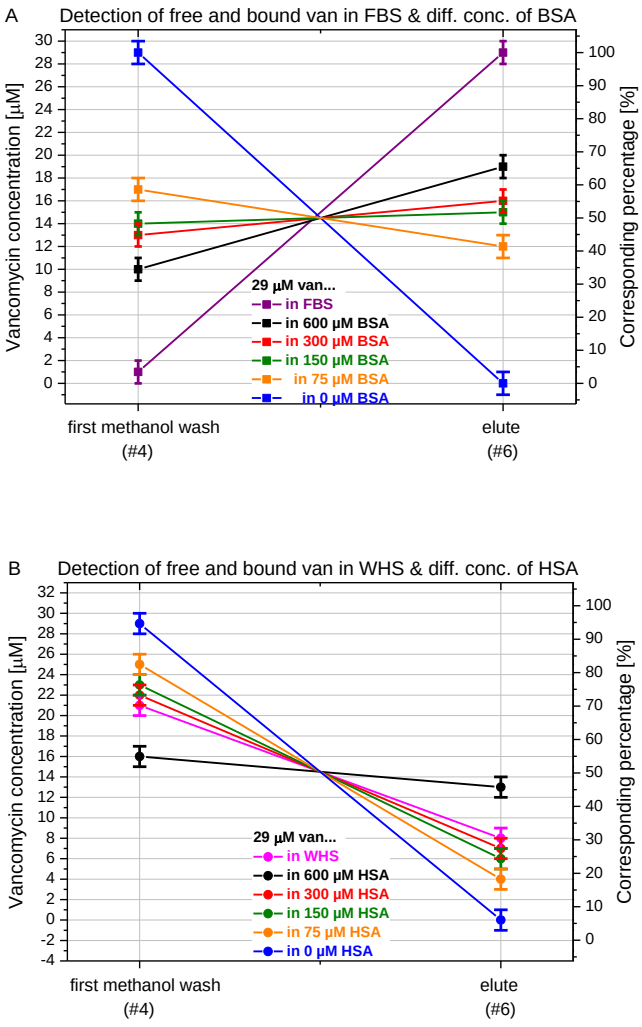

Figure 6.20: Detection of free and bound vancomycin in a single measurement. A) Percentages and the corresponding concentrations for the five concentrations of BSA plus FBS. The values for the final elute (#6) were initially calculated according to the measured free vancomycin. It was found that, except for FBS, all calculated values are matching the measured values. This allows the assumption that BSA is not significantly contributing to the absorbance of the sixth SPE stage. **B) Percentages and the corresponding concentrations for the five concentrations of HSA plus WHS.** The procedure was similar as described in figure A. It was found that, except for WHS, all calculated values are matching the measured values. This allows the assumption that also HSA is not significantly contributing to the absorbance. WHS in the sixth stage shows a larger absorbance than expected which may be due to presence of another protein or constituent of serum. For future experiments, a correction factor will be applied to account for this enlarged absorbance.

6.3.7 Selectivity Evaluation with a Subset of Interferents

This subsection reports on the specificity studies with possible cross-contaminating agents such as propofol, tyrosine, dopamine and paracetamol. The objectives were to determine whether these interferents are eluted out together with the vancomycin, whether they will react with the Gibbs reagent and subsequently whether their coupling product with the indophenolic motif would absorb in the same region as vanGibbs. The aforementioned species were chosen based on their possible presence in patient's blood and due to their chemical structure. As evident in figure 6.02 and 6.22, all of them have phenol moieties that render them potential candidates for a successful Gibbs coupling reaction. These four chosen species are most likely not all of the possible interfering species that can occur. Further specificity validation should be done. However, this lies beyond the scope of my thesis.

High concentrations (600 µM) of interferents were dissolved in FBS and WHS and then run through SPE cartridges. The collected fractions were labelled with Gibbs reagent in an identical manner as before and analysed using UV/vis spectroscopy. High concentrations were used in order to not miss any coupling event. To match these high concentrations, the chosen Gibbs concentration for this study was 3625 µM, which is within the optimal range for high vancomycin concentrations. The amino acid, tyrosine, could not be dissolved in either FBS or WHS and consequently SPE could not be carried out. For all the other interferents, figure 6.21 shows the differential absorbance spectra of all collected fractions after Gibbs coupling reaction for FBS and WHS respectively. Results found for the two sera types were fairly consistent especially for propofol. It seems as if the first methanol wash (#4) is particularly effective at extracting the interferents from the stationary phase of the SPE cartridge.

Figure 6.22 A and B summarises the absorbance values at 589 nm, which is the λ_{max} of the vanGibbs, for each SPE fraction. Although this may not be the absorbance maximum of the interfering species, absorbance at this wavelength could result in false quantification of vancomycin. It becomes evident in the figure that the washing stages, especially the first methanol wash (#4), reduces the concentration of the studies

interfering species significantly. However as previously observed and discussed, the free fraction of vancomycin is present in the first methanol wash (#4) of extraction from WHS, which of course is the serum type of interest for a future bench top device.

For the direct comparison with vancomycin, the absorbances of the interferents were adjusted according to their concentrations in patient's blood. The concentrations were chosen to be at the higher end of the corresponding therapeutic range.

- As mentioned in the preceding chapter (5.1.3.2), the clinically relevant concentrations for propofol are between 1 and 10 μg/ml, which corresponds to 5.6 – 56.2 μM (Liu et al. 2012).

- Circulating dopamine in humans occurs mainly as dopamine sulphate. The concentrations in plasma are highly depended on food intake. Typical dopamine sulphate concentrations before meals are in the region of 0.02 to 0.04 nM and raise after food intake up to 0.3 – 0.4 nM. However, after fasting overnight, they can increase up to 10 nM, which corresponds to 0.02 μg/ml of dopamine sulphate (Goldstein et al. 1999; Eisenhofer, Kopin, and Goldstein 2004).

- The therapeutic level of paracetamol typically range from 10 to 20 μg/ml, which corresponds to 66 – 132 μM (Kost, Nguyen, and Tang 2000).

Figures C and D show these adjusted absorbances according to corresponding concentrations occurring in patient's blood. In both sera types the vancomycin shows clearly the highest absorbances in the eluent (6#) as well as in the first methanol wash (#4) for WHS. In the eluent (#6), no other interferents are absorbing significantly to interfere with the vancomycin quantification. In WHS, it seems that only propofol may pose a threat as possible interferents for the free vancomycin detection in the second wash (#4).

To conclude, for the monitoring of the bound fraction of vancomycin none of the tested interferents seems to pose a risk for significant interference of the antibiotic quantification. However for quantification of the free fraction, propofol is posing a possible threat of interference. Therefore, besides extended testing of other possible interferents, further optimisation of the extraction protocol is required. This is discussed further in the conclusion and outlook chapter (6.3.8), which emphasises the requirement for optimisation and presents some ideas about how this should be approached.

Furthermore, as previously proposed in the materials and methods section (6.2.1.3), it has to be highlighted that these interferents could become the compound of interest in their own right (comparable to propofol and as opposed to vancomycin). This could lead to a foundation for the development of a multi-analyte therapeutic drug monitoring device.

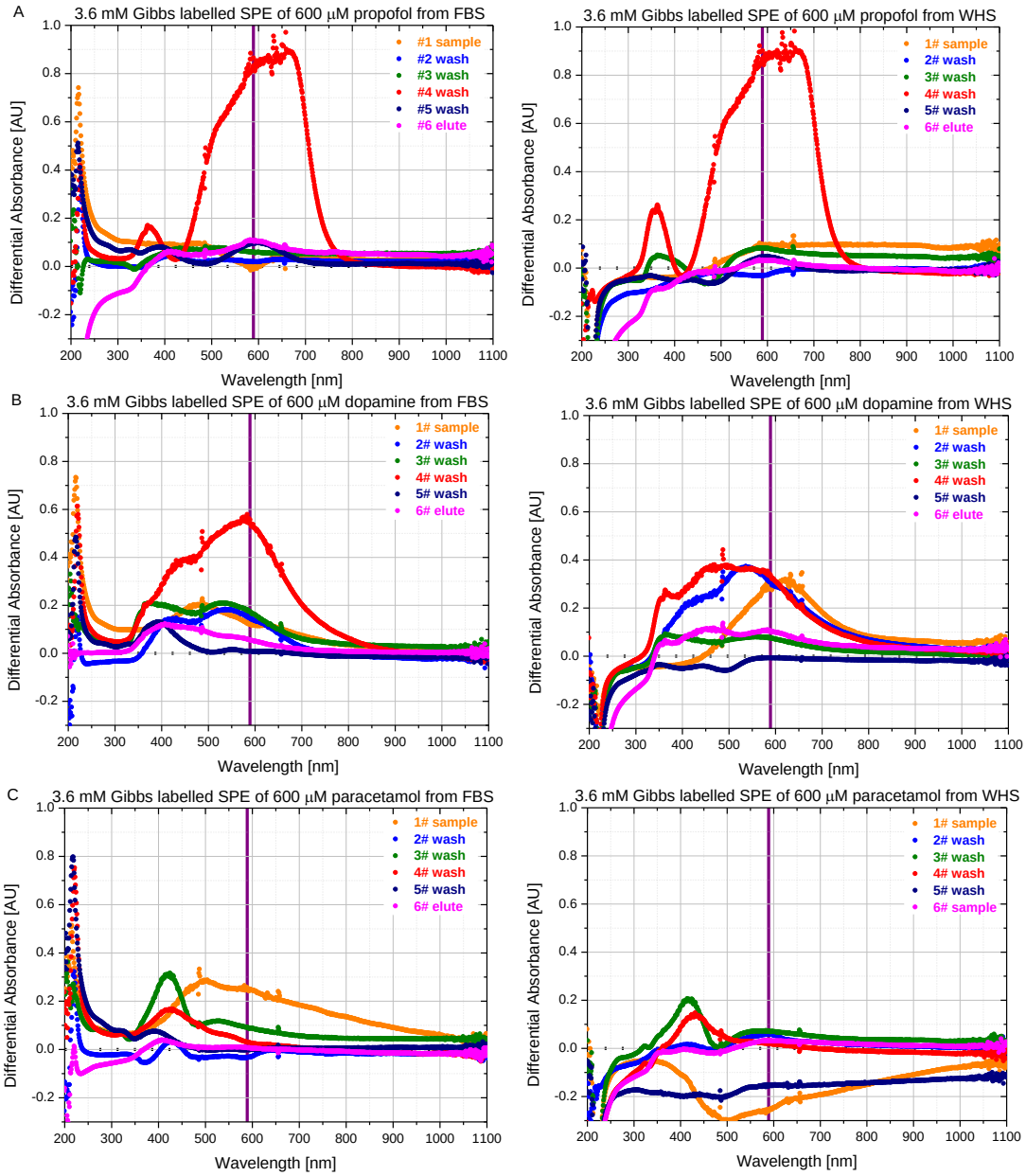

Figure 6.21: SPE stages spectra of three possible interferents for selectivity evaluation. A) Differential spectra of all SPE stages for propofol extraction from FBS and WHS. The results for the two sera types are consistent. The propofol-Gibbs molecule is mainly appearing in the first methanol wash (#4) suggesting that the aqueous organic mixture (#6) is not ideal for propofol. **B) Differential spectra for dopamine.** The results vary between the two sera. FBS shows a fairly high absorbance in stage #4, whilst WHS shows absorbance in stage #1, #2 and #4. **C) Differential spectra for paracetamol.** In comparison to the other interferents, paracetamol has a relatively low absorbance across all stages. The second water wash (#3) produces a similar peak in both sera types. In the first stage of FBS paracetmol has a broad peak and on the contrary WHS shows a comparable peak but in the negative range. These observations may suggest that paracetamol interacts with a constituent of WHS and therefore retains in the stationary phase. On the other hand if it is dissolved in FBS, it seems to run through without interacting with the polymer.

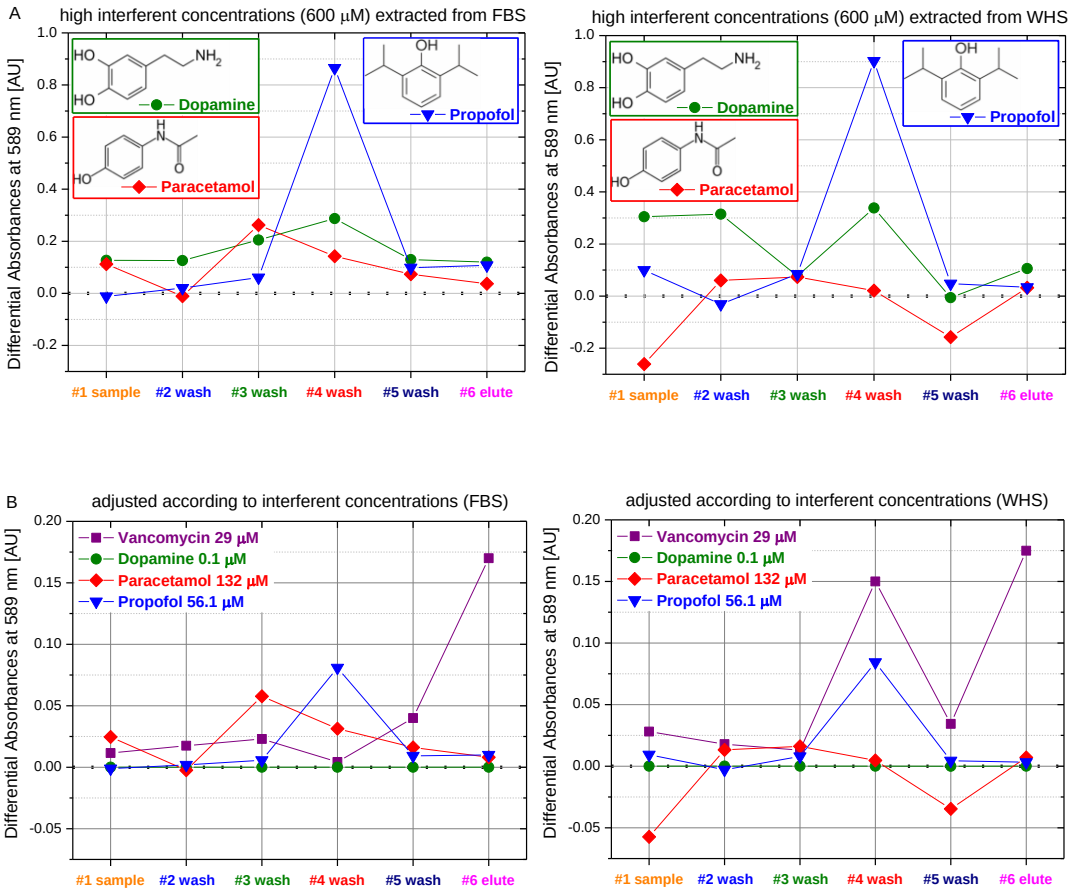

Figure 6.22: Absorbances at 589 nm for each interferent and in direct comparison to vancomycin. A) All absorbances at 589 nm for all SPE stages of each interferent dissolved at high concentrations (600 µM) in FBS and WHS respectively. The lines between the data points were added to guide the eye. It can be observed the washing stages especially the first methanol wash (#4) reduces the interferent concentrations significantly. **B) Absorbances adjustments are calculated to the top end of the therapeutic range of each interferent for direct comparison with vancomycin in FBS and WHS respectively.** Generally, it can be observed that in both sera types vancomycin shows clearly the highest absorbances in the eluent (#6) in FBS and WHS, as well as in the first methanol wash (#4) in WHS. In the eluent (#6) of both serum types, no other interferent is absorbing significantly to interfere with the vancomycin quantification. In WHS, it seems that only propofol may pose a threat as possible interferents for the free vancomycin detection in the second wash (#4).

6.3.8 Direct Comparison with a Gold Standard Technique

The very last experiment presented in this chapter is the direct comparison with a gold standard technique. The chosen gold standard technique is the homogenous enzyme immunoassay "VANC2" from COBAS®, Roche (Basel, CH) located at the diagnostic laboratories of the University College London Hospital (UCLH). Its mode of action is described in the material and methods section (6.2.2.4). The VANC2 assay has a lower detection limit of 1.7 µg/ml, which according to the technical support corresponds to 1.2 µM of vancomycin (conversion factor: µg/ml · 0.690 = µM) ("Technical Support: VANC2 COBAS® from Roche Diagnostics," 2012). The measuring range of the VANC2 is stated as 1.7 – 80.0 µg/ml of vancomycin, which corresponds to 1.2 – 55.2 µM. (I. Domke, Cremer, & Huchtemann, 2000; Ingrid Domke, 2002; Hermida, Zaera, & Tutor, 2001; "Technical Support: VANC2 COBAS® from Roche Diagnostics," 2012; Yeo, Traverse, & Horowitz, 1989)

The direct comparison experiments were conducted as follows. A stock solution of 29 µM vancomycin in WHS was used to dilute down into concentrations of 14.8, 4.7 and 1.2 µM vancomycin in WHS. Each concentration was prepared six times, so that three individual samples sets with three samples per concentration could be measured with the VANC2 and the other three sets via the herein developed colourimetric vancomycin detection. Additionally for each technique, a reference set of three samples without any vancomycin was measured as well.

Figure 6.23 and table 6.03 present the results of the VANC2 measurements. The concentrations were measured in µg/ml and the conversion factor provided by the technical support was used (µg/ml · 0.690 = µM) ("Package Insert: VANC2 COBAS® from Roche Diagnostics" 2012). The data points and the corresponding linear fit are shown in red. The linear fit has a R^2 of 0.998. The error bars highlighted in dark red correspond to the standard deviation of the three samples (n = 3). In the table 6.03, the abbreviation 'n. d.' denotes for 'not detectable', whilst 'n/a' denotes 'not applicable'. A general observation is that all errors are very small. However, it seems that the higher the concentration gets, the larger is the deviation from the diluted concentration, which is

indicated with a dotted diagonal line. Due to the dilution procedure from a stock solution in each sample preparation, errors introduced by the experimenter would either presents themselves as a constant value off the dotted line or as a propagation from higher to lower concentration and consequently be much larger for the lower concentrations. Therefore, it is believed that this deviation may be instrumental.

To initiate the herein developed colourimetric detection assay for TVM, calibration measurements had to be done. Furthermore, it has to be highlighted that for this last set of experiments a newly order batch of Gibbs reagent (see chapter 5.2.1.2) was used. Therefore the calibration was done slightly more extensively and a novel estimation of vanGibbs molar absorptivity ($\varepsilon_{589\,nm}$) was performed. The procedure was exactly the same as in previous estimation described in section 6.3.4 figure 6.17. It was found that with this new Gibbs reagent the $\varepsilon_{589\,nm}$ increased from 9100 ± 200 to 12200 ± 300 M^{-1} cm^{-1} with an adjusted R^2 of 0.998.

The measurements of the five concentrations in the three sets were performed as usual with the developed extraction protocol (see subchapter 6.3.3). The first methanol (#4) and the final elute (#6) were collected for subsequent quantification via Gibbs labelling of the free and bound fraction respectively. As usual the reference spectra were subtracted. The resulting differential absorbances were adjusted to account for the decrease in Gibbs reagent (see subsection 6.3.4), for the recovery and for the enlarged absorbance in the bound fraction (see subsection 6.3.6). Table 6.04 presents all results and calculations including the standard deviation for the three individual sets in which each sets has five different concentrations (n = 3).

The total vancomycin concentration was calculated by addition of the free and bound concentrations. For direct comparison with the gold standard these total vancomycin concentrations including their standard deviation were added to figure 6.23. They are shown in blue with navy coloured error bars. The corresponding linear fit has a R^2 of 0.992. It can be observed that the errors are significantly larger than for the Roche COBAS®' VANC2.

It has to be highlighted again that all these experiments were performed with gravity flow and manually droplet by droplet were captured from the SPE cartridge, which despite very strict experimental procedure induces errors and discrepancies. Therefore in the ultimate automated bench top device these errors should be significantly smaller. Besides these findings, the measured total vancomycin concentration with the herein developed colourimetric assay is comparable to the gold standard. Furthermore, it has the great advantage to monitor the free and bound vancomycin fraction in a single step within minutes. This will ultimately be achieved directly from whole blood in a bench top device at the PoC without any previous sample preparations.

Figure 6.24 depicts all free, bound and total concentrations per triplet including error bars and linear fits. It can be observed that the errors for the bound fractions are slightly smaller than for the free. Generally, it can be observed that the amount of free vancomycin increases more with increasing of total concentration than the amount of bound. Hence the slope for the free fraction is steeper than the slope for the bound fraction. The corresponding percentages of the two fractions in each triplet can be found in the table 6.04.

Furthermore the measurements of the control samples, which did not incorporate any vancomycin, allow a preliminary estimation of the detection limit. The procedure was the same as presented in the technical support from the Roche COBAS®' VANC2 ("Package Insert: VANC2 COBAS® from Roche Diagnostics" 2012). The VANC2 has a detection limit of 1.2 µM, which has been calculated as the value lying two standard deviations above the measured value for zero (1 + 2 StDev, n = 21). First calculations for the colourimetric assay resulted in a 1.1 µM detection limit. However, it has to be highlighted that the used sample size was only n = 3. Furthermore in light of the previous measured concentrations for 1.2 µM vancomycin that resulted in a far too large concentration, it has to be concluded that further experiments are required as well as statistical analysis.

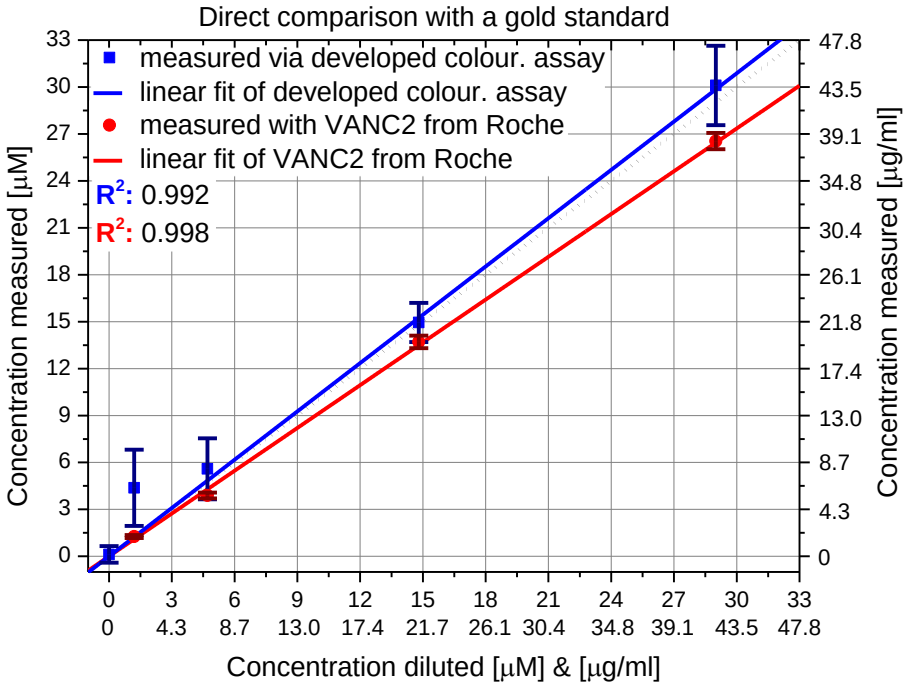

Figure 6.23: Direct comparison of the herein developed colourimetric assay with the gold standard VANC2 from Roche COBAS®. The diagonal dotted line illustrates the linear region where data points would be if the diluted and measured concentration would be exactly the same. The red points (see table 6.03) present the measured concentrations with the VANC2. The blue data points (see table 6.04 on the next page) depict the total vancomycin concentrations measured with the herein developed colourimetric assay. The errors are derived standard deviations from three independent measurements (n = 3) and are significantly larger for the colourimetric assay than for the VANC2. Furthermore, the colourimetric measured concentration for the diluted 1.2 µM of vancomycin is far too high. Besides these findings, the results of the two techniques seem comparable, as well as the calculated R^2 of the linear fits.

Table 6.03:

concentration diluted		series A: measured conc.		series B: measured conc.		series C: measured conc.		average		st. deviation (n = 3)	
[µg/ml]	[µM]	[µg/ml]	[µM]	[µg/ml]	[µM]	[µg/ml]	[µM]	[µg/ml]	[µM]	[µg/ml]	[µM]
0	0	n. d.	n. d.	n. d.	n. d.	n. d.	n. d.	n/a	n/a	n/a	n/a
1.74	1.2	1.99	1.37	1.75	1.21	1.75	1.21	1.83	1.26	0.14	0.10
6.81	4.7	5.62	3.88	5.38	3.71	5.92	4.08	5.64	3.89	0.27	0.19
21.45	14.8	20.2	13.94	19.2	13.25	20.2	13.94	19.87	13.71	0.58	0.40
42.03	29	38.8	26.77	37.6	25.94	39	26.91	38.47	26.54	0.76	0.52

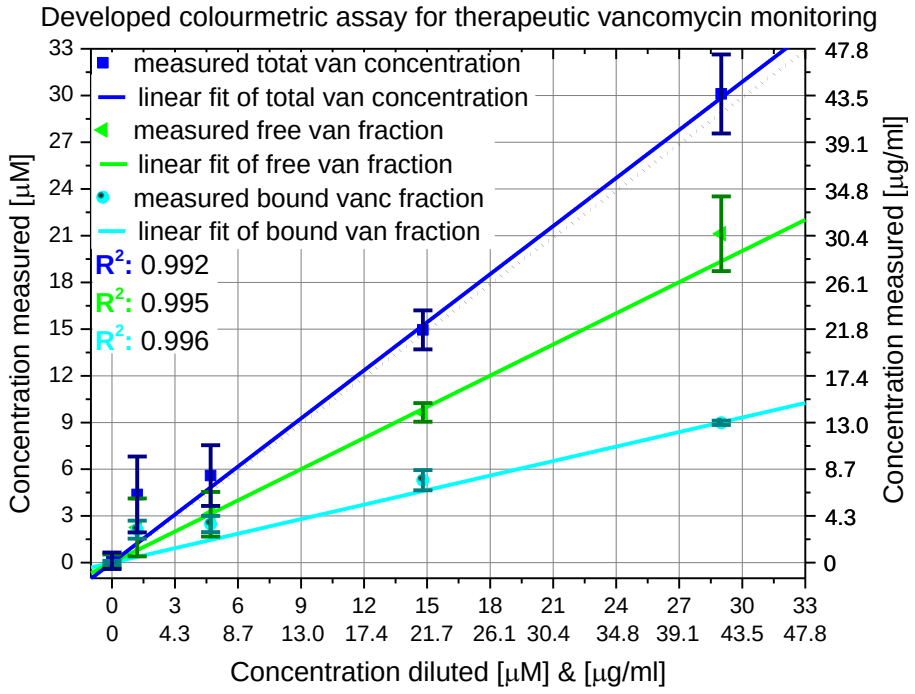

Figure 6.24: Colourimetric assay for therapeutic monitoring of free and bound vancomycin concentration. As in the previous figure (6.23), the blue values are again the total vancomycin concentrations calculated by addition of the bound and free concentrations. The cyan data points depict the bound concentrations measured from the final elute (#6), whilst the green points illustrate the free concentrations obtained by labelling the first methanol wash (#4). The errors are derived standard deviations from three independent measurements (n = 3) and it can be observed that the errors for the free concentrations are larger. The linear fits and their corresponding R^2 values seem comparable with each other. The percentages for the free and bound vancomycin concentrations can be found in the table (6.04) below.

Table 6.04:

explanation	concentration diluted		series A: measured c.		series B: measured c.		series C: measured c.		average		percentages	st. deviation (n = 3)	
	[µg/ml]	[µM]	[µg/ml]	[µM]	[µg/ml]	[µM]	[µg/ml]	[µM]	[µg/ml]	[µM]	[%]	[µg/ml]	[µM]
free	n. k.	n. k.	-0.55	-0.38	0.55	0.38	0.47	0.32	0.16	0.11	92	0.61	0.42
bound	n. k.	n. k.	0.15	0.10	-0.15	-0.10	0.05	0.03	0.02	0.01	8	0.15	0.11
total	0	0	-0.4	-0.28	0.4	0.28	0.52	0.35	0.18	0.12	100	0.76	0.53
free	n. k.	n. k.	2.76	1.91	6.18	4.27	0.89	0.62	3.28	2.26	52	2.69	1.86
bound	n. k.	n. k.	3.11	2.15	2.21	1.53	3.90	2.70	3.07	2.12	48	0.84	0.58
total	1.74	1.2	5.87	4.06	8.4	5.80	4.79	3.32	6.35	4.38	100	3.53	2.44
free	n. k.	n. k.	3.99	2.75	6.78	4.68	2.73	1.89	4.50	3.11	56	2.07	1.43
bound	n. k.	n. k.	3.49	2.41	4.41	3.04	2.91	2.01	3.60	2.48	44	0.75	0.52
total	6.81	4.7	7.48	5.16	11.19	7.72	5.64	3.9	8.1	5.59	100	2.82	1.95
free	n. k.	n. k.	9.59	9.59	14.89	10.28	13.16	9.08	13.98	9.65	65	0.87	0.60
bound	n. k.	n. k.	6.90	4.76	6.76	5.29	8.64	5.96	7.69	5.30	35	0.94	0.65
total	21.45	14.8	16.49	14.35	21.65	15.57	21.8	15.04	21.67	14.95	100	1.81	1.25
free	n. k.	n. k.	30.64	20.00	34.61	23.88	28.21	19.48	30.61	21.12	70	3.48	2.40
bound	n. k.	n. k.	12.84	8.86	12.98	8.96	13.24	9.14	13.02	8.98	30	0.20	0.14
total	42.03	29	43.48	28.86	47.59	32.84	41.45	28.62	43.63	30.1	100	3.68	2.54

6.4 Discussion and Conclusion

The objective of this chapter was to develop a colourimetric detection assay for vancomycin on the basis of the existing Pelorus device for therapeutic propofol monitoring. For the sake of brevity the major milestones and corresponding findings of this development process are listed in bullet points below. Furthermore the key characteristics of this novel colourimetric detection for TVM are stated in table 6.05 at the end.

i) It could be demonstrated that Gibbs reagent is binding to vancomycin. Its coupling product is detectable by visible spectroscopy with a maximal wavelength of 589 nm ($\lambda_{589\,nm}$) and a molar absorptivity of 12200 ± 300 M^{-1} cm^{-1} ($\varepsilon_{589\,nm}$). The coupling reaction is fast within minutes and an immediate colour change from transparent with a hint of yellow from the Gibbs reagent to bright purple can be observed. It has to be highlighted that mixing is crucial as separation of the aqueous and organic is likely to occur.

ii) An excess of Gibbs reagent of about 100 to 150 times results in the largest absorbances and consequently leads to the highest sensitivity. However, the range from 100 to 320 times does not result in an absorbance loss of more than 13 %. The reaction product or maybe products will be analysed in the next chapter (7).

iii) Detection of therapeutic vancomycin concentrations could be demonstrated. Preliminary estimations suggested a detection limit of about 1.1 µM. However, due to time limitations further experiments could not be performed. As they would lead to a strengthening of this finding and allow the crucial statistical analysis, they should be considered for future work.

Additionally in light of the required Gibbs excess, one may consider the use of two different Gibbs concentrations for the lower and the higher part of the therapeutic vancomycin to achieve best possible sensitivity.

iv) The Gibbs reagent coupling is not specific to vancomycin and it was shown that it for example in addition to propofol also couples to serum albumin. Therefore and for several other reasons, an extraction protocol seemed inevitable. Consequently an extraction protocol was developed based on the same SPE cartridge as used in the Pelorus device. Therefore it is direct compatible and only the solvents and the procedure have to be adjusted. This fulfils one another objective, which was the ability to reduce the required time for a vancomycin-focussed device to reach the market.

The extraction protocol was developed for WHS and should based on Sphere Medical's prior knowledge be directly transformable to whole blood samples. Furthermore, it was found that from one sample free and the bound vancomycin fraction could be eluted out in different stages of the extraction protocol, which therefore allows separate quantification. The free and bound concentrations can then be added to obtain the total concentration. These total concentrations were directly compared to a gold standard method and found to be comparable.

v) A small study with a subset of possible interferents was performed to evaluate the selectivity of the developed colourimetric assay for TVM. It was found that neither dopamine, nor paracetamol, nor propofol are interfering with the quantification of the bound vancomycin concentration, which is eluted out in the final elute. Again neither dopamine nor paracetamol were possible interferents for the quantification of the free vancomycin, which is included in the fourth SPE stage. However, propofol was identified as possible interfering substance.

In order to avoid potential interference of propofol, the following measures may be considered. Since propofol does not naturally occur in patients, vancomycin may be monitored when the patient is not under the influence of propofol. Alternatively, the propofol concentration may be determined independently and subsequently subtracted. The propofol could be quantified either via the Pelorus device or within a multi-analyte monitoring device that measures besides vancomycin also propofol and maybe serum albumin etc. Moreover, since the propofol-Gibbs reaction product is blue and consequently has a λ_{max} of 595 nm (see chapter 5.3.2), measuring the UV/vis spectrum over an appropriate spectral range instead of at a fixed wavelength may allow for the extraction of the propofol contribution from the overall determined concentration.

It has to be highlighted that these three interferents are most likely not all of the possible interfering species that can occur. Therefore further specificity validation should be done in the future.

To conclude the ability to monitor free and bound concentrations and consequently calculate the total concentration of vancomycin in a single step from ultimately whole blood samples without the requirement of any prior sample preparations within minutes paired with integrability into a bench top device for PoC has to the best of our knowledge never been described before. Therefore we patented this invention including the labelling reaction of vancomycin with the Gibbs reagent (Kappeler et al. 2013). The patent just entered 'Patent Cooperation Treaty' (PCT) phase on the 18th February 2014.

Table 6.05:

Sensing Technique	Colourimetric
Investigated Core Detection Technology	**Visible Spectroscopy**
Sensor Attributes or Requirements and their Feasibility and Fulfilment	
Specificity without cross-contamination	Developed extraction protocol is fairly specific for the bound fraction eluted in stage #6 and until now propofol could be identified as possible interferents for the free fraction present in stage #4.
Sensitivity according to therapeutic window/clinical range: **vancomycin's clinical range: 4 – 28 µM**	Detection limit: preliminary estimation yielded in about 1.1 µM of vancomycin, which according to conversion from the VANC2 assay corresponds to about 1.7 µg/ml ("Package Insert: VANC2 COBAS® from Roche Diagnostics" 2012)
Simplicity and requirement for specially trained staff	Very simple and no specially trained staff required.
Required sample preparation	As a final product none. Currently, SPE followed by Gibbs labelling reaction.
Stability in application environment/robustness	Assumed to last long depending on material abrasion including tubes and fittings within the device.
Shelf-life/robustness	Similar to above depending on material abrasion plus chemicals and buffer shelf life time.
Miniaturisation	Light source and light paths are the limiting factor.
Intravenous flow through application/patient attached	Not possible due to addition of chemicals and miniaturisation issue.
Safety in case of malfunction	Not tested.
Expected costs	Overall low. Single investment for the device and very low per test, which only requires a novel SPE cartridge (assumed < £ 1).
Measuring speed/rapidity	Labelling reaction & vis spectroscopic measurement: about 4 minutes. Overall assay including blood injection & SPE: less than 10 minutes.
Distinguish free vs. bound antibiotic fraction	Yes, both. In WHS, elute (#6) clearly carries the bound and wash (#4) the free fraction.

CHAPTER 7:

Structural Characterisation of the Novel Product – VanGibbs

This chapter is the last of the three chapters outlining the colourimetric detection of vancomycin. Following on the successful development of the Gibbs reagent labelling reaction for vancomycin and the specific extraction protocol discussed in the previous chapter 6, the objective of this chapter is the analysis of this reaction and its coloured product, which is herein called 'vanGibbs'. This objective serves the purposes of validating the filed patent via structural characterisation of the vanGibbs molecule, which to the best of our knowledge is a novel molecule never described before, and to acquire a better understanding of the almost 90 year old reaction mechanism, which despite its age and many publications is not fully understood (Dacre 1971; Svobodová et al. 1977; Svobodová et al. 1978; Adam et al. 1981; Josephy and Van Damme 1984; Pallagi and Dvortsák 1986; Pallagi, Toró, and Müller 1994; Pallagi, Toró, and Farkas 1994; Pallagi, Toró, and Horváth 1999). The structural analysis and study of the labelling reaction, described hereafter, were performed by mass spectrometry (MS) technique and nuclear magnetic resonance (NMR) experiments.

Similar to previous chapters, this chapter is divided into four subsections: The first subsection (7.1) introduces the Gibbs reagent literature again and summarises the relevant findings from the preceding chapters 5 and 6. The second part (7.2) lists the used materials and methods. The third subsection (7.3) presents the results including preliminary discussions and continues into the final subsection (7.4) with the overall discussion, conclusion and outlook towards future work.

7.1 Introduction

The Gibbs reagent, including its history, different reaction mechanisms and applications was introduced in chapter 5.1.2. In the original Gibbs reaction, as described by Harry D. Gibbs in 1926 and 1927, the Gibbs reagent is adding to para-unsubstituted position of the hydroxyl group in a phenol resulting in blue coloured indophenols (Gibbs 1926a; Gibbs 1926b; Gibbs 1927a; Gibbs 1927b). However later on, several research groups showed that Gibbs reagent has the ability to add to the para-substitued position of phenolic compounds (Dacre 1971; Josephy and Van Damme 1984; Pallagi, Toró, and Müller 1994; Pallagi, Toró, and Farkas 1994), as well as to some esters (Kramer, Gamson, and Miller 1959; Gamson, Kramer, and Miller 1959), certain thiols and sulfhydryl groups (Kramer and Gamson 1959; Harfoush, Zagloul, and Abdel Halim 1982; Harfoush 1983), nitroxyl groups (Pallagi, Toró, and Horváth 1999) and some amines (De Boer et al. 2007; Kovar and Teutsch 1986; Kallmayer and Thierfelder 2003; Annapurna et al. 2010).

As described in the preceding chapter (6.1) vancomycin has several aromatic groups, including some phenolic moieties. Therefore one hypothesis is that Gibbs reagent couples to one or several of these. The schematic in figure 7.01 illustrates a possible S_EAr reaction of the Gibbs reagent to position 6 in the 7th residue of vancomycin, which is the para-unsubstituted position. However, the addition may occur to another position of the vancomycin molecule such as the position 2 in the same residue (7th), other aromatic moieties that may become phenolic or to amine groups (De Boer et al. 2007; Kovar and Teutsch 1986; Kallmayer and Thierfelder 2003; Annapurna et al. 2010). Moreover, these alternative additions could result in multiple coupling reactions accompanied with possibility of fragmentation of the vancomycin molecule. These alternative reactions as well as the structural characterisation of the novel product ‘vanGibbs’ will be studied and discussed in this chapter.

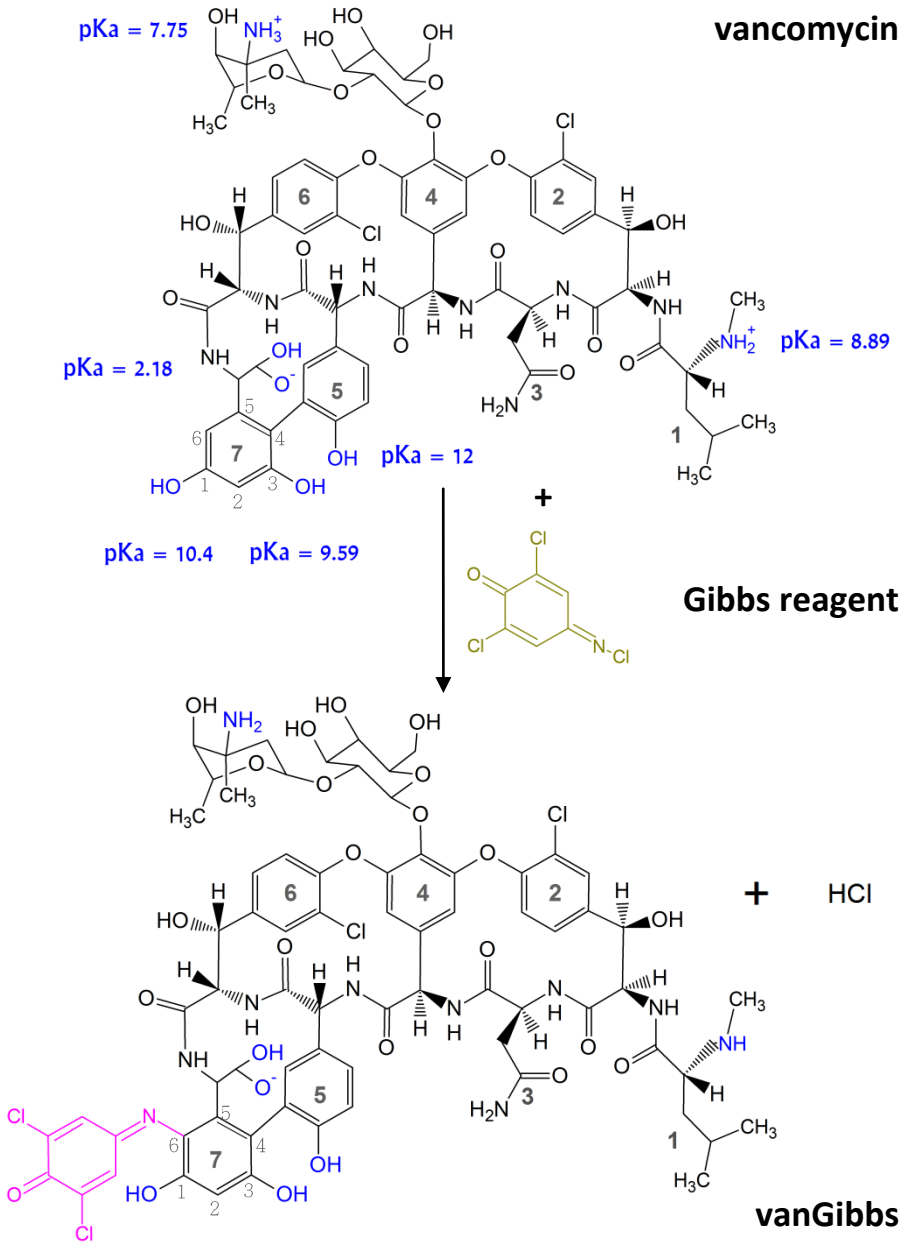

Figure 7.01: Hypothesis of Gibbs reagent coupling to vancomycin resulting in a novel vanGibbs molecule. Based on the theory of the Gibbs reaction, coupling to the para-unsubstituted position of the hydroxyl group at position 3 in 7th residues of vancomycin via a S_EAr seems a likely scenario. The coupled Gibbs molecule is indicated in purple in the vanGibbs molecule. One isomeric structure of vanGibbs was chosen as an example for many possible isomers. It has to be highlighted that the addition may occur to another position of the vancomycin molecule such as the position 2 in the same residue (7th), other aromatic moieties that may become phenolic or addition to amine groups. This could result in multiple additions accompanied with maybe even fragmentation, which will be further discussed in chapter 7. Furthermore, the coupling reaction requires high pH. Therefore the charged groups of the vancomycin scaffold were adjusted to an assumed pH of around 8.9 to 9.5 resulting in an overall charge change from $+1$ to -1. The pKa values were taken from Takács-Novák, Noszál, Tókés-Kövesdi, & Szász, 1993.

7.2 Materials and Methods

This chapter provides the information of the materials used and methods for the study of the labelling reaction and the resulting novel product vanGibbs. It is divided into three subchapters. The chemicals, including coupling reagent, the antibiotic and the solvents are described in the first subsection (7.2.1). The analytical instrumentation is presented in the second part (7.2.2). The procedure and data analysis is described in the third and last part (7.2.3).

7.2.1 Chemicals

All chemicals were purchased from Sigma-Aldrich (Dorset, UK), unless otherwise declared. They were handled, stored and disposed of in accordance with their safety guidelines stated in the corresponding 'material safety data sheets' (MSDS).

7.2.1.1 Coupling Reagent and Antibiotic

The Gibbs reagent and the vancomycin, which were used in the hereafter presented experiments, were previously described in chapter 5.2.1.2 and 6.2.1.1.

7.2.1.2 Solvents

For the mass spectrometry experiments the same solvents were used as described in the previous chapter 5.2.1.1 and 6.2.1.1. For the NMR experiments, the deuterated solvents of the aforementioned solvents were used accordingly.

7.2.2 Instrumentation

7.2.2.1 Mass Spectrometer

The mass spectra presented herein were taken by Reach Separations (Nottingham, UK). The used mass spectrometer was an Agilent 1100 series G1946D with an electrospray ionisation (ESI) probe from Agilent (Santa Clara, California, U.S.A.). The different

ionisation techniques in mass spectrometry can be separated in hard and soft ionisation techniques. ESI is the archetypal hard ionisation technique. Since in hard techniques a larger amount of energy is transferred to the analyte ion, subsequent unimolecular dissociation reactions can be expected resulting in more fragmentations than soft ionisation techniques, which include for example matrix-assisted laser desorption/ionisation (MALDI) (Kellner et al. 2004). Additionally several experiments were performed with a MALDI time-of-flight (MALDI-TOF) mass spectrometer, namely an AXIMA CFR from Shimadzu (Kyoto, Japan) located at UCL's Cancer Institute and operated by Dr. Carolyn Hyde. However, as comparable results were obtained, they are not presented herein for the sake of brevity.

7.2.2.2 NMR instrumentation

The used NMR instruments were Avance III 600 Cryo and Avance 500 both from Bruker (Billerica, Massachusetts, U.S.A.). The instruments are located in the Chemistry Department of UCL and operated by Dr. Abil Aliev. For the calibration of the chemical shift (parts per million (ppm)) the characteristic water peak was used.

7.2.3 Measurement Procedure, Data Capturing and Analysis

This chapter presents the analytical study of the reaction of vancomycin with Gibbs reagent and the structural characterisation of its product. However, it was found that the vanGibbs molecule is not stable for more than about 12 hours in various conditions including different aggregate states (liquid and solid obtained via freeze drying), pHs, temperature and molar ratios of the starting materials. Moreover, it was not stable in the purified form with an equimolar ratio of vancomycin and Gibbs reagent, which in theory should not allow further coupling reactions.[6]

In conclusion, this instability prevented a fully successful purification as well as consecutive scaling up experiments required for a complete characterisation of the

[6] Most purification attempts were performed in conjunction with Dr. Antonio Ruiz-Sanchez. The several hours stability experiments via NMR were conducted by the aforementioned. Reach Separations performed some purification attempts via HPLC and analytical studies via MS.

molecule such as elemental analysis or, besides the hereafter presented ^{1}H-NMR studies, additional ^{13}C-NMR studies.

Therefore the herein presented analytical techniques are techniques in which the crude reaction mixture could be used. These techniques include mass spectrometry (7.3.1) and one and two-dimensional ^{1}H-NMR (7.3.2).

According to the measurement procedure, the studies with both techniques were initiated with the starting materials followed by the reaction with different molar ratios of the aforementioned. Further, the procedure for capturing mass spectra and one-dimensional ^{1}H-NMR data were as usual in analytical chemistry and will not be further described in this thesis. Regarding the two-dimensional NMRs, the typical procedure is to start with COSY (**CO**rrelated **S**pectroscop**Y**) analysis, followed by TOCSY (**TO**tal **C**orrelation **S**pectroscop**Y**) spectra and then NOESY (**N**uclear **O**verhauser **E**ffect **S**pectroscop**Y**) and if required ROESY (**R**otating frame nuclear **O**verhauser **E**ffect **S**pectroscop**Y**) studies.

However in this thesis, no COSY (**CO**rrelated **S**pectroscop**Y**) study was performed because of two reasons. Firstly, the almost all protons of vanGibbs could be assigned with one-dimensional ^{1}H-NMRs (see subsection 7.3.2); Secondly, the NOESY spectrum of the product, vanGibbs, could be directly compared with the NOESY spectrum of the starting material, vancomycin. In addition, due to the fact that the Gibbs group is believed to couple to vancomycin via the heteroatom nitrogen, it has a separate spin system. This spin system separation renders results from a TOCSY not very helpful for the distinguishing of the exact coupling position in the 7th residue of vancomycin. However, an analysis via NOESY spectra was performed as it was expected to give further structural information of the vanGibbs molecule and may show where the Gibb reagent is exactly coupling to. Since the NOE (Nuclear Overhauser Effect) interaction is not through bonds but rather through space, it is a useful technique for the local assignment of different spins systems relative to each other and consequently the three-dimensional structure of molecules.

A transient NOE effect can occur via dipolar coupling of homonuclei such as H-H coupling. Each nucleus gets individually irradiated to detect whether and to which other nucleus a NOE effect occurs. The irradiated nucleus acts as source spin (S) and the nucleus which either does or does not interact upon this source spin is called interesting spin (I). The NOE range is restricted to about 3 to 6 Å, which is about 3 to 6 times the length of a carbon-hydrogen bond (~1.1 Å). However, it has to be highlighted that a proximity of 6 Å gives a fairly weak NOE signal. The NOE interactions are also influenced by the strength of the NMR magnet and the spin velocity of the molecules which gives rise to either positively or negatively signed cross peaks. Positive signals are usually obtained from fast tumbling smaller molecules, which are typically less than 1000 Daltons. Negative signals on the other hand are from slow tumbling larger molecules such as proteins. Negative signs also have diagonal peaks which can be seen as the peaks from the corresponding one-dimensional NMR plotted diagonally. Even though by convention the diagonal should be plotted negative, it is often plotted positive which inverts the signs. Therefore, small molecules are negative and large molecules positive. In a NOESY spectrum two colours indicate positive and negative signs.

Very importantly for the interpretation of NOESY spectra is that the presence of an NOE cross peak is evidence that two nuclei are in spatial proximity to each other. However, the absence of an NOE peak does not necessarily mean that they are not in close proximity to each other. This arises from the nature of the interactions which are anisotropic, hence they are asymmetric. NOESY spectra contain additional axial peaks, which typically do not provide extra information and can be eliminated. Furthermore, NOESY spectra are prone to artefacts, therefore other techniques or direct comparisons are crucial for the verification of the nuclei connections and structural interpretation. (Noggle and Schirmer 1971; Kellner et al. 2004)

7.3 Results and Discussion

This chapter presents the results of the analytical study of the reaction of vancomycin with Gibbs reagent and the structural characterisation of the novel product vanGibbs. The first section (7.3.1) describes mass spectrometry and the second (7.3.2) describes ^{1}H-NMR studies.

7.3.1 Mass Spectrometry Studies

To initiate the mass spectrometry study, a spectrum of pure vancomycin hydrochloride was taken. Vancomycin has the chemical formula $C_{66}H_{75}Cl_2N_9O_{24}$, an exact mass (monoisotopic nominal mass) of 1447.4 g/mol and a molecular weight, which equals to the average mass, of 1449.3 g/mol. Figure 7.02 A shows the theoretical prediction of the isotopic pattern of vancomycin, which has a characteristic shape mainly due to presence of the two chlorine atoms. Figure 7.02 B shows the corresponding experimental spectrum obtained by ESI mass spectrometry. The main peaks around 1447 m/z corresponding to the ionised mass of vancomycin $[M]^+$ and are in very good agreement with the predicted pattern. Both sets of peaks around 1469 m/z and 1485 m/z with comparable isotopic shapes correspond to vancomycin's mass plus a sodium $[M+Na]^+$ and a potassium cation $[M+K]^+$ respectively.

After successful initiation of the mass spectrometry studies, characterisation of the novel product vanGibbs was performed. According to the hypothesis presented above (see section 7.1) and in the previous chapter 6.1, a stoichiometric one to one reaction is expected to result in a molecule with the chemical formula $C_{72}H_{76}Cl_4N_{10}O_{25}$, a corresponding exact mass of 1620.4 g/mol and a molecular weight of 1623.2 g/mol. Figure 7.03 A shows the theoretical isotopic pattern of such a molecule. Figure 7.03 B presents the experimentally measured spectrum of two molar equivalents of Gibbs reagent reacted to one equivalent of vancomycin under alkaline condition. The main peaks around 1620 m/z represent the vanGibbs molecule in its cationic form $[M]^+$ and display a comparable pattern to the predicted isotopic shape. Similar to pure vancomycin in figure 7.02, the comparable shaped peak patterns around 1644 m/z and

1663 m/z correspond to vanGibbs' mass plus a sodium $[M+Na]^+$ and a potassium cation $[M+K]^+$ respectively. The peaks at lower masses are fragmentations of the vanGibbs molecule displaying similar isotopic pattern, which suggests that the four chlorine atoms are still attached to these main fragments. The peaks around 1579 m/z could be due to the loss of a carboxylic acid group, which equals to a loss of about 45 m/z (Kellner et al. 2004). The peaks around 1480 m/z may be due to the loss of one sugar moiety resulting in a mass loss of about 144 m/z. Furthermore, no peaks can be observed around 1447 m/z, which are displaying a vancomycin typical pattern.

A

Formula: $C_{66}H_{75}Cl_2N_9O_{24}$

mass	%
1447	100.0
1448	76.4
1449	97.6
1450	59.7
1451	34.5
1452	15.4
1453	5.3
1454	1.6
1455	0.4
1456	0.1

B

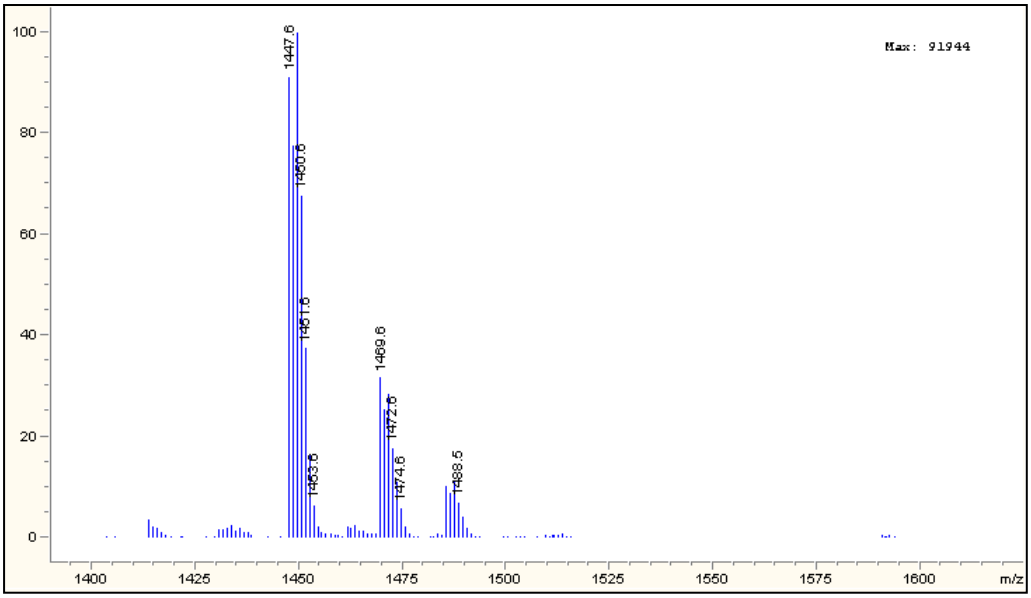

Figure 7.02: Theoretical and experimental mass spectra of pure vancomycin. A) Theoretical isotopic pattern of vancomycin. Vancomycin has a chemical formula of $C_{66}H_{75}Cl_2N_9O_{24}$, a monoisotopic nominal mass of 1447.4 g/mol and a molecular weight of 1449.3 g/mol. The characteristics in the isotopic pattern are mainly due to the presence of the two chlorine atoms. **B) Experimentally measured mass spectrum of vancomycin with an ESI mass spectrometer.** The main peaks around 1447 m/z correspond to the cationised mass of vancomycin $[M]^+$ and are in very good agreement with the predicted pattern. The both sets of peaks around 1469 m/z and 1485 m/z with comparable isotopic shapes correspond to vancomycin's mass plus a sodium $[M+Na]^+$ and a potassium cation $[M+K]^+$ respectively.

A

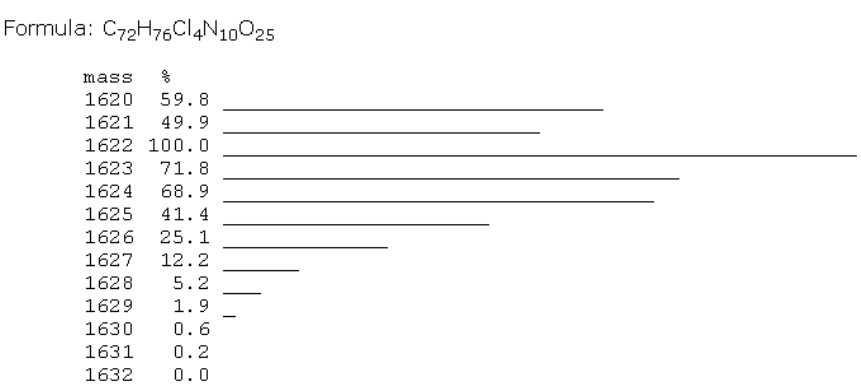

B

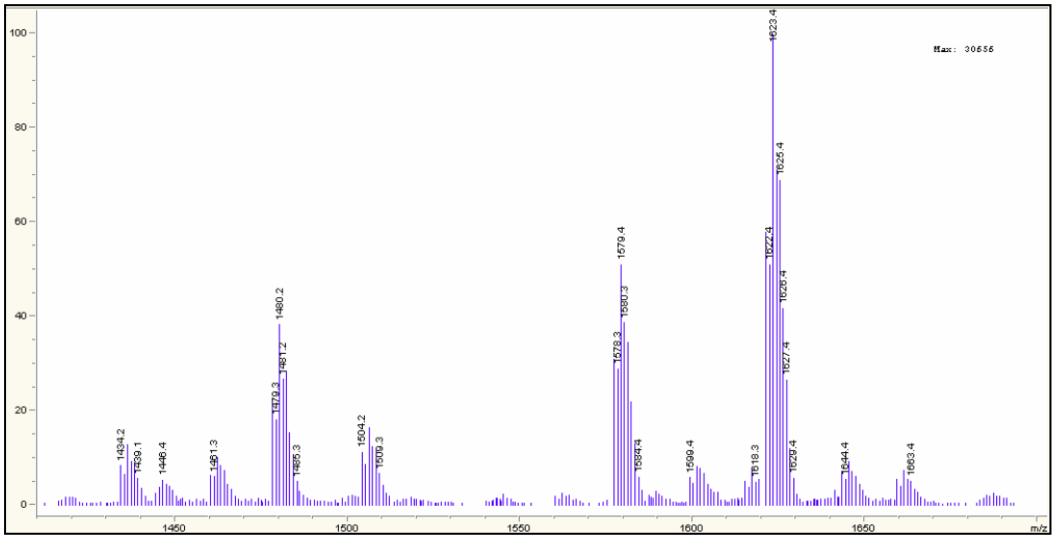

Figure 7.03: Theoretical and experimental mass spectra of the novel reaction product vanGibbs. A) Theoretical isotopic pattern of vanGibbs. The vanGibbs molecule in a one to one stochimetric reaction has an expected chemical of $C_{72}H_{76}Cl_4N_{10}O_{25}$, an exact mass of 1620.4 g/mol and a molecular weight of 1623.2 g/mol. **B) Experimentally measured mass spectrum of 2 equivalents of Gibbs reagent with one equivalent of vancomycin under alkaline conditions.** The main peaks around 1620 m/z represent the vanGibbs molecule in its cationic form $[M]^+$ and display a comparable pattern to the predicted isotopic shape. The comparable shaped peak patterns around 1644 m/z and 1663 m/z correspond to vanGibbs' mass plus a sodium $[M+Na]^+$ and a potassium cation $[M+K]^+$ respectively. The peaks at lower masses are fragmentations of the vanGibbs molecule displaying similar isotopic pattern, which suggests that the four chlorine atoms are still attached to these main fragments. The peaks around 1579 m/z could be due to the loss of a carboxylic group, which equals to a loss of about 45 m/z (Kellner et al. 2004). The peaks around 1480 m/z may be due to the loss of one sugar moiety resulting in a mass loss of about 144 m/z. Furthermore, no peaks can be observed around 1447 m/z, which are displaying a vancomycin typical pattern.

7.3.2 ^{1}H-NMR Analysis

Since to the best of our knowledge Gibbs reagent has never been successfully coupled to vancomycin molecule before, the structure of this new product is unknown. As previously hypothesised in the above section 7.1 and in chapter 6.1, the Gibbs is expected to couple to the position 6 in the resorcinol, which is the 7th residue of vancomycin. However, it has been previously highlighted that the addition may occur at another position of the vancomycin molecule, for instance in position 2 of the same residue (7th), which would be the ortho-position to both hydroxyl groups, other aromatic moieties that become phenolic or amine groups. This may result in multiple additions accompanied with possible fragmentation.

To initiate the ^{1}H-NMR study[7], spectra of the starting material, vancomycin, in deuterated dimethyl sulfoxide (DMSO-d6) were captured and compared to a spectrum taken by Clive M. Pearce and Dudley H. Williams in 1995 (Pearcea and Williams 1995). Figure 7.04 presents these two spectra and figure 7.05 in addition with table 7.01 compares their full proton assignments. The last row in table 7.01 represents the difference of the two assignments. Since both spectra are very similar and the proton shifts are highly comparable, this initial study was considered successful.

The study of the novel coupling product was proven difficult due to the required reaction conditions such as high pH and mixture of aqueous and organic solvents, as well as the stability of the produced molecule in both liquid and solid form. Therefore, structural characterisation of the product was performed by studying NMRs of the crude reaction mixture. For this reason, firstly the chemical shifts of the starting material vancomycin and their changes in the deuterated solvent mixture with increasing pD was analysed. Afterwards the novel molecule was studied and compared to this analysis of vancomycin in reaction conditions for characterisations of the structure of the novel product vanGibbs.

[7] Most NMR experiments and analysis were performed in conjunction with Dr. Antonio Ruiz-Sanchez. Additionally, their results were discussed with Dr. Stephen Hilton and Dr. Abil Aliev.

Figure 7.06 presents some ^{1}H-NMR spectra of vancomycin in deuterated water (D_2O) and deuterated methanol (MeOD) with increasing pD achieved by addition of 40% deuterated sodium hydroxide (NaOD) in D_2O. The first spectrum from the top is vancomycin in pure D_2O, the second one is in a mixture of 1/3 D_2O and 2/3 MeOD and then the subsequent four spectra have increasing amounts of NaOD. The last spectrum at the bottom shown in red has the exact reaction conditions needed for a successful Gibbs coupling as established in the previous chapter (6). These reaction conditions are hereafter called alkaline conditions and abbreviated with 'ac' in brackets. It has to be highlighted that the resolution for vancomycin in a mixture of 1/3 D_2O and 2/3 MeOD is not as good as in the other spectra. This may be due to the addition of organic solvent, which could have resulted in an aggregation of the vancomycin molecules according to the poor solubility of vancomycin in organic solvents. However, this observation and hypothesis was not further studied. In general, it can be observed that protons are shifting towards lower chemical shifts the higher the pD gets.

Figure 7.07 in addition with table 7.02 compares the full assignment of the very last spectrum shown in red with an assignment found in literature from A. S. Antipas and colleagues (Antipas et al. 2000). They have studied the ^{1}H-NMR of vancomycin in D_2O with increasing pDs. The first row of table 7.02 lists the code of the protons according to figure 7.07, the second row is the assignment copied from Antipas et al. 2000 and the third row presents the assignment of the last spectrum shown in red. In general, the vancomycin spectrum with the exact reaction conditions can be roughly divided in the following five parts:

- From 7.6 to 6.5 ppm are the aromatic protons of the 2nd, 5th and 6th residues coded with *d, e, g, f, i, j, k, m* and *l*.

- From 6.5 to 5.75 ppm are the two doublets of the aromatic protons of interest from the 7th residue – *o* and *p*.

- 5.75 to 5.2 ppm include the last two aromatic protons of the 4th residue – s_1 and s_2, the protons from the two carboxylic acids – *u* and *t*, as well as the protons neighbouring many deshielding groups such as amines, carboxylic acids and hydroxyls or oxygen atoms - r_4 and A_1.

- From 5.2 to 2.3 ppm are the peaks of aliphatic protons that directly neighbours one deshielding group such as an amine, a carboxylic acid, a carbonyl or a hydroxyl or an oxygen atom as it is the case in the disaccharide moiety. Typically in peptide chemistry, the protons which are attached to the carbon before the carbonyl carbon are called 'alpha protons' (H_α) and the corresponding protons are the 'alpha carbons' (C_α).

- Below 2.3 ppm are the peaks from aliphatic protons which have mainly aliphatic neighbouring protons. In light of the above described H_α, some of these protons are 'beta protons' (H_β) or even 'gamma protons' (H_γ) if they are attached to a 'beta carbon' (C_β) or a 'gamma carbon' (C_γ) respectively. A C_β is the second carbon to the carbonyl group whilst a C_γ is the third.

The last row in table 7.02 represents the difference in chemical shifts of the two precedent assignments. It can be observed that all differences, except of two zeros, are positive in the range between 0.01 and 0.52 ppm. Consequently, it seems that the pD of the reaction mixture is higher than 9.0. Furthermore, it can be observed that the two protons of the 7th residue (proton coded as *o* and *p* in figure 7.07) are one peak in Antipas et al. (Antipas et al. 2000). This observation is similar to the experimentally obtained spectra with 1 and 3 µl NaOD, which supports previous finding suggesting that the pD of the exact reaction conditions with 10 µl NaOD (ac) is higher than 9.0. Overall, it can be concluded that almost all peaks can be assigned to the protons of vancomycin and the experimentally obtained spectra are in good agreement with the literature.

Therefore, the next step was to study the ^{1}H-NMR spectra of the novel molecule – vanGibbs – in comparison to vancomycin in reactions conditions (ac). Figure 7.08 presents a spectra overlay of the two starting materials, Gibbs reagent and vancomycin,

and the product vanGibbs obtained with different molar ratios of the starting materials. The shown ratios of vancomycin and Gibbs reagent are equimolar (1:1), 1:2, 1:3, 1:4, 1:5 and 1:65. One of the most predominant changes is highlighted with a dotted box marking the two doublets resulting from the two protons from the 7th residue. According to the previous described hypothesis, these are the positions to which the Gibbs reagent coupling may occur resulting in an indophenolic moiety (see subsection 7.1 and figure 7.01).

It can be observed that the doublets decrease to about half of their original size from the spectrum of pure vancomycin (shown in red) to the equimolar ratio spectrum (shown in black) and finally completely disappear in the 1:2 ratio spectrum (shown in blue). This observation leads to the assumption that despite an equimolar amount of Gibbs reagent, some vancomycin starting material remains unreacted. However, with two molar equivalents of Gibbs reagent in contrast to one mol of vancomycin, no starting material could be detected via ^{1}H-NMR. The spectra with higher molar equivalents of Gibbs reagent do not show these two peaks.

Moreover, the resolution of spectra is decreasing the larger the excess of the Gibbs reagent. It was found that the peaks in the spectra of an excess above 5 equivalents of Gibbs reagent are wider and consequently the spectra is losing resolution. This finding could be an indication of multiple additions or even fragmentation of the molecule. However, the spectra of the ratios 1:2 to 1:5 show highly similar positions, shapes and integrals of peaks below 4.1 ppm to pure vancomycin. These are strong evidences that the main vancomycin structure is conserved and that this vancomycin derivative represents the majority compound in the reaction mixture. This is further supported with figure 7.09 and table 7.03 which are comparing the spectra of pure vancomycin in the second row and vanGibbs obtained by a ratio of 1:2 in the third row shaded in magenta. The fourth and last row lists the difference of the two preceding assignments. Only the chemical shifts of the protons coded as follows have changed: r_1, r_2, r_3, *o, p, k* and *d*. According to figure 7.09, all these changes are in proximity to the aromatic ring of the 7th residue or in case of *o* and *p* concerning directly the two protons of the resorcinol

itself. These findings are supporting evidence that the Gibbs reagent coupling occurs to this part of the antibiotic molecule and results in a change of electronic properties that changes the corresponding chemical shifts of these protons. Moreover, a new peak appears at a chemical shift of 7.02 ppm which is associated with the two protons of the Gibbs reagent.

Figure 7.10 shows a detailed comparison of the three ^{1}H-NMR spectra, pure vancomycin and vanGibbs obtained with an equimolar and a 1:2 ratio of vancomycin:Gibbs in the region from 8.0 to 4.2 ppm. The doublet with a chemical shift of 6.51 ppm is present and constant in all three spectra (indicated with a dark grey box). This doublet comes from the proton coded with *l* and has therefore an integral of 1. This integral serves as reference for the calculations of the other integrals in the spectra.

Similar to figure 7.08, the dotted box marks the two doublets of residue 7. Their integrals are about 1 each in pure vancomycin (shown in red). They decrease to a total of about 0.85 in middle spectra (shown in black), which is a bit less than half of their original size. Finally, they completely disappear in the spectrum obtain with a molar ratio of 1:2 vancomycin:Gibbs (shown in blue). As previously indicated, this observation leads to the assumption that with an equimolar ratio of Gibbs reagent a bit more than half of the vancomycin molecules in the sample have reacted. Then with 2 equivalents Gibbs reagent, all vancomycin molecules seems to have reacted into the novel product vanGibbs.

Upon reaction with the Gibbs reagent, it is expected that the peak of the proton at the position where the coupling occurs vanishes due to substitution with the Gibbs reagent, whilst the other proton shifts due to the change in the electronic environment. The additional substitution of the aromatic ring with a moderately activating group increases the electron density in the conjugated π system. This increase leads in a shielding effect and consequently an upfield shift to lower ppm values of the neighbouring proton. Moreover, the peak has to change its multiplicity from a doublet to a singlet. The two arrows below the peaks depict this shift of one of the two protons into the existing

multiplet *of* s_2, *t*, A_1, *u* and s_1 to a chemical shift of about 5.43 ppm (indicated with a red box). Since the shifted peak is in the middle of the existing multiplet, a superposition of various peaks is occurring which complicates the integration. Therefore, the integral differences are with about 0.73 for the difference of vancomycin and equimolar vanGibbs and with 1.54 for the difference of equimolar and 1:2 vanGibbs too large.

On the other hand, the new arising peak at 7.02 ppm (illustrated with a yellow box) has an integral of 0.88 in the equimolarly obtained vanGibbs, which is in good agreement with the expectation that this peak is associated with two similarly shifted protons of the newly attached Gibbs reagent group. The same applies for the 1:2 ratio vanGibbs in which all vancomycin molecules have reacted to vanGibbs and therefore the integral is with a value of 1.94 close to 2.

The next step was to find the exact position in the resorcinol to which the Gibbs reagent is coupling to. Therefore, a two-dimensional NMR study was performed. As described in subsection 7.2.3 neither COSY nor TOCSY spectra were captured. It was directly started with the NOESY analysis.

Figure 7.11 shows two NOESY spectra. The first one (A) is vancomycin in reaction conditions and the second one (B) is vanGibbs obtained with a molar ratio of 1:2 between vancomycin and Gibbs reagent. The blue colour indicates interactions with a negative sign whilst yellow depicts the positive interactions. As previously described in subsection 7.2.3, since vancomycin and vanGibbs are both large molecules, the NOE interactions shown as cross peaks have the same sign and consequently colour as the diagonal peaks. The axial peaks with a positive sign are arising from the water molecules present in both samples. The quantity of water seems slightly higher in spectrum B than A. In general, it can be observed that both spectra look very similar, which is expected and strongly supports previous findings.

The lines were added to the spectra to guide the eye. All horizontal lines illustrate the regions in the spectrum where cross peaks will occur if the irradiated nucleus at this chemical shift has detectable NOE interactions with nuclei in its close proximity. Hence, the nucleus of interest acts as a source spin which is further abbreviated as S. All vertical lines indicate the regions of the spectrum where peaks would occur if the nucleus of interest would interact with a nearby irradiated nucleus and upon this interaction shows as detectable NOE interaction. Hence, it would be then the interesting spin which is further abbreviated as I.

In figure 7.11 A the green lines indicates the interaction regions of the proton *o* and the grey lines of proton *p*. The cyan arrow highlights a very weak NOE interaction between the protons r_2 and *p,* where r_2 is S and *p* is I. For improved visibility, the grey line is interrupted. This dipolar coupling has also be seen by C. M. Pearce and D. H. Williams (Pearcea and Williams 1995). Besides this interaction, neither nucleus *o* nor *p* are showing any NOE interaction peaks, except of interactions as S with the water peak around 4.8 ppm. The orange lines depict the chemical shift of 5.43 ppm, which is part of the multiplet arising from the protons s_2, *t*, A_1, *u* and s_1. As previously described (see figure 7.10), this is the ppm value where one of the protons *o* and *p* will shift to in the vanGibbs molecule. Therefore, it is highlighted for simpler direct comparison with the red lines in the vanGibbs ^{1}H-NMR NOESY spectrum in figure 7.11 B.

In figure 7.11 B, it can be observed that all cross peaks are very similar to figure 7.11 A and no new interaction peaks can be found. In the region where the shifted nucleus act as S (highlighted by the horizontal red line), the peaks between 8 and 7.5 ppm have shifted slightly downfield and the peak at 6.75 ppm slightly upfield. All these shifts were previously observed in the one-dimensional ^{1}H-NMR spectra. Furthermore, some peaks seem to vanish, but as previously indicated in subsection 6.2.3 this does not necessarily mean that there is no interaction. Comparable observations can be made for the region where the shifted peak acts as I spin (illustrated with the vertical red line). Furthermore, the cyan arrow indicates again where the NOE interaction may appear if the *p* proton is the one which is shifting. However, this region is already occupied by NOE interaction

peaks from the multiplet as indicated in figure 7.11 A. The dark yellow lines in figure B indicate the NOE interaction regions of the new arising peak from the two protons of the attached Gibbs group. Both horizontal and vertical regions are not showing any cross peaks.

The yellow peaks with the opposite sign close to the diagonal peaks in the area 8 to 7.5 ppm indicate that a molecule is present in the sample with a molecular weight below 1000 Da. As visible in figure 7.08, the chemical shifts of the protons of the Gibbs reagent in the reaction conditions are in this region. Hence, these peaks are arising from the free Gibbs molecules which have not coupled to vancomycin.

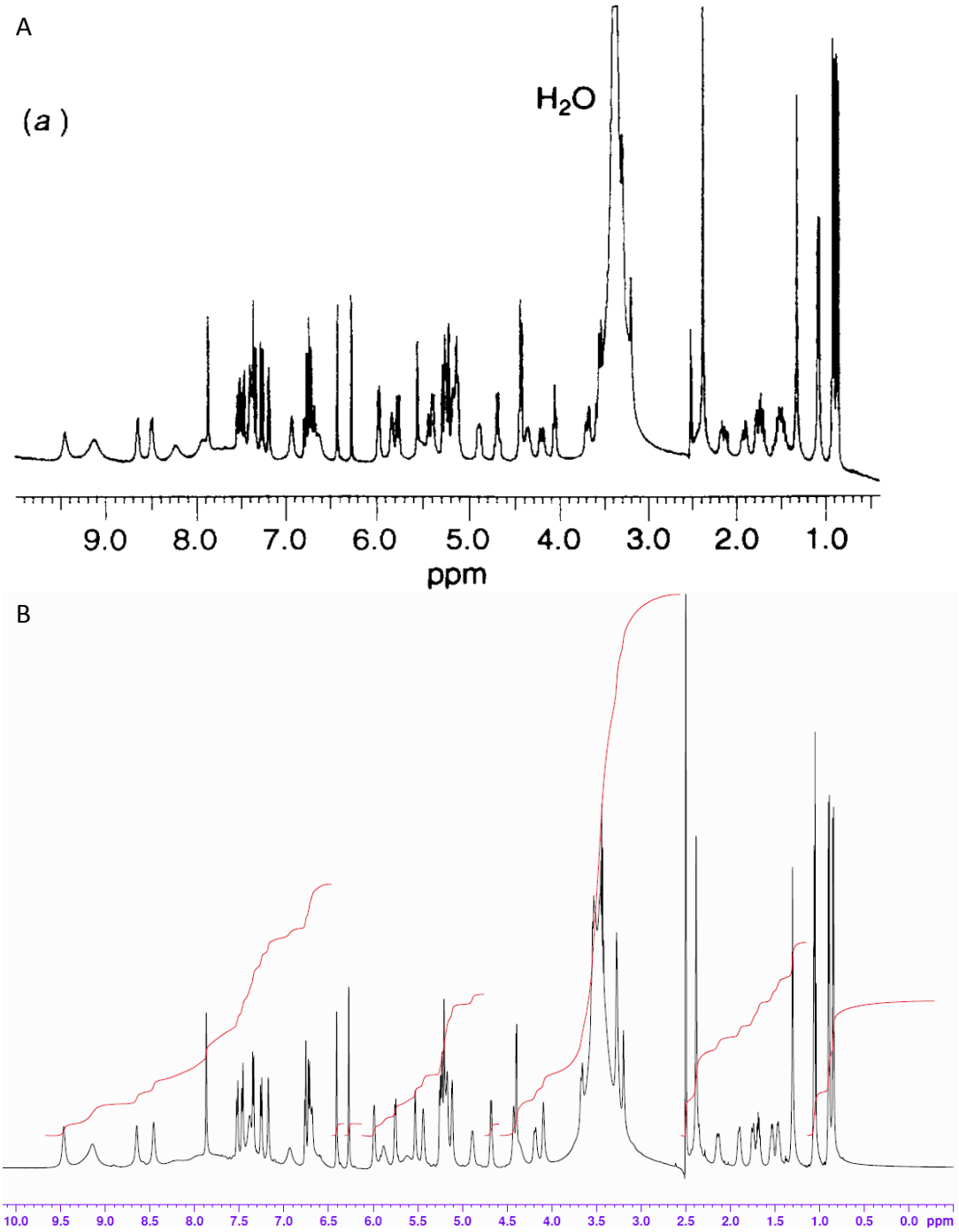

Figure 7.04: ^{1}H-NMR analysis of vancomycin in DMSO and comparison with literature. A) ^{1}H-NMR analysis of vancomycin in DMSO by Clive M. Pearce and Dudley H. Williams. Illustration adopted from Pearcea & Williams, 1995. **B) ^{1}H-NMR of vancomycin in DMSO**. The full assignment of both spectra and the direct comparison can be found on the next page in figure 7.05 and table 7.01.

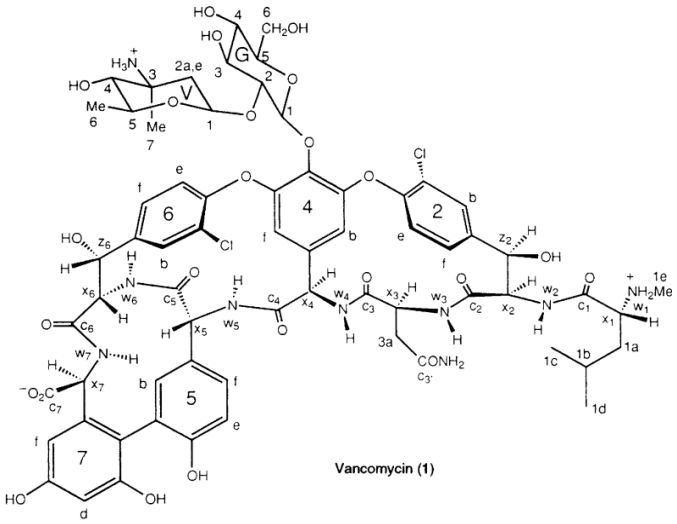

Figure 7.05: Labelled structure of vancomycin for ^{1}H-NMR assignments and comparison with literature. Proton coded structure for the full assignments of the two NMRs from figure 7.04. Schematic taken from Pearcea & Williams, 1995.

Table 7.01: Comparison of experimental full assignment with literature. The first and grey shaded assignment is taken from literature and belongs to figure 7.04 A (Pearcea and Williams 1995). The second assignment is experimentally obtained presented in figure 7.04 B. The last row presents the difference between the preceding assignments.

Table 7.01:

Multiplicity abbreviations: s = singlet, d = doublet, t = triplet, q = quartet, quin = quintet, non = nonet, m = multiplet, o = obscured, br = broad, and v br = very broad.

Proton	δ_H [ppm] (multiplicity)		$\Delta\delta_H$	Proton	δ_H [ppm] (multiplicity)		$\Delta\delta_H$
1d	0.86 (d)	0.81 (d)	0.05	*4f*	5.21 (d)	5.19 (d)	0.02
1c	0.91 (d)	0.89 (d)	0.02	V_1	5.24 (d)	5.22 (d)	0.02
V_6	1.07 (d)	1.02 (d)	0.05	G_1	5.27 (d)	5.25 (d)	0.02
V_7	1.32 (s)	1.29 (s)	0.03	G_3-*OH*	5.38 (d)	5.40 (d)	-0.02
1a'	1.47 (quin)	1.42 (quin)	0.05	V_4-*OH*	5.43 (br s)	5.43 (br s)	0
1a	1.51 (quin)	1.51 (quin)	0	*4b*	5.55 (br s)	5.50 (br s)	0.05
1b	1.72 (non)	1.70 (non)	0.02	X_4	5.75 (d)	5.75 (d)	0
V_{2eq}	1.75 (br d)	1.72 (br d)	0.03	Z_2-*OH*	5.82 (br s)	5.89 (v br s)	-0.07
V_{2ax}	1.90 (br d)	1.89 (br d)	0.01	Z_6-*OH*	5.96 (d)	5.96 (d)	0
3a'	2.14 (dd)	2.12 (dd)	0.02	*7f*	6.26 (d)	6.21 (d)	0.04
1e	2.37 (s)	2.34 (s)	0.03	*7d*	6.42 (d)	6.39 (d)	0.03
3a	2.42 (o)	2.38 (o)	0.04	W_3	6.62 (v br s)	6.60 (v br s)	0.02
V_4	3.23 (br s)	3.18 (br s)	0.05	W_6	6.67 (d)	6.65 (d)	0.02
X_1	3.31 (o)	3.31 (o)	0	*5e*	6.72 (d)	6.70 (d)	0.02
G_4	3.31 (o)	~3.31 (o)	~0	*5f*	6.77 (dd)	6.73 (dd)	0.04
G_5	3.31 (o)	~3.31 (o)	~0	$CONH_2$	6.92 (br s)	6.92 (br s)	0
G_3	3.50 (t)	3.50 (t)	0	*5b*	7.18 (br s)	7.16 (br s)	0.02
$G_{6a'}$	3.57 (dd)	3.57 (dd)	0	*2e*	7.26 (d)	7.24 (d)	0.02
G_2	3.59 (t)	3.59 (t)	0	*6e*	7.34 (d)	7.31 (d)	0.03
G_{6a}	3.68 (dd)	3.68 (dd)	0	$CONH_2$	7.37 (o)	7.34 (o)	0.03
G_{6a}-*OH*	4.05 (t)	4.08 (t)	-0.03	*2b*	7.39 (br s)	7.36 (br s)	0.03
X_6	4.19 (d)	4.19 (d)	0	*6f*	7.47 (dd)	7.44 (dd)	0.03
X_3	4.35 (br q)	4.37 (br q)	-0.02	*2f*	7.52 (d)	7.50 (d)	0.02
X_7	4.42 (d)	4.40 (d)	0.02	*6b*	7.86 (s)	7.83 (s)	0.03
X_5	4.43 (d)	4.41 (d)	0.02	W_2	7.93 (v br s)	7.89 (v br s)	0.04
V_5	4.68 (q)	4.64 (q)	0.04	W_4	8.25 (v br s)	~8.21 (o)	~0.04
X_2	4.88 (br m)	4.85 (br m)	0.03	W_7	8.48 (br d)	8.45 (br d)	0.03
G_4-*OH*	5.11 (br s)	5.09 (br s)	0.02	W_5	8.64 (br d)	8.63 (br d)	0.01
Z_6	5.13 (br s)	5.10 (br s)	0.03	*OH*	9.12 (v br s)	9.14 (v br s)	0
Z_2	5.16 (br s)	5.14 (br s)	0.02	*OH*	9.44 (br s)	9.45 (br s)	-0.01

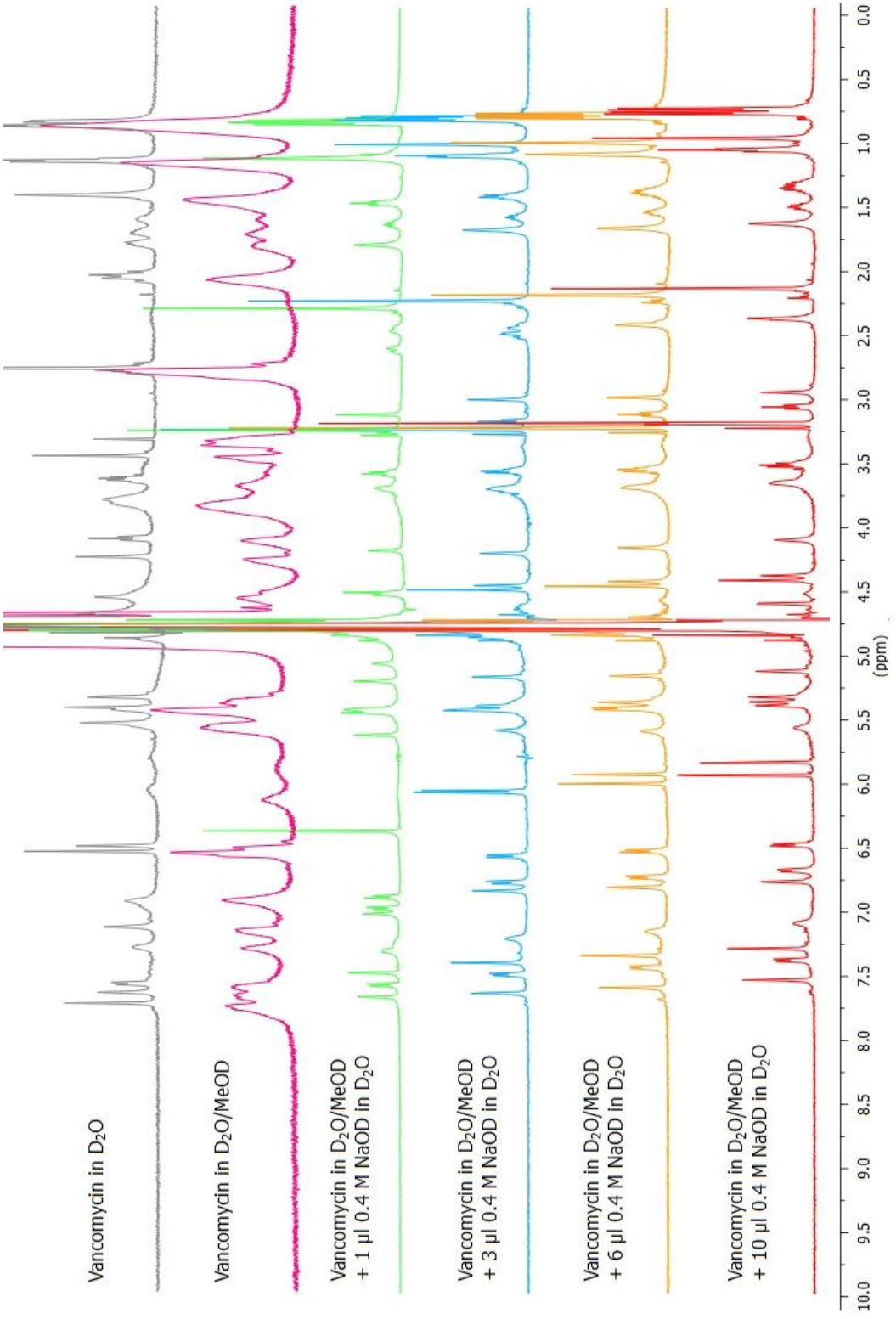

Figure 7.06: ^{1}H-NMR study of vancomycin in reaction conditions and comparison with literature. The full assignment of the last spectrum (red) is in the correct alkaline reaction condition required for the successful coupling of the Gibbs reagent. Its direct comparison with a full assignment found in literature is listed on the next page in figure 7.07 and table 7.02.

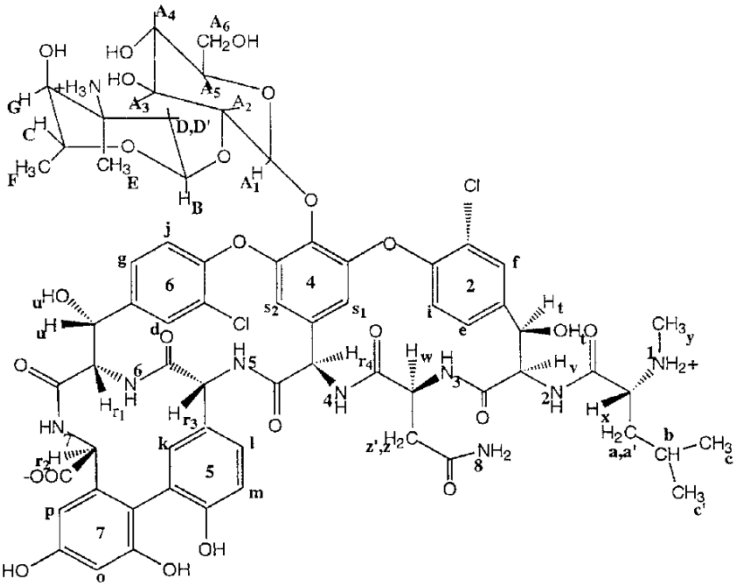

Figure 7.07: Proton coded vancomycin structure for the ^{1}H-NMR assignments and comparison with literature. Schematic taken from Antipas, Vander Velde, Jois, Siahaan, & Stella, 2000.

Table 7.02:

Proton	δ_H [ppm]		$\Delta\delta_H$ [ppm]	Proton	δ_H [ppm]		$\Delta\delta_H$ [ppm]
c'	0.90	0.82	0.08	r_2	4.50	4.41	0.09
c	0.90	0.82	0.08	r_3	4.59	4.45	0.14
F	1.19	1.12	0.07	*C*	4.85	4.66	0.19
E	1.13	1.02	0.11	*v*	5.10	4.90	0.2
a	1.50	1.50	0	*B*	5.24	5.18	0.06
b	1.63	1.55	0.08	s_2	5.46	5.30-5.45	0.16-0.01
a'	1.50	1.50	0	*t*	5.44	5.30-5.45	0.29-0.01
D, D'	1.80	1.70	0.1	A_1	-	5.30-5.45	-
z'	2.60	2.45	0.15	*u*	5.51	5.30-5.45	0.21-0.06
z	2.70	2.45	0.25	s_1	5.64	5.30-5.45	0.34-0.19
y	2.35	2.20	0.15	r_4	5.87	5.61	0.26
G	3.20	3.00	0.2	*o, p*	6.40	5.97, 5.88	0.43, 0.52
A_4	3.56	3.15	0.41	*l*	6.90	6.51	0.39
A_2	3.60	3.30	0.3	*m*	7.00	6.70	0.3
A_3	3.73	3.57	0.16	*k*	7.05	6.80	0.25
A_6	3.73	3.70	0.03	*i, j*	7.36	7.14	0.22
A_5	3.82	3.70	0.12	*f*	7.52	7.34	0.18
x	3.31	3.27	0.04	*e, g*	7.64	7.41	0.23
r_1	4.27	4.14	0.13	*d*	7.70	7.56	0.14
w	4.76	4.64	0.12				

Table 7.02: Comparison of experimental full assignment with literature at high pD. The first grey shaded assignment was taken from literature and belongs to a vancomycin in deuterated water with a pD of 9.0 (Antipas et al. 2000). The chemical shifts in the third row are experimentally obtained and taken from the ^{1}H-NMR spectrum at the bottom (red) in figure 7.06. The last row represents the differences of the two precedent assignments. Since the differences are all either zero or positive, the pD of the experimental spectrum is expected to be higher than 9.0.

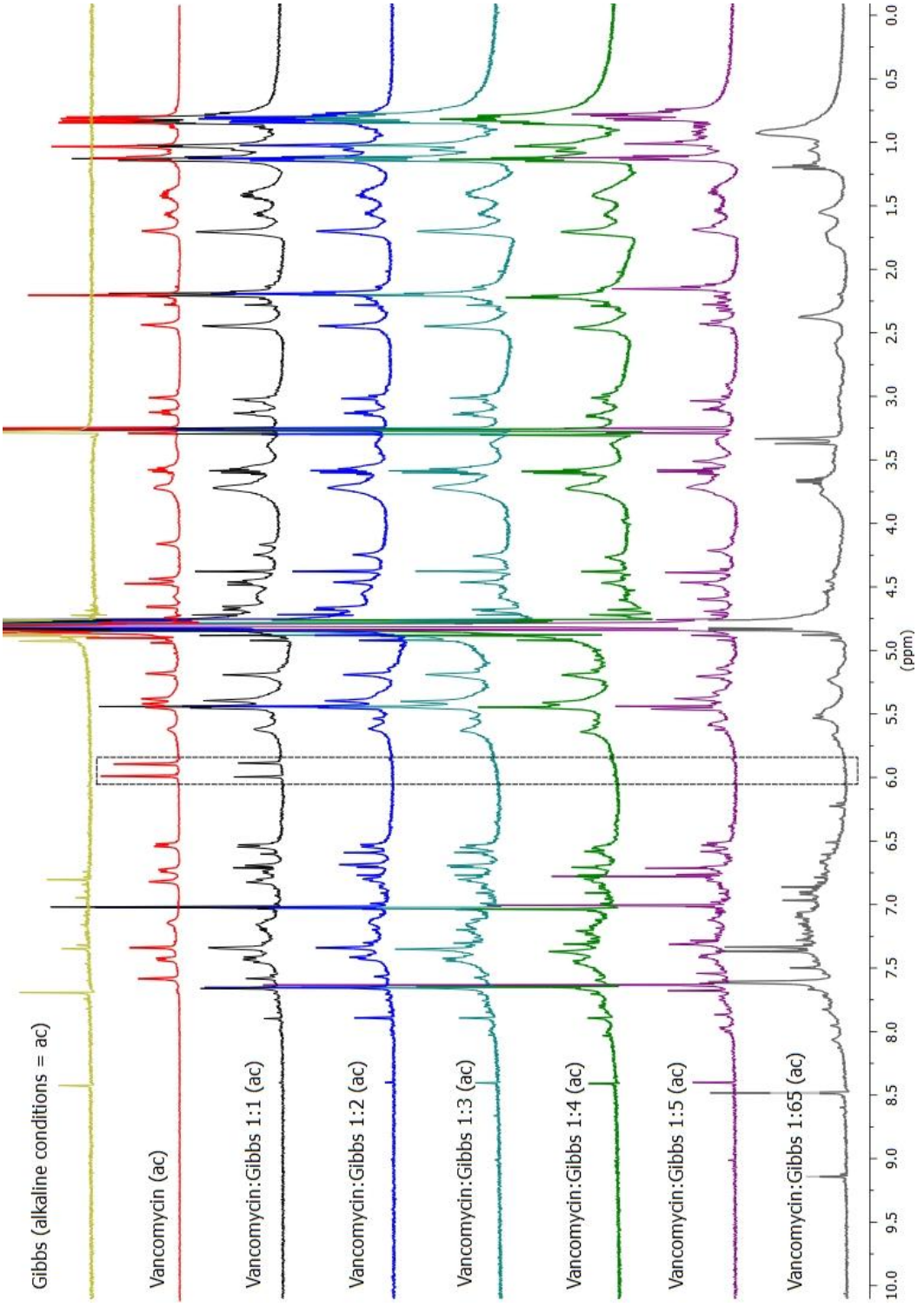

Figure 7.08: Overlay ^{1}H-NMR spectra of the starting materials and the novel product vanGibbs obtained with different molar ratios of the two starting materials. The dotted box highlights the two doublets that belong to the two protons in the resorcinol of the 7th residue of vancomycin – *o* and *p*. The abbreviation 'ac' in brackets indicates that all spectra were taken in the same alkaline conditions required for the successful coupling of Gibbs reagent to vancomycin.

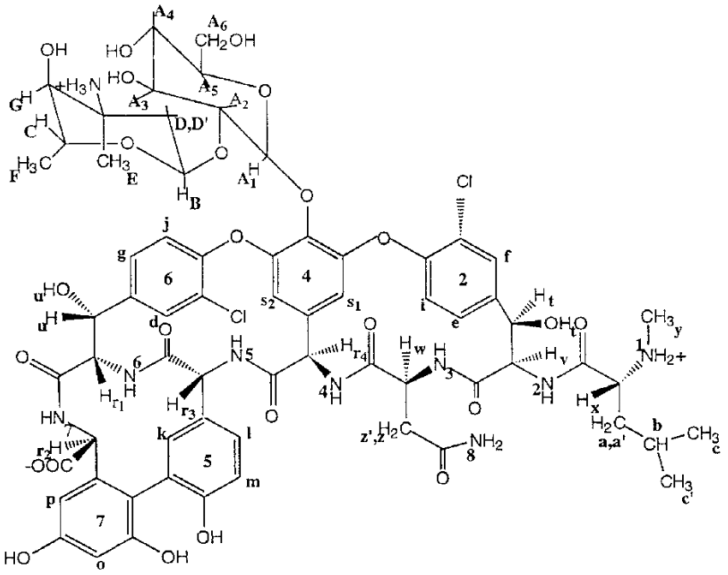

Figure 7.9: Proton coded vancomycin structure for the ^{1}H-NMR assignments of vancomycin and vanGibbs. Schematic taken from Antipas, Vander Velde, Jois, Siahaan, & Stella, 2000.

Table 7.03:

Proton	δ_H [ppm]		$\Delta\delta_H$ [ppm]	Proton	δ_H [ppm]		$\Delta\delta_H$ [ppm]
c'	0.82	0.82	0	r_2	4.41	4.37	0.04
c	0.82	0.82	0	r_3	4.45	4.46	-0.01
F	1.12	1.12	0	*C*	4.66	4.66	0
E	1.02	1.02	0	*v*	4.90	4.90	0
a	1.50	1.50	0	*B*	5.18	5.18	0
b	1.55	1.55	0	s_2	5.30-5.45	5.30-5.45	0
a'	1.50	1.50	0	*t*	5.30-5.45	5.30-5.45	0
D, D'	1.70	1.70	0	A_1	5.30-5.45	5.30-5.45	0
z'	2.45	2.45	0	*u*	5.30-5.45	5.30-5.45	0
z	2.45	2.45	0	s_1	5.30-5.45	5.30-5.45	0
y	2.20	2.20	0	r_4	5.61	5.61	0
G	3.00	3.00	0	*o, p*	5.97, 5.88	x↔~5.43	x↔~0.54
A_4	3.15	3.15	0	*l*	6.51	6.51	0
A_2	3.30	3.30	0	*m*	6.70	6.70	0
A_3	3.57	3.57	0	*k*	6.80	6.81	-0.01
A_6	3.70	3.70	0	*i, j*	7.14	7.14	0
A_5	3.70	3.70	0	*f*	7.34	7.34	0
x	3.27	3.27	0	*e, g*	7.41	7.41	0
r_1	4.14	4.24	-0.1	*d*	7.56	7.65	-0.09
w	4.64	4.64	0	*Gibbs*	not existing	7.02	-

Table 7.03: Comparison of the full assignments of vancomycin and the novel product both in reaction conditions. The second row lists the chemical shifts of vancomycin as it was previously established (see table 7.02). The assignment in the third row shaded in magenta is from the new product vanGibbs obtained by a reaction of 2 equivalents Gibbs with 1 equivalent vancomycin, which corresponds to the fourth spectrum from the top in figure 7.08 shown in blue. The symbol '↔' for the protons *o* and *p* indicates that it was not certain to which position the coupling occurs. The fourth row lists the differences between the two preceding assignments.

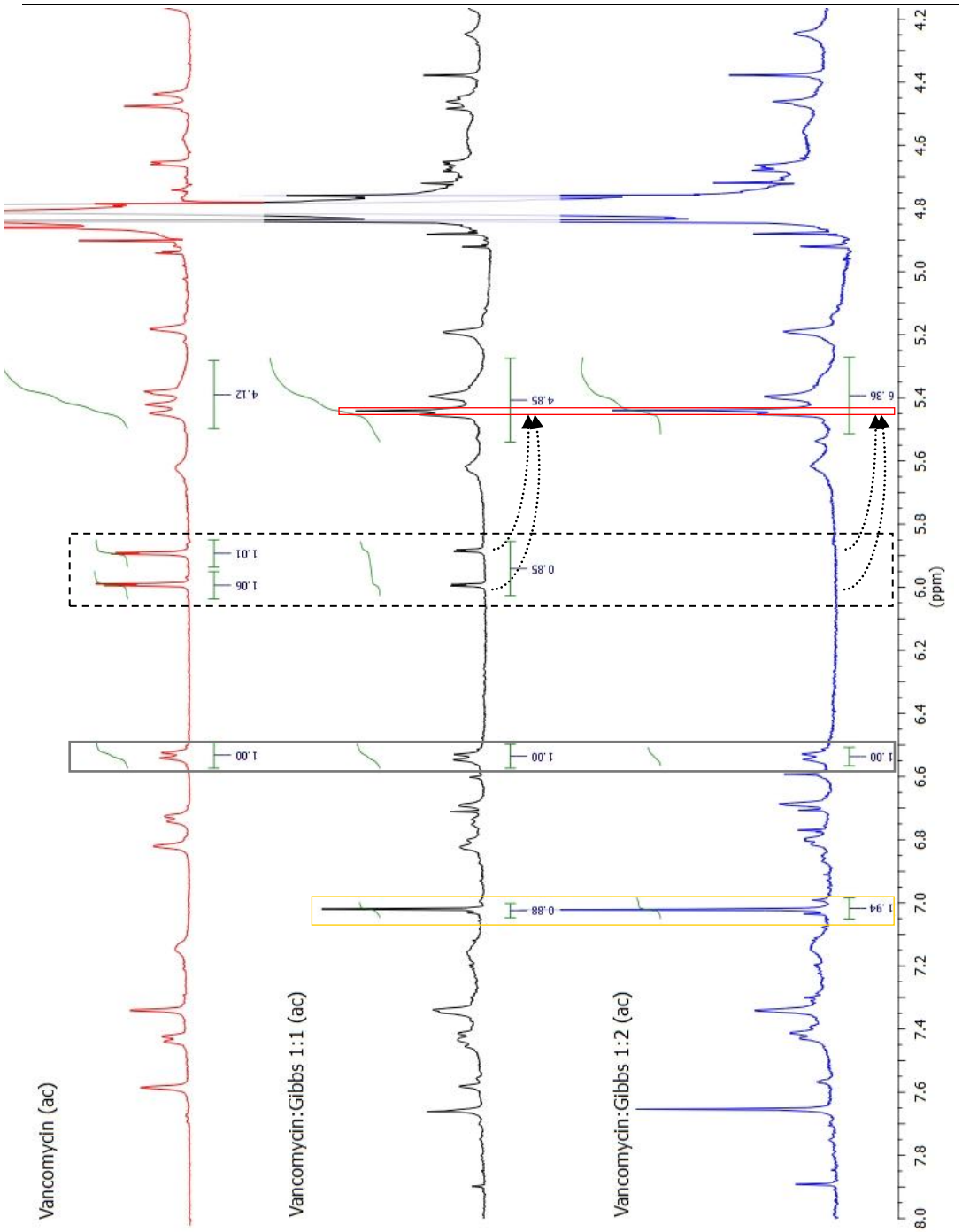

Figure 7.10: Detailed ^{1}H-NMR comparison of vancomycin and the novel product obtained with two different molar ratios in the region of 8.0 – 4.2 ppm. The doublet with integral 1 at 6.51 ppm, indicated with a grey box, is from proton *I*. It is constant in the three spectra and was taken as reference for the other integral calculations. The dotted box marks the two doublets from the 7th residue. The arrows indicate that one of the two protons is shifting towards lower chemical shifts into the multiplet of 5.30 to 5.45 ppm, whilst the other one is disappearing due to the addition of the Gibbs reagent. This shifted peak is indicated with a red box at 5.43 ppm. The novel arising peak at 7.02 ppm highlighted with a yellow box has integrals of 0.88 and 1.94. It is associated with the two protons of the added Gibbs reagent group.

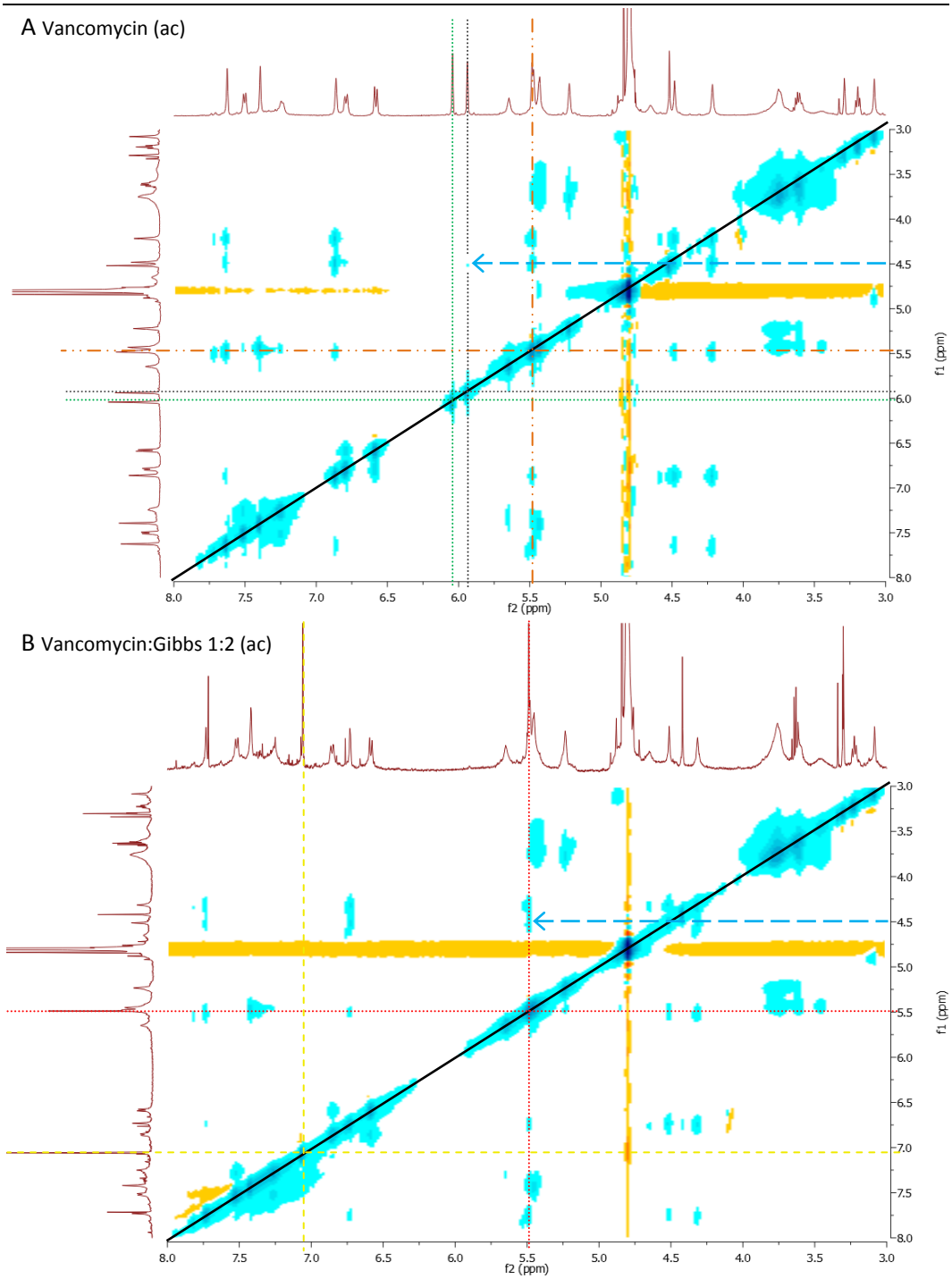

Figure 7.11: ^{1}H-NMR NOESY analysis of vancomycin and vanGibbs. All horizontal lines illustrate the regions where peaks can occur if the nucleus at this chemical shift is irradiated (S). All vertical lines indicate the regions where peaks would occur if the nucleus of interest would interact with a nearby S and would act as I. **A) Vancomycin.** The green and grey lines indicate interaction regions of the protons *o* and *p* respectively. The cyan arrow highlights a NOE interaction of *p* with r_2. For improved visibility, the grey line is interrupted. The orange lines depict 5.43 ppm as part of the multiplet to which one proton will shift after coupling (see B). **B) VanGibbs with a 1:2 molar ratio.** The dark yellow lines illustrate the new peak arising from the attached Gibbs protons. The red lines highlight the shifted peak. The cyan arrow is copied for comparison with A).

7.4 Conclusion and Outlook

The results presented herein provide very strong evidence that the Gibbs reagent is coupling to vancomycin under these reaction conditions in a one to one stoichiometry. However, two molar equivalents of Gibbs reagent are required so that vancomycin, as one of the two starting materials, is not detectable anymore via ^{1}H-NMR. The majority product of the aforementioned reaction has a molecular weight of 1623.2 g/mol and its isotope pattern supports the chemical formula of $C_{72}H_{76}Cl_4N_{10}O_2$. These observations are in an excellent agreement with the theoretically predicted values. Furthermore, the ^{1}H-NMR results show that the Gibbs reagent coupling takes place on the resorcinol ring of the 7th residue of vancomycin. However, the presented results do not show clear evidence for a coupling in either position 6 or 2 of the 7th residue. Therefore for the patent, the reaction schematic was formulated as presented in figure 7.12 (Kappeler et al. 2013). This allows leeway and assures a wide patent protection.

Nevertheless, the following arguments support a coupling to position 2 of the resorcinol ring which is the ortho-position to both hydroxyl groups.

i) If the fairly large Gibbs group with two nuclei would add to position 6, one would expect a NOE interaction with proton r_2. However, as previously indicated, no NOE interaction cross peaks in the NOESY spectra do not necessarily mean that there are no interactions.

ii) Position 2 is more nucleophilic than position 6 of the 7th residue. This increased nucleophilicity which was used by several groups for modifications of vancomycin and other glycopeptide antibiotics. For example A. Y. Pavlov and colleagues modified eremomycin with various primary and secondary amines via Mannich reactions. As illustrated in figure 7.13 A the reaction was exclusively directing to position 2 or as it is in the paper called position 7d which is the same labelling as previously proposed by C. M. Pearce and D. H. Williams (Pearcea and Williams 1995) (see figure 7.04, 7.05 and table 7.01). They also tested the antibacterial activity of their various aminomethylated eremomycin derivatives and found that

the 7d-decylaminmethyl derivative (addition of $NHC_{10}H_{21}$) was the most active one (Pavlov, Lazhok, and Preobrazhenskaya 1997).

Another very prominent example for a Mannich reaction to position 2 is the synthesis of telavancin (Leadbetter et al. 2004; Benito-Garagorry 2013; Higgins et al. 2005; Hegde et al. 2004). Telavancin was the first semi-synthetic derivative of vancomycin to receive FDA approval in September 2009 (Corey et al. 2009). Telavancin's trade name is 'Vibativ' and it is manufactured by Theravance Inc. (San Francisco, California, U.S.A.) and Astellas Pharma Inc. (Tokyo, Japan) (Corey et al. 2009; Kresse, Belsey, and Rovini 2007). It was first approved for complicated skin and skin structure infections (cSSSI) which are usually caused by *S. aureus*. Since June 2013, it can additionally be used for hospital-acquired and ventilator-associated bacterial pneumonia (HABP/VABP) also caused by *S. aureus*, but only if alternative treatments are not suitable (Yao 2013). Figure 7.13 B depicts telavancin's structure which is comparable to our vanGibbs molecule if we assume the Gibbs reagent is coupling to position 2 (figure 7.13 C).

However, despite these arguments supporting a coupling at position 2 in a one to one stoichiometric reaction, it has to be emphasised that with a larger excess of Gibbs it may be possible that a different molecule or various fractions with several Gibbs couplings are produced. Especially in light of the unexpected high absorbance in the UV/vis spectra with more than 100 times excess of Gibbs reagent (see chapter 6). This and the ultimate proof for the structure are still unsolved questions and should be considered together with purification and scaling-up as objectives for future work.

Furthermore, this novel vanGibbs molecule may be a new antibiotic which definitively should be tested for its antibacterial activity. As mentioned above, its structure is comparable to telavancin which may be promising for its antibacterial activity. Moreover, the Gibbs coupling reaction could be expanded to other members of the glycopeptide antibiotic family and could further serve as scaffold for various modifications resulting in novel semi-synthetic glycopeptide antibiotics.

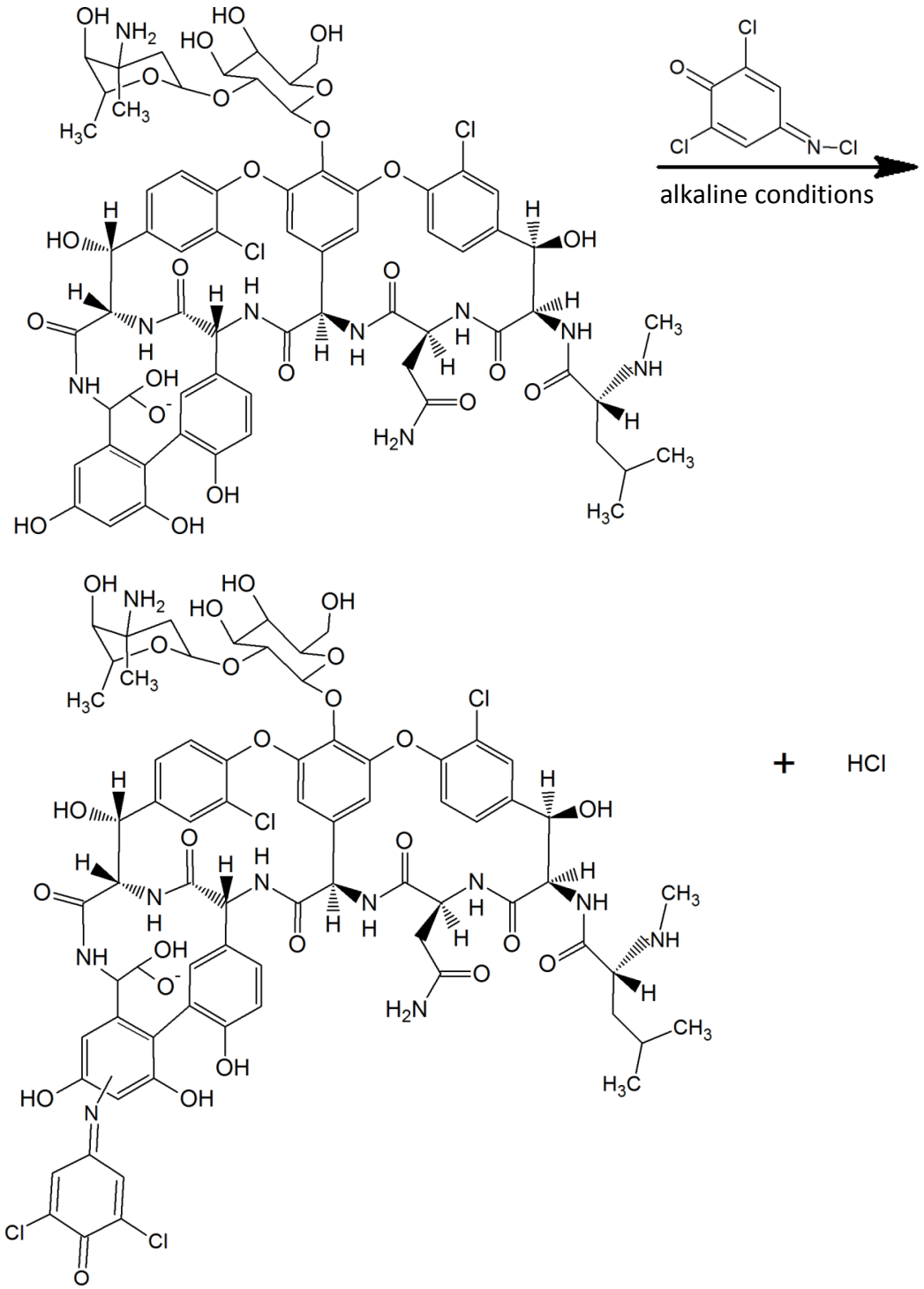

Figure 7.12: Proposed reaction scheme of the vancomycin Gibbs reaction under alkaline conditions as it is presented in our patent (Kappeler et al. 2013). It has to be highlighted that this reaction scheme is proposed for a one to one stoichiometric reaction only. It may be possible that larger excess of Gibbs results in a different molecule or that various fractions of the molecule are produced with multiple Gibbs additions.

A

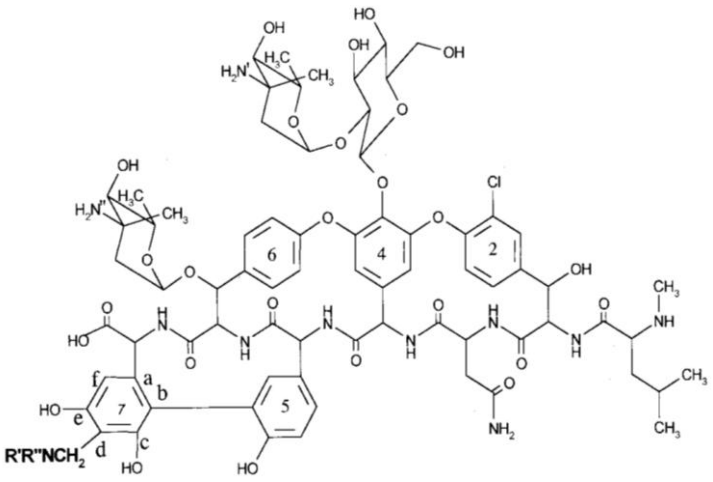

B

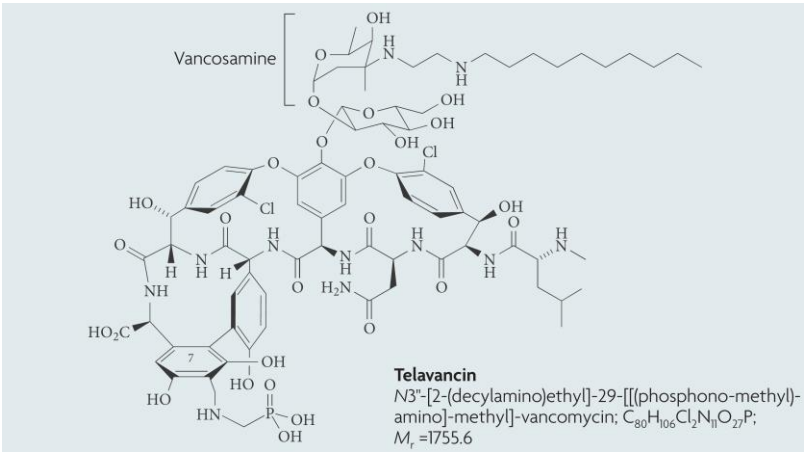

C

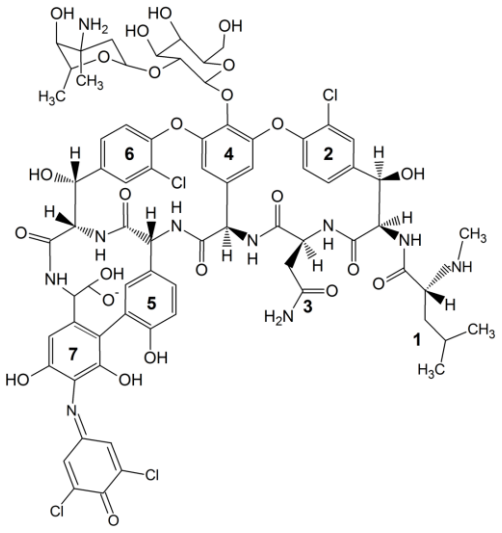

Figure 7.13: Structural comparison of different glycopeptide antibiotic derivatives obtained by Mannich reactions with our vanGibbs molecule. A) General structure of aminomethylated derivatives of eremomycin. Schematic adopted from Pavlov, Lazhok, and Preobrazhenskaya 1997. **B) Structure of telavancin.** Schematic adopted from Corey et al. 2009. **C) Structure of vanGibbs if assumed that Gibbs couples to position 2 of the 7th residue of vancomycin.**

CHAPTER 8:

Nanomechanical Detection of Vancomycin

The main objective of this PhD thesis is the development of a PoC sensor for therapeutic antibiotic monitoring, in particular for the antibiotic vancomycin. As described in the first chapter in section 1.1, the ultimate aim is to develop a patient attached real-time monitoring device by exploring the miniaturisation potentials of the different detection techniques. The starting point for this miniaturisation attempt was the colourimetric detection as a bench top device, which was previously presented in the chapters 5, 6 and 7. The technique in this chapter serves as the subsequent step in this miniaturisation development process and represents the transition from a bench top device to a future patient attached sensor (figure 1.01). In simple terms, the aim is to incorporate the sensor into the patient's the existing IV line. This platform typifies the change from intermittent measures of the drug concentration and its associated drawbacks of higher levels of staff involvement and invasiveness due to the need for repeated blood taking, to fully automated continuous and real-time monitoring, which could even feedback and regulate drug admission via automatic adjustment of drip flow rate.

The technique discussed in this chapter is cantilever array sensors. For 20 years, cantilever sensors have been used in different research fields as fast, real-time, and label-free detectors of various interactions taking place in solution, air, gas and vacuum. Due to their small size, they have the ability of being integrated into microfluidic systems and offering possibilities for various applications in lab-on-chip technology. Furthermore, multiple cantilevers, so-called cantilever arrays, provide a direct internal reference during the measuring process and enable the parallel measurement of several different analytes, making them an ideal platform for a patient attached multi-analyte sensor chip.

This approach builds on previous work by Rachel McKendry's group, which have shown that cantilever array sensors offer a unique tool to study surface-active drugs and the

nanomechanical consequences of drug-target binding interactions. Furthermore, it is speculated that these nanomechanical consequences are mimicking the antibiotic mode of action in real bacteria, where drug-target binding events introduce defects and act collectively to disrupt the cell wall leading to death of the bacteria (Watari et al. 2007; Ndieyira et al. 2008; Ndieyira et al. 2014; Watari, Ndieyira, and McKendry 2010; McKendry 2012; Kappeler 2010; Vögtli 2011; Watari 2007; Barrera 2008). Therefore cantilever array sensors paired with specific surface chemistry for antibiotic capturing create an optimal basis for a nanomechanical sensor for therapeutic vancomycin monitoring.

In this thesis, the approach using cantilever array sensors is placed in the gap between a bench top device and a patient attached sensor (see figure 1.01). Options for miniaturisation are limited, because it builds on an optical readout system. The same applies for directly monitoring analytes in blood, which is not feasible with an optical readout system. But various groups have shown that other readout systems are possible, which would allow miniaturisation and detection in opaque liquids such as whole blood (see chapter 8.1.2). Therefore, the objective of this chapter is exploring the feasibility of nanomechanical detection of antibiotics, in particular vancomycin, via cantilever array sensors. The hope is that it can be conclusively shown that with a different readout system, cantilever array sensors could become the next generation of PoC sensors for therapeutic antibiotic monitoring. In order for a sensor to be developed, it must meet the general requirements that were established in the introduction in chapter 1.2.

This chapter is divided into four subsections: The first subsection (8.1) describes the history of cantilever sensors, their application, modes of operation as well as discussions regarding surface stress and binding events. The second part (8.2) lists materials and methods. The third subsection (8.3) presents the results including preliminary discussions and continues into the final subsection (8.4) with the overall discussion and conclusion.

8.1 Introduction

This subsection introduces the nanomechanical detection via cantilever array sensors and starts with the history of cantilevers and cantilever array sensors (8.1.1), presents the modes of operation (8.1.2), reviews their applications (8.1.3), which leads to discussions on surface stress with beam deflection readouts including Stoney's equation (8.1.4) and nanomechanical detection of drug-target binding investigated via Langmuir adsorption isotherm (8.1.5 and 8.1.6), and ends in percolation model (8.1.7) followed by objectives (8.1.8).

8.1.1 History of Cantilever and Cantilever Array Sensors

The term "cantilever", as a description for a microscale beam, accompanied the development of the atomic force microscope (AFM) in the late 1980s (Binnig, Quate, and Gerber 1986; Albrecht et al. 1990). The inventors were Gerd Binnig, a German physicist, Calvin F. Quate, an American engineer, and Christoph Gerber, a Swiss physicist, at Standford University and IBM Research Laboratory, San Jose, both in California, USA. Gerd Binnig and Christoph Gerber were at that time on leave from the IBM Research Laboratory in Zürich, Switzerland. The principle of an AFM, sometimes called scanning force microscopy (SFM), is comparable to a gramophone in which interactions between a sharp tip at the end of a cantilever and underlying surface are monitored in order to obtain information from the topography. The change in topography results in a deflection of the cantilever, which can be precisely measured with a readout system such as the one described in subsections 8.1.4 and 8.2.3.1.

The deflection in the very first AFM (figure 8.01 B) has been measured with a scanning tunnelling microscope (STM) mounted on top of the AFM. The STM (figure 8.01 A) had been described just a couple of years earlier in 1983 by Heinrich Rohrer (1933 - 2013), a Swiss physicist, Gerd Binnig, Christoph Gerber and Edmund Weibel at the IBM Research Laboratory, Zürich, Switzerland (Binnig and Rohrer 1983; Binnig et al. 1982). In 1986, Gerd Binnig and Heinrich Rohrer received the Nobel Prize in physics for this invention. STM's mode of operation is based on the quantum tunnelling effect. If a conducting tip

is brought in very close proximity to a conducting or semi-conducting surface, electrons can tunnel through the vacuum between both of them. Tunnelling is induced due to an applied bias, which is a difference in voltage between tip and surface. By keeping either the height or the tunnelling current constant via a so-called feedback loop, the topography can be imaged down to atomic levels. By the year 2000, typical STM resolutions were reported in the range of 0.1 nm lateral and 0.01 nm vertical (Bai 2000). These days, low-temperature STMs even allow sub-surface imaging of different charge states induced by doping (Studer et al. 2012; Sinthiptharakoon et al. 2013) or adsorbed molecules (Dr. Cyrus Hirjibehedin, personal communication). One could argue that both STM and AFM laid foundations for the field of nanoscience and nanotechnology. Nowadays, both microscopes are key tools in nanoscale research and are used across all different nanoscientific disciplines from molecular biology to quantum physics.

If cantilevers are used as sensors by themselves, than there is no need for the tip at the end as in the AFM instrumentation, since the whole lever becomes the sensing part. Two papers published almost simultaneously at the end of 1993 marked the starting point for the use of cantilever sensors in research. Both of them were using probes developed for AFM experiments. The first paper to be published was authored by James K. Gimzewski, a Scottish physicist, and colleagues at the IBM in Zürich and the University in Basel both in Switzerland. It described a new form of calorimetric sensor usable in gas and vacuum environments. The proposed calorimeter is a silicon micromechanical lever coated with aluminium and platinum, which measures the heat flux of the catalytic conversion of hydrogen and oxygen to water with high sensitivity. Moreover, they advocated that with micromechanical technology the fabrication of an array of cantilevers is possible and could be used to construct a multi-analyte sensor similar to the human olfactory system, which they called “nose”. Furthermore, besides the photo illumination used by the group, which resulted in a temperature rise of the lever, they suggested alternative readout systems such as capacitative position sensing, changes in piezoresistance, piezoelectricity or the historically used electron tunnelling sensing technique (Gimzewski et al. 1994). The second paper, which was published only four months later by Thomas Thundat and colleagues at Oak Ridge National Laboratory in

Tennessee, USA, reported cantilever deflections upon temperature variation and adsorption of mercury and water vapours. Similar to Gimzewski et al., they observed that the optical readout results in a heating of the lever which in turn leads to cantilever deflections and continuous drift. Furthermore, they measured in static and dynamic mode, which are the two modes of operation for cantilevers also used for AFM work. Static mode refers to measurements of deflection on an idle cantilever. On the other hand, dynamic mode relates to observations of the resonance frequency of a vibrating cantilever (Thundat et al. 1994). Further information about static and dynamic mode can be found in subsection 8.1.2

Despite the proof that cantilevers possess additional sensor applicability beyond their use in AFMs as tip leverage for the amplification of topographical features, cantilever sensors did not attract large interest until 2000. In this year, Jürgen Fritz and colleagues published in the journal “Science“ that cantilevers offer a tool to measure the direct nanomechanical response of DNA hybridisation and receptor-ligand binding (Fritz et al. 2000). In the same year, A. M. Moulin and colleagues from University of Cambridge, UK, and Singapore showed that conformation changes of proteins over time and in response to adsorption of a molecule leads to surface stress that is measurable with a microcantilever-based biosensor (Moulin, O’Shea, and Welland 2000). Both papers have been denoted to be part of the breakthrough of the cantilever sensor research field (Tenje et al. 2012).

As evident in the histogram in figure 8.02, after several years of few publications incorporating cantilever sensors, the field seemed to gain momentum until its peak in 2009. The histogram visualises in blue the number of publications per year incorporating the terms “MEMS” (abbreviation of micro-electro-mechanical system), “cantilever” and “sensor” in title, keywords or abstract of publications. If the publication additionally had the term “array” in the above sections, then it is shown in yellow. Interestingly, the publication of papers pertaining to cantilever arrays seems to not have peaked yet. Moreover, their numbers appear to be fairly constant over the last five years despite the decrease in the overall publications with the terms “MEMS”, “cantilever” and “sensor”.

All publication numbers were taken from the Scopus® webpage. Scopus® is a registered trademark of Elsevier B.V. (Reed Elsevier PLC/N.V., Amsterdam, Netherlands) and offers a tool to search through various scientific journals. It has to be considered that the searches resulting in the illustrated publication numbers are not exhaustive and only serve the purpose of visualising general trends.

A

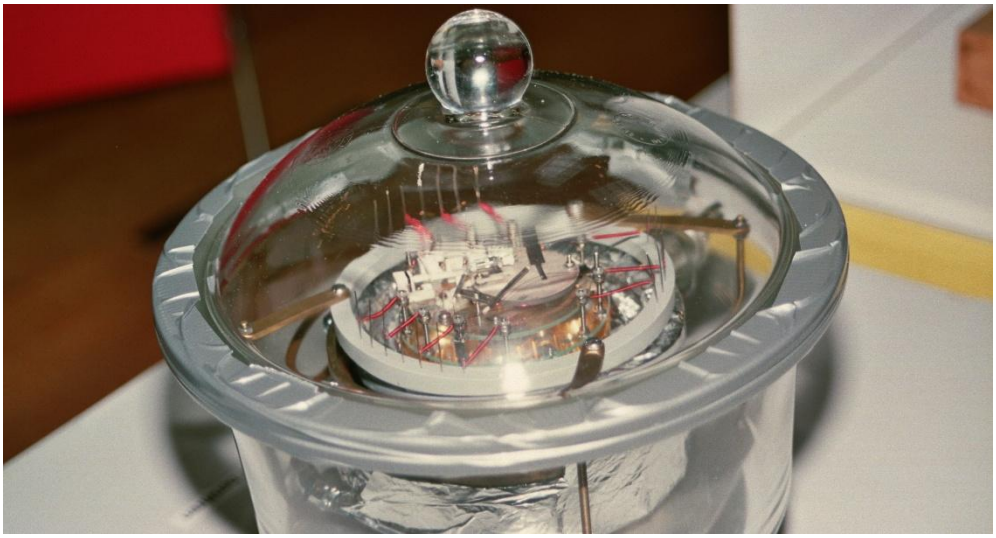

B

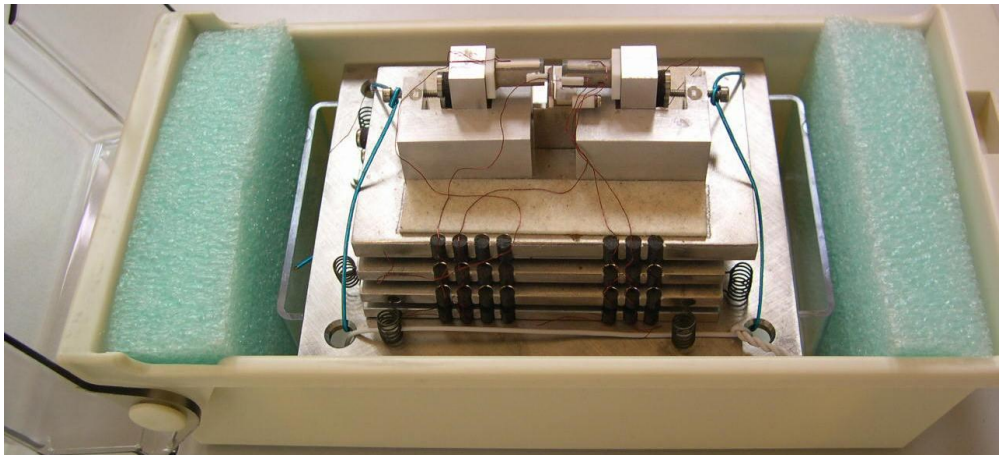

Figure 8.01: Photographs of STM and AFM replicas. A) The replica of the very first scanning tunnelling microscope (STM). It was built 1981 by Heinrich Rohrer, Gerd Binnig, Christoph Gerber and Edmund Weibel at the IBM Research Laboratory in Zürich, Switzerland. **B) The replica of the very first atomic force microscope (AFM).** Built by Gerd Binnig, Calvin F. Quate and Christoph Gerber at Standford University and IBM Research Laboratory, San Jose, California, USA in 1986. Both objects are in possession of the IBM Research Laboratory, Zürich, Switzerland.

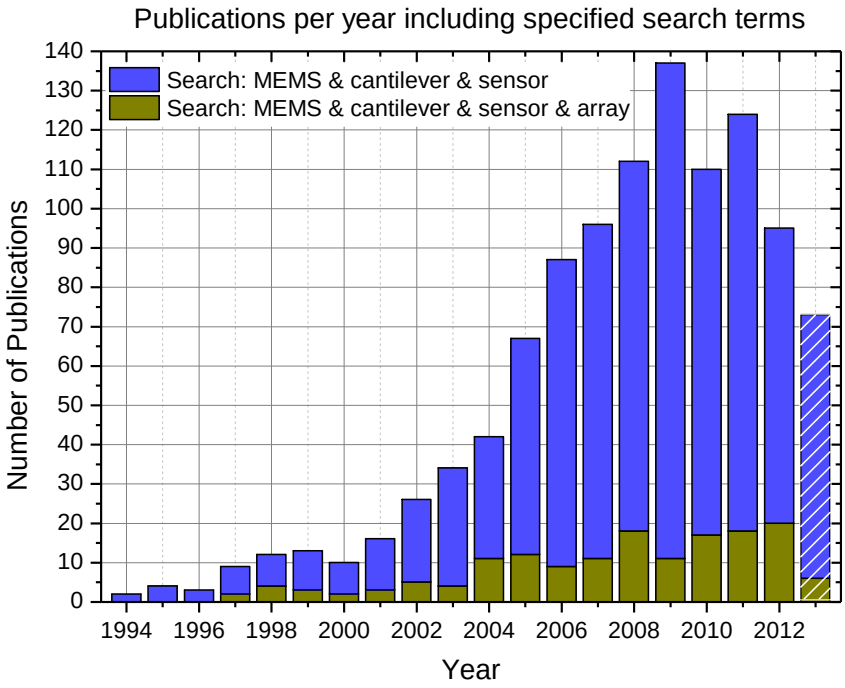

Figure 8.02: Publications per year incorporating specified search terms related to cantilever sensors. The histogram visualises in blue the number of publications per year incorporating the terms "MEMS" (abbreviation of micro-electro-mechanical system), "cantilever" and "sensor" in the title, keywords or abstract. If the publication additionally had the term "array" in at least one of these sections, then it is shown in yellow. The numbers for the search terms in blue did increase after a low in 2000 and peaked in 2009. However, the publication numbers of cantilever array seem to not have peaked yet. Moreover, their numbers appear to be fairly constant over the last five years despite the decrease in the overall publications. All publication numbers were taken from the Scopus® webpage. Scopus® is a registered trademark of Elsevier B.V. (Reed Elsevier PLC/N.V., Amsterdam, Netherlands) and is offering a tool to search through various scientific journals.

8.1.2 The Core and Mode of Operations for Cantilever Array Sensors

The core elements of a cantilever array sensor are the cantilevers, which are usually attached to a chip body. In this work a microfabricated silicon chip consisting of a chip body with eight thin rectangular silicon beams at the front was used (figure 8.03 A). Each of these cantilevers is 500 µm long, 100 µm wide and about 0.9 µm thick. More information about the fabrication of this silicon based cantilever array can be found in the materials and methods chapter on page 262.

However, the quantity of the cantilevers is variable as well as their shape and base material. For example, other groups (Zhang et al. 2007) have used a multiwell sensors with 16 cantilevers or paddle shaped cantilevers (Ilic et al. 2004; Yue et al. 2004; Stachowiak et al. 2006). Anja Boisen's group at the Technical University of Denmark (DTU) are using cantilevers made out of SU-8, which is a viscous polymer commonly used as a negative photoresist (Keller, Haefliger, and Boisen 2010; Nordström et al. 2008). Generally, due to their microscopic dimensions, the cantilevers are very flexible and have, in our case, a nominal spring constant of about 0.02 N/m. This flexibility and the corresponding sensitivity are the crucial and fundamental properties that govern how the sensors function. The advantage of multiple cantilever arrays is that each cantilever can be coated differently and is therefore able to sense various analytes simultaneously. Furthermore, single cantilevers are prone to artefacts such as thermal drifts, refraction index change and unspecific adsorption on the non-functionalised underside of the cantilever. This may cause a baseline drift during the static mode measurement. To account for these interferences, passivated, in-situ reference cantilevers are used and subsequently subtracted from the sensing cantilevers in order to obtain the veritable differential deflection signal (Watari, Ndieyira, and McKendry 2010; Shu et al. 2005). However, the entire drift causality is still subject of scientific debate. Further information about reference cantilevers can be found in subsection 8.2.1.2 in the 'Materials and Methods' chapter on page 267 including the corresponding figure 8.10 B.

Cantilever array sensors can be operated in static or dynamic mode. Static mode measures the bending of static cantilevers upon changes to the in-plane surface stress or due to mechanical expansion or contractions on one side of the lever. Dynamic mode detects the resonance frequency shift of oscillating cantilever beams after adsorption of additional mass, which is equivalent for mass sensing. The working principles for cantilever sensors can be divided into (i) temperature, (ii) mass change, and (iii) surface stress (figure 8.03 B) (Tenje et al. 2012):

i) The first principle typically involves mechanical expansion or contraction due to variations in temperature on the cantilever itself or in close proximity to it. For example an evaporated gold layer, on top of the silicon cantilever, has different thermal expansion coefficients than the underlying silicon. In this thesis this was analysed during a "heat test", which served a quality control measure for the gold layer on the upper sides of the cantilevers and the optical readout alignment. Further information referring to the heat test can be found in the subsection 8.2.4 starting on page 267, which includes figure 8.10 A.

ii) The second working principle is the change in resonance frequency of a dynamically operated cantilever due to added mass. However, the change in resonance frequency can also be triggered due to coating stiffness or changes in density or viscosity of the surrounding medium. In order to clearly distinguish between cantilever characteristics, changes in the surrounding environment and added mass, in-situ reference cantilevers besides the sensing cantilevers are of vital importance.

iii) The last principle is the change of surface stress on one side of the cantilever. This change can be generated during adsorption of a molecular layer, by surface charge as a result electrostatic repulsion, from conformational changes of the immobilised molecules, or by molecular recognition and binding events such as drug-target interactions. Stress can be caused by steric competition, structural changes, hydration, charge effects, mechanical expansion, swelling or a combination of all of

these factors. However, the stress causality is still the subject of scientific debate and is further discussed in subsection 8.1.4.

As previously mentioned, various different readout systems can be used to detect the bending of the cantilevers. The following list provides a concise summary of some of these techniques in chronological sequence and discusses their associated advantages and disadvantages:

- Original optical readout: The optical readout originated from the AFM instrumentation (Binnig, Quate, and Gerber 1986) and has been applied successfully to the cantilever sensors (Gimzewski et al. 1994; Thundat et al. 1994). A laser beam is focused at the apex of the cantilever and reflected to a position sensitive detector (PSD). By registering the deflection of this reflected laser light, the bending of each cantilever can be read out. This technique was used in the nanomechanical detection experiments and is therefore further described in the subsection '8.1.4 Surface Stress and Optical Beam Deflection Readout'. One of the advantages of the optical readout is its sensitivity. On the other hand, its size and stability is disadvantageous and renders miniaturisation towards a hand-held device almost impossible. Furthermore, the laser light has to travel through the sample, which means that opaque liquids, such as blood, cannot be measured.

- Piezoresistive readout: Piezoresistive materials change their resistivity when they are mechanically strained. For many years various groups have embedded such materials into cantilevers in order to detect the deflection by electrical property changes (Tortonese, Barrett, and Quate 1993; Mukhopadhyay, Lorentzen, et al. 2005; Wee et al. 2005; Rowe et al. 2008; Yoshikawa et al. 2009; Mukhopadhyay, Sumbayev, et al. 2005; Lang et al. 2009). The advantage of this kind of readout system is that the detector is embedded in the cantilever, which is ideal for miniaturisation and also allows analysis of opaque liquids. As such, this in theory would sound promising for a patient attached PoC sensor. However, its main disadvantage so far is a low detection sensitivity.

- Capacitive readout: In the capacitive readout, the cantilever is acting as one electrode of a capacitor and is therefore placed in parallel to a counter electrode. If the cantilever is deflecting, the distance between the two “electrodes” changes along with the capacitance, giving a measure for the extent of the cantilever’s deflection (Blanc et al. 1996; Amírola et al. 2005). The sensitivity of this technique is very high in the range of 10 picomolar. However, its application is limited to gaseous environments.

- Interferometric readout: The interferometric readout is another optical technique in which a light beam is split into a measuring and reference beam. Whilst the measuring beam is reflected on the cantilever’s surface, the reference beam stays intact. The subsequent combination of the beams leads to an interference patter due to phase shifts. This interferogram not only allows for the calculation of the deflection at the cantilever’s free end, but also gives a measure for its bending profile (Wehrmeister et al. 2007; Helm et al. 2005; Kelling et al. 2009). This technique is very sensitive and produces readouts for small cantilevers. However, similar to the original optical readout, the required optics renders miniaturisation almost impossible.

- Diffraction readout: The diffraction readout interprets the change in diffraction pattern generated by the deflection of the cantilevers. The pattern is obtained via entire illumination of the cantilevers (Hermans, Bailey, and Aeppli 2013; Aeppli and Dueck 2008). Therefore, as in the technique previously described, this readout system needs optics, which renders the miniaturisation almost impossible.

- Optical waveguide readout: This readout scheme is based on single-mode waveguides, which are integrated into the cantilevers. The deflection is determined by detecting intensity changes of the light transmitted through the cantilever (Nordström et al. 2007). The advantages of this technique are the possibility of miniaturisation and the applicability in air and opaque liquid. However, so far, it is only applicable for SU-8 cantilevers, which have the disadvantage of already being bent after the fabrication process (Keller, Haefliger, and Boisen 2010).

A

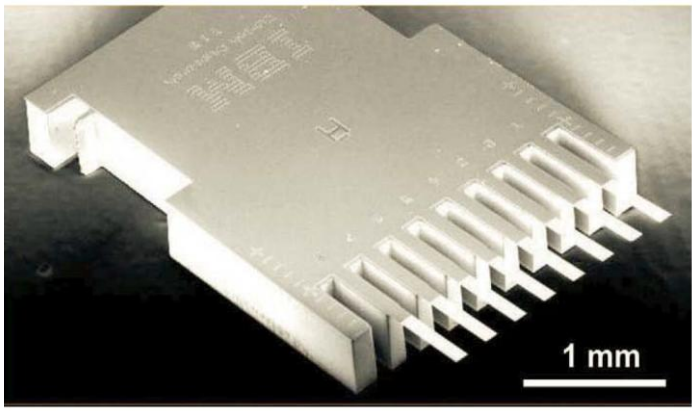

B

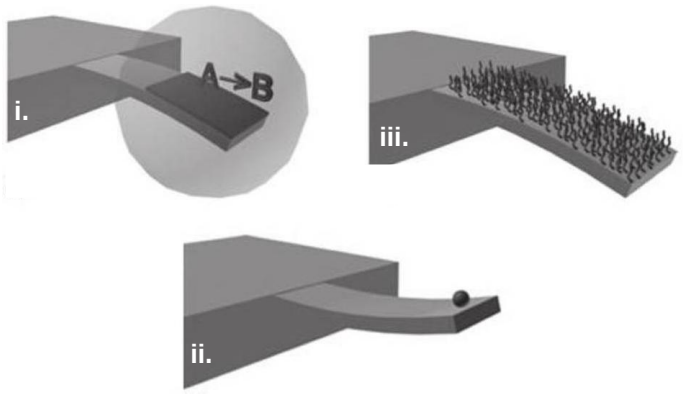

Figure 8.03: Core of a cantilever array sensor and its mode of operations. A) Scanning electron microscope image of a cantilever array fabricated by IBM Zürich, Switzerland. This silicon cantilever array consists of eight cantilevers with the dimensions of 500 µm length, 100 µm width and 0.9 µm thickness. The distance between the levers is 250 µm. Image courtesy of Dr. Hans Peter Lang and Professor Christoph Gerber. **B) The working principles of cantilever sensors.** Firstly (i) temperature, then (ii) mass change and lastly (iii) surface stress, on which this thesis will focus. Schematic adopted from Tenje et al., 2012.

8.1.3 Applications of Cantilever (Array) Sensors

Cantilever sensors and cantilever array sensors, similar to AFMs and STMs, are applicable to all the various disciplines important to nanosciece. Due to their small size, cantilevers can be integrated into microfluidic systems offering possibilities for the development of 'lab-on-chip' technologies. This is an area of immense interest for biomedicine, quality control applications as well as for proteomics and genomics research. They can be used as sensors for chemical analysis as well as biosensors for the detection of biomolecules (Raiteri, Grattarola, and Berger 2002) and cells (Antonik, D'Costa, and Hoh 1997).

The advantages of cantilever arrays are that they enable the parallel measurement of several analytes and provide direct internal references whilst measuring. Reference cantilevers are essential for subtracting all the unspecific interactions and artefacts that arise during the experimental procedure, such as temperature changes, refractive index changes and unspecific adsorption. Cantilever sensors have been successfully applied for monitoring temperature and pH-changes (Fritz 2008; Zhang et al. 2012) and for sensitive gas detection as a so-called "nose" (Lang et al. 2007; Lang et al. 1999; Yoshikawa et al. 2009; Baller et al. 2000; Lang et al. 2009). Furthermore, they can be used for characterisation of self-assembled monolayers (Backmann et al. 2010; Watari, Ndieyira, and McKendry 2010), in which they combine the two fundamental nanotechnology approaches. They integrate "top-down" miniaturisation of micro and nano-electro-mechanical systems (MEMS and NEMS) with a "bottom-up" self-assembled monolayer sensing coatings (Sushko et al. 2008; Lang, Hegner, and Gerber 2005).

The applicability of cantilever array sensor detection has also been demonstrated for various interactions such as antibody-antigen complex formation (Backmann et al. 2005; Raiteri et al. 2001), protein-ligand (Braun et al. 2009) including protein-protein (Raiteri et al. 2001) and drug-target interactions (Ndieyira et al. 2008; McKendry 2012; Ndieyira et al. 2014). Moreover they are used for the study of DNA and RNA hybridisation (McKendry et al. 2002; Shu et al. 2005; Hagan, Majumdar, and Chakraborty 2002; Zhang et al. 2006; Huber et al. 2006; Tietze, Bell, and Chandrasekhar 2003; Zhang et al. 2012;

Alvarez et al. 2004) as well as the adsorption of microorganisms. This adsorption of microorganisms includes fungi (Nugaeva et al. 2005), bacteria (Detzel, Campbell, and Mutharasan 2006; Longo et al. 2013; McKendry and Kappeler 2013; Gfeller, Nugaeva, and Hegner 2005a; Gfeller, Nugaeva, and Hegner 2005b; Ilic et al. 2000; Ramos et al. 2008), and different fungal (Nugaeva et al. 2007) and bacterial spores (Dhayal et al. 2006).

In summary, mechanical microcantilever-based sensors and arrays with multiple cantilevers in particular have the following advantages:

- **label-free detection** in real time
- high **sensitivity** i.e, attomolar (Meyer, Hug, and Bennewitz 2004), atto-joule (Raiteri, Grattarola, and Berger 2002), sub-attogramm (Ilic et al. 2004) and sub-parts-per-million (sub-ppm) (Yoshikawa et al. 2009; Mertens et al. 2004; Lang et al. 2009)
- high **specificity** with **in-situ reference** cantilevers
- **low cost** silicon microfabrication
- **miniaturised** μm and nm dimensions
- **scalable technology** i.e. for point-of-care applications
- **stress**, **mass**, **stiffness** & **viscosity** measurements in **solution**, **air, gas and vacuum**
- availability of application specific **readout** systems

8.1.4 Surface Stress and Optical Beam Deflection Readout

The principle governing the use of a rectangular or beam shaped object as a sensor for surface stress has a long history. It can be dated back more than one century when G. Gerald Stoney reported on the measurements of surface stress in 1909 (Stoney 1909). He used a several centimetre long steel ruler and measured its millimetre-ranged deformation upon the deposition of metallic thin films. The unit of surface stress is force per unit length (N/m). The surface stress difference between the upper and the lower

surface of the ruler has been in the range of kN/m. The sensitivity achieved with cantilever sensors nowadays is in the mN/m range, which is a million times smaller than with Stoney's steel ruler. Nevertheless, the "cantilever bending method", which is used to calculate surface stress as a function of cantilever deflections, is still based on Stoney's equation. The method can be described as follows (Haiss 2001): Before any adsorption takes places, the surface stresses on both sides σ^0 and σ^t of a cantilever are equal

$$\sigma^0 = \sigma^t \quad 8.1$$

thus no bending occurs (figure 8.04 A). If chemisorption takes places exclusively on one side of the cantilever, the difference ($\Delta\sigma$) in surface stress between the upper and lower surface

$$\Delta\sigma = \sigma^t - \sigma^0 \quad 8.2$$

can induce a bending of the cantilever (figure 8.04 B). Generally it is deemed that if a force acts only on one side of a cantilever and if it is large enough, then it can cause a change in the curvature of the lever. If the force is repulsive, the corresponding side of the cantilever expands, generating a compressive surface stress. On the other hand, if the force is attractive, the cantilever surface contracts and generates a tensile surface stress, which causes the beam to bend upwards (Watari et al. 2007; Ibach 1994). To simplify the analysis of the cantilever curvatures, some assumptions have to be made (Haiss 2001; Kappeler 2010; Vögtli 2011):

- The length of the cantilever has to be large in comparison to its width, which itself is large compared to the thickness.
- The adsorbate layer is of the order of several atomic layers and therefore negligible in comparison with the cantilever thickness.
- The bending of the cantilever is very small compared to its dimensions so that the coordinates can be maintained during the deformation process.
- It is assumed that the cantilever holders do not exert any forces on the cantilevers.
- The only components of stress which act in the x direction determine the bending in the x-z plane.

The bending curvatures of the cantilever in the x-z plane can be characterised as a section of a circle with radius R (figure 8.04 B), since the bending induced by the surface stress is constant along the x-axis. Therefore the induced substrate strain $\varepsilon_{xx}(z)$ can be described as:

$$\varepsilon_{xx}(z) = \frac{z - t_0}{R} \qquad 8.3$$

t_0 is the distance of the unstrained plane within the cantilever from the lower surface A^0. To achieve the bulk stress in the x direction ($\sum_{xx}(z)$) the Young's modulus (E) and the Poisson number (ν) of the cantilever material have to taken in account:

$$\sum_{xx}(z) = \frac{E}{1-\nu}\ \varepsilon_{xx}(z) \qquad 8.4$$

After integration of the bulk stress from 0 to t, substitution of equation 8.4 into 8.5, and application of the condition that in equilibrium the bending moment inside the cantilever has to be zero, Stoney's equation (Stoney 1909) can be derived as described by W. Haiss (Haiss 2001):

$$\sigma^t - \sigma^0 = \frac{Et^2}{6R(1-\nu)} \qquad 8.5$$

By considering the cantilever curvature ($k = \frac{1}{R}$), the equation (8.6) can be expressed:

$$\Delta\sigma = \frac{Et^2k}{6(1-\nu)} \qquad 8.6$$

The absolute bending was measured using a time multiplexed optical laser readout method with a position sensitive detector (PSD). For typical cantilever deflection much smaller than the length of the cantilever, the change in cantilever curvature (Δk) is linearly proportional to the change in deflection (Δz) at the free end of the cantilever. Furthermore, it is also linearly proportional to changes of the angle of laser beam reflection ($\Delta\theta$) at the effective length (L_{eff}) of the cantilever. The effective length is the distance from the hinge to the centre of the laser spot, which is in proximity to the apex of the cantilever. Therefore the change in curvature (Δk) can be defined as:

$$\Delta k = \frac{2\Delta z}{{L_{eff}}^2} = \frac{\Delta\theta}{2\,L_{eff}} \qquad 8.7$$

The change in angle of reflection ($\Delta\theta$) is linearly related to the position change of the laser spot (ΔZ) on the PSD detector located at distance (D) from the reflection point on the cantilever apex. After substituting $\Delta\theta$ into the equation 8.9, the result is:

$$\Delta Z = D \cdot \Delta\theta = \frac{4D\Delta z}{\mathrm{L_{eff}}} \qquad 8.8$$

Due to the physical distance (D) between the cantilevers and the PSD, the cantilever deflection (Δz) is amplified and can be read out by the detector.

The absolute bending signal (Δz) can be converted into surface stress ($\Delta\sigma$) between the upper and lower sides of the cantilever using the combination of Stoney's equation (8.8) and the curvature change (8.9):

$$\Delta\sigma = \frac{1}{3}\left(\frac{\mathrm{t}}{\mathrm{L_{eff}}}\right)^2 \frac{\mathrm{E}}{1-\nu}\Delta\mathrm{z} \qquad 8.9$$

t is the cantilever thickness (herein 0.9 µM), L_{eff} the effective length of the cantilever (herein 490 nm, since the size of the laser spot has been taken into account) and $\frac{E}{1-\nu} = 180\ Gpa$ is the ratio between the Youngs's modulus (E) and the Poisson ratio (ν) of Si(100) (Brantley 1973). (Kappeler 2010; Vögtli 2011)

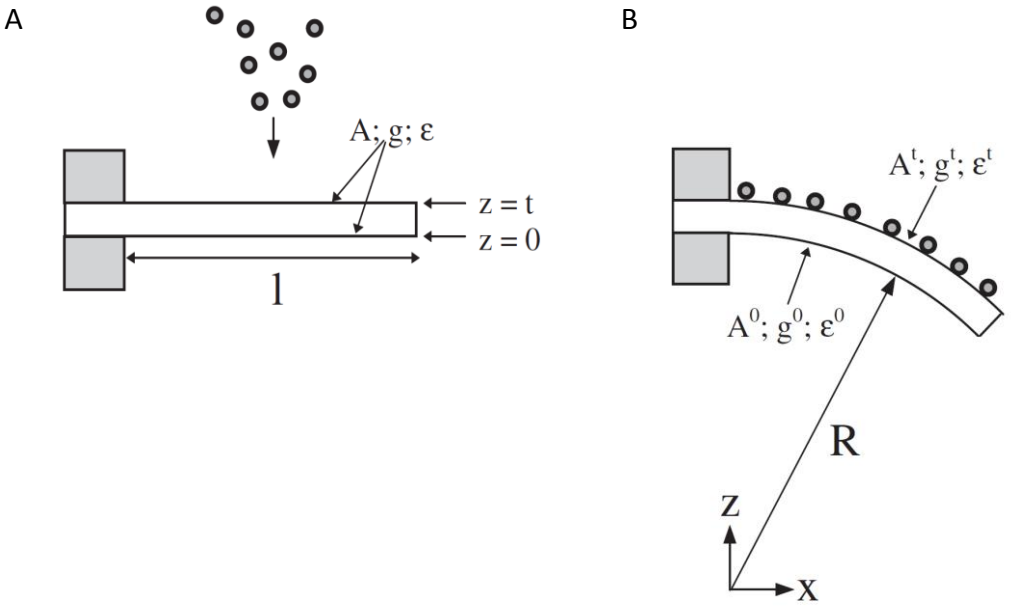

Figure 8.04: Schematic of the set-up to measure adsorbate induced surface stress with the bending cantilever method. **A**) **Schematic before any adsorption takes place.** The letter g in the schematic represents the surface stress. In the main this is named σ. $\boldsymbol{A}$ stands for the surface area and $\boldsymbol{\varepsilon}$ is the strain acting on the surface. **B) Bending of the cantilever due to chemisorptions onto the upper surface.** The superscript $\mathbf{0}$ indicates that nothing has been absorbed on this side; whereas the superscript $\boldsymbol{t}$ designates that chemisorption of any kind took place on this side. Schematic adopted from Haiss, 2001.

8.1.5 Principle of Nanomechanical Detection of Drug-Target Binding

The objective to nanomechanically detect antibiotics builds on the effect of steric competition and electrostatic repulsion upon introduction of disorders in a self assembled monolayer (SAM), which then results in an in-plane surface stress. In the case of glycopeptide antibiotics, this reflects very well the *in-vivo* drug-target mechanisms, where the antibiotic molecules bind to the precursor of the bacteria's peptidoglycan, hindering cross-linking and thus introducing defects into the bacterial cell wall.

Therefore cantilever arrays seem an optimal tool for measuring the nanomechanics of the 'antibiotics to bacterial cell wall' interactions, which are responsible for the clinical efficacy of the glycopeptide antibiotics (Watari et al. 2007; Ndieyira et al. 2008; Watari, Ndieyira, and McKendry 2010; McKendry 2012; Ndieyira et al. 2014). Herein the sensing cantilevers are functionalised with peptides that mimic cell wall precursors found in vancomycin-sensitive and vancomycin-resistant bacteria. These peptides are hereafter also designated as mucopeptides, which is the umbrella term for the polypeptides forming the crystal lattice structure of the bacterial cell wall.

To enable asymmetric adsorption of the peptides, the upper side of the cantilevers can be coated with gold. This allows semi-covalent attachment of thiol group-terminated molecules on the upper cantilever side only. Moreover, the gold layer enhances the reflectivity of cantilever surface, which is favourable for the optical readout method (Lang et al. 1998) and can be used as quality control measures. The thiolated peptides self assemble in a monolayer, whose density is concentration dependent. The formation and characteristics of these SAMs have been thoroughly investigated in Rachel McKendry's group as well as their influence on the generation of surface stress (Kappeler 2010; Vögtli 2011; Watari 2007; Barrera 2008). Therefore, in the scope of this thesis, empirical values have been used according to previously obtained findings and no secondary quality control measures and characterisations have been performed.

If binding between the bound peptides and antibiotic molecules in solution occurs, the peptides on the cantilever surface become crowded, which results in a surface stress due to electrostatic repulsion and steric hindrance. This stress leads to a downward bending of the cantilevers, which is illustrated in figure 8.05. A downward bending of a cantilever is referred to as a compressive surface stress and an upward bending as a tensile surface stress (Watari et al. 2007). The origin of the binding induced surface stress is still the subject of scientific debate and will be further discussed in the following subsection (8.1.6).

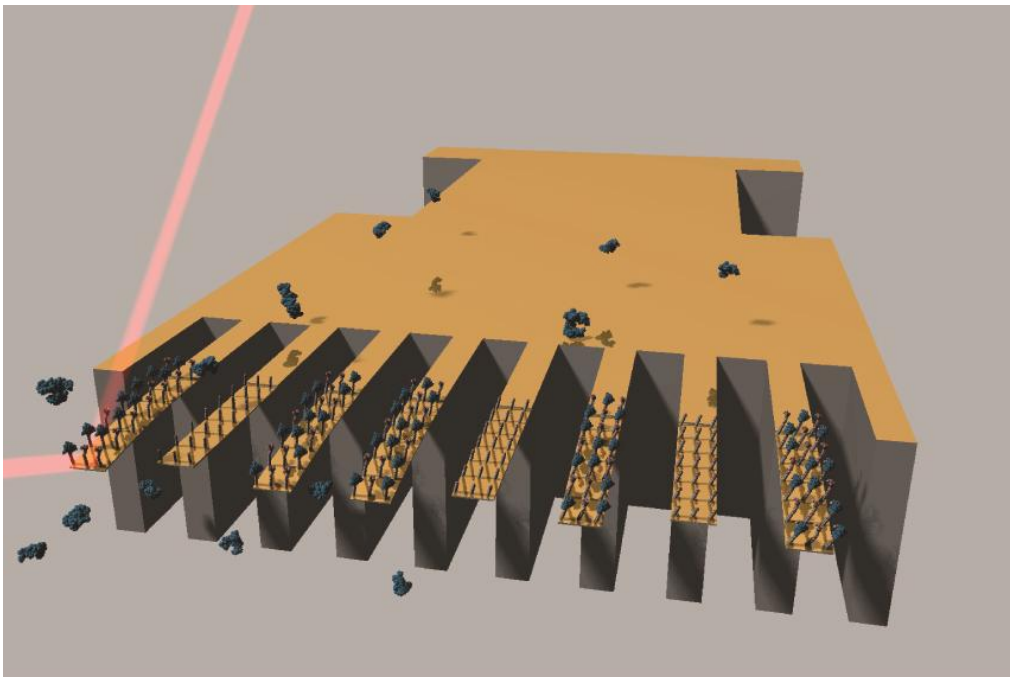

Figure 8.05: Nanomechanical detection of drug-target interactions via cantilever array sensors. This schematic shows nanomechanical sensing of drug-target interactions. The drug molecules, herein vancomycin molecules (turquoise), bind only to the cantilevers, which are coated with the specific targets or receptors and induce a downward bending momentum upon increased surface stress. No binding occurs towards the reference cantilevers, which are therefore not deflecting, and can be used to subtract for non-specific interactions and artefacts. The laser beam (red) is reflected on the apex of the cantilever and detected by position sensitive detector (PSD), which is not shown in the illustration.

8.1.6 Binding Investigation via Langmuir Adsorption Isotherm

For the characterisation of the drug-target binding interactions on the cantilever surface, the Langmuir adsorption isotherm model was used. This model has been developed by Irving Langmuir (1881 – 1957), an American chemist and physicist, in 1918. It describes the concentration dependent adsorption of gas molecules on a solid surface (Langmuir 1918). The original Langmuir's model is based on the following assumptions:

- The surface, containing the binding sites, is a flat plane.
- The substance adsorbs into an immobile state onto this plane.
- Each binding site can hold only one adsorbed molecule, and
- no interactions occur between the adsorbed molecules or between adsorbed molecules and empty sites.

This model has been adapted to describe the adsorption of antibiotic molecules in solution to immobilised mucopeptide analogues onto the cantilever surface. It has been found to model very well the experimental drug-target binding curves and therefore has been used to derive an antibiotic surface equilibrium dissociation constant K_d (McKendry et al. 2002; Vögtli 2011; Kappeler 2010).

The adapted Langmuir adsorption isotherm model can be derived as follows:
The adsorption of antibiotic molecules to mucopeptide analogues immobilised on cantilevers can be described with the following chemical equation:

$$[\mathrm{A}][\mathrm{S}] \underset{k_{\mathrm{off}}}{\overset{k_{\mathrm{on}}}{\rightleftharpoons}} [\mathrm{AS}] \qquad 8.10$$

where $[A]$ is the concentration of antibiotic molecules in solution, $[S]$ is the concentration of the free binding sites, $[AS]$ is the concentration of antibiotic molecules bound to the binding sites on the surface, and k_{on} and k_{off} are adsorption (or association) and dissociation constants respectively. The corresponding association rate r_{on} and dissociation rate r_{off} are:

$$\mathrm{r_{on}} = \mathrm{k_{on}}\,[\mathrm{A}][\mathrm{S}] \qquad 8.11$$

$$\mathrm{r_{off}} = \mathrm{k_{off}}\,[\mathrm{AS}] \quad 8.12$$

In equilibrium state, these rates are equal, $r_{on} = r_{off}$, and thus:

$$\mathrm{k_{on}}\,[\mathrm{A}][\mathrm{S}] = \mathrm{k_{off}}\,[\mathrm{A}] \quad 8.13$$

which also can be written with the equilibrium dissociation constant (K_d):

$$\frac{[\mathrm{A}][\mathrm{S}]}{[\mathrm{AS}]} = \frac{\mathrm{k_{off}}}{\mathrm{k_{on}}} = \mathrm{K_d} \quad 8.14$$

By defining the total number of available binding sites $[S_0]$ and in assumption of no depletion, $[S]$ can be written as $[S] = [S_0] - [AS]$ and this can be substituted in the equation above:

$$\mathrm{K_d} = \frac{[\mathrm{A}][\mathrm{S_0}]-[\mathrm{A}][\mathrm{AS}]}{[\mathrm{AS}]} \quad 8.15$$

and rearranged

$$[\mathrm{S_0}] = [\mathrm{AS}]\frac{\mathrm{K_d}+[\mathrm{A}]}{[\mathrm{A}]} \quad 8.16$$

By introducing the surface coverage $[S_C]$ which is the ratio of the number of bound molecules [AS] to the total number of available binding sites $[S_0]$ ($[S_C] = \frac{[AS]}{[S_0]}$) and combine it with the equation above, it yields the Langmuir adsorption isotherm:

$$[\mathrm{S_C}] = \frac{[\mathrm{A}]}{\mathrm{K_d}+[\mathrm{A}]} \quad 8.17$$

If we assume that the cantilever bending and surface stress are proportional to the surface coverage, and by introducing a factor a that describes the maximum surface stress value when all binding available site are occupied, the equation can be rewritten as:

$$\Delta\sigma_{\mathrm{eq}} = \frac{\mathrm{a}\cdot[\mathrm{antib}]}{\mathrm{K_d}+[\mathrm{antib}]} \quad 8.18$$

$\Delta\sigma_{eq}$ is the equilibrium signal of the cantilever surface stress, $[antib]$ is the antibiotic concentration in solution and $K_d$is the surface equilibrium dissociation constant on the cantilever (Ndieyira et al. 2008; McKendry et al. 2002; Kappeler 2010; Vögtli 2011). However, to be suitable for modelling the drug-target interactions the two following conditions should be fulfilled (McKendry et al. 2002):

- The drug-target binding events have to be independent, and
- they have to be unaffected by surface coverage.

In practice, this seems to be applicable only very locally and therefore a percolation model has been proposed, which will be described in the next section 8.1.7 (Ndieyira et al. 2008).

8.1.7 The Percolation Model on Cantilevers and Bacteria

The percolation model describes the surface stress in terms of chemical and geometric factors. The chemical factors describe the local drug-target binding via the Langmuir adsorption isotherm, and the geometric factors represent the large scale connectivity and mechanical consequences of the formation of a strained network. It is speculated that nanomechanical percolation plays an important role not only in the deflection of the sensor, but also in the *in-vivo* antibiotic mode of action in real bacteria, in particular for surface active antibiotics, such as glycopeptide antibiotics. Glycopeptide antibiotics are known to hinder cross-linking of peptidoglycan precursors, but the large scale mechanical consequences and the cooperative binding may put additional constraints on the bacteria. Specifically, drug-target binding events may act collectively to disrupt the bacterial cell wall leading to bacterial cell death. (Ndieyira et al. 2008)

The model was developed to fit mechanical stress response data from cantilevers with mixed monolayers of susceptible peptides to which binding occurs and reference peptides to which no binding occurs. Experiments with fixed antibiotic concentrations showed that above a certain surface coverage fraction of susceptible peptides, a steady increase in nanomechanical signal was measured. This suggests that the surface stress transduction is a “collective” phenomenon that requires connectivity of the occupied binding sites, which have to overcome a specific threshold (see figure 8.06 A). This, in turn, is dependent on a certain surface coverage and proximity of the binding targets. Based upon the assumption that the local chemical events are separable from the geometric effects responsible for the large scale connectivity, the percolation model for cantilever surface can be described as follows:

$$\Delta\sigma_{\mathrm{eq}} = \frac{\mathrm{a}\cdot[\mathrm{antib}]}{\mathrm{K_d}+[\mathrm{antib}]}\left(\frac{p-p_c}{1-p_c}\right)^{\alpha} \qquad 8.19$$

for $p > p_c$ and $zero$ if $p \leq p_c$. The first term of the equation represents the Langmuir adsorption isotherm (8.18) derived and discussed in the previous subsection (8.1.6), and the second term describes the percolation resulting in the formation of a strained network of interactions (Stauffer and Aharony 1991). p defines the surface coverage fraction, p_c the critical percolation threshold and the exponent of the power α accounts for elastic interactions between the binding sites upon antibiotic binding. For short-range interactions, including neighbouring repulsion upon steric hindrance, there will be a finite percolations threshold p_c above which a connected network will be formed that results in cantilever deflection. The experiments performed by Dr. Joseph Ndieyira led to a power α value of 1.3 and a percolation threshold p_c of 0.075, which is schematically illustrated in figure 8.06 B (Ndieyira et al. 2008). In this, p was defined as the surface coverage for the susceptible peptides with $p = 1$ for a pure layer of susceptible peptides and $p = 0$ for a pure coverage of reference peptides. This percolative triggered surface stress differs significantly from the previous studies of the Young's modulus, which is described in the previous subsection 8.1.4. (Vögtli 2011; Ndieyira et al. 2008)

As previously mentioned, the origin of the binding induced surface stress on cantilevers is still the subject of scientific debate, and several other models have been described (Wu et al. 2001; Hagan, Majumdar, and Chakraborty 2002; Zhang and Shan 2008). However, since the Langmuir adsorption isotherm paired with the percolation model has been successfully applied in Rachel McKendry's group for many years, it will also be used in the scope of this thesis.

A

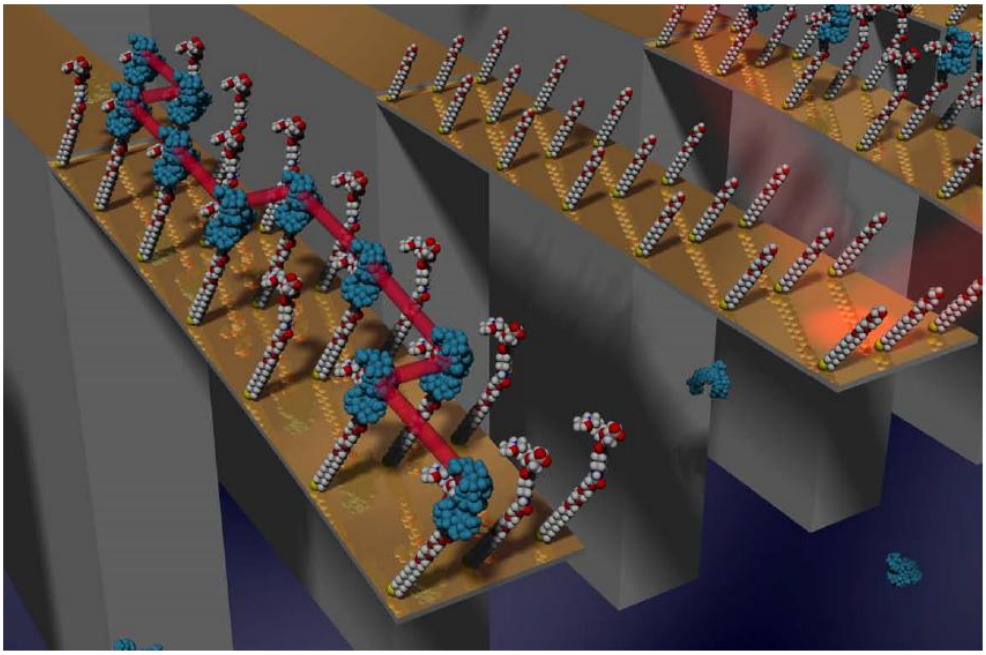

B

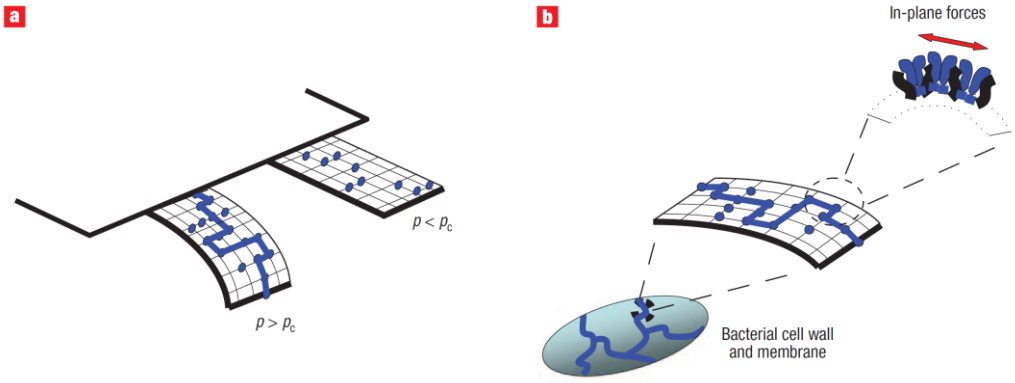

Figure 8.06: Nanomechanical drug-target percolation model on cantilever arrays and bacteria. A) Illustration of the percolation on cantilevers. The turquoise objects represent the antibiotic molecules either binding to the target peptides on the cantilever or floating freely in the solution. The red line symbolises the percolation effect and the connectivity of the drug-target binding sites. Illustration adopted from Vögtli 2011. **B) Schematic showing the percolation model on cantilever array (a) and bacteria (b).** a) If $p > p_c$ surface stress can be detected, and if $p < p_c$ the cantilevers are not deflecting, showing that there is no detectable surface stress. Schematic adopted from Ndieyira et al. 2008.

8.1.8 Objectives for Nanomechanical Detection of Vancomycin

The objective of this chapter is to explore the feasibility of nanomechanical detection of vancomycin via cantilever array sensors. The hope is that it can be conclusively shown that with a different readout system, cantilever array sensors would become the next generation of PoC sensors for therapeutic antibiotic monitoring. In order for a sensor to be developed, it must meet the general requirements that were established in the introduction in chapter 1.2 and preferably include the additional option for vancomycin listed last.

The focus of the feasibility study has been mainly laid on sensitivity and specificity whilst investigating the possibility of detecting the free and active drug fraction as opposed to the bound drug fraction. The approach of this second sensor technique builds on previous work by Rachel McKendry's group. Therefore, the first part consists of benchmarking experiments followed by requirements study for a nanomechanical therapeutic antibiotic monitoring sensor.

8.2 Materials and Methods

This subsection describes the materials and methods associated with the nanomechanical sensing technology with its core cantilever array sensors. This materials and methods subsection is divided in four subchapters, namely chemicals (8.2.1), cantilever arrays (8.2.2), the experimental set-ups (8.2.3) and measurement procedure, data processing and analysis (8.2.4). The corresponding results can be found in the successive subchapter (8.3) starting on page 271.

8.2.1 Chemicals

All chemicals were purchased from Sigma-Aldrich (Dorset, UK), unless otherwise declared. They were handled, stored and disposed of in accordance with their safety guidelines stated in the corresponding 'material safety data sheets' (MSDS).

8.2.1.1 Buffer Solution and Antibiotic

Phosphate buffer was used as buffer solution. It is a commonly used water-based salt solution abbreviated to PBS, which is the abbreviation for phosphate buffer saline. Its ion and osmotic concentration resembles human blood and it can contain different salt types as a basis for the phosphate, such as sodium phosphate or potassium phosphate. Additionally it usually contains either sodium chloride or potassium chloride. However, previous experiments performed in Rachel McKendry's group suggest that for cantilever array measurements additional sodium chloride may lead to interference, therefore mono- and di-basic sodium phosphate were dissolved in water (0.1 M) and mixed together to achieve a buffer solution of pH 7.4. The used distilled (DI) water was purified with an ELGA Purelab Ultra water purification system (ELGA, Buckinghamshire, UK).

To block the non-specific binding to the cantilevers, 0.005% bovine serum albumin (BSA) was additionally dissolved in the phosphate buffer solution. This buffer solution was filtered by syringe filters with a 0.2 µm pore size purchased from Triple Red, Long Crendon, UK and consecutively degassed by ultra-sonication for 30 minutes before every use. This phosphate buffer solution with added BSA will be denoted as phosphate buffer, buffer or PBS in this thesis. To mimic normal blood serum, additionally 600 µM BSA or human serum albumin (HSA) was also added to the phosphate buffer described above, which is further designated as pseudo-serum and specified with HSA or BSA accordingly. The amount of 600 µM BSA is well established and commonly used in the scientific community to mimic serum (Bohnert and Gan 2013; Bhattacharya, Curry, and Franks 2000). Serum albumins are the most abundant plasma proteins in mammals. They are believed to be the protein where drug molecules predominately bind to (Zeitlinger et al. 2011; Lin et al. 2013; Ndieyira et al. 2014). A more detailed discussion about the serum binding particularly of vancomycin can be found in chapter 3.3.3.

For all antibiotic solutions, the phosphate buffer or pseudo-serum as described above were used. The vancomycin solutions were prepared by dissolving various concentrations of vancomycin hydrochloride in phosphate buffer or pseudo-serum. Vancomycin hydrochloride hydrate has been described previously in chapter 6.2.1.1.

8.2.1.2 Mucopeptides Analogues, Internal Reference and SAM

The analogues of the mucopeptides used within this thesis, which are produced by vancomycin-susceptible *Enterococci* (VSE) and vancomycin-resistant *Enterococci* (VRE), as precursors for their peptidogylcan cell wall, were (figure 8.07 A):

- $HS(CH_2)_{11}(OCH_2CH_2)_3O(CH_2)(CO)NH(CH_2)_5(CO)$-L-*Lysine*-(ε-Ac)-D*Alanyl*-D*Alanine* in VSE abbreviated as **D*Ala***; and

- $HS(CH_2)_{11}(OCH_2CH_2)_3O(CH_2)(CO)NH(CH_2)_5(CO)$-L-*Lysine*-(ε-Ac)-D*Alanyl*-D*Lactate* in VRE abbreviated in this thesis as **D*Lac***.

Both peptides were synthesised by Targanta Therapeutics (Cambridge, Massachusetts, USA) (Cho, Entress, and Williams 1997). For the functionalization of the cantilevers, 1 μM ethanolic solutions of these analogues were used.

The reference cantilevers that are generally used in Rachel McKendry's group (Ndieyira et al. 2008; Watari, Ndieyira, and McKendry 2010; Vögtli 2011; Watari 2007; Kappeler 2010) are passivated with a 2 mM ethanolic solution of thiol terminating tri-ethylene glycol, $HS(CH_2)_{11}(OCH_2CH_2)_3OH$, hereafter called PEG, which is the abbreviation for polyethylene glycol (figure 8.07 A). PEG is commercially available from Sigma-Aldrich.

The peptide concentrations used for cantilever functionalization were empirically studied in previous experiments and were considered optimal for the formation of a SAM of peptidoglycan precursors for nanomechanical detection of drug-target interactions (Ndieyira et al. 2008; Vögtli 2011; Watari 2007; Kappeler 2010; Watari, Ndieyira, and McKendry 2010). For many years the adsorption of alkanethiols on gold, silver, copper, palladium, platinum and mercury surfaces has been extensively studied by various groups (Love et al. 2005; Ulman 1996; Schreiber 2000; Biebuyck, Bain, and Whitesides 1994; Bain, Biebuyck, and Whitesides 1989; Bain et al. 1989; Nuzzo and Allara 1983).

The bonding energy that anchors the adsorbed molecules of the SAM to the gold surface was first studied in 1987 by L. H. Dubois and colleagues. The strength of the heterolytic Au-S bond is believed to be in the same order as the S-S homolytic bond, which is approximately 62 kcal/mol and 259 kJ/mol respectively (Nuzzo, Zegarski, and Dubois 1987). In case of full coverage of a gold lattice with structure 111, which corresponds to the highest possible packing density, the binding of the alkanethiols is generally accepted to be based on a $(\sqrt{3}\ x\ \sqrt{3})R30^0$ structure (figure 8.07 Bi.) (Love et al. 2005). The arrangement $(\sqrt{3}\ x\ \sqrt{3})$ indicates that the distance between two sulphur atoms is $\sqrt{3}\ a$, where a is the distance between two gold atoms corresponding to a molecule-molecule spacing of 5 Å and an area per molecule of 22 Å^2. The R in the $(\sqrt{3}\ x\ \sqrt{3})R30^0$ structure represents rotation and means that the thiol axis is tilted by 30^0 to normal of the surface). Generally it is deemed that formation of SAMs is an interplay between the bond energies, the surface free energy and the lateral interactions among the adsorbed molecule to achieve the energetically most favourable confirmation (Love et al. 2005; Schreiber 2000).

Previous characterisations by Manuel Vögtli in Rachel McKendry's group suggested that from functionalization concentration of **D*Ala*** of 1 µM, the majority of the thiols must be in upright position, which allows the antibiotic molecules to bind and causes a compressive surface stress on the surface of the cantilever (Vögtli 2011). This is schematically illustrated in figure 8.07 Bii. However, it has to be highlighted that the concentrations, where the transition from 'lying down' to 'standing up' occur, are not generalizable, but rather are peptide specific. For example, preliminary data suggests that **D*Lac***, with only the alteration from amide to ester, shows transition around a functionalization concentration of 0.1 µM (Kappeler 2010).

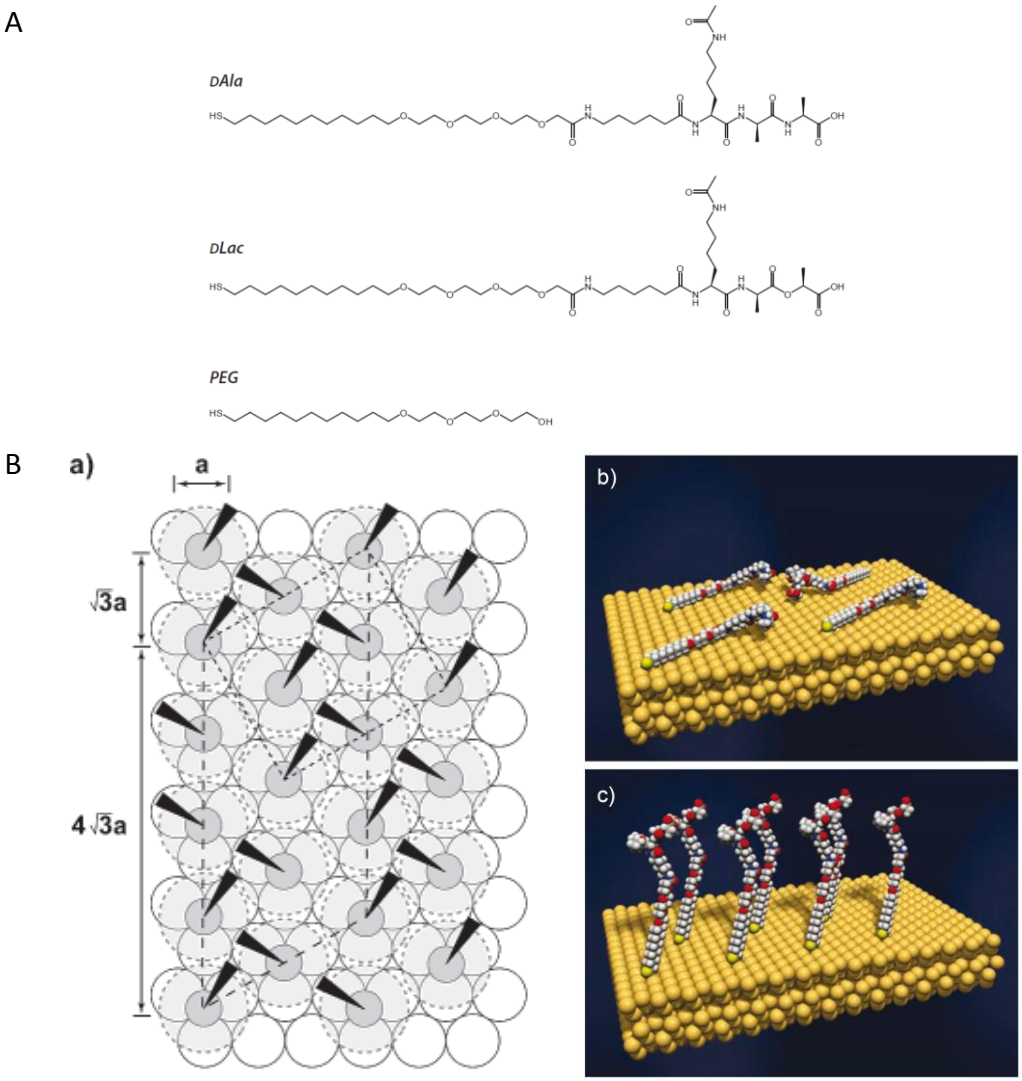

Figure 8.07: Mucopeptides analogues, internal reference and self-assembled monolayer. **A) Lewis's structures of the mucopeptide analogues (D*Ala* and D*Lac*) and the typical reference thiol (PEG) used to functionalise the cantilevers.** The only difference between the susceptible (D***Ala***) and the resistant (D***Lac***) cell wall precursors is the alteration of an amide into an ester within the binding site. PEG was typically used as internal reference. **B) Alkanethiol SAMs on a gold surface.** a) The typical $(\sqrt{3}\ x\ \sqrt{3})R30^0$ arrangement of alkanethiols on Au(111) if maximal coverage is attained. The S atoms (dark grey circles) are positioned in the 3-fold hollows of the gold lattice (white circles, a = 2.88 Å). The light grey circles surrounded with dashed lines indicate the approximate projected surface area occupied by each alkane chain; the dark triangles indicate the projection of the C-C-C plane of the alkane chain on the surface. This alternating orientation of the alkane chains defines a $c(4\ x\ 2)$ superlattice structure (marked with long dashed lines), which is an unconventional notation. The more conventional notation is rectangular $(2\sqrt{3}\ x\ 3)$ unit cell (marked with short dashed lines). The alkane chains tilt in the direction of their next nearest neighbours. Schematic adopted from Love et al., 2005. b) A 'lying down phase' is proposed for concentrations below 1 µM. It has to be highlighted that molecules are not drawn as highly packed as they would be in reality. c) A fully ordered monolayer is formed for D***Ala*** concentrations of around 50 µM. Schematics b) and c) courtesy of Dr. Manuel Vögtli.

8.2.2 Cantilever Arrays

Silicon microfabricated cantilever arrays with eight rectangular cantilevers were used. Each cantilever is 500 µm long, 100 µm wide and 0.9 µm thick. The pitch between the cantilevers is 250 µm. The arrays were fabricated via deep reactive ion etching of silicon-on-insulator (SOI) wafers at IBM Zürich Research Laboratory (Rüschlikon, Switzerland) and purchased from Concentris (Basel, Switzerland) (Kappeler 2010).

8.2.2.1 Metal Coating

The cantilever arrays were first cleaned with piranha solution (hydrogen peroxide (H_2O_2): sulphuric acid (H_2SO_4) at a ratio of 1:1) for 20 minutes. After six rinsing steps with DI water and three with ethanol, they were dried on a hotplate at 70°C. If the chip was been previously used and therefore coated with titanium and gold, it has been put in aqua regia (hydrochloride acid (HCl): nitric acid (HNO_3) at a ratio of 3:1) for 5 minutes in advance and afterwards cleaned with piranha solution.

After successful cleaning procedure, the upper surface of the array was coated with 2 nm titanium (Ti) followed by 20 nm thin gold (Au) layer at evaporation rates of 0.03 nm/s for Ti and 0.07 nm/s for Au from a base pressure of approximately 5×10^{-7} mbar. The depositions of the metal layers were performed in an electron beam (e-beam) evaporator (Edwards EB Evaporator Auto 500 – FL, Crawley, UK). This metal deposition was performed to provide a reflective surface and an interface for attaching probe molecules (Kappeler 2010).

8.2.2.2 Functionalization

Directly after the metal deposition, the cantilevers were functionalised with thiolated peptides. The functionalization was performed by immersion in a liquid-filled array of micro-capillaries. Thus, every cantilever was individually coated with a functional layer. The capillaries were arranged matching the pitch of the cantilever array. Therefore, glass capillaries with an outer diameter of 240 µm and an inner diameter of 150 µm (King Precision Glass, Claremont, CA, USA) were utilised. Figure 8.08 shows two pictures of the

cantilever functionalization 'stage'. The cantilevers were incubated within the capillaries for 20 minutes and afterwards washed three times with ethanol. During the incubation it was ensured that no crossover was occurring between any of the different functionalization liquids. As previously mentioned, this timings were also empirically studied in previous experiments and were considered optimal for the SAM formation (Ndieyira et al. 2008; Vögtli 2011; Watari 2007; Kappeler 2010; Watari, Ndieyira, and McKendry 2010). In a typical deflection experiments with vancomycin, the eight cantilevers were functionalised as follows: 2 cantilevers with PEG, 4 with **D*Ala*** and 2 with **D*Lac***. They were randomly localised over all eight cantilever, thus alignment dependencies could be excluded.

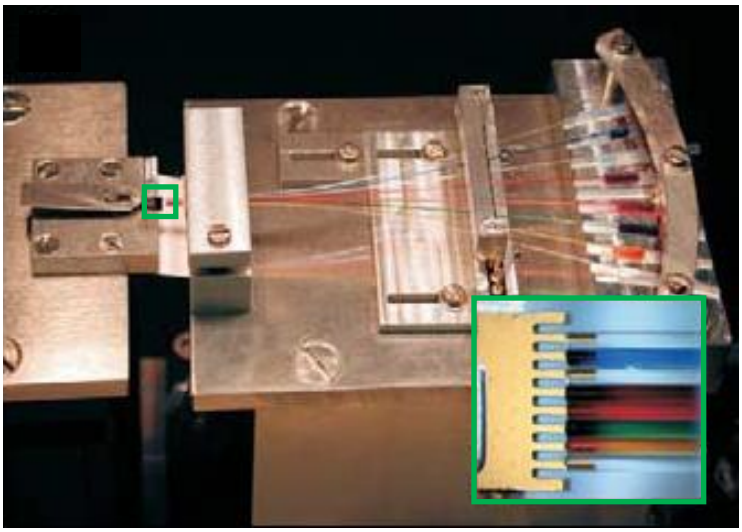

Figure 8.08: Cantilever array functionalization 'stage'. The functionalization 'stage' holds an array of eight micro-capillaries in which the cantilever array is immersed. The capillaries are filled with coloured liquids for visualisation purposes. The inset in the right corner of the picture illustrates how the each individual cantilever is inserted in an individual capillary. This functionalization 'stage' was purposely built by the University of Basel (Basel, Switzerland). Schematic adapted from H.-P. Lang, Hegner, and Gerber 2005.

8.2.3 Experimental Set-ups

Two cantilever array sensor set-ups, the Veeco Scentris and the "Basel Nose", for nanomechanical investigation of the drug-target binding interactions are in house at the London Centre for Nanotechnology (LCN). However, all binding measurements were performed with the "Basel Nose" and therefore only this experimental set-up is presented in the following subsection.

8.2.3.1 The "Basel Nose" System

The so-called "Basel Nose" is a home-built device from the University of Basel (Basel, Switzerland). A schematic of the measurement set-up is shown in figure 8.09 A and pictures in figure 8.09 B and C. The cantilever array is placed into a liquid chamber made out of polyetheretherketone (PEEK) with a volume of about 8 µl featuring an inlet and an outlet port. The liquid is pumped through the measurement chamber by a syringe pump (Kent Scientific Corporation, Torrington, CT, USA) and a ten-way-valve (Vici AG International, Schenkon, Switzerland).

As described previously, the deflection of each cantilever is read out separately via an array of eight vertical cavity surface emitting lasers (VCSELs), which are arranged at a linear pitch of 250 µm to exactly match the cantilevers pitch. They emit at a wavelength of 760 nm and are switched on and off sequentially by a time-multiplexing procedure. The laser-light is reflected off the cantilever surface and detected by a PSD. The resulting absolute deflection signals are digitised and recorded together with time information on a computer. The temperature control, the sample injection and the data acquisition hardware are all controlled by LabView software. LabView is the abbreviation for "Laboratory Virtual Instrument Engineering Workbench", which has been developed by National Instruments (Austin, Texas, USA). The whole measurement set-up, except the syringe pump, the controller and the computer, is placed in a temperature-controlled box (Lang, Hegner, and Gerber 2005; Kappeler 2010).

A

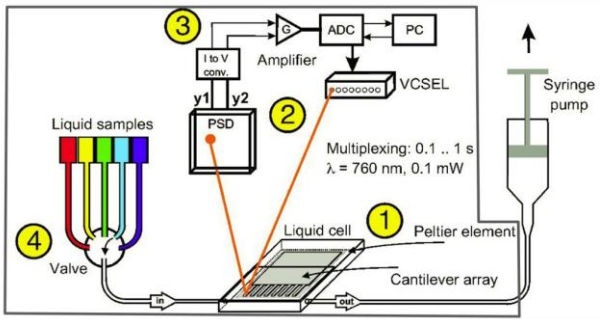

B

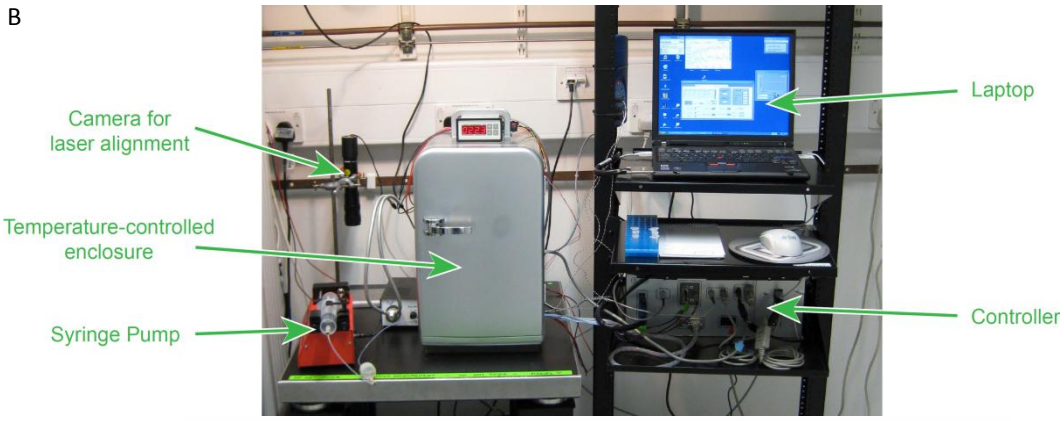

C

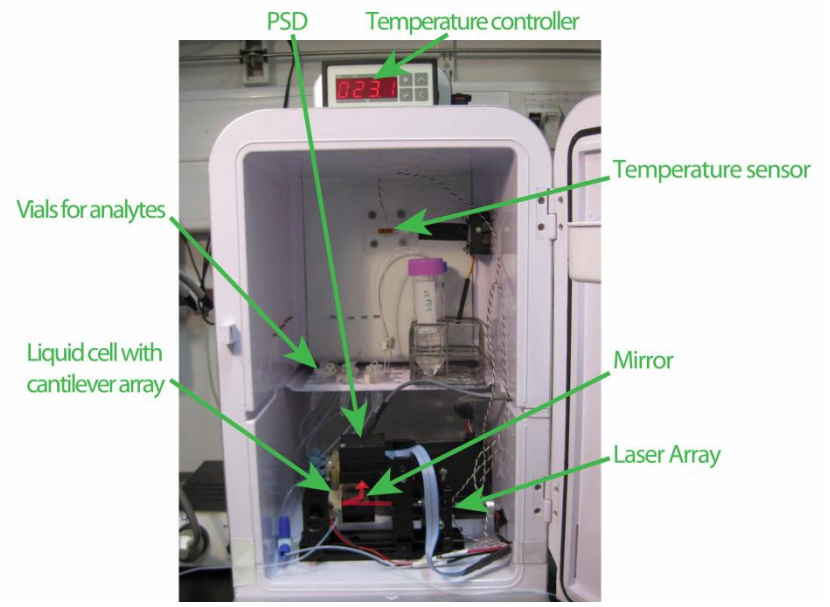

Figure 8.09: Schematic and picture of the "Basel Nose" instrumental set-up. A) Schematic drawing of the set-up. The device can be divided into four main parts: 1) the measurement cell with a mounted cantilever array shown in grey, 2) optical readout system (VCSELs and PSD), 3) data processing and acquisition and 4) valve selector connected to liquid samples. The grey box illustrates the temperature controlled chamber. The syringe pump assures a steady flow rate. Image courtesy of Dr. Hans Peter Lang. **B) Overview picture of the "Basel Nose" device. C) Zoomed picture of the device core.** The red lines indicate the laser beams emitted by the laser arrays, reflected at the apexes of the cantilevers and the mirror, and detected by the PSD. Pictures B and C courtesy of Dr. Manuel Vögtli.

8.2.4 Measurement Procedure, Data Processing and Analysis

After functionalization, the chips were inserted into the liquid chamber of the "Basel Nose" and the eight lasers were optically aligned at the apex of the cantilevers using a camera system. Then the laser positions were precisely optimised by tracking the sum of the signals and the deflections on the PSD monitored via the LabView software on the computer. To check if the alignment was successful a "heat test" was performed (figure 8.10 A). Therefore the liquid cell, which is mounted on a peltier-element, was heated by 1°C within 10 minutes and allowed to cool down for another 10 minutes. Due to the bi-metallic effect, the gold layer expands more with increased temperature than the underlying titanium and silicon, which results in a downward deflection of all cantilevers. This is due the fact that the thermal expansion coefficient for gold is larger than the ones for silicon and titanium. This property only slightly depends on the cantilever functionalization and therefore the heat test can be considered reliable as a quality control measure of the mechanics of the cantilever, the metal coating and the laser alignment. If a bending of around 200 nm was reached and the deviation of the bending signals of all eight cantilevers was less than 10%, then the heating test was considered a success and subsequent the antibiotic experiments could be started (Kappeler 2010).

The experimental procedure for the antibiotic experiments typically consisted of the following steps, which are additionally exemplified in figure 8.10 B:

I) injection of buffer solution to establish a baseline;
II) injection of antibiotic solution, which causes compressive stress in binding events that results in downward bending;
III) buffer injection, which is optional, to study the off-rate due to dissociation of the drug-target complex;
IV) injection of 10 mM hydrochloric acid (HCl) or rarely 10 mM sodium hydroxide (NaOH) to remove the bound antibiotic molecules and thereby regenerate the peptide surface; and

V) buffer injection to restore the baseline signal and to set a baseline for a new antibiotic injection

The surface regeneration (IV) via an acid injection is commonly used in surface plasmon resonance (SPR) experiments, and has been previously described, for example by Dudley Williams's group in Cambridge, UK, for different glycopeptide antibiotics binding to peptides (Cooper et al. 2000). Acidity dissociates the antibiotic molecule from the peptide by disrupting the hydrogen bond, but leaves the peptides and their semi-covalent binding to the gold intact. This regeneration step can be performed up to 10 times per chip until new functionalization is required. The regeneration and its reproducibility have been extensively studied by Rachel McKendry's group (Ndieyira et al. 2008; McKendry et al. 2002; Sushko et al. 2008; Shu et al. 2005; Houk et al. 2003; Zhang et al. 2006; Watari et al. 2007; McKendry 2012; Kappeler 2010; Vögtli 2011; Watari 2007; Barrera 2008; Watari, Ndieyira, and McKendry 2010). The same applies for the respective injection times, which were empirically studied during previous experiments. Typically, antibiotic solutions were injected for 30 minutes, and 10 minutes less for more concentrated antibiotic solutions on the grounds that saturation signals for high antibiotic concentrations were reached after a shorter time period. 10 mM HCl was injected for 40 minutes and followed by a 60 minutes buffer injection. Otherwise, if NaOH was used, 10 mM NaOH solution was injected for 5 minutes and followed by a 60 minutes buffer wash.

Furthermore, "single cycle" experiments with increasing antibiotic concentration injections were performed (figure 8.10 C). In these experiments the uncertainty, if the surface regeneration step (IV) was completely successful, did not play a role anymore and led to a gain in experimental time. Thus instead of buffer (III) or HCl/NaOH wash (IV) after each antibiotic injection (II), the next higher antibiotic concentration was injected consecutively. Experiments with vancomycin showed that the "single cycle" experiments led to results that were very comparable to the conventional experiments illustrated in figure 8.10 B. Moreover, it could be concluded that the regeneration step (IV) is sufficient to remove the bound vancomycin molecules.

The absolute deflection data of the cantilevers was recorded continuously during the experiment period via LabView software. The raw data was processed and fitted using OriginPro 8.8 software (Origin Lab Corporation, Northampton, MA, USA). The average absolute bending signals of the reference cantilevers were subtracted from the average absolute bending signals of the drug-sensitive cantilevers to get the effective differential bending upon drug-target integration. Reference cantilevers are essential to distinguish between the real drug-target binding signal and the following artefacts: temperature drift, sudden temperature changes due to solution transitions, changes in refractive index of the different solutions and non-specific binding on both or one side of the cantilever. This is especially evident in figure 8.10 B, in which both the reference and sensing cantilever are drifting. By subtracting the reference from the sensing cantilever, one can obtain the real drug-target binding with almost no drift. The estimated errors are the standard deviation of each single bending signal of D***Ala*** coated cantilevers from the average value. Due to the small number of experiments carried out, no statistical evaluation has been performed.

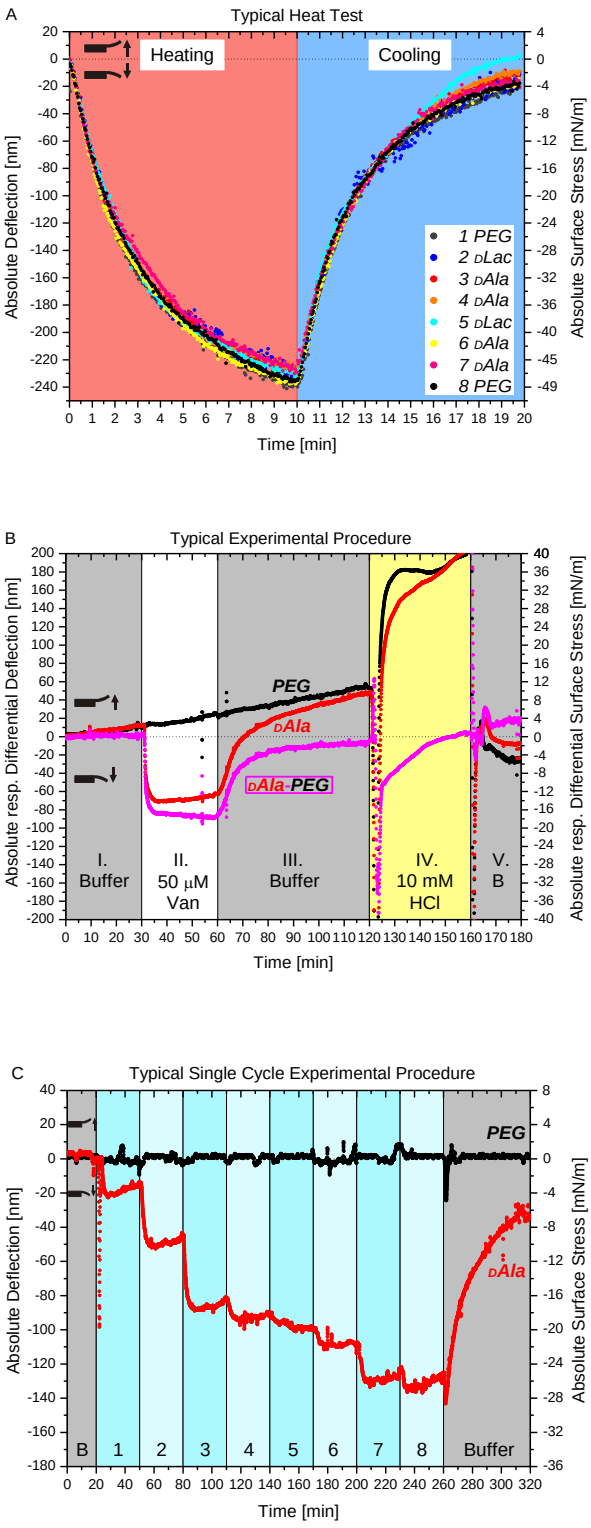

Figure 8.10: Cantilever Arrays as Nanomechanical Sensors.

A) Example of a heat test for one cantilever array. The peltier element on which the cell is mounted was heated by 1°C for 10 minutes and allowed to cool down for another 10 minutes. The heat test was considered a success, if at least 200 nm ± <10% deflections were reached. The surface stress was calculated using Stoney's equation (see page 244). Hence wherever deflection is written it can be directly converted to surface stress by dividing a factor 4.94.

B) Typical experimental procedure of an antibiotic binding experiment. After the injection of buffer or pseudo-serum (I), the antibiotic solution (II) is injected into the cell followed by an optional buffer wash (III). To remove the bound antibiotic molecules and to regenerate the sensing surface, the cell is purged in this case with a 10 mM HCl solution (IV). Afterwards buffer solution (V) is injected again to restore the baseline signal in preparation for a new antibiotic injection (I). The observed drift in both sensing (shown in red labelled **D*Ala***) and reference (shown in black labelled ***PEG***) cantilevers may be caused due to change in temperature and/or non-specific binding on both or one side of the cantilever. However, the entire drift causality is still subject of scientific debate. The purple data represent the differential deflection of the sensing minus the reference cantilever.

C) "Single cycle" experiment with increasing antibiotic concentration injections. The absolute bending signal of one PEG and one DAla coated cantilever to phosphate buffer (B) and to increasing concentrations of vancomycin, (1) 0.1 µM, (2) 1 µM, (3) 10 µM, (4) 20 µM, (5) 30 µM, (6) 50 µM, (7) 100 µM and (8) 250 µM vancomycin, are shown. Figure adopted from Kappeler, 2010.

8.3 Result and Discussions

This chapter presents and discusses the results of the second detection technique studied in this thesis. As previously mentioned, the objective of this chapter is to demonstrate that nanomechanical detection of antibiotics, particularly vancomycin, is feasible via the use of cantilever array sensors. In order for sensor development to be a viable prospect, the general requirements established in chapter 1.2 need to be fulfilled.

The approach of nanomechanical detection of vancomycin builds on previous work by Rachel McKendry's group, which showed that cantilever array sensors allow the label-free detection of antibiotic binding to bacterial cell wall precursor analogues (mucopeptides) found in vancomycin-susceptible *Enteroccoci* (VSE) (designated as **D*Ala***). Cantilevers have been proven to be highly sensitive to changes in in-plane forces caused by drug-target binding events and to have the specificity to detect the deletion of a single hydrogen bond from the antibiotic binding pocket, which is associated with the drug resistance. Additionally, they have the specificity to detect the difference in binding of different glycopeptide antibiotics (Watari et al. 2007; Ndieyira et al. 2008; Watari, Ndieyira, and McKendry 2010; McKendry 2012; Kappeler 2010; Vögtli 2011; Watari 2007; Barrera 2008; Ndieyira et al. 2014).

However, none of the previous work had investigated the use of cantilever array sensor for TDM. Therefore, the objective of this feasibility study was the investigation of cantilever array's potential to be the next generation PoC therapeutic antibiotic monitoring sensor. Hence, the focus laid on high sensitivity to clinically relevant drug concentrations, high specificity for the required drug, low interference or cross-reactivity and the possibility of detecting the free and active drug fraction rather than the total concentration, which is measured in the current gold standards. The other sensor requirements will be addressed at a later stage in the development process, especially during the adaptation of such a device for the commercial market.

Furthermore, it has to be highlighted that due to small number of experiments no statistical analysis was performed.

Accordingly, this results chapter is divided into benchmarking experiments (8.3.1), which including specificity and sensitivity experiments, and in requirement studies for nanomechanical detection of vancomycin for a therapeutic antibiotic monitoring sensor (8.3.2). The latter includes discussions regarding specificity, sensitivity studies in pseudo-serum and monitoring of total versus free drug fraction. Furthermore, it has to be highlighted that, similar to the previous results chapters, initial discussion is incorporated in this chapter, whereas the overall discussion, conclusion and outlook can be found in the next chapter (8.4).

8.3.1 Benchmarking Experiment

The results presented in this subsection are benchmarking experiments, which provide preliminary data to help guide the feasibility studies discussed in chapter 8.3.2. These initial experiments were focused on the specific detection of vancomycin in buffer (8.3.1.1) and extended to detection in the complex background of pseudo-serum according to previous work (8.3.1.2).

8.3.1.1 Benchmarking Specificity

The first set of benchmarking experiments were performed with high concentrations of vancomycin with the objective of detecting specific binding to the mucopeptides mimicking the cell wall precursor of the vancomycin-susceptible *Enteroccoci* (VSE) terminating in **D*Ala***. By functionalizing other cantilevers in the same array with mucopeptides terminating in **D*Lac***, the objective was to test the detection specificity of the deletion of one single hydrogen bond from the antibiotic binding pocket, which prevents the antibiotic from specific binding. To account for artefacts such as temperature drift and refractive index change, at least two cantilevers in each array were passivated with PEG. The description of the experimental procedure can be found in chapter 8.2.4.

Figure 8.11 A shows an example of the differential data of such a binding experiment. The three **D*Ala*** coated cantilevers in the array reached a deflection average of -169 ± 12 nm while the three **D*Lac*** cantilevers reached an average of -15 ± 9 nm, which corresponds to a surface stress of -34.2 ± 2.4 mN/m and -3.0 ± 1.8 mN/m respectively. It has to be emphasised that the errors are large due to the relative small sample sizes of only three (n = 3). Nevertheless, these deflections are in good agreement with previous results in Rachel McKendry's group. For example the 'Nature Nanotechnology' paper of 2008 reports a nanomechanical surface stress signal for 250 µM vancomycin in one array of -34.6 ± 0.9 mN/m for **D*Ala*** and -4.2 ± 0.5 mN/m for **D*Lac***, which corresponds to cantilever deflections of -171 ± 4 nm and -21 ± 2 nm respectively (Ndieyira et al. 2008).

8.3.1.2 Benchmarking Sensitivity and Detection in Pseudo-Serum

Cantilever array sensors have been proven to be highly sensitive with a detection limit of 10 nM for binding to **D*Ala*** in buffer (Ndieyira et al. 2008). In comparison, similar experiments with SPR showed detection limits of 300 nM (Rao et al. 1999) and 310 nM only (Cooper et al. 2000). For a patient attached PoC sensor, the cantilever array sensor would have to be able to detect vancomycin in the complex environment of blood. However, as previously mentioned, the current optical laser readout makes it impossible to detect the cantilever's deflection in opaque liquids. Therefore, to imitate the complex environment of blood, 600 µM HSA has been added to the PBS buffer, which is widely accepted to closely mimic the albumin concentration of normal blood serum (Bohnert and Gan 2013). It will hereafter be called pseudo-serum.

The objective is to benchmark against previous work done in the group, which has shown that cantilever array sensors are sensitive enough to detect the vancomycin in the complex environment of blood serum, which in this case has been 90% foetal calf serum mixed with 10% PBS buffer (Ndieyira et al. 2008). Moreover, these experiments should demonstrate the investigated detection technique's ability to distinguish between free and bound antibiotic fraction. Additionally, they should also show that

neither serum proteins nor the antibiotic-serum-complex bind to the ersatz bacterial cell wall precursors and, more specifically, do not result in detectable surface stress.

Therefore, experiments to compare vancomycin in buffer and pseudo-serum have been performed. Figure 8.11 B i and ii present the absolute bending signal of the same D***Ala*** coated cantilevers from upon injection of 100 µM vancomycin in buffer (i) and in pseudo-serum (ii). The vancomycin-D***Ala*** deflection signals were found to be around -175 and -100 nm, which correspond to -35 and -20 mN/m surface stress respectively. This is a decrease of about 57% in comparison to the bending signal in phosphate buffer alone. According to the literature, the proportion of vancomycin bound to serum can vary from 10 to 82% with 55% often quoted as the mean fraction bound (Sun, Maderazo, and Krusell 1993; Butterfield et al. 2011; Cantú et al. 1990; Ackerman et al. 1988; Zokufa et al. 1989; Rodvold et al. 1988; Kitzis and Goldstein 2006; Shin et al. 1992; Shin et al. 1991; Zeitlinger et al. 2011) (see chapter 3.3.3). Furthermore, this decrease supports the assumption that neither serum proteins nor antibiotic-serum-complex, herein HSA proteins and HSA-vancomycin-complex, are binding to the immobilised peptides. More specifically, they do not result in a detectable surface stress as indicated in figure 8.11 B iv.

In conclusion, these benchmarking experiments proved that cantilever arrays have the specificity and sensitivity required to detect the free antibiotic fraction in the complex environment of pseudo-serum. Therefore the benchmarking experiments were considered successful.

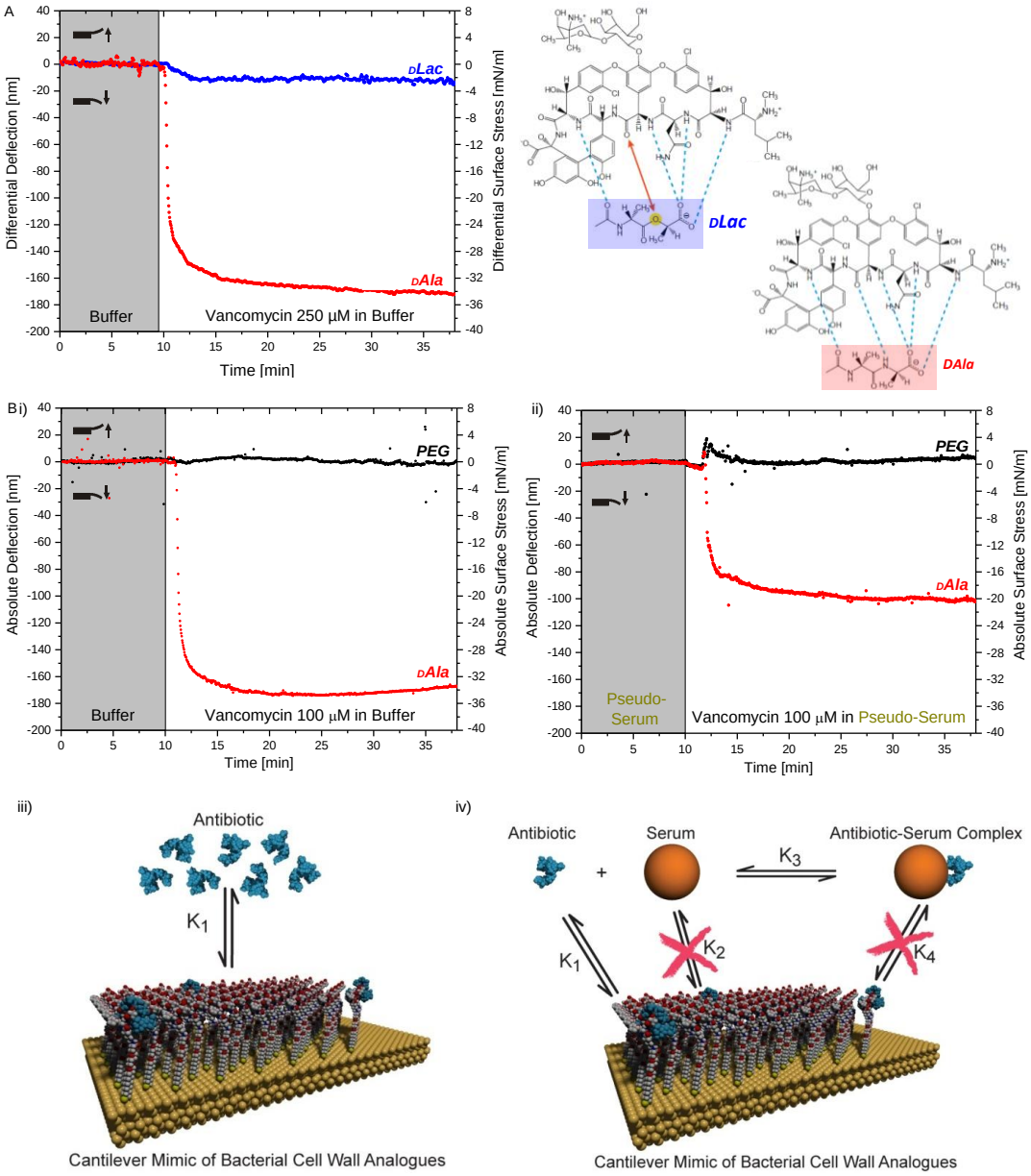

Figure 8.11: Benchmarking experiments. **A) Specificity example of vancomycin detection.** Differential deflection and surface stress of a **D*Ala*** coated cantilever (shown in red) and a **D*Lac*** coated cantilever (in blue) to buffer and 250 µM vancomycin dissolved in buffer. Almost no binding occurs to the cell wall analogues of the resistant bacteria (**D*Lac***). Resistance is caused by the deletion of one hydrogen bond from the binding pocket as illustrated in the schematics on the right. **B) Comparison of vancomycin detection in buffer and pseudo-serum.** i) Absolute deflection of a **D*Ala*** cantilever and reference cantilever upon injection of 100 µM vancomycin dissolved in buffer, and ii) in pseudo-serum. iii) Binding schematic of antibiotic molecules in buffer, and iv) in pseudo-serum. The serum proteins are competing for the antibiotic molecules, resulting in two fractions, free and bound. The decrease in deflection signal results from the reduced quantity in free drug molecules and supports the theory that neither serum proteins nor antibiotic-serum-complexes are causing any surface stress.

8.3.2 Requirements Study for Nanomechanical Antibiotic Monitoring

Continuing on from the successful benchmarking experiments, this section describes the follow up experiments. The objective was to study whether cantilever array sensors are able to fulfil important prerequisites in order to be the next generation of PoC therapeutic antibiotic monitoring sensors. These requirements include high sensitivity to clinically relevant drug concentrations, high specificity for the required drug, low interference or cross-reactivity with other drugs or blood components and the ability to detect the free drug concentration, which is associated with the antibacterial active fraction.

8.3.2.1 Specificity and Discussion of Reference

Since the binding of vancomycin to D***Ala*** terminating mucopeptides is a highly specific drug-target interaction and already the loss of one of the five hydrogen bonds results in almost no binding at low vancomycin concentrations, the specificity has not been further studied in the scope of this thesis. However, it has been contemplated whether D***Lac*** would make a better in-situ reference than PEG due to the high structural similarity to D***Ala***. Nevertheless, the following three arguments support PEG as an optimal reference coating:

i) Previous work (see chapter 8.2.1.2 on page 259) shows that despite their structural similarities, the SAMs of D***Ala*** and D***Lac*** have different formation behaviour, determined on the basis of maximal stress at different functionalisation concentrations (Vögtli 2011; Kappeler 2010).

ii) D***Lac*** has to be tailor synthesised against the commercially available PEG, which is less cost effective for a sensor, and therefore a drawback for commercialisation.

iii) PEG has been studied extensively by Rachel McKendry's group for passivation of reference cantilevers and so is better known for this kind of application. Therefore, for the subsequent experiments PEG was used as an internal reference.

8.3.2.2 Sensitivity in Vancomycin's Clinical Range

Sensitivity in the range of clinically relevant drug concentrations is one of the most crucial aspects of a TDM sensor. Cantilever array sensors have been proven to be highly sensitive with a detection limit of 10 nM for binding to D***Ala*** in buffer (Ndieyira et al. 2008). However, for a therapeutic antibiotic monitoring device, the unambiguous assignment of a single drug concentration to a single readout signal within and beyond the boundaries of the therapeutic range is also a crucial property. Thus, the function describing the function of concentration (x-axis) versus readout signal (y-axis), denoted as the cantilever deflection or surface stress, must be a strictly increasing monotonic function. As a result, the function must fulfil the following two requirements:

i) Its derivative has to be positive $f'(x) > 0$ at every single point, which is equal to a positive slope; and

ii) the slope must not be constrained to such a degree so that the noise or uncertainty of the measurement do not make the results ambiguous.

Preferably, every single point should fulfil $f'(x) \gg 0$. The simplest way to achieve this is if the dependence of drug concentration to cantilever deflection and surface stress is linear, which also means that the small changes in drug concentration have large effects on the implicit deflection and surface stress respectively.

Moreover, sensors have to be calibrated prior to the first use and additionally at regular time intervals. For vancomycin monitoring devices in clinics, this is generally done with three different known concentrations spanning the whole clinical range (Dr. Michael Kelsey, personal communication). Therefore, linear relation would render this calibration process easier and should therefore be sought after.

As previously mentioned, the used functionalization concentration for the mucopeptides has been empirically studied and optimised from previous experiments in the group. This could mean that the optimised functionalisation concentration may not be optimal for therapeutic antibiotic monitoring and should therefore be tested.

To experimentally test linearity and to investigate the sensitivity in vancomycin's clinical range, injection series of different vancomycin concentrations in buffer and pseudo-serum were performed. As an example the injection series with different antibiotic concentrations in buffer of one cantilever array is presented in figure 8.12 A. Five different arrays with three cantilevers per array (n = 15) were exposed to such injection series in buffer. Their deflection values and the corresponding errors were subsequently fitted with the Langmuir adsorption isotherm model, which is shown in black over the red deflection values in figure 8.12 B. The thermodynamic equilibrium dissociation constant K_d was found to be 1.0 ± 0.3 µM. The a value, which corresponds to the saturation signal when all available sites are occupied, was 170 ± 7 nm. These findings confirm previous work done in the group, which describes exactly the same K_d of 1.0 ± 0.3 µM and a value of 29.7 ± 1.0 mN/m that corresponds to 148 ± 5 nm (Ndieyira et al. 2008). The turquoise box in figure indicates the therapeutic window of vancomycin, which is 4 – 28 µM and corresponds to 6 – 42 µg/ml (see chapter 3.3.1).

Comparable injections series were performed with different concentrations of vancomycin in pseudo-serum. However, due to time constraints only one array with three different cantilevers has been studied (n = 3). The corresponding Langmuir adsorption isotherm model fit is shown in black over the orange data points including errors in figure 8.12 B. The thermodynamic equilibrium dissociation constant K_d was found to be 6.0 ± 2.6 µM and the a value was 110 ± 8 nm. In this context, the larger K_d value is caused by addition of another competing ligand to the system, in the form of serum proteins (see figure 8.11 B iv). These ligands and their effects upon addition are further discussed in our paper (Ndieyira et al. 2014).

As evident in figure 8.11 B, the linear region of both Langmuir fits for buffer and pseudo-serum are not within vancomycin's therapeutic range. However, the fit for pseudo-serum, which is the fit of interest based on the aims of this thesis, is still least following the previously defined requirements of a strictly increasing monotonic function and $f'(x) \gg 0$ within the clinical range. Nevertheless, these findings lead to the conclusion that the current underlying **D*Ala*** SAM is not optimal for therapeutic antibiotic monitoring and has to be further fine-tuned and optimised. This however lies beyond the scope of my thesis and is consequently discussed in the next chapter '8.4 Conclusion and Outlook'.

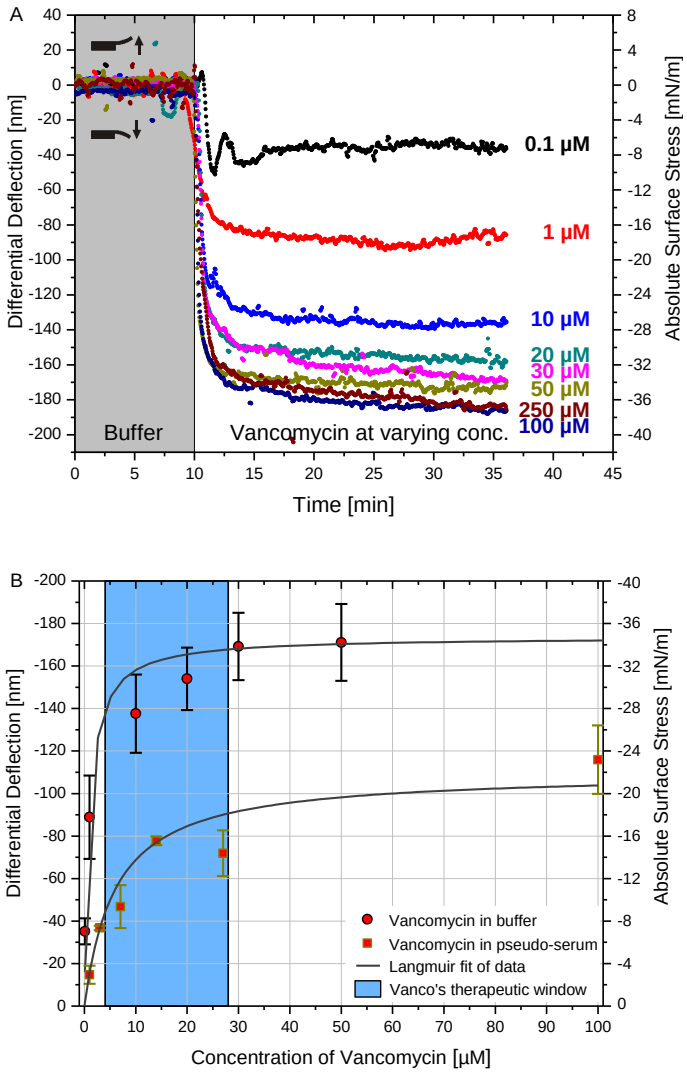

Table 8.01:

Vancomycin in buffer	n = 15
K_d [µM]	1.0 ± 0.3
a value [nm]	170 ± 7
R^2	0.96

Table 8.02:

Vancomycin in pseudo-serum	n = 3
K_d [µM]	6.0 ± 2.6
a value [nm]	110 ± 8
R^2	0.90

Figure 8.12: Requirements study for a nanomechanical therapeutic vancomycin monitoring sensor. A) Example of injections series of different concentrations performed to establish sensitivity in vancomycin's clinical range. The diagram shows differential deflections and surfaces stress of ***D*Ala** coated cantilevers to buffer and different concentrations of vancomycin dissolved in buffer. **B) Langmuir analysis of differential cantilever deflections in buffer and in pseudo-serum with reference to the clinical range.** Deflection averages of ***D*Ala** coated cantilevers upon different antibiotic concentration injections with error bars according to 5 different arrays with 3 cantilevers (n = 15) for buffer (black dot filled with red) and 3 cantilevers on 1 array (n = 3) for pseudo-serum (ochre square filled with red). The grey lines show the Langmuir adsorption isotherms fitted using Origin software, whereas the blue box indicates vancomycin's therapeutic range from 4 – 28 µM.

Table 8.01: Fitted values relating to the Langmuir fit for vancomycin injection series of different concentrations in buffer. Details about the Langmuir adsorption isotherm model can be found in chapter 8.1.6.

Table 8.02: Fitted values relating to the Langmuir fit for vancomycin injection series of different concentrations in pseudo-serum.

8.4 Conclusion and Outlook

In the introduction to this chapter (8), it has been stated that cantilever array sensors serve as the subsequent step in the miniaturisation development process required in the transition from a bench top device to a patient attached sensor. Cantilever array sensors have been placed at the transition stage because the current device in Rachel McKendry's group at the London Centre for Nanotechnology has an optical readout with an array of eight lasers. In its current state, the sensor is not directly implantable in a patient's IV line and can also not monitor the antibiotic concentration in whole blood. However, it is able to serve as a functional bench top device. Furthermore, various groups have shown that alternative readout systems are possible, which would allow miniaturisation and detection in opaque liquids, such as whole blood (see chapter 8.1.2).

Keeping that in mind, the objective of this chapter was proving the feasibility and investigating the potential for nanomechanical detection of antibiotics, particularly vancomycin, via cantilever array sensors. The focus of the feasibility study was laid on specificity, sensitivity and the possibility of detecting the free and active drug fraction. The following two bullet points present the key findings, which are also listed in table 8.03 together with other general sensor requirements that were not extensively studied in this thesis.

i) Firstly the results of the benchmarking experiments (8.3.1) were in very good agreement and confirmed previous work in Rachel McKendry's group. Therefore, they set an optimal starting point for the further requirement study for the nanomechanical antibiotic monitoring.

ii) The results of this requirement study (8.3.2) confirmed the specificity of vancomycin detection and the ability to sensitively detect vancomycin binding to the bacterial cell wall analogues in the clinically relevant concentrations (4 – 28 μM) and in the complex background of pseudo-serum. However, it was observed that the clinically relevant region is not in the linear region of the Langmuir fit, which indicates that the underlying SAM film is not optimal.

This requires further optimisation and fine-tuning. Theoretically, according to Langmuir's model, increasing the number of drug targets would reduce the surface stress and consequently the cantilever deflection upon injection of the same amount of drug molecules. Therefore the saturation stage would be reached later, which would enlarge the dynamic range wherein linearity and the constraint of the strictly increasing monotonic function would be fulfilled. However this, in turn, would lead to a loss in sensitivity. As a result there is a trade-off, which will have to be carefully investigated further.

Furthermore, it should be noted that, as discussed in chapter 8.1.7, in practice the Langmuir model is applicable only very locally. Therefore, the large scale mechanical consequence of the formation of a strained network, referred to as the percolation model, has to be taken into account as well.

This became evident in previous studies of the influence of the underlying film on surface stress by Dr. Manuel Vögtli (Vögtli 2011) for **D*Ala*** SAMs and my previous work on **D*Lac*** SAMs (Kappeler 2010). It was found that the generally used functionalization concentration of 1 µM for **D*Ala*** lies below the peak of maximal surface stress and seems to be the point where the transition from 'lying down' to 'standing up' occurs (see figures 8.13 below; and figures 8.07 Bb and 8.07 Bc in chapter 8.2.1.2). As evident in figure 8.13, the ideal functionalization concentration for a therapeutic antibiotic monitoring sensor seems to lie beyond the peak occurring at 50 µM and presumably above 100 µM.

After optimising the underlying film, the cantilever array sensors could potentially be used as a bench top device similar to the previously discussed colourimetric assay. Furthermore with a different readout system, cantilever array sensors could become the next generation of patient attached sensor for therapeutic antibiotic monitoring since they have the specificity, the sensitivity and even the ability to fulfil the additional perquisite of monitoring the free and active drug fraction.

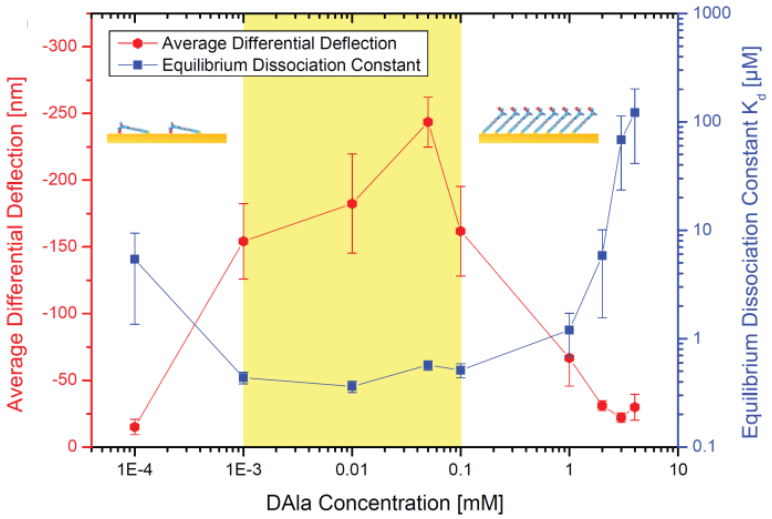

Figure 8.13: Influence of the underlying D*Ala* self-assembled monolayer (SAM) film on surface stress and equilibrium dissociation constant (K_d). This graph shows the average deflection of 250 µM vancomycin solution from five different cantilever arrays (in red) and equilibrium dissociation constant (K_d) (in blue). The yellow box indicates the area, where it is believed that the transition from the 'lying down' to the 'standing up' phase is occurring. The equilibrium dissociation constants (K_d''s) were calculated from deflection measurements with different vancomycin concentrations at the respective D***Ala*** concentrations. K_d values of 1 µM were found for D***Ala*** concentrations between 10^{-3} and 1 mM, which is consistent with previously measured binding affinities (Cooper et al. 2000; Ndieyira et al. 2008). However, K_d values for D***Ala*** concentrations above and below this range were about 1 to 2 orders of magnitude larger. Figure adopted from Vögtli 2011.

Table 8.03:

Sensing Technique	**Nanomechanical**
Investigated Core Detection Technology	**Cantilever Array Sensor**
Sensor Attributes or Requirements and their Feasibility and Fulfilment	
Specificity without cross-contamination	Highly specific, even to deletion of single hydrogen bonds from the binding pocket and for different glycopeptide antibiotics. Therefore, no further interferents tested.
Sensitivity according to therapeutic window/clinical range: **vancomycin's clinical range: 4 – 28 µM**	Detection limits: 10 nM in buffer, 7 µM in serum* (* = 90% foetal calf serum and 10% buffer) (Ndieyira et al. 2008; Ndieyira et al. 2014), and about 1 µM in pseudo-serum (see figure 8.12 B).
Simplicity and requirement for specially trained staff	Currently the readout is fairly complicated, including reaching a stable baseline, and therefore requires highly trained staff.
Required sample preparation	Measurements possible in pseudo-serum and serum (see above), but not whole blood due to the optical readout. Hence, currently requires sample preparation, but e.g. with piezoresistive readout none.
Stability in application environment/robustness	Coating stability and drift, which depend on the coating stability, may be issues. Further, sensitive temperature and vibrations.
Shelf-life/robustness	Stability depends on the coating.
Miniaturisation	Optical read-out is the limiting factor. However, other readouts are possible (e.g. piezoresistive etc.).
Intravenous flow through application/patient attached	Possible with a different readout system and if the coating is not detachable.
Safety in case of malfunction	Not tested.
Expected costs	Currently medium-high. Device approximately £ 100,000 & price per array £ 50. More efforts are needed to determine manufacturability of chips & if functionalization can be done in parallel.
Measuring speed/rapidity	After reaching a stable baseline (which may take up to 2 hours), measurement takes between 10 to 15 minutes.
Distinguish free vs. bound antibiotic fraction	Yes, only the free vancomycin fraction can be measured.

CHAPTER 9:

Conclusion and Future Work

The objective of this PhD thesis was the development of PoC sensors for therapeutic antibiotic monitoring in collaboration with industry partner, Sphere Medical Ltd. These sensors will not only allow more prudent use of our existing antibiotics whilst ensuring that their concentrations stay above the mutant prevention concentration, but also lead to better health outcomes and are associated with lower healthcare costs. Such a sensor will be a key tool for antibiotic stewardship and for personalised medicine. It will reduce the therapeutic decision time and enable the drug dose to be titrated to the desired active target concentration according to the patient's individual drug adsorption, distribution, metabolism and excretion characteristics. Furthermore, it will detect accumulation or changes in the drug clearance rate and provide early detection of faults in the drug delivery system.

In order to achieve this challenging goal, this thesis focused on the investigation of two different techniques: I) colourimetric (chapters 5, 6 and 7) and II) nanomechanical (chapter 8) detection. Along with developing each technique for TVM at the PoC, the overarching aim was to evaluate the feasibility of miniaturising the different detection techniques for patient attached real-time monitoring devices (figure 1.01). Furthermore, these technologies can be either seen as two independent approaches or one could envisage as the project matures, that a combination of detecting technologies may be an essential step towards PoC sensor for TDM.

This chapter consists of three subsections. The first subsection (9.1) gives an overall conclusion of each sensing technique and compares them in table 9.01. The second subsection presents the future work (9.2). The third and last subsection closes this thesis with closing remarks (9.3).

9.1 Conclusion

This subsection summarises the main conclusions in this thesis and is separated according to the two individual techniques: colourimetric detection (9.1.1) and nanomechanical detection (9.1.2). A detailed comparison of attributes and requirements of the different detection techniques including their feasibility and fulfilment are listed in table 9.01 starting at the end of this section.

9.1.1 Colourimetric Detection

The objective for the colourimetric detection (chapters 5, 6 and 7) was to label vancomycin with Gibbs reagent to induce a detectable colour change, which can be used to accurately quantify the antibiotic's concentration via UV/vis spectroscopy. The labelling reaction with Gibbs reagent builds on Sphere Medical's Pelorus bench top device that monitors the anaesthetic propofol.

Prior to the vancomycin detection (chapter 5), propofol assays were performed to benchmark UCL's set up to Sphere Medical's system. Furthermore experiments with the commercially available end product of the Gibbs to propofol coupling, the indophenol, were conducted to study the Beer-Lambert-Bouguer law's practical applications. Besides successful benchmarking and studying the Beer-Lambert-Bouguer law for drug monitoring applications, the experiments with indophenol showed a fast, stable, and very reliable calibration system for the therapeutic propofol monitoring device. It is now used for calibration in the commercial device.

Both, the indophenol and the propofol, experiments served further purposes, such as identification and minimisation of errors in the experimental procedure, which were highly beneficial for the following development of therapeutic vancomycin detection assay in chapter 6.

Starting from chapter 6.3.1, it was found that Gibbs reagent is binding to vancomycin and that the resulting coupling product is detectable by visible spectroscopy. The developed extraction protocol via SPE reduced the sample complexity, eliminated some possible interfering species, especially free serum proteins, and pre-concentrated the analyte of interest. Furthermore, it enables the separate elution of free and bound vancomycin fraction from the same sample. This is of particular importance for TVM device as it is generally accepted that only the free drug fraction is pharmacologically active. However, measurements of free antibiotic concentrations are not routinely performed in health care facilities as they require several preparation steps and consequently are very time consuming and expensive (Berthoin et al. 2009). Therefore, routine drug monitoring currently only measures the total antibiotic concentration, even though protein binding can vary dramatically and studies have suggested that the correlation between free and total fraction is poor (chapter 3.3.3) (Zeitlinger et al. 2011; Estes and Derendorf 2010; Butterfield et al. 2011).

However, it has to be emphasised that is not clear yet how the free and bound vancomycin gets separated in the SPE cartridge and whether the extraction alters the serum binding. Furthermore, experiments suggested that the serum protein to which the vancomycin binds either stays in the sorbent material of the SPE cartridge or is not coupling to Gibbs reagent and consequently not contributing to the absorbance. However, on the other hand, the origin of the enhanced absorbance in WHS in contrast to HSA remains unclear and can only be assumed to arise from another serum protein to which vancomycin is binding to, such as alpha-1-acid glycoprotein (Fournier, Medjoubi-N, and Porquet 2000; Zokufa et al. 1989; Dawidowicz, Kobielski, and Pieniadz 2008b; Sun, Maderazo, and Krusell 1993; Shin et al. 1991; Bohnert and Gan 2013) or interaction to other serum constituents including antibodies, antigens and hormones.

The experimental results suggested that 48 to 30 % of vancomycin is serum bound for clinical concentrations ranging from 1.2 to 29 µM vancomycin in WHS (see subsection 6.3.8). These percentages fall broadly into the literature range, which extends from 10 to 82 %, however are lower than the typical mean fraction of 55 %.

Future work should include direct comparison with current methods measuring the free and bound vancomycin fraction, such as described by K. Berthoin and colleagues (Berthoin et al. 2009), who were using extensive sample preparation followed by HPLC analysis.

The experiments with 600 µM HSA and 29 µM vancomcyin, on the other hand, can be compared to the findings of the nanomechanical vancomycin detection described in chapter 8.3.1.2. Via cantilever array sensors, it was found that approximately 57 % of the total vancomycin is bound to the HSA. In contrast via the colourimetric assay (chapter 6.3.6), it was found that 46 ± 3 % was bound to HSA. Hence, both values are in the same range. However, more experements are needed to confirm the staticstical significance of these differences and to test different batches of serum proteins and WHS.

By colourimetric quantification of free and bound concentration, facilitated via prior Gibbs labelling, the total concentration can additionally be determined by simple addition of the two aforementioned. These total concentrations were compared directly with a gold standard technique, the Roche COBAS® VANC2 assay based at the UCLH laboratory. The colourimetrically measured vancomycin concentrations were found to be in excellent agreement to the concentrations obtained by the gold standard technique. The preliminary calculation of the detection limit (1.1 µM) was found to be in good agreement with the VANC2 system (1.2 µM).

In a small study of a subset of possible interferents, it was found that neither dopamine nor paracetamol are interfering with the vancomycin detection. However, propofol is a possible interferent for the free vancomycin quantification, which can be avoided or overcome with various different approaches described in chapter 6.4. Furthermore, this propofol interference could also be an opportunity for a multi-analyte drug monitoring device, which will be further discussed in subsection (9.2.1). This small interferents study most likely did not cover all the possible interfering species and further specificity validation should be performed.

To conclude the herein developed assay has the ability to monitor free and bound vancomycin concentrations, and the total concentration in a single step, within minutes and ultimately from whole blood samples. The method does not require any prior sample preparation s and can be integrated into a bench top device for PoC. To the best of our knowledge this demonstration is the first of its kind and has never been described before. Therefore, this invention together with the labelling reaction of vancomycin with the Gibbs reagent was patented (Kappeler et al. 2013). The patent just entered PCT on the 18th February 2014.

The novel product of the coupling reaction vanGibbs was structurally characterised and the reaction mechanism studied (chapter 7). Strong evidence was found that Gibbs and vancomycin couple in a one to one stoichiometric ratio. The ^{1}H-NMR study showed that the S_EAr reaction takes place on the resorcinol ring of the 7th residue of vancomycin. However, coupling to position 6 or 2 of the 7th residue could not be distinguished. Nevertheless, two strong arguments, which are further described in subsection 7.4, supported the coupling to position 2 of the resorcinol ring. Furthermore, since the ^{1}H-NMRs were losing their resolution at higher Gibbs excesses and due to difficulties in purification and scaling-up, it is plausible that a different molecule is produced or fragmentation of the vanGibbs molecule due to a large Gibbs excess. Thus, purification and scaling-up studies as well as solving the definitive structure of the vanGibbs molecule are objectives for the future.

Future work should also involve integration of this patented assay into a bench top device in which adjustment to automation and whole blood samples have to be performed. However, since the extraction protocol could be developed based on the same SPE cartridge as used in the Pelorus device, the required adjustment time could therefore be successfully reduced. Further the vancomycin-focused bench top device also requires clinical evaluation for whole blood samples, more extensive interferents

study as well as the development of the most optimal calibration procedure. After successful completion of all these steps, commercialisation follows.[8]

9.1.2 Nanomechanical Detection

The objective for the nanomechanical sensing technique (chapter 8) was to demonstrate the feasibility of therapeutic antibiotic monitoring via cantilever array sensors. The focus was laid on specificity, sensitivity and the possibility of detecting the free and active vancomycin fraction in serum samples.

Prior to the therapeutic vancomycin detection, benchmarking experiments were performed (subsection 8.3.1). They were found to be in very good agreement and confirmed previous work in Rachel McKendry's group. Therefore subsequent requirements studies focusing on specificity and sensitivity for the nanomechanical antibiotic monitoring were conducted (subsection 8.3.2). These results confirmed the specificity of vancomycin detection and the ability to sensitively detect vancomycin binding to the bacterial cell wall analogues in the clinically relevant concentrations (4 - 28 µM) and in the complex background of pseudo-serum (600 µM of serum albumin proteins). However, the clinically relevant region was not in the linear region of the Langmuir fit, which indicated that the underlying SAM film is not optimal. This requires further optimisation and fine-tuning as described in subsection 8.4, which should be considered for future work.

[8] On a personal note, I would like to take this opportunity to propose two names for the future PoC bench top device for therapeutic vancomycin monitoring. The first suggestion is "Vanolorus" in the style of Pelorus. In the case that this is too similar to the four ships of the Royal Navy, named "HMS Valorous" (Lyon and Winfield 2004), then I would like to suggest "Vancolorus", which in a brief search through the internet did not come up with any hits.

In the overarching miniaturisation development process cantilever array sensors were placed as the transition step from a bench top device to a patient attached sensor. This is due to the fact that the current device has an optical readout system, which renders monitoring in whole blood impossible. Therefore in its current state, the sensor is not directly implantable in a patient's IV line. Nonetheless, it is able to serve as a sensor in a bench top device, which pre-treats the whole blood sample to serum similarly to Sphere Medical's Pelorus device. Various groups have shown that alternative cantilever readout systems that allow detection in opaque liquids are possible, e.g. piezoresistive readout (subsection 8.1.2). This would then allow miniaturisation and should be considered for future work.

Conclusively, it can be said, that cantilever array sensors are meeting many of the requirements for a PoC sensor for TVM, which are listed in table 9.01 at the end of this chapter. However, further optimisation according to the readout system, coating stability and usability are needed and should be considered for future work.

The herein described experiments combined with findings from a different setup and in association with an established surface-solution equilibrium theory were recently published in a *Nature Nanotechnology* paper (Ndieyira et al. 2014). The nanomechanical detection of active free antibiotic concentration combined with the equilibrium theory led to better understanding of the biophysical mode of action of antibiotics, which will improve future drug discovery and development as well as treatment and dosage.

Moreover, general interest on new cantilever array methods for studying antibiotic resistance and stewardship led to a *Nature Nanotechnology* 'News & Views' article (McKendry and Kappeler 2013) and in an enquiry for a review article on "Cantilevers for Biological Monitoring" in *Contemporary Physics.* Furthermore, an image could be designed for the 'News & Views' article, which was written for our paper by F. Huber, H. P. Lang and Ch. Gerber in *Nature Nanotechnology* (Huber, Lang, and Gerber 2014).

Table 9.01:

Sensing Technique	**Colourimetric**	**Nanomechanical**
Investigated Core Detection Technology	**Visible Spectroscopy**	**Cantilever Array Sensor**
Specificity without cross-contamination	Developed extraction protocol is fairly specific for the bound fraction eluted in stage #6 and until now propofol could be identified as possible interferents for the free fraction present in stage #4.	Highly specific, even to deletion of single hydrogen bonds from the binding pocket and for different glycopeptide antibiotics. Therefore, no further interferents tested.
Sensitivity according to therapeutic window/ clinical range: **vancomycin's clinical range: 4 – 28 µM**	Detection limit: preliminary estimation yielded in about 1.1 µM of vancomycin, which according to conversion from the VANC2 assay corresponds to about 1.7 µg/ml ("Package Insert: VANC2 COBAS® from Roche Diagnostics" 2012)	Detection limits: 10 nM in buffer, 7 µM in serum* (* = 90% foetal calf serum and 10% buffer) (Ndieyira et al. 2008; Ndieyira et al. 2014), and about 1 µM in pseudo-serum (see figure 8.11B).
Simplicity and requirement for specially trained staff	Very simple and no specially trained staff required.	Currently the readout is fairly complicated, including reaching a stable baseline, and therefore requires highly trained staff.
Required sample preparation	As a final product none. Currently, SPE followed by Gibbs labelling reaction.	Measurements possible in pseudo-serum and serum (see above), but not whole blood due to the optical readout. Hence, currently requires sample preparation, but e.g. with piezoresistive readout none.
Stability in application environment/ robustness	Assumed to last long depending on material abrasion including tubes and fittings within the device.	Coating stability and drift, which depend on the coating stability, may be issues. Further, sensitive temperature and vibrations.

Shelf-life/ robustness	Similar to above depending on material abrasion plus chemicals and buffer shelf life time.	Stability depends on the coating.
Miniaturi-sation	Light source and light paths are the limiting factor.	Optical read-out is the limiting factor. However, other readouts are possible (e.g. piezoresistive etc.).
Intravenous flow through application/ patient attached	Not possible due to addition of chemicals and miniaturisation issue.	Possible with a different readout system and if the coating is not detachable.
Safe in case of malfunction	Not tested.	Not tested.
Expected costs	Overall low. Single investment for the device and very low per test, which only requires a novel SPE cartridge (assumed < £ 1).	Currently medium-high. Device approximately £ 100,000 & price per array £ 50. More efforts are needed to determine manufacturability of chips & if functionalization can be done in parallel.
Measuring speed/ rapidness/ rapidity	Labelling reaction & vis spectroscopic measurement: about 4 minutes. Overall assay including blood injection & SPE: less than 10 minutes.	After reaching a stable baseline (which may take up to 2 hours), measurement takes between 10 to 15 minutes.
Distinguish free vs. bound antibiotic fraction	Yes, both. In WHS, elute (#6) clearly carries the bound and wash (#4) the free fraction.	Yes, only the free vancomycin fraction can be measured.

9.2 Future Work

Besides the previously indentified objectives for future work, this section presents some further visions. It is divided into three subsections. The first subsection describes a multi-analyte sensor for therapeutic drug monitoring (9.2.1), the second (9.2.2) a hand-held device and the third and last subsection (9.2.3) goes into a different direction, namely antibiotic drug discovery on the basis of vanGibbs.

9.2.1 Multi-analyte Sensor for Therapeutic Drug Monitoring

A multi-analyte sensor that monitors serum albumin, propofol and free and bound vancomycin concentrations seems to be obvious according to previous findings. One could therefore consider collecting the fractions #1 – #3 for the serum albumin monitoring, #4 for the propofol and free vancomycin, and #6 for the bound vancomycin.

Furthermore, beyond the aforementioned analytes, an extension towards other antibiotics should be considered, especially in light of the recent treatment approaches with combinatorial antibiotic therapy (Ndieyira et al. 2014; Tamma et al. 2013; Rodrigo et al. 2013; Edgeworth et al. 2014). Combination antibiotic therapies have shown better efficacy against many multi-resistant bacteria as well Gram-negative bacteraemia than single antibiotic therapy. However, most of the antibiotics are not fully tested in combination with other antibiotics and therefore such therapies have a high risk of unwanted and toxic side effects. Hence, a multi-antibiotic therapeutic monitoring sensor would be a useful device for antibiotic stewardship whilst maximising efficacy and minimising side effects and can additionally be used as early detection system for accumulations or changes in drug clearance rate.

Furthermore, as previously emphasised in the thesis, such a multi-analyte sensor may possibly also be approached by combination of the two investigated sensor techniques.

9.2.2 Hand-held Device

In light of the overarching objective of miniaturisation, further miniaturisation of the colourimetric drug monitoring assay into a handheld device may be investigated. The extraction may be further optimised so that for instance the manual injection of blood with a syringe is sufficient to elute out the compound of interest. The readout may be done either optically by eye, with a smart phone camera or with Google glasses, as it was proposed for lateral flow PoC tests (Feng et al. 2014).

Figure 9.02 illustrates a photograph of four different therapeutic vancomycin concentrations and a control preparation treated according to the herein developed colourimetric assay. It is evident that especially the two high concentrations, 14.8 and 29 µM vancomycin, are optically clearly distinguishable from each other as well as from the other concentrations including the control preparation. Hence this illustrates that with further optimisation an optical detection without the use of an UV/vis spectrometer may be possible. Besides general TDM, such a handheld device may have further specific applications in antibiotic stewardship to test whether patients are compliant in their prescribed course of medication or in food safety for rapid determination of drug levels, which improves the ease with which food standards may be controlled.

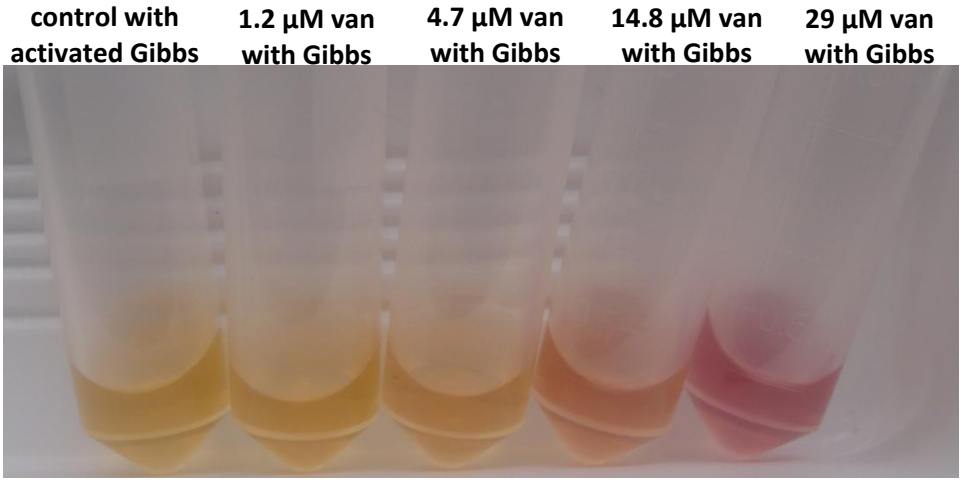

Figure 9.01: Therapeutic vancomycin concentrations for a future handheld device. Photograph of four different therapeutic vancomycin concentrations and a control preparation treated according to the herein developed colourimetric assay. Especially the two high concentrations, 14.8 and 29 µM of vancomycin, show strong colouration and are clearly distinguishable from each other as well as from the other concentrations including the control preparation. This observation illustrates that with further optimisation an optical detection without the use of an UV/vis spectrometer may be possible. The readout could for example be done either optically by eye, with a smart phone camera or with Google glasses. If the extraction could be further optimised so that for instance the manual injection of blood with a syringe is sufficient to elute out the compound of interest, then this colourimetric assay may be integrated into a handheld device. Besides general TDM, such a handheld device may have further specific applications in antibiotic stewardship to test whether patients are completing their prescribed course of medication or in food safety for rapid determination of drug levels, which improves the ease with which food standards may be controlled.

9.2.3 Antibiotic Drug Discovery on the Basis of the novel VanGibbs

As previously mentioned in chapter 7.4, the vanGibbs molecule is to the best of our knowledge a novel molecule never been described before. Furthermore, it is a derivative of vancomycin and has structural similarities to telavancin. Consequently, it is plausible that the vanGibbs molecule may be a novel antibiotic belonging to the class of semi-synthetic vancomycin derivative. Therefore, testing vanGibbs' antibacterial activity should also be considered for future work. Moreover, the Gibbs coupling reaction could be expanded to other antibiotics from the same or different families and could further serve as a scaffold for various modifications that may resulting in novel antibiotics.

9.3 Closing Remarks

My thesis is an excellent example of interdisciplinary research spanning various different scientific fields. Furthermore, due to the collaboration with industry and the objective to develop a medical assay for improvement in healthcare and antibiotic stewardship, my project led to exciting work at the interface of industry, clinic and academia and therefore included meeting clinicians, scientists and researchers from various different backgrounds. In my opinion all these aspects were perfect to me and made me enjoy my thesis very much.

Therefore, I would like to round off with reference to the quotation from Sir Gareth G. Roberts quoted at the very beginning of the thesis, and conclude, besides the measurable outcomes of my doctoral study, the development of myself was very important and will carry on in my hopefully successful academic career.

Bibliography

Ackerman, B. H., E. H. Taylor, K. M. Olsen, W. Abdel-Malak, and A. A. Pappas. 1988. "Vancomycin Serum Protein Binding Determination by Ultrafiltration." *Drug Intelligence & Clinical Pharmacy* 22 (4): 300–303.

Adam, H. K., E. J. Douglas, G. F. Plummer, and M. B. Cosgrove. 1981. "Estimation of ICI 35,868 (Diprivan R) in Blood by High-Performance Liquid Chromatography, Following Coupling with Gibbs' Reagent." *Journal of Chromatography* 223 (1): 232–37. doi:10.1016/S0378-4347(00)80092-4.

Adam, H. K., J. B. Glen, and P. A. Hoyle. 1980. "Pharmacokinetics in Laboratory Animals of ICI 35 868, A New I.V. Anaesthetic Agent." *BJA: British Journal of Anaesthesia* 52 (8): 743–46. doi:10.1093/bja/52.8.743.

Adamczyk, Maciej, Elaine M. Brate, Mary M. Perkowitz, and Sushil D. Rege. 2004. "Reagents and Methods for the Detection and Quantification of Vancomycin in Biological Fluids." *United States Patent*. Patent No.: US 6,797,479 B2.

Adamczyk, Maciej, Jonathan Grote, Jeffrey A. Moore, Sushil D. Rege, and Zhiguang Yu. 1999. "Structure-Binding Relationships for the Interaction between a Vancomycin Monoclonal Antibody Fab Fragment and a Library of Vancomycin Analogues and Tracers." *Bioconjugate Chemistry* 10 (2): 176–85. doi:10.1021/bc980135i.

Aeppli, Gabriel, and Benjamin Dueck. 2008. "Apparatus and Method for Measuring Deformation of a Cantilever Using Interferometry." *International Patent*. International Publication No.: WO2008/129272 A1.

Albrecht, T. R., S. Akamine, T. E. Carver, and C. F. Quate. 1990. "Microfabrication of Cantilever Styli for the Atomic Force Microscope." *Journal of Vacuum Science & Technology A: Vacuum, Surfaces, and Films* 8 (4): 3386. doi:10.1116/1.576520.

Alekshun, Michael N., and Stuart B. Levy. 2007. "Molecular Mechanisms of Antibacterial Multidrug Resistance." *Cell* 128 (6): 1037–50. doi:10.1016/j.cell.2007.03.004.

Allen, Norris E., and Thalia I. Nicas. 2003. "Mechanism of Action of Oritavancin and Related Glycopeptide Antibiotics." *FEMS Microbiology Reviews* 26 (5): 511–32. doi:10.1111/j.1574-6976.2003.tb00628.x.

Alvarez, M., L. G. Carrascosa, M. Moreno, A. Calle, A. Zaballos, L. M. Lechuga, C. Martínez-A, and J. Tamayo. 2004. "Nanomechanics of the Formation of DNA Self-Assembled Monolayers and Hybridization on Microcantilevers." *Langmuir: The ACS Journal of Surfaces and Colloids* 20 (22): 9663–68. doi:10.1021/la0489559.

Amírola, Jorge, Angel Rodríguez, Luis Castañer, J. P. Santos, J. Gutiérrez, and M. C. Horrillo. 2005. "Micromachined Silicon Microcantilevers for Gas Sensing Applications with Capacitive Read-Out." *Sensors and Actuators B: Chemical* 111-112 (November): 247–53. doi:10.1016/j.snb.2005.07.053.

Annapurna, V., G. Jyothi, V. Nagalakshmi, and B. B. V. Sailaja. 2010. "Spectrophotometric Methods for the Assay of Fluvoxamine Using Chromogenic Reagents." *E-Journal of Chemistry* 7 (4): 1539–45. doi:10.1155/2010/137178.

Antipas, Amy S., David G. Vander Velde, Seetharama D. S. Jois, Teruna Siahaan, and Valentino J. Stella. 2000. "Effect of Conformation on the Rate of Deamidation of Vancomycin in Aqueous Solutions." *Journal of Pharmaceutical Sciences* 89 (6): 742–50. doi:10.1002/(SICI)1520-6017(200006)89:6<742::AID-JPS5>3.0.CO;2-9.

Antoci, Valentin, Christopher S. Adams, Javad Parvizi, Helen M. Davidson, Russell J. Composto, Theresa A. Freeman, Eric Wickstrom, et al. 2008. "The Inhibition of Staphylococcus Epidermidis Biofilm Formation by Vancomycin-Modified Titanium Alloy and Implications for the Treatment of Periprosthetic Infection." *Biomaterials* 29 (35). Elsevier Ltd: 4684–90. doi:10.1016/j.biomaterials.2008.08.016.

Antonik, Matthew D., Neill P. D'Costa, and Jan H. Hoh. 1997. "A Biosensor Based an Micromechanical Interrogation of Living Cells." *IEEE Engineering in Medicine and Biology Magazine* 16 (2): 66–72. doi:10.1109/51.582178.

Arthur, Michel, Catherine Molinas, Timothy D. H. Bugg, Gerard D. Wright, Christopher T. Walsh, and Patrice Courvalin. 1992. "Evidence for in Vivo Incorporation of D-Lactate into Peptidoglycan Precursors of Vancomycin-Resistant Enterococci." *Antimicrobial Agents and Chemotherapy* 36 (4): 867–69. doi:10.1128/AAC.36.4.867.

Arthur, Michel, Peter E. Reynolds, F. Depardieu, S. Evers, S. Dutka-Malen, R. Quintiliani, and Patrice Courvalin. 1996. "Mechanisms of Glycopeptide Resistance in

Enterococci." *The Journal of Infection* 32 (1): 11–16. doi:10.1016/S0163-4453(96)80003-X.

Ashcroft, Stephen, and Chris Pereira. 2003. *Practical Statistics for the Biological Sciences*. palgrave macmillan, ISBN: 978-0-333-96044-8.

Atkins, Peter, and Julio De Paula. 2002. *Atkin's Physical Chemistry*. Oxford University Press, ISBN: 978-0-19-879285-7.

Avent, M. L., V. L. Vaska, B. A. Rogers, A. C. Cheng, S. J. van Hal, N. E. Holmes, B. P. Howden, and D. L. Paterson. 2013. "Vancomycin Therapeutics and Monitoring: A Contemporary Approach." *Internal Medicine Journal* 43 (2): 110–19. doi:10.1111/imj.12036.

Backmann, Natalija, Natascha Kappeler, Thomas Braun, François Huber, Hans Peter Lang, Christoph Gerber, and Roderick Y. H. Lim. 2010. "Sensing Surface PEGylation with Microcantilevers." *Beilstein Journal of Nanotechnology* 1 (January): 3–13. doi:10.3762/bjnano.1.2.

Backmann, Natalija, Christian Zahnd, François Huber, Alexander Bietsch, Andreas Plückthun, Hans Peter Lang, Hans-Joachim Günterodt, Martin Hegner, and Christoph Gerber. 2005. "A Label-Free Immunosensor Array Using Single-Chain Antibody Fragments." *PNAS* 102 (41): 14587–92. doi:10.1073/pnas.0504917102.

Baggi, T. R., N. V. Ram Rao, and H. R. K. Murty. 1976. "Visualisation of Opium Alkaloids on TLC Plates by Gibbs Reagent Spray." *Forensic Science* 8: 265–67. doi:10.1016/0300-9432(76)90141-2.

Bai, Chunli. 2000. *Scanning Tunneling Microscopy and Its Application*. Springer-Verlag Berlin Heidelberg New York, ISBN: 3-540-65715-0.

Bain, Colin D., Hans A. Biebuyck, and George M. Whitesides. 1989. "Comparison of Self-Assembled Monolayers on Gold: Coadsorption of Thiols and Disulfides." *Langmuir* 5: 723–27. doi:10.1021/la00087a027.

Bain, Colin D., E. Barry Troughton, Yu-Tai Tao, Joseph Evall, George M. Whitesides, and Ralph G. Nuzzo. 1989. "Formation of Monolayer Films by the Spontaneous Assembly of Organic Thiols from Solution onto Gold." *Journal of the American Chemical Society* 335 (58): 321–35. doi:10.1021/ja00183a049.

Baller, Marko K., Hans Peter Lang, Jürgen Fritz, Christoph Gerber, James K. Gimzewski, Ute Drechsler, H. Rothuizen, et al. 2000. "A Cantilever Array-Based Artificial Nose." *Ultramicroscopy* 82 (1-4): 1–9. doi:10.1016/S0304-3991(99)00123-0.

Barnes, Marion D., and Victor K. LaMer. 1942. "Kinetics and Equilibria of the Carbinol Formation of Phenolphthalein." *Journal of the American Chemical Society* 1844 (6). doi:10.1021/ja01262a026.

Barrera, Alejandra Donoso. 2008. "Nanomechanical Sensor Arrays for Antibiotic Drug Analysis." *PhD Thesis*. University College London (UCL).

Basford, R. E., and F. M. Huennekens. 1955. "Studies on Thiols. I. Oxidation of Thiol Groups by 2, 6-Dichlorophenol Indophenol1." *Journal of the American Chemical Society* 2609 (13): 3873–77. doi:10.1021/ja01619a058.

Bashir, Sajid, and Jingbo L. Liu. 2009. "Construction and Characterization of Phenol-Based Sensor Derived from Colloidal Chemistry." *Sensors and Actuators B: Chemical* 139 (2): 584–91. doi:10.1016/j.snb.2009.02.072.

Beer, August. 1852. "Bestimmung Der Absorption Des Rothen Lichts in Farbigen Flüssigkeiten." *Annalen Der Physik Und Chemie by J. C. Poggendorff* 162 (5): 78–88. doi:10.1002/andp.18521620505.

Begg, Evan J., Murray L. Barclay, and Carl J. M. Kirkpatrick. 1999. "The Therapeutic Monitoring of Antimicrobial Agents." *British Journal of Clinical Pharmacology* 47 (1): 23–30. doi:10.1046/j.1365-2125.1999.00850.x.

Benito-Garagorry, David. 2013. "Process for the Synthesis of Telavancin and Its Pharmaceutically Acceptable Salts as Well as N-Protected Derivatives Thereof." *International Patent*. International Publication No.: WO 2013/034675 A1: Sandoz AG, Basel, Switzerland.

Berthoin, Karine, Els Ampe, Paul M. Tulkens, and Stephane Carryn. 2009. "Correlation between Free and Total Vancomycin Serum Concentrations in Patients Treated for Gram-Positive Infections." *International Journal of Antimicrobial Agents* 34 (6): 555–60. doi:10.1016/j.ijantimicag.2009.08.005.

Bhattacharya, Ananyo A., Stephen Curry, and Nicholas P. Franks. 2000. "Binding of the General Anesthetics Propofol and Halothane to Human Serum Albumin. High

Resolution Crystal Structures." *The Journal of Biological Chemistry* 275 (49): 38731–38. doi:10.1074/jbc.M005460200.

Biebuyck, Hans A., Colin D. Bain, and George M. Whitesides. 1994. "Comparison of Organic Monolayers on Polycrystalline Gold Spontaneously Assembled from Solutions Containing Dialkyl Disulfides or Alkanethiols." *Langmuir* 10 (33): 1825–31. doi:10.1021/la00018a034.

Binnig, Gerd, Calvin F. Quate, and Christoph Gerber. 1986. "Atomic Force Microscope." *Physical Review Letters* 56 (9): 930–33. doi:10.1103/PhysRevLett.56.930.

Binnig, Gerd, and Heinrich Rohrer. 1983. "Scanning Tunneling Microscopy." *Surface Science* 126 (1-3): 236–44. doi:10.1016/0039-6028(83)90716-1.

Binnig, Gerd, Heinrich Rohrer, Christoph Gerber, and Edmund Weibel. 1982. "Surface Studies by Scanning Tunneling Microscopy." *Physical Review Letters* 49 (1): 57–61. doi:10.1103/PhysRevLett.49.57.

Blanc, N., J. Brugger, N. F. de Rooij, and U. Dürig. 1996. "Scanning Force Microscopy in the Dynamic Mode Using Microfabricated Capacitive Sensors." *Journal of Vacuum Science & Technology B: Microelectronics and Nanometer Structures* 14 (2): 901–5. doi:10.1116/1.589171.

Blázquez, Jesús. 2003. "Hypermutation as a Factor Contributing to the Acquisition of Antimicrobial Resistance." *Clinical Infectious Diseases: An Official Publication of the Infectious Diseases Society of America* 37 (9): 1201–9. doi:10.1086/378810.

Bohnert, Tonika, and Liang-shang Gan. 2013. "Plasma Protein Binding: From Discovery to Development." *Journal of Pharmaceutical Sciences* 102 (9): 2953–94. doi:10.1002/jps.23614.

Born, M. 1948. "Max Karl Ernst Ludwig Planck. 1858-1947." *Obituary Notices of Fellows of the Royal Society* 6 (17): 161–88. doi:10.1098/rsbm.1948.0024.

Bouguer, Pierre. 1729. *Essai D'optique Sur La Gradation de La Lumière*. Claude Jombert.

Boyd, Jeff A., and Thomas E. Eling. 1984. "Evidence for a One-Electron Mechanism of 2-Aminofluorene Oxidation by Prostaglandin H Synthase and Horseradish Peroxidase." *The Journal of Biological Chemistry* 259 (22): 13885–96.

Brantley, W. A. 1973. “Calculated Elastic Constants for Stress Problems Associated with Semiconductor Devices.” *Journal of Applied Physics* 44 (1): 534–35. doi:10.1063/1.1661935.

Braun, Thomas, Murali Krishna Ghatkesar, Natalija Backmann, Wilfried Grange, Pascale Boulanger, Lucienne Letellier, Hans Peter Lang, Alex Bietsch, Christoph Gerber, and Martin Hegner. 2009. “Quantitative Time-Resolved Measurement of Membrane Protein-Ligand Interactions Using Microcantilever Array Sensors.” *Nature Nanotechnology* 4 (3): 179–85. doi:10.1038/nnano.2008.398.

Burdon-Sanderson, John Scott. 1871. “The ORIGIN and DISTRIBUTION of MICROZYMES (BACTERIA) in WATER, and the CIRCUMSTANCES Which Determine Their EXISTENCE in the TISSUES and LIQUIDS of the LIVING BODY. By Dr. BUKDON-SANDERSON, F.R.S.” *Quarterly Journal of Microscopical Science* XI (s2-11): 323–52.

Butler, Mark S., and Matthew A. Cooper. 2011. “Antibiotics in the Clinical Pipeline in 2011.” *The Journal of Antibiotics* 64 (6). Nature Publishing Group: 413–25. doi:10.1038/ja.2011.44.

Butterfield, Jill M., Nimish Patel, Manjunath P. Pai, Thomas G. Rosano, George L. Drusano, and Thomas P. Lodise. 2011. “Refining Vancomycin Protein Binding Estimates: Identification of Clinical Factors That Influence Protein Binding.” *Antimicrobial Agents and Chemotherapy* 55 (9): 4277–82. doi:10.1128/AAC.01674-10.

Calderón, Cassandra B., and Beulah Perdue Sabundayo. 2007. “Antimicrobial Classifications: Drugs for Bugs.” In *Antimicrobial Susceptibility Testing Protocols by Richard Schwalbe, Lynn Steele-Moore, Avery C. Goodwin*. CRC Press, Taylor & Francis Group, ISBN: 978-0-8247-4100-6.

Calfee, David P. 2012. “Methicillin-Resistant Staphylococcus Aureus and Vancomycin-Resistant Enterococci, and Other Gram-Positives in Healthcare.” *Current Opinion in Infectious Diseases* 25 (4): 385–94. doi:10.1097/QCO.0b013e3283553441.

Cantú, Thomas G., James D. Dick, David E. Elliott, Richard L. Humphrey, and David M. Kornhauser. 1990. “Protein Binding of Vancomycin in a Patient with Immunoglobulin A Myeloma.” *Antimicrobial Agents and Chemotherapy* 34 (7): 1459–61. doi:10.1128/AAC.34.7.1459.

Cantú, Thomas G., Nancy A. Yamanaka-Yuen, and Paul S. Lietman. 1994. "Serum Vancomycin Concentrations: Reappraisal of Their Clinical Value." *Clinical Infectious Diseases: An Official Publication of the Infectious Diseases Society of America* 18 (4): 533–43. doi:10.1093/clinids/18.4.533.

Carroll, Lewis. 1871. *Through the Looking-Glass*. Macmillan.

Casati, Andrea, Guido Fanelli, Elisabetta Casaletti, Eleonora Colnaghi, Valeria Cedrati, and Giorgio Torri. 1999. "Clinical Assessment of Target-Controlled Infusion of Propofol during Monitored Anesthesia Care." *Canadian Journal of Anaesthesia = Journal Canadien D'anesthésie* 46 (3): 235–39. doi:10.1007/BF03012602.

Casey, A. L., D. Adams, T. J. Karpanen, P. A. Lambert, B. D. Cookson, P. Nightingale, L. Miruszenko, R. Shillam, P. Christian, and T. S. J. Elliott. 2010. "Role of Copper in Reducing Hospital Environment Contamination." *The Journal of Hospital Infection* 74 (1). Elsevier Ltd: 72–77. doi:10.1016/j.jhin.2009.08.018.

Chan, Margaret. 2013. "Antimicrobial Resistance in the European Union and the World @ 'Combating Antimicrobial Resistance: Time for Action' Conference on 14/03/13 in Copenhagen, Denmark." *Last Accessed: 07/08/2013*. http://www.who.int/dg/speeches/2012/amr_20120314/en/#.

Chandrasekhar, S. 1943. "Stochastic Problems in Physics and Astronomy." *Reviews of Modern Physics* 15 (1): 1–89. doi:10.1103/RevModPhys.15.1.

Chen, Luke F. 2013. "The Changing Epidemiology of Methicillin-Resistant Staphylococcus Aureus: 50 Years of a Superbug." *American Journal of Infection Control* 41 (5). Association for Professionals in Infection Control and Epidemiology, Inc. 448–51. doi:10.1016/j.ajic.2012.06.013.

Cheng, Anthony K., and Julie S. Kim. 2004. "Homogeneous Assay of Vancomycin Using a Stable Particle-Vancomycin Conjugate, a Novel Rate Enhancer, and a Novel Dose Response Modulator." *United States Patent*. Patent No.: US 6,800,608 B2.

Cho, Younghoon R., Richard M. H. Entress, and Dudley H. Williams. 1997. "Synthesis of Cell-Wall Analogues of Vancomycin-Resistant Enterococci Using Solid Phase Peptide Synthesis." *Tetrahedron Letters* 38 (29): 5229–32. doi:10.1016/S0040-4039(97)01110-6.

Cirz, Ryan T., Jodie K. Chin, David R. Andes, Valérie de Crécy-Lagard, William A. Craig, and Floyd E. Romesberg. 2005. "Inhibition of Mutation and Combating the Evolution of Antibiotic Resistance." *PLoS Biology* 3 (6): e176. doi:10.1371/journal.pbio.0030176.

Coia, J.E., G.J. Duckworth, D.I. Edwards, M. Farrington, C. Fry, H. Humphreys, C. Mallaghan, and D.R. Tucker. 2006a. "Guidelines for the Control and Prevention of Meticillin-Resistant Staphylococcus Aureus (MRSA) in Healthcare Facilities." *The Journal of Hospital Infection* 63 (1): S1–44. doi:10.1016/j.jhin.2006.01.001.

———. 2006b. "Erratum to 'Guidelines for the Control and Prevention of Meticillin-Resistant Staphylococcus Aureus (MRSA) in Healthcare Facilities [Journal of Hospital Infection 2006;63:S1–S44].'" *Journal of Hospital Infection* 64 (1): 97–98. doi:10.1016/j.jhin.2006.06.001.

Compton, Richard Guy, and Craig Edward Banks. 2006. "Detection of Phenols." *United States Patent*. Publication No.: US 2009/0294298 A1.

Coop, Andrew, Konstantinos Grivas, Stephen Husbands, and John W. Lewis. 1995. "Methylation of the Enolates of Thevinone and Some Analogues." *Tetrahedron* 51 (35): 9681–98. doi:10.1016/0040-4020(95)00553-K.

Cooper, Matthew A., Maria T. Fiorini, Chris Abell, and Dudley H. Williams. 2000. "Binding of Vancomycin Group Antibiotics to D-Alanine and D-Lactate Presenting Self-Assembled Monolayers." *Bioorganic & Medicinal Chemistry* 8 (11): 2609–16. doi:10.1016/S0968-0896(00)00184-X.

Cooper, Matthew A., and David Shlaes. 2011. "Fix the Antibiotics Pipeline." *Nature* 472 (7341): 32. doi:10.1038/472032a.

Cooper, Matthew A., and Dudley H. Williams. 1999. "Binding of Glycopeptide Antibiotics to a Model of a Vancomycin-Resistant Bacterium." *Chemistry & Biology* 6 (12): 891–99. doi:10.1016/S1074-5521(00)80008-3.

Corey, G. Ralph, Martin E. Stryjewski, Wim Weyenberg, Uma Yasothan, and Peter Kirkpatrick. 2009. "Telavancin." *Nature Reviews Drug Discovery* 8 (December): 929–30. doi:10.1038/nrd3051.

Craig, William A. 2003. "Basic Pharmacodynamics of Antibacterials with Clinical Applications to the Use of B-Lactams, Glycopeptides, and Linezolid." *Infectious*

Disease Clinics of North America 17 (3): 479–501. doi:10.1016/S0891-5520(03)00065-5.

Curry, Stephen. 2011. "X-RAY CRYSTALLOGRAPHY OF ALBUMIN." *Functional Impacts and Pharmaceutical Applications* 2011: 1–20.

Cussonneau, Xavier, Els De Smet, Kristof Lantsoght, Jean-Paul Salvi, Magali Bolon-Larger, and Roselyne Boulieu. 2007. "A Rapid and Simple HPLC Method for the Analysis of Propofol in Biological Fluids." *Journal of Pharmaceutical and Biomedical Analysis* 44 (3): 680–82. doi:10.1016/j.jpba.2006.10.020.

D'Orazio, Paul. 2003. "Biosensors in Clinical Chemistry." *Clinica Chimica Acta* 334 (1-2): 41–69. doi:10.1016/S0009-8981(03)00241-9.

Daabees, H. G., M. S. Mahrous, A. S. Issa, Y. A. Beltagy, and H. Fouad. 1998. "The Use of 2,6-Dichloroquinone Chlorimide for the Colorimetric Determination of Some Antibiotics." *Bull. Fac. Pharm. Cairo Univ.* 36 (1): 67–75.

Dacre, Jack C. 1971. "Nonspecificity of the Gibbs Reaction." *Analytical Chemistry* 43 (4). ACS Publications: 589–91. doi:10.1021/ac60299a015.

Dandliker, W. B., R. J. Kelly, J Dandliker, J. Farquhar, and J. Levin. 1973. "Fluorescence Polarization Immunoassay. Theory and Experimental Method." *Immunochemistry* 10 (4): 219–27. doi:10.1016/0019-2791(73)90198-5.

Dantas, Gautam, Morten O. A. Sommer, Rantimi D. Oluwasegun, and George M. Church. 2008. "Bacteria Subsisting on Antibiotics." *Science* 320 (5872): 100–103. doi:10.1126/science.1155157.

Darwin, Charles. 1859. *On the Origin of Species by Means of Natural Selection, or the Preservation of Favoured Races in the Struggle for Life.* 1st ed. London: John Murray.

Davies, Julian, and Dorothy Davies. 2010. "Origins and Evolution of Antibiotic Resistance." *Microbiology and Molecular Biology Reviews : MMBR* 74 (3): 417–33. doi:10.1128/MMBR.00016-10.

Davies, Sally C. 2011. "Annual Report of the Chief Medical Officer - Volume Two, 2011: Infections and the Rise of Antimicrobial Resistance". London, 1–153.

Davy, Humphry. 1800. “Researchers, Chemical And Philosophical; Chiefly Concerning Nitrous Oxide, Or Dephlogisticated Nitrous Air, And Its Respiration.” In *The Collect Works of Sir Humphry Davy*. By Biggs and Cottle, Bristol.

Davy, John. 1839. *The Collected Works of Sir Humphry Davy*. London: Smith, Elder And Company, Cornhill.

Dawidowicz, Andrzej L., and E. Fornal. 2000. “The Advantages of Cell Lysis before Blood Sample Preparation by Extraction for HPLC Propofol Analysis.” *Biomedical Chromatography: BMC* 14 (7): 493–97. doi:10.1002/1099-0801(200011)14:7<493::AID-BMC999>3.0.CO;2-T.

Dawidowicz, Andrzej L., and Rafal Kalitynski. 2005. “Effects of Intraoperative Fluid Infusions, Sample Storage Time, and Sample Handling on Unbound Propofol Assay in Human Blood Plasma.” *Journal of Pharmaceutical and Biomedical Analysis* 37 (5): 1167–71. doi:10.1016/j.jpba.2004.09.022.

Dawidowicz, Andrzej L., Rafal Kalitynski, Mateusz Kobielski, and Jaroslaw Pieniadz. 2006. “Influence of Propofol Concentration in Human Plasma on Free Fraction of the Drug.” *Chemico-Biological Interactions* 159 (2): 149–55. doi:10.1016/j.cbi.2005.10.108.

Dawidowicz, Andrzej L., Mateusz Kobielski, and Jaroslaw Pieniadz. 2008a. “Anomalous Relationship between Free Drug Fraction and Its Total Concentration in Drug-Protein Systems I. Investigation of Propofol Binding in Model HSA Solution.” *European Journal of Pharmaceutical Sciences : Official Journal of the European Federation for Pharmaceutical Sciences* 34 (1): 30–36. doi:10.1016/j.ejps.2008.02.004.

———. 2008b. “Anomalous Relationship between Free Drug Fraction and Its Total Concentration in Drug-Protein Systems II. Binding of Different Ligands to Plasma Proteins.” *European Journal of Pharmaceutical Sciences : Official Journal of the European Federation for Pharmaceutical Sciences* 35 (1-2): 136–41. doi:10.1016/j.ejps.2008.06.011.

De Boer, Eric J. M., Harry Van Der Heijden, Wilhelmina C. Verhoef-Van Wijk, and Arie Van Zon. 2007. “Ligands and Catalyst Systems Thereof for Ethylene Oligomerisation to Linear Alpha Olefins.” *United States Patent*. Patent No.: US 7,304,159 B2.

DeLong, Edward F., and Norman R. Pace. 2001. “Environmental Diversity of Bacteria and Archaea.” *Systematic Biology* 50 (4): 470–78. doi:10.1080/10635150118513.

Demain, Arnold L., and Sergio Sanchez. 2009. “Microbial Drug Discovery: 80 Years of Progress.” *The Journal of Antibiotics* 62 (1): 5–16. doi:10.1038/ja.2008.16.

Department of Health. 2013. “UK Five Year Antimicrobial Resistance Strategy 2013 to 2018.” *Crown. Last Accessed: 22/02/2014*. https://www.gov.uk/government/uploads/system/uploads/attachment_data/file/244058/20130902_UK_5_year_AMR_strategy.pdf.

Detzel, Andrew J., Gossett A. Campbell, and Raj Mutharasan. 2006. “Rapid Assessment of Escherichia Coli by Growth Rate on Piezoelectric-Excited Millimeter-Sized Cantilever (PEMC) Sensors.” *Sensors and Actuators B: Chemical* 117 (1): 58–64. doi:10.1016/j.snb.2005.10.045.

Dhand, Abhay, and George Sakoulas. 2012. “Reduced Vancomycin Susceptibility among Clinical Staphylococcus Aureus Isolates (’the MIC Creep'): Implications for Therapy.” *F1000 Medicine Reports* 4 (February): 1–11. doi:10.3410/M4-4.

Dhayal, Babita, Walter A. Henne, Derek D. Doorneweerd, Ronald G. Reifenberger, and Philip S. Low. 2006. “Detection of Bacillus Subtilis Spores Using Peptide-Functionalized Cantilever Arrays.” *Journal of the American Chemical Society* 128 (11): 3716–21. doi:10.1021/ja0570887.

Domke, Ingrid. 2002. “Therapeutic Drug Monitoring on COBAS INTEGRA 400: Reply to Hermida, et Al. in Therapeutic Drug Monitoring 2001;23:725-727.” *Therapeutic Drug Monitoring* 24 (6): 789–90.

Domke, Ingrid, P. Cremer, and M. Huchtemann. 2000. “Therapeutic Drug Monitoring on COBAS INTEGRA 400--Evaluation Results.” *Clinical Laboratory* 46 (9-10): 509–15.

Don, Burl R., and George Kaysen. 2004. “Serum Albumin: Relationship to Inflammation and Nutrition.” *Seminars in Dialysis* 17 (6): 432–37. doi:10.1111/j.0894-0959.2004.17603.x.

Drury, Bradley, John Scott, Emma J. Rosi-Marshall, and John J. Kelly. 2013. “Triclosan Exposure Increases Triclosan Resistance and Influences Taxonomic Composition of Benthic Bacterial Communities.” *Environmental Science & Technology* 47 (15): 8923–30. doi:10.1021/es401919k.

Dwyer, Daniel J., Michael A. Kohanski, and James J. Collins. 2009. “Role of Reactive Oxygen Species in Antibiotic Action and Resistance.” *Current Opinion in Microbiology* 12 (5): 482–89. doi:10.1016/j.mib.2009.06.018.

Edgeworth, Jonathan D., Irina Chis Ster, Duncan Wyncoll, Manu Shankar-Hari, and Catherine A. McKenzie. 2014. “Long-Term Adherence to a 5 Day Antibiotic Course Guideline for Treatment of Intensive Care Unit (ICU)-Associated Gram-Negative Infections.” *The Journal of Antimicrobial Chemotherapy*, February. doi:10.1093/jac/dku038.

Ehrlich, Paul. 1913. “CHEMIOTHERAPY.” *The British Medical Journal*, 353–59.

Eiland, Lea S., Thomas M. English, and Edward H. Eiland. 2011. “Assessment of Vancomycin Dosing and Subsequent Serum Concentrations in Pediatric Patients.” *The Annals of Pharmacotherapy* 45 (5): 582–89. doi:10.1345/aph.1P588.

Eisenhofer, Graeme, Irwin J. Kopin, and David S. Goldstein. 2004. “Catecholamine Metabolism: A Contemporary View with Implications for Physiology and Medicine.” *Pharmacological Reviews* 56 (3): 331–49. doi:10.1124/pr.56.3.1.

El-Nahhal, Issa M., Shehata M. Zourab, and Nizam M. El-Ashgar. 2001. “Encapsulation of Phenolphthalein pH-Indicator into a Sol-Gel Matrix.” *Journal of Dispersion Science and Technology* 22 (6): 583–90. doi:10.1081/DIS-100107757.

Estes, Kerry S., and Hartmut Derendorf. 2010. “Comparison of the Pharmacokinetic Properties of Vancomycin, Linezolid, Tigecyclin, and Daptomycin.” *European Journal of Medical Research* 15 (12): 533–43. doi:10.1186/2047-783X-15-12-533.

Eswaranandam, S., N. S. Hettiarachchy, and M. G. Johnson. 2006. “Antimicrobial Activity of Citric, Lactic, Malic, or Tartaric Acids and Nisin-Incorporated Soy Protein Film Against Listeria Monocytogenes, Escherichia Coli O157:H7, and Salmonella Gaminara.” *Journal of Food Science* 69 (3): FMS79–FMS84. doi:10.1111/j.1365-2621.2004.tb13375.x.

Fearon, W. R. 1944. “The Detection and Estimation of Uric Acid by 2:6-Dichloroquinone-Chloroimide.” *The Biochemical Journal* 38 (5): 399–402.

Feng, Steve, Romain Caire, Bingen Cortazar, Mehmet Turan, Andrew Wong, and Aydogan Ozcan. 2014. “Immunochromatographic Diagnostic Test Analysis Using Google Glass.” *ACS Nano*, no. 3 (February): 3069–79. doi:10.1021/nn500614k.

Fernandes, Prabhavathi. 2006. “Antibacterial Discovery and Development--the Failure of Success?” *Nature Botechnology* 24 (12): 1497–1503. doi:10.1038/nbt1206-1497.

Fernandez de Gatta, del Mar, Victoria Calvo, Jesus M. Hernández, Dolores Caballero, Jesus F. San Miguel, and Alfonso Dominguez-Gil. 1996. “Cost-Effectiveness Analysis of Serum Vancomycin Concentration Monitoring in Patients with Hematologic Malignancies.” *Clinical Pharmacology & Therapeutics* 60 (3). Nature Publishing Group: 332–40.

Fieser, Louis F., Mary Fieser, and Srinivasa Rajagopalan. 1948. “Absorption Spectroscopy and the Structures of the Diosterols.” *The Journal of Organic Chemistry* 13 (6): 800–806. doi:10.1021/jo01164a003.

Firsov, Alexander A., Maria V. Smirnova, Irene Yu. Lubenko, Sergey N. Vostrov, Yury A. Portnoy, and Stephen H. Zinner. 2006. “Testing the Mutant Selection Window Hypothesis with Staphylococcus Aureus Exposed to Daptomycin and Vancomycin in an in Vitro Dynamic Model.” *The Journal of Antimicrobial Chemotherapy* 58 (6): 1185–92. doi:10.1093/jac/dkl387.

Fish, Richard, Robert Nipah, Chris Jones, Hazel Finney, and Stanley L. S. Fan. 2012. “Intraperitoneal Vancomycin Concentrations during Peritoneal Dialysis-Associated Peritonitis: Correlation with Serum Levels.” *Peritoneal Dialysis International* 32 (3): 332–38. doi:10.3747/pdi.2010.00294.

Fleming, Alexander. 1922. “On a Remarkable Bacteriolytic Element Found in Tissues and Secretions.” *Proceedings of the Royal Society B: Biological Sciences* 93 (653): 306–17. doi:10.1098/rspb.1922.0023.

———. 1929. “On the Antibacterial Action of Cultures of a Penicillium, with Special Reference to Their Use in the Isolation of B. Influenzae.” *British Journal of Experimental Pathology* 10: 226–36.

Fong, Kei-Lai, Dah-Hsi Ho, Laurie Bogerd, Theresa Pan, Nita S. Brown, Layne Gentry, and Gerald P. Bodey. 1981. “Sensitive Radioimmunoassay for Vancomycin.” *Antimicrobial Agents and Chemotherapy* 19 (1): 139–43. doi:10.1128/AAC.19.1.139.

Foster, Laurence S., and Irving J. Gruntfest. 1937. “Demonstration Experiments Using Universal Indicators.” *Journal of Chemical Education* 14 (6): 274–77. doi:10.1021/ed014p274.

Foster, William, and Alain Raoult. 1974. “Early Descriptions of Antibiosis.” *The Journal of the Royal College of General Practitioners* 24 (149): 889–94.

Fournier, Thierry, Najet Medjoubi-N, and Dominique Porquet. 2000. “Alpha-1-Acid Glycoprotein.” *Biochimica et Biophysica Acta (BBA) - Protein Structure and Molecular Enzymology* 1482 (1-2): 157–71. doi:10.1016/S0167-4838(00)00153-9.

French, G. L. 2006. “Bactericidal Agents in the Treatment of MRSA Infections--the Potential Role of Daptomycin.” *The Journal of Antimicrobial Chemotherapy* 58 (6): 1107–17. doi:10.1093/jac/dkl393.

Freshney, R. Ian. 2005. “Culture of Specific Cell Types.” In *Culture of Animal Cells*, 375–420. John Wiley & Sons, Inc. doi:10.1002/0471747599.cac023.

Fritz, Jürgen. 2008. “Cantilever Biosensors.” *The Analyst* 133 (7): 855–63. doi:10.1039/b718174d.

Fritz, Jürgen, Marko K. Baller, Hans Peter Lang, H. Rothuizen, Peter Vettiger, Ernst Meyer, Hans-Joachim Güntherodt, Christoph Gerber, and James K. Gimzewski. 2000. “Translating Biomolecular Recognition into Nanomechanics.” *Science* 288 (5464): 316–18. doi:10.1126/science.288.5464.316.

Gamson, Robert M., David N. Kramer, and F. M. Miller. 1959. “A Study of the Physical and Chemical Properties of the Esters of Indophenols. II. Structural Studies of the Isomeric Esters.” *The Journal of Organic Chemistry* 24 (11): 1747–50. doi:10.1021/jo01093a033.

Gensini, Gian Franco, Andrea Alberto Conti, and Donatella Lippi. 2007. “The Contributions of Paul Ehrlich to Infectious Disease.” *The Journal of Infection* 54 (3): 221–24. doi:10.1016/j.jinf.2004.05.022.

Gfeller, Karin Y., Natalia Nugaeva, and Martin Hegner. 2005a. “Rapid Biosensor for Detection of Antibiotic-Selective Growth of Escherichia Coli.” *Applied and Environmental Microbiology* 71 (5): 2626–31. doi:10.1128/AEM.71.5.2626-2631.2005.

———. 2005b. “Micromechanical Oscillators as Rapid Biosensor for the Detection of Active Growth of Escherichia Coli.” *Biosensors & Bioelectronics* 21 (3): 528–33. doi:10.1016/j.bios.2004.11.018.

Ghuman, Jamie, Patricia A. Zunszain, Isabelle Petitpas, Ananyo A. Bhattacharya, Masaki Otagiri, and Stephen Curry. 2005. “Structural Basis of the Drug-Binding Specificity of Human Serum Albumin.” *Journal of Molecular Biology* 353 (1): 38–52. doi:10.1016/j.jmb.2005.07.075.

Gibbs, Harry Drake. 1923. “Process of Manufacturing Anthraquinone and Phthalic Anhydride.” *United States Patent*. Patent No.: 1,444,068.

———. 1926a. “Phenol Tests. I. A. Classification of the Tests and a Review of the Literature.” *The Journal of Biological Chemistry*, 291–319.

———. 1926b. “Phenol Tests. II. Nitrous Acid Tests. The Millon and Similar Tests. Spectrophotometric Investigations.” *The Journal of Biological Chemistry* 71 (2). ASBMB: 445–59.

———. 1927a. “Phenol Tests. III. The Indophenol Test.” *The Journal of Biological Chemistry* 72: 649–64.

———. 1927b. “Phenol Tests. IV. A Study of the Velocity of Indophenol Formation 2, 6-Dibromobenzenoneindophenol.” *The Journal of Physical Chemistry* 31 (7). ACS Publications: 1053–81.

———. 1927c. “PARA-CRESOL. A NEW METHOD OF SEPARATING PARACRESOL FROM ITS ISOMERS AND A STUDY OF THE BOILING POINT.” *Journal of the American Chemical Society* 49 (3): 839–44.

Gibbs, Harry Drake, and C. C. James. 1905. “ON THE OCCURRENCE OF ARSENIC IN WINES.” *Journal of the American Chemical Society*, 1484–96.

Gill, Stanley C., and Peter H. von Hippel. 1989. “Calculation of Protein Extinction Coefficients from Amino Acid Sequence Data.” *Analytical Biochemistry* 182 (2): 319–26. doi:10.1016/0003-2697(89)90602-7.

Gimzewski, James K., Christoph Gerber, Ernst Meyer, and R. R. Schlittler. 1994. “Observation of a Chemical Reaction Using a Micromechanical Sensor.” *Chemical Physics Letters* 217 (5-6): 589–94. doi:10.1016/0009-2614(93)E1419-H.

Ginbserg, Judah. 2005. “Selman Waksman and Antibiotics.” *American Chemical Society National Historic Chemical Landmarks*.

Glass, P. S. A, L. S. Shafer, J. G. Reves, and Ronald D. Miller (Editor). 2010. “Intravenous Drug Delivery Systems.” In *Miller’s Anesthesia*, 720 et seqq. Churchill Livingstone, Elsevier, ISBN: 978-0-443-06959-8.

Glen, J. B. 1980. “Animal Studies Of The Anaesthetic of ICI 35 868.” *BJA: British Journal of Anaesthesia* 52 (8): 731–42. doi:10.1093/bja/52.8.731.

Glen, J. B., and S. C. Hunter. 1984. “Pharmacology Of An Emulsion Formulation Of ICI 35 868.” *BJA: British Journal of Anaesthesia* 56 (6): 617–26. doi:10.1093/bja/56.6.617.

Goldstein, David S., Kathryn J. Swoboda, John M. Miles, Simon W. Coppack, Anders Aneman, Courtney Holmes, Isaac Lamensdorf, and Graeme Eisenhofer. 1999. “Sources and Physiological Significance of Plasma Dopamine Sulfate.” *The Journal of Clinical Endocrinology and Metabolism* 84 (7): 2523–31. doi:10.1210/jc.84.7.2523.

Gordon, Claire L., Chantelle Thompson, Jonathan R. Carapetis, John Turnidge, Charles Kilburn, and Bart J. Currie. 2012. “Trough Concentrations of Vancomycin: Adult Therapeutic Targets Are Not Appropriate for Children.” *The Pediatric Infectious Disease Journal* 31 (12): 1269–71. doi:10.1097/INF.0b013e31826a3eaf.

Gospodarowicz, D., and J. S. Moran. 1976. “Growth Factors in Mammalian Cell Culture.” *Annual Review of Biochemistry* 45 (January): 531–58. doi:10.1146/annurev.bi.45.070176.002531.

Gould, Ian M. 2010. “VRSA-Doomsday Superbug or Damp Squib?” *The Lancet Infectious Diseases* 10 (12): 816–18. doi:10.1016/S1473-3099(10)70259-0.

———. 2011. “Clinical Activity of Anti-Gram-Positive Agents against Methicillin-Resistant Staphylococcus Aureus.” *The Journal of Antimicrobial Chemotherapy* 66 Suppl 4 (May): iv17–iv21. doi:10.1093/jac/dkr073.

Green, Steven M. 2007. “Propofol in Emergency Medicine: Further Evidence of Safety.” *Emergency Medicine Australasia* 19 (5): 389–93. doi:10.1111/j.1742-6723.2007.01016.x.

Griffith, R. S. 1981. “Introduction to Vancomycin.” *Reviews of Infectious Diseases* Nov-Dec (3 suppl): S200–204. doi:10.1093/clinids/3.Supplement_2.S200.

Gross, Annette S. 2002. “Best Practice in Therapeutic Drug Monitoring.” *British Journal of Clinical Pharmacology* 46 (2): 95–99. doi:10.1046/j.1365-2125.1998.00770.x.

Gwynn, Michael N., Alison Portnoy, Stephen F. Rittenhouse, and David J. Payne. 2010. “Challenges of Antibacterial Discovery Revisited.” *Annals of the New York Academy of Sciences* 1213 (December): 5–19. doi:10.1111/j.1749-6632.2010.05828.x.

Hackbusch, W., H. R. Schwarz, and E. Zeidler. 1996. *Teubner-Taschenbuch Der Mathematik*. B. G. Teubner, Stuttgart Leipzig, ISBN: 3-8154-2001-6.

Hagan, Michael F., Arun Majumdar, and Arup K. Chakraborty. 2002. “Nanomechanical Forces Generated by Surface Grafted DNA.” *The Journal of Physical Chemistry B* 106 (39): 10163–73. doi:10.1021/jp020972o.

Haiss, W. 2001. “Surface Stress of Clean and Adsorbate-Covered Solids.” *Reports on Progress in Physics* 64 (5): 591–648. doi:10.1088/0034-4885/64/5/201.

Harfoush, A. A. 1983. “Medium Effect on the Reaction of Gibb’s Reagent with Sodium Thiosulphate.” *Journal of Chemical Technology and Biotechnology* 33A (6): 281–85. doi:10.1002/jctb.504330602.

Harfoush, A. A., A Zagloul, and F. M. Abdel Halim. 1982. “Kinetics of the Reaction of N-2,6-Trichlorobenzoquinonimine with Sodium Thiosulphate.” *Monatshefte Für Chemie Chemical Monthly* 113 (6-7): 837–43. doi:10.1007/BF00809024.

Harris, Constance M., and Thomas M. Harris. 1982. “Structure of the Glycopeptide Antibiotic Vancomycin. Evidence for an Asparagine Residue in the Peptide.” *Journal of the American Chemical Society* 104 (15): 4293–95. doi:10.1021/ja00379a062.

Harrison, G. R., A. D. J. Critchley, C. A. Mayhew, and J. M. Thompson. 2003. “Real-Time Breath Monitoring of Propofol and Its Volatile Metabolites during Surgery Using a Novel Mass Spectrometric Technique: A Feasibility Study.” *British Journal of Anaesthesia* 91 (6): 797–99. doi:10.1093/bja/aeg271.

Hegde, Sharath S., Noe Reyes, Tania Wiens, Nicole Vanasse, Robert Skinner, Julia McCullough, Koné Kaniga, et al. 2004. “Pharmacodynamics of Telavancin (TD-6424), a Novel Bactericidal Agent, against Gram-Positive Bacteria.” *Antimicrobial Agents and Chemotherapy* 48 (8): 3043–50. doi:10.1128/AAC.48.8.3043-3050.2004.

Helgason, Kristjan O., Alison H. Thomson, and Craig Ferguson. 2008. “A Review of Vancomycin Therapeutic Drug Monitoring Recommendations in Scotland.” *The Journal of Antimicrobial Chemotherapy* 61 (6): 1398–99. doi:10.1093/jac/dkn114.

Helm, M., J. J. Servant, F. Saurenbach, and R. Berger. 2005. “Read-out of Micromechanical Cantilever Sensors by Phase Shifting Interferometry.” *Applied Physics Letters* 87 (6): 064101. doi:10.1063/1.2008358.

Hermans, Rodolfo I., Joe M. Bailey, and Gabriel Aeppli. 2013. “Direct and Alignment-Insensitive Measurement of Cantilever Curvature”. Instrumentation and Detectors; Optics. *Applied Physics Letters* 103 (3): 1–6. doi:10.1063/1.4813265.

Hermida, Jesús, Sofia Zaera, and J. Carlos Tutor. 2001. “Therapeutic Drug Monitoring in the COBAS Integra 400 Analyzer.” *Therapeutic Drug Monitoring* 23 (6): 725.

Higgins, Deborah L., Ray Chang, Dmitri V. Debabov, Joey Leung, Terry Wu, Kevin M. Krause, Erik Sandvik, et al. 2005. “Telavancin, a Multifunctional Lipoglycopeptide, Disrupts Both Cell Wall Synthesis and Cell Membrane Integrity in Methicillin-Resistant Staphylococcus Aureus.” *Antimicrobial Agents and Chemotherapy* 49 (3): 1127–34. doi:10.1128/AAC.49.3.1127-1134.2005.

Hiramatsu, Keiichi. 2001. “Vancomycin-Resistant Staphylococcus Aureus: A New Model of Antibiotic Resistance.” *The Lancet Infectious Diseases* 1 (3): 147–55. doi:10.1016/S1473-3099(01)00091-3.

Hofmann, Christopher M., James M. Anderson, and Roger E. Marchant. 2012. “Targeted Delivery of Vancomycin to Staphylococcus Epidermidis Biofilms Using a Fibrinogen-Derived Peptide.” *Journal of Biomedical Materials Research. Part A* 100 (9): 2517–25. doi:10.1002/jbm.a.34166.

Holmes, Natasha E., Paul D. R. Johnson, and Benjamin P. Howden. 2012. “Relationship between Vancomycin-Resistant Staphylococcus Aureus, Vancomycin-Intermediate S. Aureus, High Vancomycin MIC, and Outcome in Serious S. Aureus Infections.” *Journal of Clinical Microbiology* 50 (8): 2548–52. doi:10.1128/JCM.00775-12.

Hopewood, David, Stuart Levy, Richard P. Wenzel, Nafsika Georgopapadakou, Richard H. Baltz, Sujata Bhavnani, and Edward Cox. 2007. “A Call to Arms.” *Nature Reviews. Drug Discovery* 6 (1): 8–12. doi:10.1038/nrd2225.

Hornero-Méndez, Dámaso, and M. Isabel Mínguez-Mosquera. 2001. "Rapid Spectrophotometric Determination of Red and Yellow Isochromic Carotenoid Fractions in Paprika and Red Pepper Oleoresins." *Journal of Agricultural and Food Chemistry* 49 (8): 3584–88. doi:10.1021/jf010400l.

Hornuss, Cyrill, Siegfried Praun, Johannes Villinger, Albert Dornauer, Patrick Moehnle, Michael Dolch, Ernst Weninger, et al. 2007. "Real-Time Monitoring of Propofol in Expired Air in Humans Undergoing Total Intravenous Anesthesia." *Anesthesiology* 106 (4): 665–74. doi:10.1097/01.anes.0000264746.01393.e0.

Houk, K. N., Andrew G. Leach, Susanna P. Kim, and Xiyun Zhang. 2003. "Binding Affinities of Host-Guest, Protein-Ligand, and Protein-Transition-State Complexes." *Angewandte Chemie (International Ed. in English)* 42 (40): 4872–97. doi:10.1002/anie.200200565.

Housecroft, Catherine E., and Edwin C. Constable. 2010. *Chemistry: An Introduction to Organic, Inorganic and Physical Chemistry*. Prentice-Hall, ISBN: 978-0-273-71545-0.

Howell, Lee. 2013. "World Econmic Forum (WEF) - Global Risks 2013 Eighth Edition." *www3.weforum.org/docs/WEF_GlobalRisks_Report_2013.pdf Accessed: 28/1/2014*, 1–80.

Hubbard, Brian K., and Christopher T. Walsh. 2003. "Vancomycin Assembly: Nature's Way." *Angewandte Chemie (International Ed. in English)* 42 (7): 730–65. doi:10.1002/anie.200390202.

Huber, François, Martin Hegner, Christoph Gerber, Hans-Joachim Güntherodt, and Hans Peter Lang. 2006. "Label Free Analysis of Transcription Factors Using Microcantilever Arrays." *Biosensors & Bioelectronics* 21 (8): 1599–1605. doi:10.1016/j.bios.2005.07.018.

Huber, François, Hans Peter Lang, and Christoph Gerber. 2014. "Nanomechanical Sensors: Measuring a Response in Blood." *Nature Nanotechnology* 9 (3). Nature Publishing Group: 165–67. doi:10.1038/nnano.2014.42.

Hückel, Erich. 1931. "Quantentheoretische Beiträge Zum Benzolproblem." *Zeitschrift Für Physik* 70 (3-4): 204–86. doi:10.1007/BF01339530.

Ibach, H. 1994. "Adsorbate-Induced Surface Stress." *Journal of Vacuum Science & Technology A: Vacuum, Surfaces, and Films* 12 (4): 2240. doi:10.1116/1.579122.

Ichikawa, Tetsuo, and Hiroshi Terada. 1979. “Estimation of State and Amount of Phenylalanine Residues in Proteins by Second Derivative Spectrophotometry.” *Biochimica et Biophysica Acta (BBA) - Protein Structure* 580 (1): 120–28. doi:10.1016/0005-2795(79)90203-4.

Ilic, B., H. G. Craighead, S. Krylov, W. Senaratne, C. Ober, and P. Neuzil. 2004. “Attogram Detection Using Nanoelectromechanical Oscillators.” *Journal of Applied Physics* 95 (7): 3694–3703. doi:10.1063/1.1650542.

Ilic, B., D. Czaplewski, H. G. Craighead, P. Neuzil, C. Campagnolo, and C. Batt. 2000. “Mechanical Resonant Immunospecific Biological Detector.” *Applied Physics Letters* 77 (3): 450. doi:10.1063/1.127006.

Imamovic, Lejla, and Morton O. A. Sommer. 2013. “Use of Collateral Sensitivity Networks to Design Drug Cycling Protocols That Avoid Resistance Development.” *Science Translational Medicine* 5 (204): 204ra132–204ra132. doi:10.1126/scitranslmed.3006609.

Jelassi, Mohamed Larbi, Amine Benlmouden, Sandrine Lefeuvre, Jean-Luc Mainardi, and Eliane M. Billaud. 2011. “Level of Evidence for Therapeutic Drug Monitoring of Vancomycin.” *Thérapie* 66 (1): 29–37. doi:10.2515/therapie/2011005.

Jesús Valle, María José De, Francisco González López, and Amparo Sánchez Navarro. 2008. “Development and Validation of an HPLC Method for Vancomycin and Its Application to a Pharmacokinetic Study.” *Journal of Pharmaceutical and Biomedical Analysis* 48 (3): 835–39. doi:10.1016/j.jpba.2008.05.040.

Johnson, Alan. P., Anne H. C. Uttley, Neil Woodford, and Robert C. George. 1990. “Resistance to Vancomycin and Teicoplanin: An Emerging Clinical Problem.” *Clinical Microbiology Reviews* 3 (3): 280–91. doi:10.1128/CMR.3.3.2803.

Johnston, James B., and V. Renganathan. 1987. “Production of Substituted Catechols from Substituted Benzenes by a Pseudomonas Sp.” *Enzyme and Microbial Technology* 9 (12). Elsevier: 706–8. doi:10.1016/0141-0229(87)90028-7.

Jolley, M. E., S. D. Stroupe, K. S. Schwenzer, C. J. Wang, H. D. Hill, S. R. Popeika, J. T. Holen, and D. M. Kelso. 1981. “FluorescencePolarizationImmunoassay. Ill. An Automated System for Therapeutic Drug Determiniation.” *Clinical Chemistry* 27 (9): 1575–79.

Josephy, P. David, and Anjel Van Damme. 1984. “Reaction of Gibbs Reagent with Para-Substituted Phenols.” *Analytical Chemistry* 56 (4). ACS Publications: 813–14.

Kahne, Daniel, Catherine Leimkuhler, Wei Lu, and Christopher T. Walsh. 2005. “Glycopeptide and Lipoglycopeptide Antibiotics.” *Chemical Reviews* 105 (2): 425–48. doi:10.1021/cr030103a.

Kallmayer, H.-J., and B. Thierfelder. 2003. “Die Reaktion Des Iminodibenzyls Mit 2,6-Dichlor- 1,4-Benzochinon-4-Chlorimid.” *Die Pharmazie* 58 (3): 218–19.

Kalsi, P. S. 2004. *Spectroscopy Of Organic Compounds*. New Age International, ISBN: 978-8122415438.

Kang, Ju Seop, and Min Ho Lee. 2009. “Overview of Therapeutic Drug Monitoring.” *The Korean Journal of Internal Medicine* 24 (1): 1–10. doi:10.3904/kjim.2009.24.1.1.

Kannan, Rajamoorthi, Constance M. Harris, Thomas M. Harris, Jonathan P. Waltho, Nicholas J. Skelton, and Dudley H. Williams. 1988. “Function of the Amino Sugar and N-Terminal Amino Acid of the Antibiotic Vancomycin in Its Complexation with Cell Wall Peptides.” *Journal of the American Chemical Society* 110 (9): 2946–53. doi:10.1021/ja00217a042.

Kappeler, Natascha. 2010. “Nanomechanical Detection of Antibiotic- Mucopeptide Binding on Cantilever Array Sensors in a Model for Superbug Drug Resistance.” *Master’s Thesis*. University of Basel & University College London (UCL).

Kappeler, Natascha, Rachel A. McKendry, Daren Joseph Caruana, Russell Keay, David Michael Pettigrew, and Steve Andrew Fowler. 2013. “Analyte Extraction Apparatus and Method.” *United Kingdom Patent*.

Kar, Indrajit, B. M. Mandal, and S. R. Palit. 1969. “Retardation of Free Radical Polymerization by Redox Dyes.” *Die Makromolekulare Chemie* 127 (3089): 195–203. doi:10.1002/macp.1969.021270113.

Keller, Stephan, Daniel Haefliger, and Anja Boisen. 2010. “Fabrication of Thin SU-8 Cantilevers: Initial Bending, Release and Time Stability.” *Journal of Micromechanics and Microengineering* 20 (4): 045024. doi:10.1088/0960-1317/20/4/045024.

Kelling, Sven, François Paoloni, Juzheng Huang, Victor P. Ostanin, and Stephen R. Elliott. 2009. “Simultaneous Readout of Multiple Microcantilever Arrays with Phase-

Shifting Interferometric Microscopy." *The Review of Scientific Instruments* 80 (9): 093101–18. doi:10.1063/1.3212667.

Kellner, Robert, Jean-Michel Mermet, Matthias Otto, Miguel Valcárcel, and H. Michael Widmer. 2004. *Analytical Chemistry: A Modern Approach to Analytical Science*. WILEY-VCH, ISBN: 3527305904.

Khachik, Frederick, and Gary R. Beecher. 1987. "Application of a C-45-.beta.-Carotene as an Internal Standard for the Quantification of Carotenoids in Yellow/orange Vegetables by Liquid Chromatography." *Journal of Agricultural and Food Chemistry* 35 (5): 732–38. doi:10.1021/jf00077a022.

Khoo, L. E., F. Morsingh, and K. Y. Liew. 1979. "The Adsorption of B-Carotene I. by Bleaching Earths." *Journal of the American Oil Chemists …*, no. c: 672–75.

Kitzis, M. D., and F. W. Goldstein. 2006. "Monitoring of Vancomycin Serum Levels for the Treatment of Staphylococcal Infections." *Clinical Microbiology and Infection: The Official Publication of the European Society of Clinical Microbiology and Infectious Diseases* 12 (1): 92–95. doi:10.1111/j.1469-0691.2005.01306.x.

Kohanski, Michael A., Mark A. DePristo, and James J. Collins. 2010. "Sublethal Antibiotic Treatment Leads to Multidrug Resistance via Radical-Induced Mutagenesis." *Molecular Cell* 37 (3). Elsevier Ltd: 311–20. doi:10.1016/j.molcel.2010.01.003.

Kohanski, Michael A., Daniel J. Dwyer, Boris Hayete, Carolyn A. Lawrence, and James J. Collins. 2007. "A Common Mechanism of Cellular Death Induced by Bactericidal Antibiotics." *Cell* 130 (5): 797–810. doi:10.1016/j.cell.2007.06.049.

Kollanoor Johny, A., M. J. Darre, A. M. Donoghue, D. J. Donoghue, and K. Venkitanarayanan. 2010. "Antibacterial Effect of Trans-Cinnamaldehyde, Eugenol, Carvacrol, and Thymol on Salmonella Enteritidis and Campylobacter Jejuni in Chicken Cecal Contents in Vitro." *The Journal of Applied Poultry Research* 19 (3): 237–44. doi:10.3382/japr.2010-00181.

Kost, Gerald J., Tam H. Nguyen, and Zuping Tang. 2000. "Whole-Blood Glucose and Lactate. Trilayer Biosensors, Drug Interference, Metabolism, and Practice Guidelines." *Archives of Pathology & Laboratory Medicine* 124 (8): 1128–34. doi:10.1043/0003-9985(2000)124<1128:WBGAL>2.0.CO;2.

Kovar, Karl-Artur, and Michael Teutsch. 1986. “Die Umsetzung von Harnsäure Mit 2,6-Dichlorchinon-4-Chlorimin.” *Archiv Der Pharmazie* 319 (1): 81–83. doi:10.1002/ardp.19863190116.

Kramer, David N., and Robert M. Gamson. 1959. “Preparation of Quinone Sulfenimines.” *The Journal of Organic Chemistry* 24 (8): 1154–55. doi:10.1021/jo01090a623.

Kramer, David N., Robert M. Gamson, and F. M. Miller. 1959. “A Study of the Physical and Chemical Properties of the Esters of Indophenols I. Preparation.” *The Journal of Organic Chemistry* 24 (11): 1742–47. doi:10.1021/jo01093a032.

Kresse, Hedwig, Mark J. Belsey, and Holger Rovini. 2007. “The Antibacterial Drugs Market.” *Nature Reviews. Drug Discovery* 6 (1): 19–20. doi:10.1038/nrd2226.

Krishna, K. Bala Murali. 2010. “Chapter III - Development and Validation of Analytical Procedure for the Estiamtion of Dobutamine Hydrochloride through New RP-HPLC Method”. Acharya Nagarjuna University.

Kumarasamy, Karthikeyan K., Mark A. Toleman, Timothy R. Walsh, Jay Bagaria, Fafhana Butt, Ravikumar Balakrishnan, Uma Chaudhary, et al. 2010. “Emergence of a New Antibiotic Resistance Mechanism in India, Pakistan, and the UK: A Molecular, Biological, and Epidemiological Study.” *The Lancet Infectious Diseases* 10 (9): 597–602. doi:10.1016/S1473-3099(10)70143-2.

Lai, Cheng-Chou, Jeng-Fu You, Chien-Yuh Yeh, Jinn-Shiun Chen, Reiping Tang, Jeng-Yi Wang, and Chih-Chien Chin. 2011. “Low Preoperative Serum Albumin in Colon Cancer: A Risk Factor for Poor Outcome.” *International Journal of Colorectal Disease* 26 (4): 473–81. doi:10.1007/s00384-010-1113-4.

Laitenberger, Peter G., Rachel A. McKendry, and Joseph W. Ndieyira. 2010. Nanomechanical Point-of-Care Devices for Antibiotic Monitoring EPSRC/Healthtech and Medicines KTN Industrial CASE Studentship Proposal 1–5.

Lambert, D. G. 2008. “Volume 100: Basic Sciences in the British Journal of Anaesthesia.” *BJA: British Journal of Anaesthesia* 100 (5): 595–96. doi:10.1093/bja/aen091.

Lambert, Johann Heinrich. 1760. *Photometria, Sive de Mensura et Gradibus Luminis, Colorum et Umbrae*. Sumptibus Vidae Eberhardi Klett.

Landsberg, H. 1949. “Prelude to the Discovery of Penicillin.” *Isis* 40 (3): 225–27.

Lang, Hans Peter, Murali K. Baller, Rüdiger Berger, Christoph Gerber, James K. Gimzewski, F. M. Battiston, P. Fornaro, Jean-Pierre Ramseyer, Ernst Meyer, and Hans-Joachim Güntherodt. 1999. "An Artificial Nose Based on a Micromechanical Cantilever Array." *Analytica Chimica Acta* 393 (1-3): 59–65. doi:10.1016/S0003-2670(99)00283-4.

Lang, Hans Peter, Rüdiger Berger, C. Andreoli, J. Brugger, Michel Despont, Peter Vettiger, Christoph Gerber, et al. 1998. "Sequential Position Readout from Arrays of Micromechanical Cantilever Sensors." *Applied Physics Letters* 72 (3): 383–85. doi:10.1063/1.120749.

Lang, Hans Peter, A. Filippi, A. Tonin, François Huber, Natalija Backmann, Jiayun Zhang, and Christoph Gerber. 2009. "Towards a Modular, Versatile and Portable Sensor System for Measurements in Gaseous Environments Based on Microcantilevers." *Procedia Chemistry* 1 (1). Elsevier B.V. 208–11. doi:10.1016/j.proche.2009.07.052.

Lang, Hans Peter, Martin Hegner, and Christoph Gerber. 2005. "Cantilever Array Sensors." *Materials Today* 5 (5): 30–36. doi:10.1021/nn103626q.

Lang, Hans Peter, J. P. Ramseyer, Wilifrid Grange, Thomas Braun, D. Schmid, Patrick Hunziker, C. Jung, Martin Hegner, and Christoph Gerber. 2007. "An Artificial Nose Based on Microcantilever Array Sensors." *Journal of Physics: Conference Series* 61 (March): 663–67. doi:10.1088/1742-6596/61/1/133.

Langmaier, Jan, Fernando Garay, Francine Kivlehan, Edward Chaum, and Erno Lindner. 2011. "Electrochemical Quantification of 2,6-Diisopropylphenol (propofol)." *Analytica Chimica Acta* 704 (1-2): 63–67. doi:10.1016/j.aca.2011.08.003.

Langmuir, Irving. 1918. "The Adsorption of Gases on Plane Surfaces of Glass, Mica and Platinum." *Journal of the American Chemical Society* 40 (9): 1361–1403. doi:10.1021/ja02242a004.

Leadbetter, Michael R., Stacy M. Adams, Bettina Bazzini, Paul R. Fatheree, Dane E. Karr, Kevin M. Krause, Bernice M. T. Lam, et al. 2004. "Hydrophobic Vancomycin Derivatives with Improved ADME Properties: Discovery of Telavancin (TD-6424)." *The Journal of Antibiotics* 57 (5): 326–36. doi:10.7164/antibiotics.57.326.

"Leaflet: Boots Paracetamol 500 Mg Capsules from Boots Pharmaceuticals." 2011, no. Reference number: 12063/0006.

Ledford, Heidi. 2012. “FDA under Pressure to Relax Drug Rules.” *Nature* 492 (7427): 19. doi:10.1038/492019a.

Levine, Donald P. 2006. “Vancomycin: A History.” *Clinical Infectious Diseases: An Official Publication of the Infectious Diseases Society of America* 42 Suppl 1 (Suppl 1): S5–12. doi:10.1086/491709.

Levison, Matthew E. 2004. “Pharmacodynamics of Antimicrobial Drugs.” *Infectious Disease Clinics of North America* 18 (3): 451–65, vii. doi:10.1016/j.idc.2004.04.012.

Levy, Stuart B, and Bonnie Marshall. 2004. “Antibacterial Resistance Worldwide: Causes, Challenges and Responses.” *Nature Medicine* 10 (12 Suppl): S122–9. doi:10.1038/nm1145.

Lewis, Kim. 2012. “Antibiotics: Recover the Lost Art of Drug Discovery.” *Nature* 485 (7399): 439–40. doi:10.1038/485439a.

Ligon, B.Lee. 2004. “Penicillin: Its Discovery and Early Development.” *Seminars in Pediatric Infectious Diseases* 15 (1): 52–57. doi:10.1053/j.spid.2004.02.001.

Lin, Yongxin, Genlong Jiao, Guodong Sun, Lili Zhang, Shilong Wang, Hanchao Liu, and Zhizhong Li. 2013. “Binding of Teicoplanin and Vancomycin to Bovine Serum Albumin in Vitro: A Multispectroscopic Approach and Molecular Modeling.” *Luminescence : The Journal of Biological and Chemical Luminescence*, no. October 2012 (April). doi:10.1002/bio.2512.

Liu, Bo, David Michael Pettigrew, Stephen Bates, Peter Georg Laitenberger, and Gavin Troughton. 2012. “Performance Evaluation of a Whole Blood Propofol Analyser.” *Journal of Clinical Monitoring and Computing* 26 (1): 29–36. doi:10.1007/s10877-011-9330-0.

Livermore, David M. 2007. “Introduction: The Challenge of Multiresistance.” *International Journal of Antimicrobial Agents* 29 Suppl 3 (May): S1–7. doi:10.1016/S0924-8579(07)00158-6.

Lloyd, Nicholas C., Hugh W. Morgan, Brian K. Nicholson, and Ron S. Ronimus. 2005. “The Composition of Ehrlich’s Salvarsan: Resolution of a Century-Old Debate.” *Angewandte Chemie (International Ed. in English)* 44 (6): 941–44. doi:10.1002/anie.200461471.

Loll, Patrick J., Russ Miller, Charles M. Weeks, and Paul H. Axelsen. 1998. "A Ligand-Mediated Dimerization Mode for Vancomycin." *Chemistry & Biology* 5 (5): 293–98. doi:10.1016/S1074-5521(98)90622-6.

Lomaestro, Ben M. 2011. "Vancomycin Dosing and Monitoring 2 Years after the Guidelines." *Expert Review of Anti-Infective Therapy* 9 (6): 657–67. doi:10.1586/eri.11.46.

Longo, G., L. Alonso-Sarduy, L. Marques Rio, A. Bizzini, A. Trampuz, J. Notz, G. Dietler, and S. Kasas. 2013. "Rapid Detection of Bacterial Resistance to Antibiotics Using AFM Cantilevers as Nanomechanical Sensors." *Nature Nanotechnology* 8 (7). Nature Publishing Group: 522–26. doi:10.1038/nnano.2013.120.

Love, J. Christopher, Lara A. Estroff, Jennah K. Kriebel, Ralph G. Nuzzo, and George M. Whitesides. 2005. "Self-Assembled Monolayers of Thiolates on Metals as a Form of Nanotechnology." *Chemical Reviews* 105 (4): 1103–69. doi:10.1021/cr0300789.

Lowe, Eleanor R., Craig Edward Banks, and Richard Guy Compton. 2005. "Indirect Detection of Substituted Phenols and Cannabis Based on the Electrochemical Adaptation of the Gibbs Reaction." *Analytical and Bioanalytical Chemistry* 383 (3). Springer: 523–31. doi:10.1007/s00216-005-0043-4.

Luppa, Peter B., Carolin Müller, Alice Schlichtiger, and Harald Schlebusch. 2011. "Point-of-Care Testing (POCT): Current Techniques and Future Perspectives." *TrAC Trends in Analytical Chemistry* 30 (6): 887–98. doi:10.1016/j.trac.2011.01.019.

Lyon, D., and R. Winfield. 2004. *The Sail & Steam Navy List*. Chatham Publishing, ISBN: 1-86176-032-9.

MacLean, R. Craig, Clara Torres-Barceló, and Richard Moxon. 2013. "Evaluating Evolutionary Models of Stress-Induced Mutagenesis in Bacteria." *Nature Reviews. Genetics* 14 (3). Nature Publishing Group: 221–27. doi:10.1038/nrg3415.

MacManus-Spencer, Laura A., and Kristopher McNeill. 2005. "Quantification of Singlet Oxygen Production in the Reaction of Superoxide with Hydrogen Peroxide Using a Selective Chemiluminescent Probe." *Journal of the American Chemical Society* 127 (25): 8954–55. doi:10.1021/ja052045b.

Malabarba, Adriano, Thalia I. Nicas, and Richard C. Thompson. 1997. “Structural Modifications of Glycopeptide Antibiotics.” *Medicinal Research Reviews* 17 (1): 69–137. doi:10.1002/(SICI)1098-1128(199701)17:1<69::AID-MED3>3.0.CO;2-R.

Marsh, Max, and Wayne Hilty. 1955. “Review - Pharmaceuticals and Natural Drugs.” *Analytical Chemistry* 27 (4): 636–53. doi:10.1021/ac60100a608.

Marshall, C., S. Wesselingh, M. McDonald, and D. Spelman. 2004. “Control of Endemic MRSA-What Is the Evidence? A Personal View.” *The Journal of Hospital Infection* 56 (4): 253–68. doi:10.1016/j.jhin.2004.02.001.

Marshall, Frederick J. 1965. “Structure Studies on Vancomycin.” *Journal of Medicinal Chemistry* 8: 18–22. doi:10.1021/jm00325a004.

McAllister, Ronald A. 1950. “A New Colour Reaction for Methylthiouracil.” *Nature* 166 (4227): 789–789. doi:10.1038/166789a0.

———. 1951. “Colour Reaction for Certain Mercaptoimidazoles.” *Nature* 167 (4256): 863–863. doi:10.1038/167863a0.

McCormick, Mack H., James M. McGuire, G. E. Pittenger, R. C. Pittenger, and W. M. Stark. 1956. “Vancomycin, a New Antibiotic. I. Chemical and Biologic Properties.” *Antibiotics Annual* 3 (1955-1956): 606–11.

McCormick, Mack H., Lawrence McGuire, and James M. McGuire. 1962. “Vancomycin and Method for Its Preparation.” *United States Patent*. Patent No.: US3067099A.

McGaughran, L., L. J. Voss, R. Oliver, M. Petcu, P. Schaare, J. P. M. Barnard, and J. W. Sleigh. 2006. “Rapid Measurement of Blood Propofol Levels: A Proof of Concept Study.” *Journal of Clinical Monitoring and Computing* 20 (2): 109–15. doi:10.1007/s10877-006-9014-3.

McKendry, Rachel A. 2012. “Nanomechanics of Superbugs and Superdrugs: New Frontiers in Nanomedicine.” *Biochemical Society Transactions* 40 (4): 603–8. doi:10.1042/BST20120082.

McKendry, Rachel A., and Natascha Kappeler. 2013. “Sensors: Good Vibrations for Bad Bacteria.” *Nature Nanotechnology* 8 (7). Nature Publishing Group: 483–84. doi:10.1038/nnano.2013.127.

McKendry, Rachel A., Jiayun Zhang, Youri Arntz, Torsten Strunz, Martin Hegner, Hans Peter Lang, Marko K. Baller, et al. 2002. “Multiple Label-Free Biodetection and

Quantitative DNA-Binding Assays on a Nanomechanical Cantilever Array." *Proceedings of the National Academy of Sciences of the United States of America* 99 (15): 9783–88. doi:10.1073/pnas.152330199.

Mertens, Johann, Eric Finot, Marie-Hélène Nadal, Vincent Eyraud, Olivier Heintz, and Eric Bourillot. 2004. "Detection of Gas Trace of Hydrofluoric Acid Using Microcantilever." *Sensors and Actuators B: Chemical* 99 (1): 58–65. doi:10.1016/j.snb.2003.10.030.

Meyer, Ernst, Hans Josef Hug, and Roland Bennewitz. 2004. *Prospects for SPM - The Lab on a Tip*. Springer-Verlag Berlin Heidelberg. doi:10.1007/978-3-662-09801-1_7.

MHRA. 2010. "Management and Use of IVD Point of Care Test Devices." *Crown. Last Accessed: 17/03/2014*. http://www.mhra.gov.uk/home/groups/dts-bi/documents/publication/con071105.pdf.

Miekisch, Wolfram, Patricia Fuchs, Svend Kamysek, Christine Neumann, and Jochen K. Schubert. 2008. "Assessment of Propofol Concentrations in Human Breath and Blood by Means of HS-SPME-GC-MS." *Clinica Chimica Acta; International Journal of Clinical Chemistry* 395 (1-2): 32–37. doi:10.1016/j.cca.2008.04.021.

Miles, Michael V., Li Li, Hassan Lakkis, John Youngblood, and Paul McGinnis. 1997. "Special Considerations for Monitoring Vancomycin Concentrations in Pediatric Patients." *Therapeutic Drug Monitoring* 19 (June 1997): 265–70.

Miller, Christine, Line Elnif Thomsen, Carina Gaggero, Ronen Mosseri, Hanne Ingmer, and Stanley N. Cohen. 2004. "SOS Response Induction by Beta-Lactams and Bacterial Defense against Antibiotic Lethality." *Science (New York, N.Y.)* 305 (5690): 1629–31. doi:10.1126/science.1101630.

Miller, Ronald D., and Manuel C. Pardo. 2011. *Basics of Anesthesia*. Elsevier Saunders, ISBN: 978-1437716146.

Moellering, Robert C. 2006. "Vancomycin: A 50-Year Reassessment." *Clinical Infectious Diseases: An Official Publication of the Infectious Diseases Society of America* 42 Suppl 1 (Suppl 1): S3–S4. doi:10.1086/491708.

Moulin, A. M., S. J. O'Shea, and Mark E. Welland. 2000. "Microcantilever-Based Biosensors." *Ultramicroscopy* 82 (1-4): 23–31. doi:10.1016/S0304-3991(99)00145-X.

Mukhopadhyay, Rupa, Martin Lorentzen, Jørgen Kjems, and Fleming Besenbacher. 2005. "Nanomechanical Sensing of DNA Sequences Using Piezoresistive Cantilevers." *Langmuir: The ACS Journal of Surfaces and Colloids* 21 (18): 8400–8408. doi:10.1021/la0511687.

Mukhopadhyay, Rupa, Vadim V. Sumbayev, Martin Lorentzen, Jørgen Kjems, Peter A. Andreasen, and Flemming Besenbacher. 2005. "Cantilever Sensor for Nanomechanical Detection of Specific Protein Conformations." *Nano Letters* 5 (12): 2385–88. doi:10.1021/nl051449z.

Muppidi, Krishna, Andrew S. Pumerantz, Jeffrey Wang, and Guru Betageri. 2012. "Development and Stability Studies of Novel Liposomal Vancomycin Formulations." *Internation Scholarly Research Netweork (ISRN) Pharmaceutics* 2012 (January): 1–8. doi:10.5402/2012/636743.

Nagarajan, R. 1994. *Glycopeptide Antibiotics*. *Drugs and Pharmaceutical Sciences*. Vol. 63. Marcel Dekker Inc., ISBN: 0-8247-9193-2.

Nandí-Lozano, Eugenia, Eduardo Ramírez-López, and Carlos Avila-Figueroa. 2003. "Pharmacologic Clinical Monitoring of Serum Vancomycin Levels in Pediatric Patients." *Revista de Investigación Clínica; Organo Del Hospital de Enfermedades de La Nutrición* 55 (3): 276–80.

Ndieyira, Joseph W., Natascha Kappeler, Stephen Logan, Matthew A. Cooper, Chris Abell, Rachel A. McKendry, and Gabriel Aeppli. 2014. "Surface-Stress Sensors for Rapid and Ultrasensitive Detection of Active Free Drugs in Human Serum." *Nature Nanotechnology* 9 (3). Nature Publishing Group: 225–32. doi:10.1038/nnano.2014.33.

Ndieyira, Joseph W., Moyu Watari, Alejandra Donoso Barrera, Dejian Zhou, Manuel Vögtli, Matthew Batchelor, Matthew A. Cooper, et al. 2008. "Nanomechanical Detection of Antibiotic-Mucopeptide Binding in a Model for Superbug Drug Resistance." *Nature Nanotechnology* 3 (11): 691–96. doi:10.1038/nnano.2008.275.

Nieto, Manuel, and Harold R. Perkins. 1971. "Modifications of the Acyl-D-Alanyl-D-Alanine Terminus Affecting Complex-Formation with Vancomycin." *The Biochemical Journal* 123 (5): 789–803.

Nitanai, Yasushi, Takanori Kikuchi, Kouji Kakoi, Shinji Hanamaki, Ikuhide Fujisawa, and Katsuyuki Aoki. 2009. “Crystal Structures of the Complexes between Vancomycin and Cell-Wall Precursor Analogs.” *Journal of Molecular Biology* 385 (5). Elsevier Ltd: 1422–32. doi:10.1016/j.jmb.2008.10.026.

Noggle, Joseph H., and Roger E. Schirmer. 1971. *Nuclear Overhauser Effect: Chemical Applications*. ACADEMIC PRESS INC., ISBN: 978-0125206501.

Nordström, Maria, Stephan Keller, Michael Lillemose, Alicia Johansson, Søren Dohn, Daniel Haefliger, Gabriela Blagoi, Mogens Havsteen-Jakobsen, and Anja Boisen. 2008. “SU-8 Cantilevers for Bio/chemical Sensing; Fabrication, Characterisation and Development of Novel Read-out Methods.” *Sensors* 8 (3): 1595–1612. doi:10.3390/s8031595.

Nordström, Maria, Dan A. Zauner, Montserrat Calleja, Jörg Hübner, and Anja Boisen. 2007. “Integrated Optical Readout for Miniaturization of Cantilever-Based Sensor System.” *Applied Physics Letters* 91 (10): 103512. doi:10.1063/1.2779851.

Nostro, Antonia, Andrea Sudano Roccaro, Giuseppe Bisignano, Andreana Marino, Maria a Cannatelli, Francesco C Pizzimenti, Pier Luigi Cioni, Francesca Procopio, and Anna Rita Blanco. 2007. “Effects of Oregano, Carvacrol and Thymol on Staphylococcus Aureus and Staphylococcus Epidermidis Biofilms.” *Journal of Medical Microbiology* 56 (Pt 4): 519–23. doi:10.1099/jmm.0.46804-0.

Nugaeva, Natalia, Karin Y. Gfeller, Natalija Backmann, Marcel Düggelin, Hans Peter Lang, Hans-joachim Güntherodt, and Martin Hegner. 2007. “An Antibody-Sensitized Microfabricated Cantilever for the Growth Detection of Aspergillus Niger Spores.” *Microscopy and Microanalysis : The Official Journal of Microscopy Society of America, Microbeam Analysis Society, Microscopical Society of Canada* 13 (1): 13–17. doi:10.1017/S1431927607070067.

Nugaeva, Natalia, Karin Y. Gfeller, Natalija Backmann, Hans Peter Lang, Marcel Düggelin, and Martin Hegner. 2005. “Micromechanical Cantilever Array Sensors for Selective Fungal Immobilization and Fast Growth Detection.” *Biosensors & Bioelectronics* 21 (6): 849–56. doi:10.1016/j.bios.2005.02.004.

Nuzzo, Ralph G., and David L. Allara. 1983. “Adsorption of Bifunctional Organic Disulfides on Gold Surfaces.” *Journal of the American Chemical Society*, no. 11: 4481–83. doi:10.1021/ja00351a063.

Nuzzo, Ralph G., Bernard R. Zegarski, and Lawrence H. Dubois. 1987. “Fundamental Studies of the Chemisorption of Organosulfur Compounds on Gold (111). Implications for Molecular Self-Assembly on Gold Surfaces.” *Journal of the American Chemical Society* 109 (7): 733–40. doi:10.1021/ja00237a017.

O’Gorman, J., and H. Humphreys. 2012. “Application of Copper to Prevent and Control Infection. Where Are We Now?” *The Journal of Hospital Infection* 81 (4). Elsevier Ltd: 217–23. doi:10.1016/j.jhin.2012.05.009.

Ogata, Masahiro, Kanae Tutumimoto Sato, Takao Kunikane, Kentaro Oka, Masako Seki, Shiro Urano, Keiichi Hiramatsu, and Toyoshige Endo. 2005. “Antibacterial Activity of Dipropofol and Related Compounds.” *Biological & Pharmaceutical Bulletin* 28 (6): 1120–22. doi:10.1248/bpb.28.1120.

Ojeil, M., C. Jermann, J. Holah, S. P. Denyer, and J.-Y. Maillard. 2013. “Evaluation of New in Vitro Efficacy Test for Antimicrobial Surface Activity Reflecting UK Hospital Conditions.” *The Journal of Hospital Infection*, September. Elsevier Ltd. doi:10.1016/j.jhin.2013.08.007.

Otten, H. 1986. “Domagk and the Development of the Sulphonamides.” *Journal of Antimicrobial Chemotherapy* 17 (6): 689–90. doi:10.1093/jac/17.6.689.

Owen, J. A., and Betty Iggo. 1956. “The Use of P-Chloromercuribenzoic Acid in the Determination of Ascorbic Acid with 2:6-Dichlorophenolindophenol.” *The Biochemical Journal* 62 (4): 675–80.

“Package Insert: AXSYM® SYSTEM Vancomycin II from Abbott.” 2005, no. REF:5B75-1 34-3919/R6.

“Package Insert: VANC2 COBAS® from Roche Diagnostics.” 2012, no. 04491050190V10.

Padidem, Chandra, Sajid Bashir, and Liu Jingbo. 2011. “Sensor Enhancement Using Nanomaterials to Detect Pharmaceutical Residue: Nanointegration Using Phenol as Environmental Pollutant.” In *New Perspectives in Biosensors Technology and Applications. Edited by Prof. Pier Andrea Serra*, 421–48. InTech.

Paladino, Joseph A., Jenna L. Sunderlin, Martin H. Adelman, Mendel E. Singer, and Jerome J. Schentag. 2007. “Observations on Vancomycin Use in U.S. Hospitals.” *American Journal of Health-System Pharmacy : AJHP : Official Journal of the American Society of Health-System Pharmacists* 64 (15): 1633–41. doi:10.2146/ajhp060651.

Pallagi, István, and Peter Dvortsák. 1986. “Gibbs Reaction. Part 1. Reduction of Benzoquinone N-Chloroimines to Benzoquinone Imines.” *J. Chem. Soc., Perkin Trans. 2*, no. 1. The Royal Society of Chemistry: 105–10. doi:10.1039/P29860000105.

Pallagi, István, András Toró, and Ödön Farkas. 1994. “Mechanism of the Gibbs Reaction. 3. Indophenol Formation via Radical Electrophilic Aromatic Substitution (SREAr) on Phenols.” *The Journal of Organic Chemistry* 59 (22). ACS Publications: 6543–57. doi:10.1021/jo00101a013.

Pallagi, István, András Toró, and Gyula Horváth. 1999. “Mechanism of the Gibbs Reaction. Part 4.(1) Indophenol Formation via N-Chlorobenzoquinone Imine Radical Anions. The Aza-S(RN)2 Chain Reaction Mechanism. Chain Initiation with 1,4-Benzoquinones and Cyanide Ion.” *The Journal of Organic Chemistry* 64 (18): 6530–40. doi:10.1021/jo00101a013.

Pallagi, István, András Toró, and Jozsef Müller. 1994. “The Mechanism of the Gibbs Reaction. Part 2: The Ortho Ortho 2, 4-Cyclohexadiene-1-One Rearrangement of the Reaction Product of 2, 6-Di- Tert-Butyl-4-Chlorophenol and 2, 6-Dichlorobenzoquinone N-Chloroimine.” *Tetrahedron* 50 (29). Elsevier: 8809–14. doi:10.1016/S0040-4020(01)85354-0.

Pan, Sheng-Wei, Hsin-Kuo Kao, Wen-Kuang Yu, Te-Cheng Lien, Yen-Wen Chen, Jia-Horng Wang, and Yu Ru Kou. 2013. “Synergistic Impact of Low Serum Albumin on Intensive Care Unit Admission and High Blood Urea Nitrogen during Intensive Care Unit Stay on Post-Intensive Care Unit Mortality in Critically Ill Elderly Patients Requiring Mechanical Ventilation.” *Geriatrics & Gerontology International* 13 (1): 107–15. doi:10.1111/j.1447-0594.2012.00869.x.

Pavlov, Andrei Y., Eduard I. Lazhok, and Maria N. Preobrazhenskaya. 1997. “A New Type of Chemical Modification of Glycopeptides Antibiotics: Aminomethylated

Derivatives of Eremomycin and Their Antibacterial Activity." *The Journal of Antibiotics* 50 (6): 509–13. doi:10.7164/antibiotics.50.509.

Pearcea, Clive M., and Dudley H. Williams. 1995. "Complete Assignment of the 13C NMR Spectrum of Vancomycin." *J. Chem. Soc., Perkin Trans. 2*, no. 1. The Royal Society of Chemistry: 153–57. doi:10.1039/P29950000153.

Percival, S. L., P. G. Bowler, and D. Russell. 2005. "Bacterial Resistance to Silver in Wound Care." *The Journal of Hospital Infection* 60 (1): 1–7. doi:10.1016/j.jhin.2004.11.014.

Pérez-Capilla, Tatiana, María-Rosario Baquero, José-María Gómez-Gómez, Alina Ionel, Soledad Martín, and Jesús Blázquez. 2005. "SOS-Independent Induction of dinB Transcription by Beta-Lactam-Mediated Inhibition of Cell Wall Synthesis in Escherichia Coli." *Journal of Bacteriology* 187 (4): 1515–18. doi:10.1128/JB.187.4.1515-1518.2005.

Perkins, Harold R. 1969. "Specificity of Combination between Mucopeptide Precursors and Vancomycin or Ristocetin." *The Biochemical Journal* 111 (2): 195–205.

Perrin, Fred H. 1948. "Whose Absorption Law?" *Journal of the Optical Society of America* 38 (1): 72–74. doi:10.1364/JOSA.38.000072.

Pettigrew, David Michael, Peter Georg Laitenberger, and Bo Liu. 2012. "Analyte Detection Method." *International Patent*. International Publication No.: WO2012049486.

Pfaller, Michael A., Donald J. Krogstad, George G. Granich, and Patrick R. Murray. 1984. "Laboratory Evaluation of Five Assay Methods for Vancomycin: Bioassay, High-Pressure Liquid Chromatography, Fluorescence Polarization Immunoassay, Radioimmunoassay, and Fluorescence Immunoassay." *Journal of Clinical Microbiology* 20 (3): 311–16.

Portolés, A., E. Palau, M. Puerro, E. Vargas, and J. J. Picazo. 2006. "Health Economics Assessment Study of Teicoplanin versus Vancomycin in Gram-Positive Infections." *Rev Esp Quimioterap* 19 (1): 65–75.

Pumerantz, Andrew, Krishna Muppidi, Sunil Agnihotri, Carlos Guerra, Vishwanath Venketaraman, Jeffrey Wang, and Guru Betageri. 2011. "Preparation of Liposomal Vancomycin and Intracellular Killing of Meticillin-Resistant Staphylococcus Aureus

(MRSA)." *International Journal of Antimicrobial Agents* 37 (2). Elsevier B.V. 140–44. doi:10.1016/j.ijantimicag.2010.10.011.

Raiteri, Roberto, Massimo Grattarola, and Rüdiger Berger. 2002. "Micromechanics Senses Biomolecules." *Materials Today* 5 (1): 22–29. doi:10.1016/S1369-7021(02)05139-8.

Raiteri, Roberto, Massimo Grattarola, Hans-Jürgen Butt, and Petr Skládal. 2001. "Micromechanical Cantilever-Based Biosensors." *Sensors and Actuators B: Chemical* 79 (2-3): 115–26. doi:10.1016/S0925-4005(01)00856-5.

Raju, Tonse N. K. 1998. "The Nobel Chronicles." *The Lancet* 352 (9128): 661. doi:10.1016/S0140-6736(05)79625-2.

———. 1999. "The Nobel Chronicles." *The Lancet* 353 (9153). Elsevier Ltd: 681. doi:10.1016/S0140-6736(05)75485-4.

Ramos, D., J. Tamayo, J. Mertens, M. Calleja, L. G. Villanueva, and A. Zaballos. 2008. "Detection of Bacteria Based on the Thermomechanical Noise of a Nanomechanical Resonator: Origin of the Response and Detection Limits." *Nanotechnology* 19 (3): 035503. doi:10.1088/0957-4484/19/03/035503.

Rang, H. P., M. M. Dale, J. M. Ritter, and R. J. Flower. 2007. *Rang and Dale's Pharmacology*. Churchill Livingstone, ISBN: 978-0443069116.

Rao, Jianghong, Lin Yan, Bing Xu, and George M. Whitesides. 1999. "Using Surface Plasmon Resonance to Study the Binding of Vancomycin and Its Dimer to Self-Assembled Monolayers Presenting D -Ala- D -Ala." *Journal of the American Chemical Society* 121 (11): 2629–30. doi:10.1021/ja9838763.

Raybin, Harry W. 1945. "Reaction of Theophylline with Gibbs' Reagent." *Journal of the American Chemical Society* 67 (9): 1621–22. doi:10.1021/ja01225a512.

Rello, Jordi, Jordi Sole-Violan, Marcio Sa-Borges, Jose Garnacho-Montero, Emma Muñoz, Gonzalo Sirgo, Montserrat Olona, and Emili Diaz. 2005. "Pneumonia Caused by Oxacillin-Resistant Staphylococcus Aureus Treated with Glycopeptides*." *Critical Care Medicine* 33 (9): 1983–87. doi:10.1097/01.CCM.0000178180.61305.1D.

Roberts, Jason A., Carl M. J. Kirkpatrick, and Jeffrey Lipman. 2011. "Monte Carlo Simulations: Maximizing Antibiotic Pharmacokinetic Data to Optimize Clinical

Practice for Critically Ill Patients." *The Journal of Antimicrobial Chemotherapy* 66 (2): 227–31. doi:10.1093/jac/dkq449.

Roberts, Jason A., Peter Kruger, David L. Paterson, and Jeffrey Lipman. 2008. "Antibiotic Resistance--What's Dosing Got to Do with It?" *Critical Care Medicine* 36 (8): 2433–40. doi:10.1097/CCM.0b013e318180fe62.

Roberts, Jason A., and Jeffrey Lipman. 2009. "Pharmacokinetic Issues for Antibiotics in the Critically Ill Patient." *Critical Care Medicine* 37 (3). Society of Critical Care Medicine and Lippincott Williams & Wilkins: 840–51. doi:10.1097/CCM.0b013e3181961bff.

Roberts, Jason A., Jeffrey Lipman, Stijn Blot, and Jordi Rello. 2008. "Better Outcomes through Continuous Infusion of Time-Dependent Antibiotics to Critically Ill Patients?" *Current Opinion in Critical Care* 14 (4): 390–96. doi:10.1097/MCC.0b013e3283021b3a.

Roberts, Jason A., Michael S. Roberts, Andrew Semark, Andrew A. Udy, Carl M. J. Kirkpatrick, David L. Paterson, Matthew J. Roberts, Peter Kruger, and Jeffrey Lipman. 2011. "Antibiotic Dosing in the 'at Risk' Critically Ill Patient: Linking Pathophysiology with Pharmacokinetics/pharmacodynamics in Sepsis and Trauma Patients." *BMC Anesthesiology* 11 (1). BioMed Central Ltd: 1–7. doi:10.1186/1471-2253-11-3.

Rodrigo, Chamira, Tricia M. Mckeever, Mark Woodhead, and Wei Shen Lim. 2013. "Single versus Combination Antibiotic Therapy in Adults Hospitalised with Community Acquired Pneumonia." *Thorax* 68 (5): 493–95. doi:10.1136/thoraxjnl-2012-202296.

Rodvold, Keith A., Robert A. Blum, James H. Fischer, Humphrey Z. Zokufa, John C. Rotschafer, Kent B. Crossley, and Louise J. Riff. 1988. "Vancomycin Pharmacokinetics in Patients with Various Degrees of Renal Function." *Antimicrobial Agents and Chemotherapy* 32 (6): 848–52. doi:10.1128/AAC.32.6.848.

Rossi, Roberto A., Adriana B. Pierini, and Alicia B. Peñéñory. 2003. "Nucleophilic Substitution Reactions by Electron Transfer." *Chemical Reviews* 103 (1): 71–167. doi:10.1021/cr960134o.

Rottman, Martin, Joel Goldberg, and S. Adam Hacking. 2012. "Titanium-Tethered Vancomycin Prevents Resistance to Rifampicin in Staphylococcus Aureus in Vitro." *PloS One* 7 (12): 1–6. doi:10.1371/journal.pone.0052883.

Rowe, A. C. H., A. Donoso-Barrera, Ch. Renner, and S. Arscott. 2008. "Giant Room-Temperature Piezoresistance in a Metal-Silicon Hybrid Structure." *Physical Review Letters* 100 (14): 145501. doi:10.1103/PhysRevLett.100.145501.

Rybak, Michael J. 2006. "The Pharmacokinetic and Pharmacodynamic Properties of Vancomycin." *Clinical Infectious Diseases: An Official Publication of the Infectious Diseases Society of America* 42 (Suppl 1): S35–39. doi:10.1086/491712.

Rybak, Michael J., Ben M. Lomaestro, John C. Rotschafer, Robert C. Moellering, Willam A. Craig, Marianne Billeter, Joseph R. Dalovisio, and Donald P. Levine. 2009a. "Vancomycin Therapeutic Guidelines: A Summary of Consensus Recommendations from the Infectious Diseases Society of America, the American Society of Health-System Pharmacists, and the Society of Infectious Diseases Pharmacists." *Clinical Infectious Diseases : An Official Publication of the Infectious Diseases Society of America* 49 (3): 325–27. doi:10.1086/600877.

Rybak, Michael J., Ben Lomaestro, John C. Rotschafer, Robert Moellering, William Craig, Marianne Billeter, Joseph R. Dalovisio, and Donald P. Levine. 2009b. "Therapeutic Monitoring of Vancomycin in Adult Patients: A Consensus Review of the American Society of Health-System Pharmacists, the Infectious Diseases Society of America, and the Society of Infectious Diseases Pharmacists." *American Journal of Health-System Pharmacy : AJHP : Official Journal of the American Society of Health-System Pharmacists* 66 (1): 82–98. doi:10.2146/ajhp080434.

Sandiumenge Camps, A., J. A. Sanchez-Izquierdo Riera, D. Toral Vazquez, M. Sa Borges, J. Peinado Rodriguez, and E. Alted Lopez. 2000. "Midazolam and 2% Propofol in Long-Term Sedation of Traumatized Critically Ill Patients: Efficacy and Safety Comparison." *Critical Care Medicine* 28 (11): 3612–19.

Saribas, Suat, and Yasar Bagdatli. 2004. "Vancomycin Tolerance in Enterococci." *Chemotherapy* 50 (5): 250–54. doi:10.1159/000081946.

Sawyer, Heineman, and Beebe. 1984. *Chemistry Experiments for Instrumental Methods*. John Wiley & Sons.

Schäfer, Martina, Thomas R. Schneider, and George M. Sheldrick. 1996. “Crystal Structure of Vancomycin.” *Structure* 4 (12): 1509–15. doi:10.1016/S0969-2126(96)00156-6.

Scheller, Frieder W., Ulla Wollenberger, Axel Warsinke, and Fred Lisdat. 2001. “Research and Development in Biosensors.” *Current Opinion in Biotechnology* 12 (1): 35–40. doi:10.1016/S0958-1669(00)00169-5.

Schneider, Tanja, and Hans-Georg Sahl. 2010. “An Oldie but a Goodie - Cell Wall Biosynthesis as Antibiotic Target Pathway.” *International Journal of Medical Microbiology : IJMM* 300 (2-3). Elsevier: 161–69. doi:10.1016/j.ijmm.2009.10.005.

Schouten, James A., Sangeev Bagga, Adrian J. Lloyd, Gianfranco de Pascale, Christopher G. Dowson, David I. Roper, and Timothy D. H. Bugg. 2006. “Fluorescent Reagents for in Vitro Studies of Lipid-Linked Steps of Bacterial Peptidoglycan Biosynthesis: Derivatives of UDPMurNAc-Pentapeptide Containing D-Cysteine at Position 4 or 5.” *Molecular BioSystems* 2 (10): 484–91. doi:10.1039/b607908c.

Schreiber, Frank. 2000. “Structure and Growth of Self-Assembling Monolayers.” *Progress in Surface Science* 65 (5-8). Elsevier: 151–257. doi:10.1016/S0079-6816(00)00024-1.

Schwartz, Robert S. 2004. “Paul Ehrlich’s Magic Bullets.” *The New England Journal of Medicine* 350 (11): 1079–80. doi:10.1056/NEJMp048021.

Schwenzer, Kathryn S., Chao-Huei J. Wang, and John P. Anhalt. 1983. “Automated Fluorescence Polarization Immunoassay for Monitoring Vancomycin.” *Therapeutic Drug Monitoring* 5: 341–45.

Scudi, John V. 1941. “On the Colorimetric Determination of Vitamin B6.” *Journal of Biological Chemistry* 139: 707–20.

Scudi, John V., and Rudolf P. Buhs. 1941. “A Colorimetric Oxidation-Reduction Method for the Determination of the K Vitamins.” *Journal of Biological Chemistry* 141: 451–64.

Selim, Samy. 2011. “Antimicrobial Activity of Essential Oils against Vancomycin-Resistant Enterococci (vre) and Escherichia Coli o157:h7 in Feta Soft Cheese and Minced Beef Meat.” *Brazilian Journal of Microbiology : [publication of the Brazilian Society for Microbiology]* 42 (1): 187–96. doi:10.1590/S1517-83822011000100023.

Servin, Jacqueline A., Craig W. Herbold, Ryan G. Skophammer, and James A. Lake. 2008. "Evidence Excluding the Root of the Tree of Life from the Actinobacteria." *Molecular Biology and Evolution* 25 (1): 1–4. doi:10.1093/molbev/msm249.

Seve, Pascal, Isabelle Ray-Coquard, Veronique Trillet-Lenoir, Michael Sawyer, John Hanson, Christiane Broussolle, Sylvie Negrier, Charles Dumontet, and John R. Mackey. 2006. "Low Serum Albumin Levels and Liver Metastasis Are Powerful Prognostic Markers for Survival in Patients with Carcinomas of Unknown Primary Site." *Cancer* 107 (11): 2698–2705. doi:10.1002/cncr.22300.

Shee, Chandan, P. J. Hastings, and Susan M. Rosenberg. 2013. "Mutagenesis Associated with Repair of DNA Double-Strand Breaks Under Stress." In *Stress-Induced Mutagenesis*, edited by David Mittelman, 21–39. New York, NY: Springer New York. doi:10.1007/978-1-4614-6280-4_2.

Sheldrick, George M., Peter G. Jones, Olga Kennard, Dudley H. Williams, and Gerald A. Smith. 1978. "Structure of Vancomycin and Its Complex with Acetyl-D-Alanyl-D-Alanine." *Nature* 271 (5642): 223–25. doi:10.1038/271223a0.

Shin, Wan G., Myung G. Lee, Min H. Lee, and Nak D. Kim. 1991. "Factors Influencing the Protein Binding of Vancomycin." *Biopharmaceutics & Drug Disposition* 12 (9): 637–46. doi:10.1002/bdd.2510120902.

———. 1992. "Pharmacokinetics of Drugs in Blood VII: Unusual Distribution and Blood Storage Effect of Vancomycin." *Biopharmaceutics & Drug Disposition* 13 (4): 305–10. doi:10.1002/bdd.2510130409.

Shu, Wenmiao, Dongsheng Liu, Moyu Watari, Christian K. Riener, Torsten Strunz, Mark E. Welland, Shankar Balasubramanian, and Rachel A. McKendry. 2005. "DNA Molecular Motor Driven Micromechanical Cantilever Arrays." *Journal of the American Chemical Society* 127 (48): 17054–60. doi:10.1021/ja0554514.

Singh, Sheo B., and John F. Barrett. 2006. "Empirical Antibacterial Drug Discovery--Foundation in Natural Products." *Biochemical Pharmacology* 71 (7): 1006–15. doi:10.1016/j.bcp.2005.12.016.

Sinthiptharakoon, Kitiphat, Steven R. Schofield, Philipp Studer, Veronika Brázdová, Cyrus F. Hirjibehedin, David R. Bowler, and Neil J. Curson. 2013. "Investigating Individual

Arsenic Dopant Atoms in Silicon Using Low-Temperature Scanning Tunnelling Microscopy". Mesoscale and Nanoscale Physics. *arXiv Preprint arXiv*, July.

Slater, Leo B. 2002. "Instruments and Rules: R. B. Woodward and the Tools of Twentieth-Century Organic Chemistry." *Studies in History and Philosophy of Science* 33 (1): 1–33. doi:10.1016/S0039-3681(01)00024-3.

Smith-Palmer, A., J. Stewart, and L. Fyfe. 1998. "Antimicrobial Properties of Plant Essential Oils and Essences against Five Important Food-Borne Pathogens." *Letters in Applied Microbiology* 26 (2): 118–22. doi:10.1046/j.1472-765X.1998.00303.x.

Sneader, Walter. 2000. "The Discovery of Aspirin: A Reappraisal." *BMJ* 321 (7276): 1591–94. doi:10.1136/bmj.321.7276.1591.

Sommer, Morten O. A., Gautam Dantas, and George M. Church. 2009. "Functional Characterization of the Antibiotic Resistance Reservoir in the Human Microflora." *Science* 325 (5944): 1128–31. doi:10.1126/science.1176950.

Spellberg, Brad, John G. Bartlett, and David N. Gilbert. 2013. "The Future of Antibiotics and Resistance." *The New England Journal of Medicine* 368 (4): 299–302. doi:10.1056/NEJMp1215093.

"Sphere Medical Ltd.'s Homepage: About Sphere Medical." 2014. *Last Accessed: 07/03/2014*. http://www.spheremedical.com/about_us.

"Sphere Medical Ltd.'s Homepage: Pelorus Propofol Measurement System." 2014. *Last Accessed: 04/02/2014*. http://www.spheremedical.com/pelorus.

"Sphere Medical Ltd.'s Homepage: Proxima System." 2014. *Last Accessed: 12/02/2014*. http://www.spheremedical.com/proxima_system.

Stachowiak, Jeanne C., Min Yue, Kenneth Castelino, Arup Chakraborty, and Arun Majumdar. 2006. "Chemomechanics of Surface Stresses Induced by DNA Hybridization." *Langmuir : The ACS Journal of Surfaces and Colloids* 22 (1): 263–68. doi:10.1021/la0521645.

Stauffer, Dietrich, and Ammon Aharony. 1991. *Introduction to Percolation Theory*. Taylor & Francis, ISBN: 978-0748400270.

Stein, Gary E., and Elizabeth M. Wells. 2010. "The Importance of Tissue Penetration in Achieving Successful Antimicrobial Treatment of Nosocomial Pneumonia and Complicated Skin and Soft-Tissue Infections Caused by Methicillin-Resistant

Staphylococcus Aureus: Vancomycin and Linezolid." *Current Medical Research and Opinion* 26 (3): 571–88. doi:10.1185/03007990903512057.

Stoney, G. Gerald. 1909. "The Tension of Metallic Films Deposited by Electrolysis." *Proceedings of the Royal Society of London.* 82 (553): 172–75.

Stuart, P. C., S. M. Stott, A. Millar, G. N. C. Kenny, and D. Russell. 2000. "Cp50 of Propofol with and without Nitrous Oxide 67%." *British Journal of Anaesthesia* 84 (5): 638–39. doi:10.1093/bja/84.5.638.

Studer, Philipp, Veronika Brázdová, Steven R. Schofield, David R. Bowler, Cyrus F. Hirjibehedin, and Neil J. Curson. 2012. "Site-Dependent Ambipolar Charge States Induced by Group V Atoms in a Silicon Surface." *ACS Nano* 6 (12): 10456–62. doi:10.1021/nn3039484.

Sułkowska, Anna. 2002. "Interaction of Drugs with Bovine and Human Serum Albumin." *Journal of Molecular Structure* 614 (1-3): 227–32. doi:10.1016/S0022-2860(02)00256-9.

Sun, He, Eufronio G. Maderazo, and Allan R. Krusell. 1993. "Serum Protein-Binding Characteristics of Vancomycin." *Antimicrobial Agents and Chemotherapy* 37 (5): 1132–36.

Sushko, Maria L., John H. Harding, Alexander L. Shluger, Rachel A. McKendry, and Moyu Watari. 2008. "Physics of Nanomechanical Biosensing on Cantilever Arrays." *Advanced Materials* 20 (20): 3848–53. doi:10.1002/adma.200801344.

Svobodová, D., P. Křenek, M Fraenkl, and J. Gasparič. 1977. "Colour Reaction of Phenols with the Gibbs Reagent. The Reaction Mechanism and Decomposition and Stabilisation of the Reagent." *Mikrochimica Acta* 67 (3-4): 251–64. doi:10.1007/BF01213035.

Svobodová, D., P. Krenek, M. Fraenkl, and J. Gasparič. 1978. "The Colour Reaction of Phenols with the Gibbs Reagent." *Microchimica Acta* 70 (3). Springer: 197–211.

Takács-Novák, Kristztina, Béla Noszál, Márta Tókés-Kövesdi, and György Szász. 1993. "Acid-Base Properties and Proton-Speciation of Vancomycin." *International Journal of Pharmaceutics* 89 (3): 261–63. doi:10.1016/0378-5173(93)90252-B.

Tamma, Pranita D., Alison E. Turnbull, Anthony D. Harris, Aaron M. Milstone, Alice J. Hsu, and Sara E. Cosgrove. 2013. "Less Is More: Combination Antibiotic Therapy for

the Treatment of Gram-Negative Bacteremia in Pediatric Patients." *JAMA Pediatrics* 167 (10): 903–10. doi:10.1001/jamapediatrics.2013.196.

Tateishi, K., W. Ando, C. Higuchi, D. A. Hart, J. Hashimoto, K. Nakata, H. Yoshikawa, and N. Nakamura. 2008. "Comparison of Human Serum with Fetal Bovine Serum for Expansion and Differentiation of Human Synovial MSC: Potential Feasibility for Clinical Applications." *Cell Transplantation* 17 (5): 549–57. doi:10.3727/096368908785096024.

Tenje, Maria, Stepan S. Keller, Zachary J. Davis, Anja Boisen, Joseph W. Ndieyira, Manuel Vögtli, Carlo Morasso, and Rachel A. McKendry. 2012. "Cantilever-Based Sensor." In *Optochemical Nanosensors*. CRP Press, Taylor & Francis Group, ISBN: 978-1-4398-5489-1.

"The Merck Index Online - Vancomycin." 2013. *CAS Registry Number: 1404-90-6. Last Accessed: 25/02/2014*. Accessed 2/25/2014. https://www.rsc.org/Merck-Index/monograph/mono1500010116/vancomycin derivative monohydrochloride?q=authorize.

Theuretzbacher, Ursula. 2013. "Global Antibacterial Resistance: The Never-Ending Story." *Journal of Global Antimicrobial Resistance* 1 (2). Taibah University: 63–69. doi:10.1016/j.jgar.2013.03.010.

Thévenot, Daniel R., Klara Toth, Richard A. Durst, and George S. Wilson. 2001. "Electrochemical Biosensors: Recommended Definitions and Classification." *Biosensors and Bioelectronics* 16 (1-2): 121–31. doi:10.1016/S0956-5663(01)00115-4.

Thompson, A., P. Griffin, R. Stuetz, and E. Cartmell. 2005. "The Fate and Removal of Triclosan during Wastewater Treatment." *Water Environment Research* 77 (1): 63–67. doi:10.2175/106143005X41636.

Thomson, A. H., C. E. Staatz, C. M. Tobin, M. Gall, and A. M. Lovering. 2009. "Development and Evaluation of Vancomycin Dosage Guidelines Designed to Achieve New Target Concentrations." *The Journal of Antimicrobial Chemotherapy* 63 (5): 1050–57. doi:10.1093/jac/dkp085.

Thundat, T., R. J. Warmack, G. Y. Chen, and D. P. Allison. 1994. "Thermal and Ambient-Induced Deflections of Scanning Force Microscope Cantilevers." *Applied Physics Letters* 64 (21): 2894–96. doi:10.1063/1.111407.

Tietze, Lutz F., Hubertus P. Bell, and Srivari Chandrasekhar. 2003. "Natural Product Hybrids as New Leads for Drug Discovery." *Angewandte Chemie (International Ed. in English)* 42 (34): 3996–4028. doi:10.1002/anie.200200553.

Tillmans, J., P. Hirsch, and E. Reinshagen. 1928. "Über Die Anwendung von 2, 6-Dichlorphenol-Indophenol Als Reduktionsindicator Bei Der Untersuchung von Lebensmitteln." *Zeitschrift Für Untersuchung Der Lebensmittel.* 40: 272–92.

Tobin, C. M. 2002. "Vancomycin Therapeutic Drug Monitoring: Is There a Consensus View? The Results of a UK National External Quality Assessment Scheme (UK NEQAS) for Antibiotic Assays Questionnaire." *Journal of Antimicrobial Chemotherapy* 50 (5): 713–18. doi:10.1093/jac/dkf212.

Tortonese, M., R. C. Barrett, and C. F. Quate. 1993. "Atomic Resolution with an Atomic Force Microscope Using Piezoresistive Detection." *Applied Physics Letters* 62 (8): 834. doi:10.1063/1.108593.

Touw, Daan J., Cees Neef, Alison H. Thomson, and Alexander A. Vinks. 2007. "Cost-Effectiveness of Therapeutic Drug Monitoring: A Systematic Review." *The European Journal of Hospital Pharmacy Science* 13 (4): 83–91.

Trujillo, T. N., K. M. Sowinski, R. A. Venezia, M. K. Scott, and B. A. Mueller. 1999. "Vancomycin Assay Performance in Patients with Acute Renal Failure." *Intensive Care Medicine* 25 (11): 1291–96. doi:10.1007/s001340051060.

Tyndall, John. 1881. *Essays on the Floating Matter of the Air in Relation to Putrefaction and Infection. By John Tyndall, F.R.S.* London: D. Appleton and Co., New York, 1882.

Udy, Andrew A., Jason A. Roberts, Robert J. Boots, David L. Paterson, and Jeffrey Lipman. 2010. "Augmented Renal Clearance: Implications for Antibacterial Dosing in the Critically Ill." *Clinical Pharmacokinetics* 49 (1): 1–16. doi:10.2165/11318140-000000000-00000.

Ulman, Abraham. 1996. "Formation and Structure of Self-Assembled Monolayers." *Chemical Reviews* 96 (4): 1533–54. doi:10.1021/cr9502357.

Van Hal, S. J., T. P. Lodise, and D. L. Paterson. 2012. "The Clinical Significance of Vancomycin Minimum Inhibitory Concentration in Staphylococcus Aureus Infections: A Systematic Review and Meta-Analysis." *Clinical Infectious Diseases: An Official Publication of the Infectious Diseases Society of America* 54 (6): 755–71. doi:10.1093/cid/cir935.

Van Valen, Leigh. 1973. "A New Evolutionary Law." *Evolutionary Theory* 1: 1–30.

VanderJagt, Dorothy J., Philip J. Garry, and William C. Hunt. 1986. "Ascorbate in Plasma as Measured by Liquid Chromatography and by Dichlorophenolindophenol Colorimetry." *Clinical Chemistry* 32 (6): 1004–6.

Varma, Archana, Miguel A. de Pedro, and Kevin D. Young. 2007. "FtsZ Directs a Second Mode of Peptidoglycan Synthesis in Escherichia Coli." *Journal of Bacteriology* 189 (15): 5692–5704. doi:10.1128/JB.00455-07.

Vögtli, Manuel. 2011. "Nanomechanical Detection of Drug-Target Interactions Using Cantilever Sensors." *PhD Thesis - University College London (UCL)*. University College London (UCL).

Vollhardt, K. Peter C., and N. E. Shore. 2005. *Organische Chemie*. WILEY-VCH, ISBN: 978-3-527-31380-8.

Von Nussbaum, Franz, Michael Brands, Berthold Hinzen, Stefan Weigand, and Dieter Häbich. 2006. "Antibacterial Natural Products in Medicinal Chemistry--Exodus or Revival?" *Angewandte Chemie (International Ed. in English)* 45 (31): 5072–5129. doi:10.1002/anie.200600350.

Wachtmeister, Carl Alex. 1954. "Studies on the Chemistry of Lichens." *Acta Chemica Scandinavica* 10 (9): 1404–13.

Wainwright, Milton. 1989. "Moulds in Ancient and More Recent Medicine." *Mycologist* 3 (1): 21–23. doi:10.1016/S0269-915X(89)80010-2.

Waksman, Selman A. 1947. "What Is an Antibiotic or an Antibiotic Substance?" *Mycologia* 39 (5): 565–96. doi:10.2307/3755196.

Walsh, Christopher T., and Gerard D. Wright. 2005. "Introduction: Antibiotic Resistance." *Chemical Reviews* 105 (2): 391–94. doi:10.1021/cr030100y.

Wan, Qian-Hong, and X. Chris Le. 1999. “Fluorescence Polarization Studies of Affinity Interactions in Capillary Electrophoresis.” *Analytical Chemistry* 71 (19): 4183–89. doi:10.1021/ac9902796.

Wang, Jiun-Ling, Chung-Hsu Lai, Hsi-Hsun Lin, Wei-Fang Chen, Yi-Chun Shih, and Chih-Hsin Hung. 2013. “High Vancomycin Minimum Inhibitory Concentrations with Heteroresistant Vancomycin-Intermediate Staphylococcus Aureus in Meticillin-Resistant S. Aureus Bacteraemia Patients.” *International Journal of Antimicrobial Agents* 42 (5): 390–94. doi:10.1016/j.ijantimicag.2013.07.010.

Watari, Moyu. 2007. “In-Plane Mechanochemistry at Model Biological Interfaces.” *PhD Thesis*. University College London (UCL).

Watari, Moyu, Jane Galbraith, Hans Peter Lang, Marilyne Sousa, Martin Hegner, Christoph Gerber, Mike A. Horton, and Rachel A. McKendry. 2007. “Investigating the Molecular Mechanisms of in-Plane Mechanochemistry on Cantilever Arrays.” *Journal of the American Chemical Society* 129 (3): 601–9. doi:10.1021/ja065222x.

Watari, Moyu, Joseph W. Ndieyira, and Rachel A. McKendry. 2010. “Chemically Programmed Nanomechanical Motion of Multiple Cantilever Arrays.” *Langmuir: The ACS Journal of Surfaces and Colloids* 26 (7): 4623–26. doi:10.1021/la100448v.

Wee, Kyung Wook, Ghi Yuun Kang, Jaebum Park, Ji Yoon Kang, Dae Sung Yoon, Jung Ho Park, and Tae Song Kim. 2005. “Novel Electrical Detection of Label-Free Disease Marker Proteins Using Piezoresistive Self-Sensing Micro-Cantilevers.” *Biosensors & Bioelectronics* 20 (10): 1932–38. doi:10.1016/j.bios.2004.09.023.

Wehrmeister, Jana, Achim Fuss, Frank Saurenbach, Rüdiger Berger, and Mark Helm. 2007. “Readout of Micromechanical Cantilever Sensor Arrays by Fabry-Perot Interferometry.” *The Review of Scientific Instruments* 78 (10): 104105. doi:10.1063/1.2785028.

White, L. O. 2000. “UK NEQAS in Antibiotic Assays.” *Journal of Clinical Pathology* 53 (11): 829–34. doi:10.1136/jcp.53.11.829.

Wild, David. 2013. *The Immunoassay Handbook*. Elsevier Science, ISBN: 978-0080970387.

Williams, Dudley H. 1984. “Structural Studies on Some Antibiotics of the Vancomycin Group, and on the Antibiotic-Receptor Complexes, by Proton NMR.” *Accounts of Chemical Research* 17 (10): 364–69. doi:10.1021/ar00106a004.

———. 1996. “The Glycopeptide Story ? How to Kill the Deadly ?superbugs?” *Natural Product Reports* 13 (6): 469. doi:10.1039/np9961300469.

Williams, Dudley H., and Ben Bardsley. 1999. “The Vancomycin Group of Antibiotics and the Fight against Resistant Bacteria.” *Angewandte Chemie International Edition* 38 (9): 1172–93. doi:10.1002/(SICI)1521-3773(19990503)38:9<1172::AID-ANIE1172>3.0.CO;2-C.

Williams, Dudley H., and John R. Kalman. 1977. “Structural and Mode of Action Studies on the Antibiotic Vancomycin. Evidence from 270-MHz Proton Magnetic Resonance.” *Journal of the American Chemical Society* 99 (8): 2768–74. doi:10.1021/ja00450a058.

Williams, Dudley H., Michael P. Williamson, David W. Butcher, and Stephen J. Hammond. 1983. “Detailed Binding Sites of the Antibiotics Vancomycin and Ristocetin A: Determination of Intermolecular Distances in Antibiotic/substrate Complexes by Use of the Time-Dependent NOE.” *Journal of the American Chemical Society* 105 (5): 1332–39. doi:10.1021/ja00343a043.

Wilson, John F., Alan C. Davis, and Caroline M. Tobin. 2003. “Evaluation of Commercial Assays for Vancomycin and Aminoglycosides in Serum: A Comparison of Accuracy and Precision Based on External Quality Assessment.” *The Journal of Antimicrobial Chemotherapy* 52 (1): 78–82. doi:10.1093/jac/dkg296.

Windler, Lena, Murray Height, and Bernd Nowack. 2013. “Comparative Evaluation of Antimicrobials for Textile Applications.” *Environment International* 53 (March). Elsevier Ltd: 62–73. doi:10.1016/j.envint.2012.12.010.

Woodford, Neil. 2003. “Novel Agents for the Treatment of Resistant Gram-Positive Infections.” *Expert Opinion on Investigational Drugs* 12 (2): 117–37. doi:10.1517/13543784.12.2.117.

Woodford, Neil, and David M. Livermore. 2009. “Infections Caused by Gram-Positive Bacteria: A Review of the Global Challenge.” *The Journal of Infection* 59 (Suppl 1). The British Infection Society: S4–S16. doi:10.1016/S0163-4453(09)60003-7.

Woodward, Robert Burns. 1941. “Structure and the Absorption Spectra of A, B-Unsaturated Ketones.” *Journal of the American Chemical Society* 63: 1123–26.

———. 1942a. “Structure and Absorption Spectra. III. Normal Conjugated Dienes.” *Journal of the American Chemical Society* 64: 72–75.

———. 1942b. “Structure and Absorption Spectra. IV. Further Observations on A,β-Unsaturated Ketones.” *Journal of the American Chemical Society* 64: 1941–42.

Woodward, Robert Burns, and A. F. Clifford. 1941. “Structure and Absorption Spectra. II. 3-Acetoxy-Δ5-(6)-nor-Cholestene-7-Carboxylic Acid.” *Journal of the American Chemical Society* 102: 2727–29.

Wright, Gerard D. 2010. “Antibiotic Resistance in the Environment: A Link to the Clinic?” *Current Opinion in Microbiology* 13 (5). Elsevier Ltd: 589–94. doi:10.1016/j.mib.2010.08.005.

Wu, Guanghua, Haifeng Ji, Karolyn Hansen, Thomas Thundat, Ram Datar, Richard Cote, Michael F. Hagan, Arup K. Chakraborty, and Arunava Majumdar. 2001. “Origin of Nanomechanical Cantilever Motion Generated from Biomolecular Interactions.” *Proceedings of the National Academy of Sciences of the United States of America* 98 (4): 1560–64. doi:10.1073/pnas.031362498.

Wysocki, Marc, Frederique Delatour, F. Faurisson, A. Rauss, Y. Pean, B. Misset, F. Thomas, et al. 2001. “Continuous versus Intermittent Infusion of Vancomycin in Severe Staphylococcal Infections: Prospective Multicenter Randomized Study.” *Antimicrobial Agents and Chemotherapy* 45 (9): 2460–67. doi:10.1128/AAC.45.9.2460-2467.2001.

Yamasaki, Keishi, Victor Tuan Giam Chuang, Toru Maruyama, and Masaki Otagiri. 2013. “Albumin-Drug Interaction and Its Clinical Implication.” *Biochimica et Biophysica Acta* 1830 (12). Elsevier B.V. 5435–43. doi:10.1016/j.bbagen.2013.05.005.

Yao, Stephanie. 2013. “FDA Approves Vibativ for Hospitalized Patients with Bacterial Pneumonia.” *U.S. Food and Drug Administration. Last Accessed: 21/03/2014*. http://www.fda.gov/newsevents/newsroom/pressannouncements/ucm358209.htm.

Yeo, Klang-Teck, Wiliiam Traverse, and Gary L. Horowitz. 1989. “Clinical Performance of the EMIT Vancomycin Assay.” *Clinical Chemistry* 35 (7): 1504–7.

Yoshikawa, Genki, Hans Peter Lang, Terunobu Akiyama, Laure Aeschimann, Urs Staufer, Peter Vettiger, Masakazu Aono, Toshio Sakurai, and Christoph Gerber. 2009. "Sub-Ppm Detection of Vapors Using Piezoresistive Microcantilever Array Sensors." *Nanotechnology* 20 (1): 015501. doi:10.1088/0957-4484/20/1/015501.

Yu, Linliang, Meng Zhong, and Yinan Wei. 2010. "Direct Fluorescence Polarization Assay for the Detection of Glycopeptide Antibiotics." *Analytical Chemistry* 82 (16): 7044–48. doi:10.1021/ac100543e.

Yue, M., H. Lin, D. E. Dedrick, S. Satyanarayana, A. Majumdar, A. S. Bedekar, J. W. Jenkins, and S. Sundaram. 2004. "A 2-D Microcantilever Array for Multiplexed Biomolecular Analysis." *Journal of Microelectromechanical Systems* 13 (2): 290–99. doi:10.1109/JMEMS.2003.823216.

Zechmeister, L., and A. Polgár. 1943. "Cis-Trans Isomerization and Spectral Characteristics of Carotenoids and Some Related Compounds." *Journal of the American Chemical Society* 65: 1522–28. doi:10.1021/ja01248a025.

Zeitlinger, Markus A., Hartmut Derendorf, Johan W. Mouton, Otto Cars, William A. Craig, David Andes, and Ursula Theuretzbacher. 2011. "Protein Binding: Do We Ever Learn?" *Antimicrobial Agents and Chemotherapy* 55 (7): 3067–74. doi:10.1128/AAC.01433-10.

Zhang, Jiayun, Hans Peter Lang, François Huber, Alexander Bietsch, Wilfried Grange, Ulrich Certa, Rachel A. McKendry, Hans-Joachim Güntherodt, Martin Hegner, and Christoph Gerber. 2006. "Rapid and Label-Free Nanomechanical Detection of Biomarker Transcripts in Human RNA." *Nature Nanotechnology* 1 (3): 214–20. doi:10.1038/nnano.2006.134.

Zhang, Jiayun, Hans Peter Lang, Genki Yoshikawa, and Christoph Gerber. 2012. "Optimization of DNA Hybridization Efficiency by pH-Driven Nanomechanical Bending." *Langmuir: The ACS Journal of Surfaces and Colloids* 28 (15): 6494–6501. doi:10.1021/la205066h.

Zhang, Neng-Hui, and Jin-Ying Shan. 2008. "An Energy Model for Nanomechanical Deflection of Cantilever-DNA Chip." *Journal of the Mechanics and Physics of Solids* 56 (6): 2328–37. doi:10.1016/j.jmps.2007.12.003.

Zhang, R., A. Best, R. Berger, S. Cherian, S. Lorenzoni, E. Macis, R. Raiteri, and R. Cain. 2007. “Multiwell Micromechanical Cantilever Array Reader for Biotechnology.” *The Review of Scientific Instruments* 78 (8): 084103. doi:10.1063/1.2775433.

Zokufa, Humphrey Z., Lynn D. Solem, Keith A. Rodvold, Kent B. Crossley, J. H. Fischer, and John C. Rotschafer. 1989. “The Influence of Serum Albumin and Alpha 1-Acid Glycoprotein on Vancomycin Protein Binding in Patients with Burn Injuries.” *The Journal of Burn Care & Rehabilitation* 10 (5): 425–28.

Appendix

Contents

A. Statistical Analysis

This chapter presents the statistical analysis and is divided into four subsections. The first two subsections present the two tests used in this thesis, a one-way analysis of variance (ANOVA) (subsection A.1) and a post hoc Fisher's least significant difference (LSD) (subsection A.2). These are followed by two subsections presenting the analysis of the absorbances of the six extraction protocol stages (#1 - #6) of chapter 6.3.3 (subsection A.3) and chapter 6.3.5 (subsection A.4).

To initiate the statistical analysis of the absorbances a one-way ANOVA was used. The one-way ANOVA test compares the means of several groups with each other in a single test. It was chosen on the basis that the data is quantitative so demands a parametric test, has more than two unpaired data sets without direct relationship, and has one independent variable - the antibiotic concentration - that influences the depended variable - the absorbance. The null hypothesis H_0 states that none of the absorbances of any extraction stage is significantly different from any other stage. If this null hypothesis H_0 could be rejected, a post hoc Fisher's LSD was performed subsequently to decide which stages are significantly different from each other (Ashcroft and Pereira 2003).

A.1. One-way ANOVA

The theory behind the ANOVA test is the rejection of the null hypothesis H_0 on the basis that the variability between the mean values of the samples is greater than can be accounted for by the intrinsic variability of the data within the samples. Therefore, the variabilities between and within the samples have to be estimated. This estimation is typically done as a mean square deviation of the general form: the sum of squares divided by the degrees of freedom. If the null hypothesis H_0 is correct, which means that the samples are drawn from a normal distribution with equal means and variances, the two estimations of the within- and the between-samples variability are the same. These two estimates are compared via the F-test that tests whether their ratio is close enough

to 1 allowing the conclusion that the null hypothesis H_0 is true at a certain level of significance (Ashcroft and Pereira 2003).

The formulae used for the one-way ANOVA test are the listed below, wherein x_{iJ} depicts the value of the observation j in the sample i, k is the number of samples or the population and n_i is the number of observation in sample i (Ashcroft and Pereira 2003).

The between-samples sum of squares (SS_B) is defined as:

$$\mathrm{SS_B} = \sum_{i=1}^{k} \mathrm{n_i} \cdot (\overline{\mathrm{x_i}} \cdot \overline{\mathrm{X}})^2 \qquad \text{I.I}$$

wherein $\overline{x_i}$ is the mean of the samples i and $\overline{X}$ is the overall mean of all observation.
And the within-samples sum of squares ($\mathrm{SS_W}$) is defined as:

$$\mathrm{SS_W} = \sum_{i=1}^{k} \sum_{j=1}^{n_i} (\mathrm{x_{ij}} \cdot \overline{\mathrm{x_i}})^2 \qquad \text{I.II}$$

And the addition of equations I.I and I.II results in the total sum of squares (SS_T):

$$\mathrm{SS_T} = \mathrm{SS_B} + \mathrm{SS_W} \qquad \text{I.III}$$

The between-samples degrees of freedom ($\mathrm{df_B}$) and the within-samples degrees of freedom ($\mathrm{df_W}$) are defined as:

$$\mathrm{df_B} = \mathrm{k} - 1 \qquad \text{I.IV}$$

and:

$$\mathrm{df_W} = \sum_{i=1}^{k} \mathrm{n_i} - \mathrm{k} \qquad \text{I.V}$$

The between-samples mean square ($\mathrm{MS_B}$) and the within-samples mean square ($\mathrm{MS_B}$), which are the estimates of the variabilities, are defined as the sums of the squares (I.I and I.II) over the corresponding degrees of freedom (I.IV and I.V):

$$MS_B = \frac{SS_\mathrm{B}}{df_B} \qquad \text{I.VI}$$

and:

$$MS_W = \frac{SS_\mathrm{W}}{df_W} \qquad \text{I.VII}$$

These estimates are then compared via the F-test using the F-ratio (F) with the formula:

$$F = \frac{MS_\mathrm{B}}{\mathrm{MS}_W} \qquad \text{I.VIII}$$

To compare the calculated F, the corresponding predefined critical value for F-distribution has to be found in literature such as in Ashcroft & Pereira, 2003. This critical F value is dependent on the level of significance and the two degrees of freedom for between- and within-samples. If the calculated F exceeds the critical F then it can be concluded that there is significant difference between at least two of the mean values of the data set, hence the null hypothesis H_0 can be rejected at the chosen significance level (Ashcroft and Pereira 2003).

A.2. Fisher's LSD test

When the results of an ANOVA analysis indicates that at least one mean is significantly different from another mean in the analysis, a multiple comparison has to be performed to indentify which mean or means are different. These comparisons are called post hoc tests and many different tests exist. The Fisher's Least Significant Difference (LSD) test was chosen as it is one of the commonly used tests following an ANOVA. The Fisher's LSD is a pair-wise comparison of all the means and calculates a modified t-statistic based on the within samples mean squares. It is also known as Protected t-test.

The three important formulae for the Fisher's LSD test are the following.

The number of comparisons N_c for k samples:

$$N_c = \frac{\mathrm{k(k-1)}}{2} \qquad \text{I.IX}$$

The t-test:

$$\mathrm{t} = \frac{|\overline{\mathrm{x}_1} - \overline{\mathrm{x}_2}|}{\sqrt{\mathrm{MS_W}\left[\frac{1}{\mathrm{n}_1} + \frac{1}{\mathrm{n}_2}\right]}} \qquad \text{I.X}$$

where $\mathrm{MS_W}$ is the within-samples mean square from the ANOVA test (see chapter A.1 and $\overline{\mathrm{x}_1}$ and $\overline{\mathrm{x}_2}$ are the mean value for the two pairs, which are compared with n_1 and n_2 values respectively.

Lastly, the calculated t-value of equation I.X has to be compared to the corresponding critical t-value, which can be found in literature such as in Ashcroft & Pereira, 2003. If the calculated t-value is greater than the critical t-value, it can be concluded that the corresponding pair, which was been compared, is significantly different at the chosen level of significance. To find the corresponding critical t-value the total degrees of

freedom (df) has to be calculated by the formula, which was previously described for df_W (I.V):

$$df = \sum_{i=1}^{m} n_i - k \qquad \text{I.XI}$$

wherein k samples are subtracted from $\sum_{i=1}^{m} n_i$, which is the total number of observations (Ashcroft and Pereira 2003).

A.3. Statistical Analysis of Subsection 6.3.3 Extraction Protocol Development from Foetal Bovine Serum

This subsection presents the statistical analysis of chapter 6.3.3 in particular the data presented in figure 6.11 D, which is shown below. As described above, firstly a one-way ANOVA analysis was performed. If the ANOVA indicated that at least one mean is significantly different from another mean, a post hoc Fisher's LSD was performed. For the sake of brevity, the interpretation of the statistical analysis results were not included in the appendix and can be found in the main part of the thesis in the corresponding chapter.

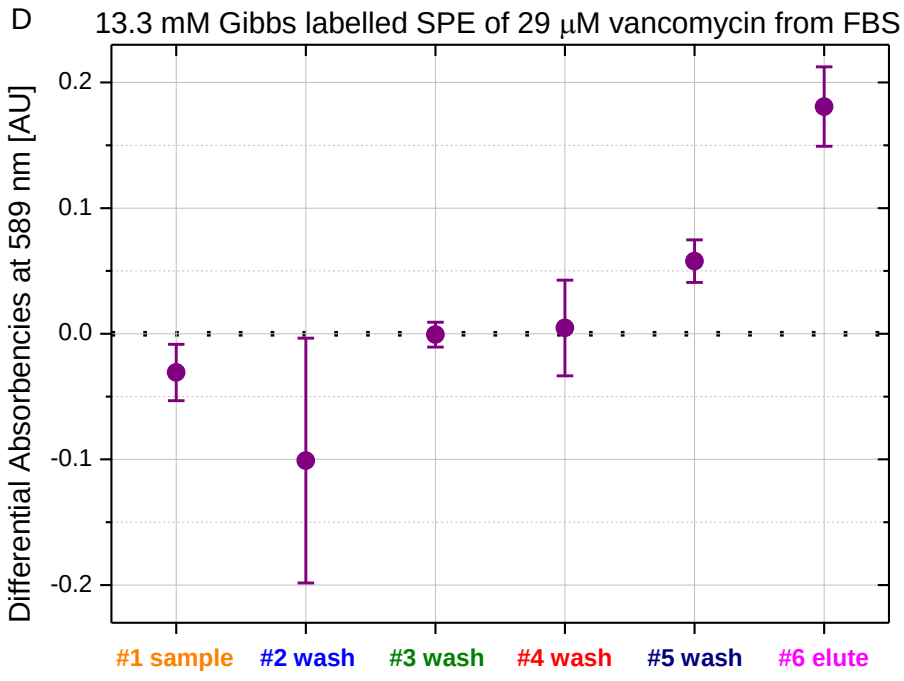

Table I:

one-way ANOVA	SS	DF	MS	*F*-ratio
between-samples (*b*)	0.135	5	0.027	**12.668**
within-samples (*w*)	0.026	12	0.002	
critical *F*-value at 1% significance level				**5.06**

Table II:

Fisher's LSD		***t*-value**	
critical *t*-value at 1% significance level for 12 df		**3.055**	
Nc = 15	**sample pair for comparison**	***t*-value**	**Significant?**
1	#1 sample vs. #2 wash	1.857	no
2	#1 sample vs. #3 wash	0.798	no
3	#1 sample vs. #4 wash	0.939	no
4	#1 sample vs. #5 wash	2.349	no
5	#1 sample vs. #6 elute	5.605	yes
6	#2 wash vs. #3 wash	2.655	no
7	#2 wash vs. #4 wash	2.796	no
8	#2 wash vs. #5 wash	4.206	yes
9	#2 wash vs. #6 elute	7.462	yes
10	#3 wash vs. #4 wash	0.141	no
11	#3 wash vs. #5 wash	1.550	no
12	#3 wash vs. #6 elute	4.807	yes
13	#4 wash vs. #5 wash	1.409	no
14	#4 wash vs. #6 elute	4.666	yes
15	#5 wash vs. #6 elute	3.256	yes

A.4. Statistical Analysis of Subsection 6.3.5 Change from Foetal Bovine to Whole Human Serum

This subsection presents the statistical analysis of chapter 6.3.3 in particular the data presented in figure 6.16 C, which is again shown below. The procedure was similar as described in the previous subsection A.3. Again for the sake of brevity, the interpretation of the statistical analysis results were not included in the appendix and can be found in the main part of the thesis in the corresponding chapter. The tables III and IV present the analyses for FBS and the tables V and VI the analyses for WHS.

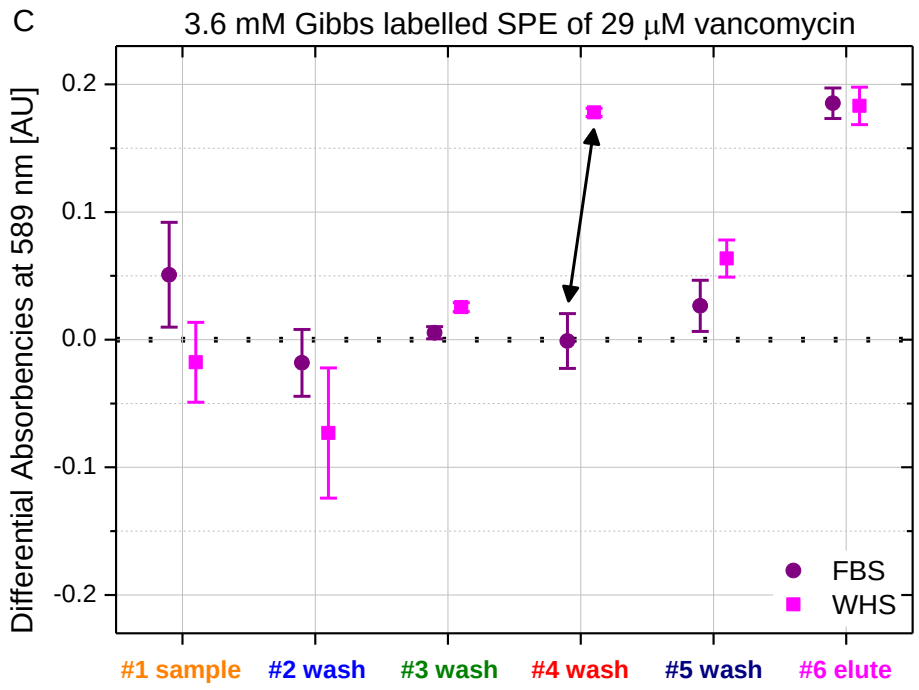

Table III: FBS

one-way ANOVA	SS	DF	MS	F-ratio
between-samples (*b*)	0.089	5	0.018	**31.411**
within-samples (*w*)	0.007	12	0.001	
critical F-value at 1% significance level				**5.06**

Table IV: FBS

Fisher's LSD		***t*-value**	
critical *t*-value at 1% significance level for 12 df		**3.055**	
Nc = 15	**sample pair for comparison**	***t*-value**	**Significant?**
1	#1 sample vs. #2 wash	3.549	yes
2	#1 sample vs. #3 wash	2.337	no
3	#1 sample vs. #4 wash	2.666	no
4	#1 sample vs. #5 wash	1.254	no
5	#1 sample vs. #6 elute	6.913	yes
6	#2 wash vs. #3 wash	1.212	no
7	#2 wash vs. #4 wash	0.883	no
8	#2 wash vs. #5 wash	2.294	no
9	#2 wash vs. #6 elute	10.462	yes
10	#3 wash vs. #4 wash	0.329	no
11	#3 wash vs. #5 wash	1.083	no
12	#3 wash vs. #6 elute	9.250	yes
13	#4 wash vs. #5 wash	1.412	no
14	#4 wash vs. #6 elute	9.579	yes
15	#5 wash vs. #6 elute	8.168	yes

Table V: WHS

one-way ANOVA	SS	DF	MS	F-ratio
between-samples (*b*)	0.162	5	0.032	**48.308**
within-samples (*w*)	0.008	12	0.001	
critical F-value at 1% significance level				**5.06**

Table VI: WHS

Fisher's LSD		***t*-value**	
critical *t*-value at 1% significance level for 12 df		**3.055**	
Nc = 15	**sample pair for comparison**	***t*-value**	**Significant?**
1	#1 sample vs. #2 wash	2.617	no
2	#1 sample vs. #3 wash	2.042	no
3	#1 sample vs. #4 wash	9.252	yes
4	#1 sample vs. #5 wash	3.842	yes
5	#1 sample vs. #6 elute	9.495	yes
6	#2 wash vs. #3 wash	4.660	yes
7	#2 wash vs. #4 wash	11.870	yes
8	#2 wash vs. #5 wash	6.459	yes
9	#2 wash vs. #6 elute	12.112	yes
10	#3 wash vs. #4 wash	7.210	yes
11	#3 wash vs. #5 wash	1.800	no
12	#3 wash vs. #6 elute	7.453	yes
13	#4 wash vs. #5 wash	5.410	yes
14	#4 wash vs. #6 elute	0.243	no
15	#5 wash vs. #6 elute	5.653	yes